ISSN: 2687 - 4539

CHAOS

THEORY AND APPLICATIONS

IN APPLIED SCIENCES AND ENGINEERING

Special Issue: Advanced Fractional Mathematics, Fractional Calculus, Algorithms and Artificial Intelligence with Applications in Complex Chaotic Systems

Editors: Yeliz Karaca, Dumitru Baleanu

VOLUME 5, ISSUE 4, DECEMBER 2023 (SPECIAL ISSUE)

AN INTERDISCIPLINARY JOURNAL OF NONLINEAR SCIENCE

Chaos Theory and Applications (CHTA)
ISSN: 2687-4539
Volume: 5 – Issue No: 4 (December 2023)
Special Issue: Advanced Fractional Mathematics, Fractional Calculus, Algorithms and Artificial Intelligence with Applications in Complex Chaotic Systems (Editors: Yeliz Karaca, Dumitru Baleanu)
https://dergipark.org.tr/en/pub/chaos/issue/81404

Editorial Board Members

ISSN: 2687-4539

Chaos Theory and Applications (CHTA)
Volume: 5 – Issue No: 4 (December 2023)
Special Issue: Advanced Fractional Mathematics, Fractional Calculus, Algorithms and Artificial Intelligence with Applications in Complex Chaotic Systems
Editors: Yeliz Karaca, Dumitru Baleanu
https://dergipark.org.tr/en/pub/chaos/issue/81404

Contents:

Advanced Fractional Mathematics, Fractional Calculus, Algorithms and Artificial Intelligence with Applications in Complex Chaotic Systems (Editorial) 257-266
Yeliz KARACA, Dumitru BALEANU

Unveiling the Complexity of Medical Imaging through Deep Learning Approaches (Review Article) 267-280
Novsheena RASOOL, Javaid IQBAL BHAT

Novel Traveling Wave Solutions of Jaulent-Miodek Equations and Coupled Konno-Oono Systems and Their Dynamics (Research Article) 281-285
Raj KUMAR, Krıpa Shankar PANDEY, Avneesh KUMAR, Anshu KUMAR

Study of Fixed Points and Chaos in Wave Propagation for the Generalized Damped Forced Korteweg-de Vries Equation using Bifurcation Analysis (Research Article) 286-292
Shruti TOMAR, Naresh M. CHADHA

Different Variants of Bernstein Kantorovich Operators and Their Applications in Sciences and Engineering Field (Research Article) 293-299
Parveen BAWA, Neha BHARDWAJ, Sumit Kaur BHATİA

Weighted and Well-Balanced Nonlinear TV-Based Time-Dependent Model for Image Denoising (Research Article) 300-307
Alka CHAUHAN, Santosh KUMAR, Khursheed ALAM

Analysis of the n-Term Klein-Gordon Equations in Cantor Sets (Research Article) 308-317
Nikhil SHARMA, Pranay GOSWAMİ, Sunil JOSHİ

Fractalization of Fractional Integral and Composition of Fractal Splines (Research Article) 318-325
Gowrisankar ARULPRAKASH

CHAOS
Theory and Applications
in Applied Sciences and Engineering

e-ISSN: 2687-4539
EDITORIAL
Vol.5 / No.4 / 2023 / pp.257-266
Special Issue

Advanced Fractional Mathematics, Fractional Calculus, Algorithms and Artificial Intelligence with Applications in Complex Chaotic Systems

Yeliz Karaca *,1 **and Dumitru Baleanu** β,2

*University of Massachusetts (UMass) Chan Medical School, Worcester, MA 01655, USA, βLebanese American University, Beirut 11022801, Lebanon.

ABSTRACT Chaos, comprehended characteristically, is the mathematical property of a dynamical system which is a deterministic mathematical model in which time can be either continuous or discrete as a variable. These respective models are investigated as mathematical objects or can be employed for describing a target system. As a long-term aperiodic and random-like behavior manifested by many nonlinear complex dynamic systems, chaos induces that the system itself is inherently unstable and disordered, which requires the revealing of representative and accessible paths towards affluence of complexity and experimental processes so that novelty, diversity and robustness can be generated. Hence, complexity theory focuses on non-deterministic systems, whereas chaos theory rests on deterministic systems. These entailments demonstrate that chaos and complexity theory provide a synthesis of emerging wholes of individual components rather than the orientation of analyzing systems in isolation. Therefore, mathematical modeling and scientific computing are among the chief tools to solve the challenges and problems related to complex and chaotic systems through innovative ways ascribed to data science with a precisely tailored approach which can examine the data applied. The complexity definitions need to be weighed over different data offering a highly extensive applicability spectrum with more practicality and convenience owing to the fact that the respective processes lie in the concrete mathematical foundations, which all may as well indicate that the methods are required to be examined thoroughly regarding their mathematical foundation along with the related methods to be applied. Furthermore, making use of chaos theory can be considered to be a way to better understand the internal machinations of neural networks, and the amalgamation of chaos theory as well as Artificial Intelligence (AI) can open up stimulating possibilities acting instrumental to tackle diverse challenges, with AI algorithms providing improvements in the predictive capabilities via the introduction of adaptability, enabling chaos theory to respond to even slight changes in the input data, which results in a higher level of predictive accuracy. Therefore, chaos-based algorithms are employed for the optimization of neural network architectures and training processes. Fractional mathematics, with the application of fractional calculus techniques geared towards the problems' solutions, describes the existence characteristics of complex natural, applied sciences, scientific, engineering related and medical systems more accurately to reflect the actual state properties co-evolving entities and patterns of the systems concerning nonlinear dynamic systems and modeling complexity evolution with fractional chaotic and complex systems. Complexity entails holistic understanding of various processes through multi-stage integrative models across spanning scales for expounding complex systems while following actuality across evolutionary path. Moreover, Fractional Calculus (FC), related to the dynamics of complicated real-world problems, ensures emerging processes adopting fractional dynamics rather than the ordinary integer-ordered ones, which means the related differential equations feature non-integer valued derivatives. Given that slight perturbation leads to a significantly divergent future concatenation of events, pinning down the state of different systems precisely can enable one to unveil uncertainty to some extent. Predicting the future evolution of chaotic systems can screen the direction towards distant horizons with extensive applications in order to understand the internal machinations of neural and chaotic complex systems. Even though many problems are solvable and have been solved, they remain to be open constantly under transient circumstances. Thus, fields with a broad range of spectrum range from mathematics, physics, biology, fluid mechanics, medicine, engineering, image analysis, based on differing perspectives in our special issue which presents a compilation of recent research elaborating on the related advances in foundations, theory, methodology and topic-based implementations regarding fractals, fractal methodology, fractal spline, non-differentiable fractal functions, fractional calculus, fractional mathematics, fractional differential equations, differential equations (PDEs, ODEs), chaos, bifurcation, Lie symmetry, stability, sensitivity, deep learning approaches, machine learning, and so forth through advanced fractional mathematics, fractional calculus, data-intensive schemes, algorithms and machine learning applications surrounding complex chaotic systems.

KEYWORDS
Fractional mathematics
Complexity
Fractional calculus
Deep learning
Computational complexity
Fractal methodology
Fractalization
Complex versus chaotic systems and chaos
Bifurcation
Control and optimization
Strange attractors
Approximation theory
Lie symmetry
Complex chaotic systems
Complex systems
Data-intensive computational application processes
Real data interpolation and applications
Differential equations
Machine learning
Deep neural network.

INTRODUCTION, PRELIMINARY REMARKS AND OVERVIEW

Theory of chaos, as having been referred to the qualitative exploration of unstable aperiodic behaviors in deterministically nonlinear dynamical complex systems, bears a plenus of definitions where unstability means the system does not settle into a form of behavior resisting small disturbances, while aperiodic behavior signifies the variables' description of a state of a system that does not go through an iteration of values, which comes to mean that the system in question does not repeat itself at all continuing to manifest the impacts of any slight perturbation. Notwithstanding, these conditions render exact predictions impossible, yielding a series of measurements that are apparent randomly on small disturbances, which is a situation more commonly known as the 'butterfly effect' referring to the fact that even a very minor and remote factor can produce disruptions with a large-scale magnitude; and thus, sensitive dependence on initial conditions marks

Manuscript received: 7 December 2023,
Accepted: 8 December 2023.

[1]yeliz.karaca@ieee.org (**Corresponding author**)
[2]dumitru.baleanu@lau.edu.lb, dumitru.baleanu@gmail.com

the chaotic systems' distinctive features among which being topologically mixing and having dense periodic orbit happen to be the other ones. The indication of time-chaos, on the other hand, referring to sensitivity to initial conditions means that when one has you have two sets of initial conditions or as another option two points in phase space, extremely in proximity with each other, the two ensuing trajectories, are close to each other at the beginning, will show eventual and exponential divergence away from each other. The other principle chaos theory lies on is uncertainty that interdicts accuracy while the third principle belongs to strange attractors showing that complex systems are inclined to settle in one specific situation. When the situation is dynamic, it is known as "strange attractor", whereas it is referred to as attractor when it is static. Given all these, small perturbations bring about chaos in a chaotic system, and chaos theory is involved with the way order irrupts into chaos, whereas complexity theory, suggesting the conception that there is order within chaos, emphasizes self-organization related to chaos into order. With a plethora of diverse independent variables and constituents in nonlinear interaction with one another, complex systems exhibiting a unique characteristic known as emergence, with interactions among subcomponents producing novel properties surpassing individual capabilities can be stated to provide balance in order and chaos (Farsi 2017).

Key Constructs of Complexity Theory, Complex versus Chaotic Systems, and Chaos

Complex systems are said to be more coherent compared to chaotic systems, with uncertainty arising differently in both systems. Complexity theory, providing the implications of analysis and explanation of complex systems, addresses the emergence of order in complex systems at the edge of chaos which signifies a point across the boundary oscillating between randomness and determinism. Thus, complexity theory focuses on non-deterministic systems, whereas chaos theory rests on deterministic systems (Karaca 2022b). Furthermore, uncertainty in chaotic systems results from the inability of knowing the initial condition of the system, whereas uncertainty arises from the notion of emergence in a complex system (Lartey *et al.* 2020). Concerning the uncertainty quantification, which is the quantitative characterization and estimation of uncertainties in both computational and real-world applications, attempts to determine the degree of likelihood regarding certain outcomes if certain aspects of the system are not know in an exact sense. Aleatoric uncertainty refers to a sort of uncertainty that is peculiar to a problem or to an experimental setup in which it is not possible to do reduction to additional experimental knowledge or physical lineage (Barbano *et al.* 2022). As Pierre Simon Laplace put forth, the theory regarding probabilities lies at the bottom of common sense that is reduced to calculus, which enables one to appreciate the exactness an accurate mind can feel based on a kind of instinctive hunch that cannot often be accounted for (Pierre-Simon 1986). Chaos-based applications in science, engineering and other relevant domains require the understanding that some chaotic systems display a unique feature by having two or more coexisting attractors with every attractor being achieved due to the same range of parameters which depend on the initial condition at stake. In these respects, multistable chaotic systems are equipped with the potential applications correspondingly with several parameters of multistable dynamical systems that have sensitivity to initial conditions, noise as week as system parameters. The appearance of hidden attractors, associated with multistability, demonstrates the existence of self-excited attractors in multistable systems with the employment of computational processes. Yet, it is not possible to predict the hidden attractors by typical computational approaches, and thus, the growing level of complexity in physical problems requires more complex and advanced mathematical differential operators. Fractal-fractional operator provides the combination of fractional differentiation with fractal derivative for performing a single differentiation. All these physical processes exhibit attributes characterized by a fractal nature (Khan *et al.* 2023). Both complexity and chaos, being deeply rooted in physics, display the endeavor through an attempt to observe similar systematics across an extensive varying range of phenomena so that a more profound and precise understanding thereof can be achieved. Comprised of a set of mathematical concepts, chaos and complexity theory provides the description of the way systems change over time. Mathematical modeling, oriented towards describing multiple and diverse facets of the real world, reciprocal interactions and dynamics of them from the lenses of mathematics, needs to tackle universal concepts efficiently, promptly and accurately. From this point of view, mathematical models are unique in that they enable the control, mechanization and automation of intellectual activities as well as processes. Mathematical models depending on specialized knowledge are those which with inherent mathematical nature encompass the process of determining the properties of a model with rigor elucidating the different multiple components being identified, revised, designed, organized, formulated and arranged in harmony. Given all these, chaos and complexity theory provide a synthesis of emerging wholes of individual components unlike some of the traditional scientific approaches that analyze systems in isolation.

Both mathematical modeling and scientific computing are considered to be amongst the chief tools for the purpose of solving the challenges and problems related to complex systems by means of innovative ways attributable to data science with a precisely-tailored approach so that sense can be derived from chunks of big data. This kind of tailor-made customized approach can only realize the opportunity of examining data applied, which heavily relies on the capacity of the computer at work as different capacities of computers can have impact on the computational outputs, and thus, the application of the method in question is based on the code by step to be taken into account. Therefore, the complexity definitions needs to be weighed over different data offering a highly extensive applicability spectrum endowed with more practicality, convenience and availability due to the fact that the respective processes lie in the concrete mathematical foundations, which all may as well indicate that the methods are required to be examined thoroughly regarding their mathematical foundation in conjunction the methods to be applied. This is the sole manner which can make foreseeability possible as regards what level of complexity will emerge concerning any data chosen to be employed.

Key Constructs of Nonlinearity, Complex Dynamics Systems, Chaos and Order

Nonlinearity, being a required condition for chaos, with almost all nonlinear systems whose phase space having three or more dimensions, display chaotic features in at least part of the phase space. Exhibiting complex dynamics, complex systems which span across several scales, display order and chaos in a simultaneous way, operating at the critical "edge of chaos", which provides maximization of emergence, spanning from micro-level to macro-level to illustrate the propagation of critical decisions ranging from lower to higher levels, adaptability, creativity and evolvability. While complex systems may have several scales, chaos may reign upon scale n, with the coarser scale above it (scale n-1) which

might be self-organizing, which indicates that it is the opposite of chaos in some sense. When there is the case of the edge of chaos, the precise value of the control manifests a switching dynamics, which happens to be a critical point in phase transitions where the long-range correlations are significant. At this point, adaptability with memory, the capability of modifying the environment to be able to operate appropriately at the edge of chaos, becomes evident and it is this place where self-organization becomes likely to occur. Consequently, the interplay between chaos that producing new possibilities and order coupled with them ensures self-organization and open-ended evolution (Baranger 2000). As a dynamical system dependent on diverse parameters, complex systems manifest themselves in a constant sort of evolution formed by a huge number of unities and distances along trajectories increase or decrease in a polynomial way not exponential way. Furthermore, fractal structures are to be seen in many complex systems (Palis 2002).

Sharing fundamental features with chaos theory, complexity theory encompasses nonlinearity, dynamism, feedback, loops, and so forth. Both being sensitive to initial conditions result in unpredictable outcomes, and self-organization, in this regard, is emphasized with global patterns emerging from local reciprocal interactions. As a compelling challenge, chaotic systems are ones belonging to the unknown unknowns with chaotic motion being almost impossible or very challenging to forecast. Thus, the chaotic behaviors of correlations in chaotic systems prove the hardships concerning prediction of the chaotic systems, while the identified state transitions of correlations can lend a quantitative rule for the selection of appropriate methods. Systems that are deterministic, made up of simple differential equations, are not attributed to reference points to implicit chance mechanisms. Complex systems ofttimes display self-organization which arises when systems spontaneously order themselves optimally or in a more stable way without the external adjustment of any control parameters, which is a feature not found in chaotic systems. This situation is often referred to as anti-chaos in chaotic systems that are inclined to be out of equilibrium, meaning that the system does not settle into a steady state of behavior, which refers to the notion of openness. Most of the real-world systems are open, which poses problems in terms of modeling and experimentation. One other feature related to complex systems is the notion of feedback where the output of a process in the system is exposed to being recycled, as a result of which the output becomes the new input of the system. Feedback occurrences in complex systems are seen to be across the levels of organization, which are micro levels and macro levels. Between the subunits of micro level interactions, some patterns are generated, reacting back again which is a global o local positive feedback known as coevolution which is a concept originating from evolutionary biology for the description of how organisms create their environments and how they are in return molded by the environment they exist in (Rickles *et al.* 2007), (Ruhl 1995). Chaotic systems do not depend on their history unlike the complex systems which rely on their history. Across this line, chaotic behaviors push a system acting in equilibrium into chaotic order out of order. Complex systems, on the other hand, evolve distantly from the equilibrium at the edge of chaos.

Chaos theory posits that even the most seemingly random processes can be described and predicted through the use of a set of complex mathematical equations. Concerning nonlinearity and complex dynamics with chaos, it was noticed by French mathematician Henri Poincaré that nonlinear deterministic systems could behave in an apparently chaotic and unpredictable way. Despite this important contribution, the significance of chaos was accredited with full appreciation after the extensive availability and exponential growth of computational processes through digitalization employed for numerical simulations as well as for the demonstration of chaos in various physical systems. Figure 1 depicts the Poincaré section in z = 0 along with the return maps having three associated elements and the scaled axis system, demonstrating the sensitivity to changes in initial conditions, which is an important characteristic of chaotic systems.

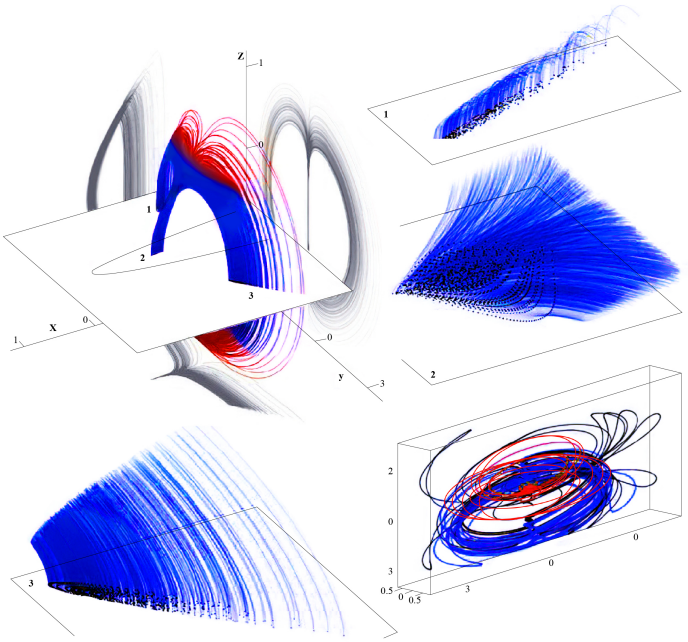

Figure 1 3D perspective segment of a typical chaotic attractor system having a hyperbolic equilibrium.

Given these notions, facts and considerations, the role of mathematical modeling and scientific computation comes to the foreground in processes, including analyses, decision-making, solution of real-world problems, prediction and simulation. These processes entail the definition of which level of detail needs to be introduced in different parts of a mode along with which simplifications are to be conducted to achieve its integration into different models emulating highly complex problems while considering uncertainty as well.

Key Constructs of Bifurcation Theory, Control, Strange Attractors in Complex Chaotic Systems

Bifurcation theory is concerned with the examination of changes in topological or qualitative structure of a given family of curves including the integral curves of vector fields as well as the solutions concerning differential equations. Bifurcation theory is generally applied to the mathematical study of dynamical systems with bifurcation introduced by Henri Poincaré in 1885 occurring both in continuous, characterized by ordinary, delay or partial differential equations, and in discrete systems, described by maps, when a slight smooth change made to the parameter values of a given system brings about an abrupt change in its behavior (Poincaré 1885), (Blanchard *et al.* 2006). Local bifurcations can be analyzed by changes in local stability of equilibrium, periodic orbits and other sets which are invariant as parameters across critical thresh-

olds, whereas global bifurcations often occur as larger invariant system sets collide with one another, which cannot be detected by fixed points. Causing sudden changes in the system's direction, outcomes and characteristics, bifurcation points are those in the system being unstable, leading the system to change structure, character or direction in a dramatic way (Lartey *et al.* 2020). If these unstable points are known, prediction of a bifurcation can be ensured, however, the outcome of the bifurcation or the next state of the system remains unpredictable.

Control theory, in these regards, are concerned with the questions of how the behavior of a system is influenced through the inputs appropriately chosen in order that the output of the system adopts a desired final state or trajectory. Feedback process happens to be the key notion of control theory, with the difference between actual and desired output is implemented as feedback into the input of the system so that the output of the system is completed to converge into the output desired. Correspondingly, bifurcation is used to describe significant qualitative changes occurring in the trajectories of a generally nonlinear dynamical system, considering that the key system parameters are varied. Since a control input and feedback are involved in a nonlinear control system, its nature is very complex as a dynamical system (Chen and Moiola 1994). Even though control input is given and fixed, the controlled system is a non-autonomous dynamical system. Therefore, control input is necessary to be determined to achieve a certain performance considering the combination of the design and dynamics of controllers, which is challenging. All in all, bifurcation equilibrium, oscillation and therefore chaos is found in many systems and new kinds of attractors representing a new sort of behavior entails the understanding that nonrandom chaotic behavior enables the handling of the system. Demonstrating the repetitive abilities, chaotic systems may enable the identification of strange patterns, and although dynamic systems are unpredictable, they still keep the boundaries where they operate their transformations. This creates patterns which are referred to as strange attractors which have different shapes and forms characterizing chaotic systems (Murphy 1996). It is these strange attractors which define the dynamic systems' boundaries since such systems show progress towards chaos owing to their constant growth, and they are identifiable as well as measurable through the use of fractals.

Key Constructs of Fractal Methodology, Real Data Interpolation and Applications in Complex Chaotic Systems

In mathematics, fractal, signifying any of a class of complex geometric shapes with a common attribute of fractional dimension was first introduced as a concept by mathematician Felix Hausdorff in 1918. Distinctive from the simple figures pertaining to Euclidean or classical geometry, fractals are endowed with the capability of describing diverse irregularly shaped objects or spatially nonuniform phenomena in nature from cliffs to seashores, coastlines to mountain ranges. The term *fractal*, as derived from *fractus* meaning fragmented or broken in Latin was coined by Benoit B. Mandelbrot. A fractal system, as a complex, nonlinear interactive system, has the ability of adapting to a changing environment, and it is marked by the self-organization potential existent within a nonequilibrium setting. Fractal theory, on the other hand, has sought to comprehend seeks to complexity in order to ensure an innovative way for the identification of irregularity and complex dynamical systems. The applications that deal with fractal geometry concern various subject matters from turbulence to errors, word frequencies to aggregation and fragmentation-related processes. The growth of the use of fractals in application areas has spawned not only new directions but also new methodological issues. Furthermore, multifractals, arising as a more complex form of fractals, have paved the way of multifractal analysis with the assignment of fractal spectrum to an object, while fractal analysis provides the assignment to a single fractal value. Consequently, multifractal algorithms have been proposed to be employed for practical applications to characterize the signals in medicine, clinical research, biology, and so forth (Karaca 2022a), (Karaca *et al.* 2022).

These developments challenge the prescriptions of reductionism, which assumes that the resultant component behavior and dynamics provide the representation of the entire system behavior by synthesizing approaches and showing that in most complex systems, there is a high level of interconnectivity, dynamic aspects and reasons attributed to nonlinear behaviors (Gowrisankar and Banerjee 2021). While complexity theory explores the way individual components generate simple outcomes by nonlinear and intense interactions, chaos theory explores the possible ways simple systems generate complex outcomes which cannot be described through the components per se (Watt and Willey 2005). Fractals, as very complex, having symmetry of scale and being infinitely detailed geometric shapes show the direction of a procedure that describes the way of constructing and defining a small section in which their small sections resemble the large ones. For a function, one can consider fractal as follows: $f(x)$ to x, $g(x)$, $g(g(x))$, $g(g(g(x)))$, $g(g(g(g(x))))$, $g(g(g(g(g(x)))))$, etc. Given all these aspects, fractals are related to chaos as they both are complex systems with similar properties (Meta 2016). By assessing the fractal characteristics of data, fractal analysis is made up of different methods for assigning a fractal dimension to a dataset, whether it be pattern or signal, which makes it helpful in understanding the functions, structures as well as *spatial and temporal complexity* of various systems, and thus, facilitation is provided quantifying patterns in nature and identifying deviations from such natural sequences.

As the process of using known data values for the estimation of the unknown data values or a missing value, data interpolation is used as a method to predict the future based on the past trends and data, which improves the way to collect data and work on it (Karaca and Cattani 2018). Among some of the elements interpolated are dense evenly space points, extreme changes in terrains, obstacles, and increase or decrease amount of sample points which influence cell values. The values of non-sampled data from a set of discrete sensory data are measured by interpolation which is required in different fields as sensors cannot constantly cover the region under study. Natural systems include complex dynamics which extend across multiple spatiotemporal scales, and efforts to understand and forecast the dynamics of these systems have brought about advances in large-scale simulations along with the dimensionality reduction techniques and a multitude of complementing forecasting methods. High dimensionality and chaotic behavior of the systems reveals a convergence of different approaches as a result of the advances in innovations in algorithms, computing power and ample data accessibility.

Key Constructs of Fractional Mathematics, Fractional Calculus and Data-intensive Computational Application Processes in Complex Chaotic Systems

Fractional mathematics along with the application of fractional calculus techniques oriented towards the solution of problems can describe the existence characteristics of complex natural, scientific and engineering-related as well as medical systems in a more accurate way to reflect the actual state properties, besides the coevolving entities observations and patterns of such systems truly

concerning the nonlinear dynamic systems and modeling complexity evolution in combination with order of fractional chaotic as well as complex systems (Karaca 2022a). Notwithstanding, Fractional calculus (FC), deeply related to the dynamics of complicated real-world problems, allows emerging processes in various fields adopting fractional dynamics rather than the ordinary integer-ordered ones, which means the respective differential equations feature non-integer valued derivatives (Jacob *et al.* 2020), (Karaca 2023).

Fractal patterns, albeit in an array of scales rather than in an infinite manner, having been modeled extensively due to the time and space-related limits concerning practice-wise elements (Karaca and Cattani 2017), (Karaca *et al.* 2020). It is possible that the models might simulate theoretical fractals or natural phenomena with fractal features, and the results derived from modeling processes can be employed as benchmarks for fractal analysis purposes. Fractional calculus, which emerged as a formulation extending ordinary calculus, procures a constructive and algorithmic approach towards the smooth differentiable-structured modeling of natural processes through fractals. Fractal calculus procures a constructive approach towards the smooth differentiable-structured modeling of natural processes through fractals which are perplexing to solve, while differential equations concerning fractals congregate a profound understanding of analysis along with different constructions. The models constructed accordingly can be applied to processes that occur in fractal time and spaces, which propounds the dimensionality aspects as well as the endless patterns at temporal and spatial scales. To put differently, the application of calculus concepts as well as techniques can be beneficial for analyzing and describing the behavior of not fractal objects only but also systems.

With the inherent feature of fractional derivatives in terms of spatiotemporal memory as well as the capability of expressing phenomena occurring in a naturally complex way, machine learning, as a powerful tool, has also come to the foreground in an integrated way owing to its learning behavior and patterns based on historical data lending upper hand in analyzing data, solving problems, modeling, prediction, and so forth by providing new genesis and points of view. The potential of the combination of these approaches facilitates the description process of complex dynamics based on the schemes relying on fractional derivatives and machine learning with novel and innovative corresponding techniques. Furthermore, with its differentiation and integration of non-integer order, FC provides the representation of the generalization of classical differential and integral calculus, providing an amalgam of computational methods concerning various complex systems in tandem with fractional derivatives, fractional differential equations, fractional wavelet, fractional entropy, fractional neural networks, fractional fuzzy, and so on to open the frontiers towards systematic optimized solutions, tackling the systemic properties holistically by seeing through the spontaneous processes (Karaca and Baleanu 2022b), (Karaca and Baleanu 2022a).

Data, being at the center of many compelling challenges in system design, modeling and other related processes, require the need of figuring out reliability, efficiency, consistence, maintainability, scalability. The real-life applications of data-intensive systems and applications make an intensive use of data in all their heterogeneous forms, and computational problems can be solved in this sort of a nested network with concurrent or distributed systems paying attention to operational processes, memory, communication between nodes, machine instructions, among many other processes and elements. Based on the voluminous amounts of data produced by experiments as well as high-throughput technologies disseminated by cyberinfrastructures, data-intensive research comprises a rich variety of scientific methodology that shares the common feature of relying on the accumulation and sharing of evidences across an extensive scale and research contexts, ranging from automated data analysis and automated reasoning to extraction of significant patterns in exact sciences based on data through computational means with human intervention as minimized as possible. With these amenities, applications of data-driven methods have demonstrated that computational methods are empowered with transforming research substantially in terms of how it is performed and the ways by which experiments are set up, conducted and verified. Considering that slight perturbation leads to a significantly divergent future concatenation of events, pinning down the state of different systems in a precise way can to some extent unveil uncertainty. Predicting the future evolution of chaotic systems can show the direction to distant horizons with extensive applications to understand the internal machinations of neural and chaotic complex systems.

Key Constructs of Machine Learning, Algorithmic and Artificial Intelligence-related Application Processes in Complex Chaotic Systems

Chaos theory evolved from a niche mathematical field into a transformative force, demonstrated that quite simple mathematical equations were able to model systems with each bit as violent as a waterfall (Gleick 2008) Rooted in the exploration and investigation of dynamic systems with extreme sensitivity to initial conditions, the world of chaos theory has projected an exponential impact on the realm of Artificial Intelligence (AI) by empowering it in terms of tackling complex problems and providing enhancement in adaptability and learning capabilities related to the AI algorithms. Besides sensitivity to initial conditions, chaos also arises in nonlinear systems with relationships across variables may not be proportional, which is known as nonlinearity that presents intricate and unpredictable behaviors. Another characteristic is the strange attractors as chaotic systems are known to exhibit randomly appearing but deterministic and self-similar complex patterns in a related system's behavior, known as strange attractors. Randomness abruptly becomes an orderly disorder, both in existential terms and in the real-world scenarios where there is a hidden order to chaos. The incorporation of chaos theory and AI provides other improvements in the predictive capabilities of AI algorithms through the introduction of adaptability, which makes chaos theory respond to even slight changes in the input data bringing about a higher level of predictive accuracy. Furthermore, chaos-based algorithms are employed for the optimization of neural network architectures and training processes. That being said, chaos theory also provides facilitation in feature selection, namely the identification of significant attributes in complex and big datasets, leading to more efficient AI models and more streamlined in the meantime. Sensitivity to initial conditions make chaos theory a significant one in the detection of anomalies, which allows the AI systems to identify critical deviations from normal behaviors or those which are unexpected. Besides these, chaos-based data augmentation techniques host controlled perturbations, which improves the generalization capabilities concerning the AI models. Last but not least, reinforcement learning attribute in chaos theory is applied to enhance the AI agents to discover the related environments in a more effective way, which also results in coming up with optimal policies.

Referring to models employed to find patterns within data, a wide variety of advanced machine learning methods, including su-

pervised, unsupervised and reinforcement learning, can be utilized effectively for prediction and classification with a nested hierarchy of features. As for deep learning, it is utilized for solving the same kind of problems as in conventional machine learning means, yet the difference lies in the models' architecture to comprehend the way the decisions are made. Machine learning means are run through the estimation of parameters bringing about the optimal outcome possible, with parameters being existent for each input feature in simple linear cases of models. Deep learning models also exhibit corresponding parallelism, and yet, they integrate more features compared to conventional means oriented towards making predictions. Generating new features from the input features as integral to the training process, deep learning does not use the combination of input features for direct prediction. Machine learning, as the prediction state evolution of chaotic systems, is considered to be an emerging paradigm along with reservoir computing that has a core with dynamical network made up of artificial neurons, which can provide facilitation in predicting unexpected situations like system collapse and chaotic transients linked with crisis situations as well as bifurcation points and asymptotic behaviors (Kong *et al.* 2021). Managing uncertainties and changes in processes can happen on machine learning level with pattern recognition in addition to algorithmic processes which lends applicable processes to solve mathematical problems in a finite set of steps involving recurrence broadly. Artificial Neural Networks (ANNs) and AI systems, in that regard, have their applications with overlapping fields concerning process modeling, adaptive control issues and tool condition monitoring with a focus on learning abilities with the recognition that it is not possible to treat learning separate from other points like signal processing, fusion abilities, critical decision making and self-calibration, among others (Monostori 2003). Thus, different machine learning techniques have significant impacts on building effective models in various application terrains based on the learning capabilities, the particular nature of data as well as the targeted outcome.

The rest of the Editorial for our special issue is organized as follows: Section 2 presents the Work in Progress providing the overview information and inputs of the accepted papers compiled and published. Finally, Section 3 is comprised of Concluding Remarks, Challenges and Future Directions.

WORK IN PROGRESS

Comprising of a set of mathematical concepts, chaos and complexity theory propounds the description of the way particular systems evolve over time, and in this context, chaos-based applications in engineering, science, applied sciences, mathematics, physics, medicine, biology, and other related realms require the reflective, holistic and accurate comprehension, which unveils a rigorous attempt to observe similar systematics spanning across a broad varying range of phenomena. Mathematical modeling and scientific computing also serve these purposes while describing, analyzing and interpreting multiple aspects of the real-world problems blended with the dynamics, complexities and reciprocal interactions in addressing universal concepts effectively. Thus, the integration of mathematical modeling and computational methods empower solution-oriented approaches related to chaotic and complex systems based on innovative ways that can be ascribed to data science from a precisely customized perspective while dealing with large chunks of big data. With reference to the content of accepted papers, the aim of our special issue has been to provide novel directions based on advanced mathematical modeling and computational practicalities in conjunction with chaos-driven model training as well as optimization methods.

Across these strands of thought and aspects, deep learning approaches, deep neural networks, fractional calculus, approximation theory, medical imaging, image denoising, machine learning methods, learning algorithms, complexity, wave propagation, Newtonian mechanics on fractals subset, bifurcation, PDEs, ODEs, wave equations with different models as Nonlinear Coupled Konno-Oono model, Jaulent–Miodek, Korteweg–de Vries (KdV) equation, peak signal-to-noise ratio, Cantor sets, n-Term Klein-Gordon equations, local fractional Laplace equation related to complexity and chaos in electromagnetic fields, fractal methodology, fractal spline, non-differentiable fractal functions and linear fractal function have been addressed, explained and exemplified through the schemes of different areas including physics, mathematics, fluid dynamics, medicine engineering, science, control, optimization geared towards applicable solutions. The theoretical and applied dimensions of nonlinear dynamics and complex systems, merging mathematical analysis, advanced methods and computational technologies have been presented for exhibiting the implications of applicable approaches in real systems and other related domains. Accordingly, the main contributions, novelties and contents of the seven papers accepted for our special issue are provided herein.

Deep learning and machine learning have had a pivotal impact in healthcare systems owing to their capability of handling large complex data with as minimal human intervention as possible, and thus, the applications of deep learning and machine learning are geared towards the achievement of a higher level of service quality besides the quality of health concerning patients, doctors, researchers, practitioners and healthcare professionals. Among the critical tasks deep learning and machine learning have proven to be effective are acute disease detection, disease diagnosis, classification, image analysis, signal analysis, drug discovery and delivery as well as smart health monitoring, among others. Accordingly, The first manuscript in our special issue entitled "Unveiling the Complexity of Medical Imaging through Deep Learning Approaches" presents a comprehensive review of deep learning methodologies which are applied to different healthcare aspects with a focus on various tasks among which disease segmentation, classification and detection are included (Rasool and Iqbal Bhat 2023). The study provides contributions in terms of the intricate nature of medical imaging, revealing the hidden patterns by the application of deep learning-related approaches. Furthermore, the authors of the manuscript provide the discussion of the key features and characteristics of deep learning approaches and significant contributions made by different deep learning techniques in the field of medicine, highlighting the classification approaches and advancements in medical imaging, with a specific emphasis placed on the Convolutional Neural Network (CNN) as a popular method in computer vision tasks. The merits and demerits of various deep learning methods are also depicted through an evaluation in tabular format. The findings indicated through the study reveal the immense potential and benefits belonging to deep learning technology in healthcare, which can empower researchers and practitioners while navigating through the complexities of medical imaging with enhanced diagnostics and interpretation.

Wave propagation is one of the cornerstones in the study of linear and nonlinear Partial Differential Equations (PDEs) where a wave is referred to as a recognizable signal transferred from one part of the medium to another part of it at an identifiable speed of propagation. In this regard, the transfer of energy occurs as the wave propagates, yet, for the matter, it may not be the case. A trav-

elling wave, advancing in a particular direction with the addition of retaining a fixed shape is associated with a constant velocity throughout its related propagation course. It is possible to observe these kinds of waves in various scientific areas such as in combustion occurring after a chemical reaction. In addition, PDEs are one result of the mathematical modeling of dynamical systems, and phenomena such as conservation, reaction and diffusion, to name some can be expressed by means of PDEs which owing to their quintessence are examined profusely in science and engineering. In this regard, Lie symmetry analysis is known to be a robust tool to mathematically analyze PDEs, and it can be employed to secure analytic solutions or to converge PDEs into solvable ordinary differential equations (ODEs). Correspondingly, Nonlinear Coupled Konno-Oono model (NCKOM) represents a current-field string interaction with an external magnetic field, whereas Jaulent–Miodek (JM) equation is a kind of evolution equation possible to be identified in physics, remarkably fluid dynamics, matter physics as well as optics to describe these aspects. The next research paper with the title "Novel Traveling Wave Solutions of Jaulent-Miodek Equations and Coupled Konno-Oono Systems and Their Dynamics" provides the contributions with regard to deriving of some novel variety of solutions for Jaulent-Miodek equations (JMEs) and coupled Konno-Oono equations (CKOEs) (Kumar *et al.* 2023a). (1+1) coupled Jaulent-Miodek system of equations is associated with the energy-dependent Schrödinger potential, while the coupled Konno-Oono system related to complexity and chaos in electromagnetic fields are solved analytically in the research in question. Similarity reductions via Lie-symmetry analysis is carried out for the systems to derive their analytical solutions. The authors supplement the analytical solutions graphically to shed light on the dynamical behavior of the solutions. The research paper, which has dealt with the Lie-symmetry analysis as explored, provides the obtaining of seven analytic solutions for the CKOEs and two analytic solutions for the JMEs. Similarity reductions are conducted by the authors via Lie-symmetry analysis so that it can be possible to derive the related analytical solutions. As another contribution, traveling wave profiles are obtained and solution for CKOEs are shown to different from the one obtained by an earlier research.

As a prototypical example of an exactly solvable nonlinear system, the Korteweg–de Vries (KdV) equation aims at describing shallow water waves which are in nonlinear and weak interactions, concerning long internal waves in a density-stratified fluid, ion acoustic waves in a plasma as well as acoustic waves on a crystal lattice. As a model for many physical phenomena including the propagation of small-amplitude large-wavelength waves in plasma physics and shallow waters, the Korteweg–de Vries (KdV) equation is considered to be an extensively-employed model. On the other hand, bifurcation in dynamical system happens in the case a slight smooth change exerted to the parameter values, namely bifurcation parameters, of a system leads to an abrupt topological or qualitative change in its behavior. Within this regard, the authors of the subsequent work "Study of Fixed Points and Chaos in Wave Propagation for the Generalized Damped Forced KdV (GDFKdV) Equation using Bifurcation Analysis" consider the Generalized Damped Forced KdV (GDFKdV) equation given by $U_t + PU^nU_x + QU_{xxx} + SU = \gamma F(U, x, t, v_i)$ with P, Q and S denoting non-linear, dispersion, damping coefficients, respectively (Chadha and Tomar 2023). The authors also investigate the behavior of the fixed points evaluated for the corresponding dynamical system of their model problem. In addition, the effects of significant parameters involved in the model, which are the free parameters v_1 and v_2, the nonlinear, dispersion and damping coefficients denoted by P, Q and S respectively, are analyzed using the bifurcation tools. Another input to note is the obtaining of the plots for the critical values of the nonlinear and dispersion coefficients for which the system becomes unstable and exhibit chaotic behavior. The chaos in the related dynamical system under various conditions is confirmed with the help of the Lyapunov exponents.

Approximation theory having a significant role in machine learning regarding its tasks like classification or regression plays a key role with its techniques in terms of learning from the data. Via a learning algorithm, many machine learning methods approximate a function or a mapping between the inputs and outputs, and a typical example of models approximating functions in classification tasks is one that belongs to neural networks which are as a whole assumed to be able to approximate a true function mapping the inputs to the class labels. Deep neural networks, on the other hand, own the same order of computational complexity as deep convolutional neural networks. Across these lines, another paper entitled "Different variants of Bernstein Kantorovich operators and their applications in Sciences and Engineering field" aims to highlight the different variants of Bernstein-Kantorovich operators which are used extensively for the approximation of functions in L^p spaces (Bhardwaj and Bawa 2023). The authors put forth the benefit of employing Kantorovich variants over discrete operators that are not suitable for approximating functions which are not continuous. Thus, the operators are generalized into operators of integral type, Kantorovich being one technique which helps to approximate integral functions. The study provides the other inputs addressing the discussion of the important applications of Kantorovich operators that depict the pragmatic and theoretical aspects of approximation theory which concerned with the approximation of complicated quantities by simpler functions.

Having become more significant over the recent times in different fields including but not limited to medical imaging, defect detection, machine vision, image processing provides practical benefits like making the digital image available in any wanted format which improves the images for human interpretation and enables the processing and extracting of information for machine interpretation. Likewise, the process of denoising aims at enhancing the quality of the image through noise reduction while preserving the significant structures and details. Image denoising removes noise from a noisy image so that the true image can be restored, yet, due to factors such as edge, texture, noise, sharp structures and texture pose difficulties in these processes. It is possible that denoised images cause to lose some details, so when an image is being denoised, it is of importance to keep the visual details and components mentioned above. The peak signal-to-noise ratio (PSNR) is the one of the frequently emplpyed objective measure to assess perceptual image quality in tasks related to images and video compression. In the next paper entitled "Weighted and well-balanced non linear TV based time-dependent model for image denoising", the authors address image denoising and deblurring issues which require the adoption of a time-dependent model as a fundamental idea (Kumar *et al.* 2023b). The aim of the research is to enhance the image formation process, and weighted well-balanced flow as a total variation-based time-dependent model is utilized by the authors for the purpose of removing additive noise while preserving the edges successfully. As another contribution, the authors apply the new variation of the flow in the TV-based time-dependent model. The weighted model is said to improve the quality of the restored images and preserve the edges better. The numerical results, which are expressed as a static known as

the peak signal-to-noise ratio (PSNR), demonstrate that the scheme proposed yields better results compared to the previous model.

As a method used to solve for a broad range of problems that have mathematical models yielding equations or systems thereof, the differential transform scheme is effective. The Cantor set, created by repeatedly deleting the open middle thirds of a set of line segment, is a closed set that entirely consists of boundary points, which is a noteworthy counterexample in the fields of set theory and general topology. The local fractional calculus is applied for modeling and processing non-differentiable phenomena in different fractal physical phenomena, with some local fractional models being wave equations on the Cantor sets, local fractional mechanics of elastic materials, Newtonian mechanics on fractals subset of real-line, local fractional Laplace equation, and so forth. The subsequent paper named "Analysis of the n-Term Klein-Gordon Equations in Cantor Sets" aims at demonstrating the effectiveness of the local fractional reduced differential transformation method (LFRDTM) in approximating the solution of the extended n-term local fractional Klein-Gordon equation (Goswami *et al.* 2023). For this aim, the authors use the fractional complex transform and the local fractional derivative, in combination, to analyze the n-term Klein-Gordon equations and in cantor sets. The method proposed by the paper is said to provide a powerful mathematical instrument for solving fractional linear differential equations. As the other contributions, the authors address the existence of the solution followed by some examples. Ultimately, the study provides an effective and accurate method for modeling complex physical systems displaying fractal or self-similar behavior at various length scales. The authors conclude that the fractional complex transform with the local fractional differential transform method proves to be a powerful and flexible approach for obtaining effective approximate solutions of local fractional partial differential equations. By demonstrating the effectiveness of the LFRDTM in approximating the solution of the local fractional Klein-Gordon equation of term n, the authors also expect to encourage its use in an extensive range of applications in fields like physics and engineering.

Providing a general setting and context to understand real-world phenomena, fractal methodology provides the generalization of real-data interpolation by means of fractal techniques. Numerous mathematical models developed and which can generate free-form shapes show two varieties which are known to be deterministic and stochastic. With deterministic qualities, spline models have established themselves to be powerful and convenient to model smooth shapes. On the other hand, fractal models are used to recreate different shapes which are found in nature, and most fractal models are endowed with stochastic components, which render them appropriate to generate irregular, nonsmooth shapes. In this regard, a fractal spline is a function which is made of spline functions having different sclaes maintaining the self-similarity attribute. Consequently, the last study in our special issue "Fractalization of Fractional Integral and Composition of Fractal Splines" is concerned with the perturbation of fractional integral of a continuous function f defined on a real compact interval, namely $(I^v f)$ by means of a family of fractal functions $(I^v f)^\alpha$ reliant upon the scaling parameter α (Apulprakash 2023). The authors of the study propose a fractal operator within the space of continuous functions, an analogue to the existing fractal interpolation operator perturbing f, which results with α-fractal function f^α to elicit the phenomenon. The composition of differentiable fractal function $h^{(k)}$ with a non-differentiable fractal function g yields a non-differentiable fractal function $g(h^{(k)})$, which satisfies the end point conditions that are necessary. Furthermore, the study provides the discussion regarding the composition of α-fractal function with the linear fractal function besides the extension of the composition operation on the fractal interpolation functions to the case of differentiable fractal functions.

CONCLUDING REMARKS, CHALLENGES AND FUTURE DIRECTIONS

Chaos theory is capable of offering an alternative that describes and explains the particular behavior of some nonlinear systems, fundamentally almost in all naturally occurring physical, biological, chemical or social systems or structures. This qualitative exploration of unstable aperiodic behaviors in deterministically nonlinear dynamical complex systems also holds a plethora of definitions in which unstability means the system resists small disturbances and does not settle into a form of behavior whereas aperiodic behavior denotes the variables in a state of a system which does not go through an iteration of values. These particular conditions can make exact predictions not possible; and thus, generates a series of measurements appearing randomly on small disturbances. Butterfly effect, uncertainty and strange attractors are some of the most notable features chaotic systems, whereas more coherence is attributed to complex systems where complexity theory addresses the emergence of order there at the edge of chaos, signifying a boundary point between randomness and determinism. Chaos-based applications in engineering, science and other related trajectories entail the profound and precise comprehension revealing a rigorous attempt to observe similar systematics over an extensive varying range of phenomena. Made up of a set of mathematical concepts, chaos and complexity theory grants the description how particular systems evolve over time. Mathematical modeling geared towards the description of diverse multiple aspects of the real world in addition to the dynamics and reciprocal interactions tackles universal concepts in a prompt, accurate and efficient way. As they are unique in enabling the mechanization, automation and control of intellectual activities and processes, mathematical models are acknowledged to be unique. The integration of mathematical modeling and scientific computing are the principles that empower means to solve challenges pertaining to complex systems through innovative ways attributable to data science with a precisely customized approach plausible sense can be derived from large chunks of big data.

Fractional mathematics encompassing the application of fractional calculus techniques can be used to solve problems that describe the existence characteristics of complex natural, scientific, engineering-related and medical systems accurately. FC is profoundly concerned with the dynamics of real-world problems, which allows emerging processes in diverse trajectories by adopting fractional dynamics rather than the ordinary integer-ordered ones. Fractal patterns, in an array of scales rather than in an infinite manner, have been modeled extensively owing to the time and space-related limits concerning practice-wise elements. It is possible that the models might simulate theoretical fractals or natural phenomena with fractal features, and the outcomes derived from modeling processes can be employed as benchmarks for fractal analysis purposes. As a result, the application of calculus concepts as well as techniques are highly beneficial to describe and analyze both behavior of fractal objects and that of systems. Owing to the inherent feature of fractional derivatives in terms of spatiotemporal memory and the capability of expressing phenomena that occur in a naturally complex way, machine learning is an integrated way through its learning behavior and patterns based on historical data, which provides benefits in analyzing data, solving

problems, modeling, forecasting, prediction, and so forth by providing new genesis and perspectives. The coherent combination of these approaches facilitates the description process of complex dynamics based on the schemes relying on fractional derivatives and machine learning with novel corresponding techniques. Furthermore, with its differentiation and integration of non-integer order, FC provides the representation of the generalization of classical differential and integral calculus, providing an amalgam of computational methods concerning various complex systems in tandem with fractional derivatives, fractional differential equations, fractional wavelet, fractional entropy, fractional neural networks, fractional fuzzy, and so on to open the frontiers towards systematic optimized solutions, tackling the systemic properties holistically by seeing through the spontaneous processes. Data, while causing compelling challenges in system design, modeling and other related processes, also require the need of sorting out efficiency, reliability, consistence, maintainability and scalability. The real-life applications of data-intensive systems and applications make an intensive use of data in all their heterogeneous forms, and computational problems can be solved in this sort of a nested network with concurrent or distributed systems paying attention to operational processes, memory, communication between nodes, machine instructions, among many other processes and elements.

Challenges also become evident considering the asymptomatic, chaotic, complex, dynamic and nonlinear systems. If one has the aim of managing chaos and complex systems, it is important to identify the correct level of the system and consider it within its particular setting adopting vigilance by interpreting and analyzing the system. Therefore, the related challenge and wrongdoing is identifying individual agents as the agents of the system. Another compelling issue is the dependent components regarding the system's complexity as the result is coupled systems in a tight way if multiple components depend on each other, while the other one is managing work in progress with common delays in a certain workflow concerning feedback and making use of the related information. This causes somehow overload leading to problems and challenges due to highly chaotic and complex issues. To solve this challenge, tasks need to be managed constantly on track with no delays if possible. One more challenge worthy of mentioning has to do with predicting changes that are possible to occur. This challenge can be sorted out by managing chaos and complex systems by using advanced technologies and probing the trends as well as establishing forecasting models so that the evolutions of complex systems can be predicted with a relatively strong precision.

Based on these aspects, trends and challenges, the following points can be provided as future directions to unlock new frontiers in research and application terrains: novel and solution-oriented avenues can be explored for the ultimate the medical, clinical impacts of machine learning in imaging and signal processing. In addition to deep learning methods and parallel training implementation techniques, having become dominant in computer vision-related tasks, Convolutional Neural Networks (CNNs), made up of multiple building blocks, can be oriented for automatic and adaptive learning in spatial hierarchies. Another direction is related to large medical datasets and enhancing of the potential in minimizing overfitting and providing generalizability through better pre-trained sets of unis so that deep learning research can be fostered. Moreover, experiments with high dimensional or multimodal data to represent and analyze them through the selection of powerful tools. All these challenges and directions show that further research may be carried out so that it can be figured out how it could be possible to control and manage the chaotic behavior of different systems for the purpose of expanding validity, coherence and reliability concerning future plans, schemes and models. Chaos theory, in this regard, provides an alternative to explain and describe the behavior of nonlinear systems, and the rationale behind the use of chaos theory is to better understand the internal machinations of neural networks. As a matter of fact, being profoundly rooted in physics, complexity and chaos attempt to observe comparable similar systematics over a broad range of phenomena. Taken together, chaos and complexity theory provide a version synthesis comprising emerging wholes of individual components unlike some traditional scientific approaches which handle the analysis of systems in isolation. Unpredictability, being at the pedestal of some challenges, this approach is one way which can render foreseeability possible concerning what level of complexity will emerge related to the data chosen to be employed. As a last resort, what needs to be endowed with is the ability to see deep relationships and how they can fit in a whole coherently, which can be put differently as the simplicity on the other side of complexity.

Acknowledgements

We, as the Editors of our special issue, would like to extend our sincere thanks to Professor Akif Akgül, the Editor-in-Chief, the Editorial Board members and the staff of the *Chaos Theory and Applications* Journal for enabling the publication of our special issue where significant contributions from the authors from diverse fields have been included. We would also like to extend our many sincere thanks to all the referees for their rigorous reviewing processes during the related course of time. Last but not least, much earnest appreciation is conveyed to all the authors who have contributed to our special issue with their papers.

Special Acknowledgements

Yeliz Karaca would like to extend her genuine gratitude to late Professor Abul Hasan Siddiqi (1943-2020), a highly prominent and respectable Indian mathematician and Professor of Applied Mathematics, whose academic positions include being the President of the Indian Society of Industrial and Applied Mathematics (ISIAM) and Editor-in-Chief of a series of Industrial and Applied Mathematics of Springer Nature. Some of the papers accepted in this special issue have been through the International Conference on Applied and Industrial Mathematics (ICAIM) held by the A.H. Siddiqi Centre for Advanced Research in Applied Mathematics & Physics (CARAMP). Dr. Karaca would like to extend her sincere thanks to all the members of CARAMP for their efforts and continual projects which were initiated by the dedicated work of Professor Abul Hasan Siddiqi and his team.

Authors' contributions

The Editorial for the special issue entitled *Advanced Fractional Mathematics, Fractional Calculus, Algorithms and Artificial Intelligence with Applications in Complex Chaotic Systems* has been written by Yeliz Karaca. Having conducted the related editorial duties and assignments, both Editors, Yeliz Karaca and Dumitru Baleanu, have approved the submission of the Editorial work pertaining to the special issue.

Conflicts of interest

The authors declare that there is no conflict of interest regarding the publication of this paper.

Availability of data and material

Not applicable.

LITERATURE CITED

Apulprakash, G., 2023 Fractalization of fractional integral and composition of fractal splines. Chaos Theory and Applications **5**: 318–325.

Baranger, M., 2000 Chaos, complexity, and entropy. New England Complex Systems Institute, Cambridge **17**.

Barbano, R., S. Arridge, B. Jin, and R. Tanno, 2022 Uncertainty quantification in medical image synthesis. In *Biomedical Image Synthesis and Simulation*, pp. 601–641, Elsevier.

Bhardwaj, N. and P. Bawa, 2023 Different variants of bernstein kantorovich operators and their applications in sciences and engineering field. Chaos Theory and Applications **5**: 293–299.

Blanchard, P., R. Devaney, and G. Hall, 2006 Differential equations. London: Thompson. Technical report, ISBN 0-495-01265-3.

Chadha, N. M. and S. Tomar, 2023 Study of fixed points and chaos in wave propagation for the generalized damped forced korteweg-de vries equation using bifurcation analysis. Chaos Theory and Applications **5**: 286–292.

Chen, G. and J. L. Moiola, 1994 An overview of bifurcation, chaos and nonlinear dynamics in control systems. Journal of the Franklin Institute **331**: 819–858.

Farsi, R., 2017 Chaos/complexity theory and postmodern poetry: A case study of Jorie Graham's "fuse". SAGE Open **7**: 2158244017725130.

Gleick, J., 2008 *Chaos: Making a new science*. Penguin.

Goswami, P., N. Sharma, and S. Joshi, 2023 Analysis of the n-term klein-gordon equations in cantor sets. Chaos Theory and Applications **5**: 308–317.

Gowrisankar, A. and S. Banerjee, 2021 Frontiers of fractals for complex systems: recent advances and future challenges. The European Physical Journal Special Topics **230**: 3743–3745.

Jacob, J. S., J. H. Priya, and A. Karthika, 2020 Applications of fractional calculus in science and engineering. J. Crit. Rev **7**: 4385–4394.

Karaca, Y., 2022a Multi-chaos, fractal and multi-fractional AI in different complex systems. In *Multi-Chaos, Fractal and Multi-Fractional Artificial Intelligence of Different Complex Systems*, pp. 21–54, Elsevier.

Karaca, Y., 2022b Theory of complexity, origin and complex systems. In *Multi-Chaos, Fractal and Multi-fractional Artificial Intelligence of Different Complex Systems*, pp. 9–20, Elsevier.

Karaca, Y., 2023 Fractional calculus operators–bloch–torrey partial differential equation–artificial neural networks–computational complexity modeling of the micro–macrostructural brain tissues with diffusion mri signal processing and neuronal multicomponents. Fractals p. 2340204.

Karaca, Y. and D. Baleanu, 2022a Computational fractional-order calculus and classical calculus AI for comparative differentiability prediction analyses of complex-systems-grounded paradigm. In *Multi-Chaos, Fractal and Multi-fractional Artificial Intelligence of Different Complex Systems*, pp. 149–168, Elsevier.

Karaca, Y. and D. Baleanu, 2022b Evolutionary mathematical science, fractional modeling and artificial intelligence of nonlinear dynamics in complex systems.

Karaca, Y., D. Baleanu, and R. Karabudak, 2022 Hidden markov model and multifractal method-based predictive quantization complexity models vis-á-vis the differential prognosis and differentiation of multiple sclerosis' subgroups. Knowledge-Based Systems **246**: 108694.

Karaca, Y. and C. Cattani, 2017 Clustering multiple sclerosis subgroups with multifractal methods and self-organizing map algorithm. Fractals **25**: 1740001.

Karaca, Y. and C. Cattani, 2018 *Computational methods for data analysis*. Walter de Gruyter GmbH & Co KG.

Karaca, Y., M. Moonis, and D. Baleanu, 2020 Fractal and multifractional-based predictive optimization model for stroke subtypes' classification. Chaos, Solitons & Fractals **136**: 109820.

Khan, N., Z. Ahmad, J. Shah, S. Murtaza, M. D. Albalwi, *et al.*, 2023 Dynamics of chaotic system based on circuit design with ulam stability through fractal-fractional derivative with power law kernel. Scientific Reports **13**: 5043.

Kong, L.-W., H. Fan, C. Grebogi, and Y.-C. Lai, 2021 Emergence of transient chaos and intermittency in machine learning. Journal of Physics: Complexity **2**: 035014.

Kumar, A., R. Kumar, K. S. Pandey, and K. Anshu, 2023a Novel traveling wave solutions of jaulent-miodek equations and coupled konno-oono systems and their dynamics. Chaos Theory and Applications **5**: 281–285.

Kumar, S., A. Chauhan, and K. Alam, 2023b Weighted and well-balanced nonlinear tv based time dependent model for image denoising. Chaos Theory and Applications **5**: 300–307.

Lartey, F. M. *et al.*, 2020 Chaos, complexity, and contingency theories: a comparative analysis and application to the 21st century organization. Journal of Business Administration Research **9**: 44–51.

Meta, A., 2016 An overview for chaos fractals and applications .

Monostori, L., 2003 AI and machine learning techniques for managing complexity, changes and uncertainties in manufacturing. Engineering applications of artificial intelligence **16**: 277–291.

Murphy, P., 1996 Chaos theory as a model for managing issues and crises. Public relations review **22**: 95–113.

Palis, J., 2002 Chaotic and complex systems. Current science **82**: 403–406.

Pierre-Simon, L., 1986 Essai philosophique sur les probabilités, 1814. Paris, Christian Bourgois .

Poincaré, H., 1885 Sur l'équilibre d'une masse fluide animée d'un mouvement de rotation. Bulletin astronomique, Observatoire de Paris **2**: 109–118.

Rasool, N. and J. Iqbal Bhat, 2023 Unveiling the complexity of medical imaging through deep learning approaches. Chaos Theory and Applications **5**: 267–280.

Rickles, D., P. Hawe, and A. Shiell, 2007 A simple guide to chaos and complexity. Journal of Epidemiology & Community Health **61**: 933–937.

Ruhl, J. B., 1995 Complexity theory as a paradigm for the dynamical law-and-society system: A wake-up call for legal reductionism and the modern administrative state. Duke LJ **45**: 849.

Watt, D. and K. Willey, 2005 The complex, chaotic, and fractal nature of complex systems. In *2005 IEEE International Conference on Systems, Man and Cybernetics*, volume 4, pp. 3155–3160, IEEE.

How to cite this article: Karaca, Y., and Baleanu, D. Advanced Fractional Mathematics, Fractional Calculus, Algorithms and Artificial Intelligence with Applications in Complex Chaotic Systems. *Chaos Theory and Applications*, 5(4), 257-266, 2023.

CHAOS
Theory and Applications
in Applied Sciences and Engineering

e-ISSN: 2687-4539
REVIEW ARTICLE
Vol.5 / No.4 / 2023 / pp.267-280
Special Issue
https://doi.org/10.51537/chaos.1326790

Unveiling the Complexity of Medical Imaging through Deep Learning Approaches

Novsheena Rasool *,[1] **and Javaid Iqbal Bhat** *,[2]
*Department of Computer Science, Islamic University of Science & Technology, Kashmir, J & K, 192122, India.

ABSTRACT Recent advancements in deep learning, particularly convolutional networks, have rapidly become the preferred methodology for analyzing medical images, facilitating tasks like disease segmentation, classification, and pattern quantification. Central to these advancements is the capacity to leverage hierarchical feature representations acquired solely from data. This comprehensive review meticulously examines a variety of deep learning techniques applied across diverse healthcare domains, delving into the intricate realm of medical imaging to unveil concealed patterns through strategic deep learning methodologies. Encompassing a range of diseases, including Alzheimer's, breast cancer, brain tumors, glaucoma, heart murmurs, retinal microaneurysms, colorectal liver metastases, and more, the analysis emphasizes contributions succinctly summarized in a tabular form.The table provides an overview of various deep learning approaches applied to different diseases, incorporating methodologies, datasets, and outcomes for each condition.Notably, performance metrics such as accuracy, specificity, sensitivity, and other crucial measures underscore the achieved results. Specifically, an in-depth discussion is conducted on the Convolutional Neural Network (CNN) owing to its widespread adoption as a paramount tool in computer vision tasks. Moreover, an exhaustive exploration encompasses deep learning classification approaches, procedural aspects of medical image processing, as well as a thorough examination of key features and characteristics. At the end, we delve into a range of research challenges and put forth potential avenues for future improvements in the field.

KEYWORDS
Deep learning
Complexity
CNN
Medical image analysis
Pattern recognition
Segmentation

INTRODUCTION

Deep learning (DL) stands as an advanced form of machine learning (ML), centred on the utilization of artificial neural networks (ANNs) for the analysis and prediction of data.The inception of deep learning dates back to 1943, when Warren McCulloch and Walter Pitts formulated a computational framework inspired by the neural networks within the human brain (Wang and Raj 2017). These DL models draw inspiration from the intricate communication observed among biological neurons within the brain, serving as a structural framework to understand information. Furthermore, similar to their biological counterparts, DL models comprise multiple layers of artificial neurons,including an initial input layer, a conclusive output layer, and a varying number of intermediate processing layers positioned between them.These intermediary layers, collectively referred to as hidden layers,play a pivotal role in extracting crucial features from the input images and recognizing intricate patterns.In each layer, artificial neurons activate upon receiving impulses from neighboring neurons in subsequent layers,leveraging multiple processing levels within the deep architecture (LeCun *et al.* 2015).In essence, each layer within a deep architecture holds a specific algorithm that employs a designated activation function.The amalgamation of these algorithms constructs complex and generalized machines, endowed with remarkable capabilities to address a diverse range of medical image-related challenges (Saba *et al.* 2020).

Over the past few decades,DL has risen to prominence as an incredibly powerful technology.This is primarily due to its remarkable ability to handle and make sense of enormous amounts of data (Islam and Zhang 2018).These algorithms have demonstrated superior capabilities in learning and categorizing

Manuscript received: 13 July 2023,
Revised: 22 August 2023,
Accepted: 27 August 2023.

[1]novsheena.rasool@iust.ac.in (**Corresponding author**).
[2]javaid.iqbal@iust.ac.in

across various domains.For instance, they excel in transfer learning, where insights gained from one task are applied to solve another (Tan *et al.* 2018). They've also been instrumental in speech recognition,enabling computers to understand and interpret human speech effectively Chen and Mak (2015).In the domain of recognizing handwritten digits, these models play a pivotal role in identifying characters and symbols accurately (Alwzwazy *et al.* 2016).Furthermore, DL has made significant strides in disease detection, contributing to the early and precise identification of various medical conditions Pereira *et al.* (2016). It has also been instrumental in disease segmentation, allowing for the precise delineation of affected areas within medical images (Trajanovski *et al.* 2020). The field of computational medicine (see Figure 1) has also benefited greatly from DL's capabilities (Islam and Zhang 2018). Consequently,deep learning has become a revolutionary technology that has the ability to completely revolutionise a wide range of industries. Its exceptional ability to process information and undertake intricate tasks with unparalleled proficiency marks it as a technology with immense possibilities for reshaping diverse industries.

In the field of diagnosing medical conditions using historical radiological screening methods,the process is time-intensive, subjecting patients to prolonged waiting times spanning from hours to weeks for test outcomes.Moreover,discrepancies in outcomes among labs may arise due to reliance on individual proficiencies. To address these issues, the medical field has turned to the application of deep learning algorithms. These algorithms have been leveraged to diagnose diverse conditions, including cancer(Albarqouni *et al.* 2016), tongue tumor(Trajanovski *et al.* 2020), Alzheimer's disease(Islam and Zhang 2018), glaucoma(Yang *et al.* 2021),brain tumor(Pereira *et al.* 2016; Muhammad *et al.* 2020; Dong *et al.* 2017; Abiwinanda *et al.* 2019; Rasool and Bhat 2023), and other life-threatening diseases with increased accuracy and speed. These models highlight irregularities in medical imagery, which primarily include X-rays, MRI scans, CT scans, and similar types of medical images (Arif *et al.* 2022; Meena and Roy 2022; Albarqouni *et al.* 2016). Furthermore, these sophisticated algorithms have proven to be immensely valuable in expediting the assessment of medical images and mitigating the time-consuming nature of conventional scans. They excel in precision, as they adeptly extract intricate features from medical images (Pereira *et al.* 2016). This capability enables them to undertake a variety of tasks, including medical image classification (see Figure 6), object detection, pattern recognition, and various other tasks within computer vision. Table 1 highlights the key features, merits and demerits of different deep learning architectures. Meanwhile, in Table 2, the proficient effectiveness of deep learning across various healthcare tasks is highlighted.

This paper examines a broad range of diseases and presents a comprehensive analysis of the methodologies employed,using deep learning in the field of healthcare. The primary focus of this analysis centers on the tasks of disease detection, segmentation, and classification.Encompassing a wide spectrum of health-related ailments, this comprehensive review delves deeply into the substantial advancements achieved, with special attention given to convolutional neural networks (CNNs) in the context of medical imaging. The findings of this research underscore the transformative potential of deep learning within the healthcare sector. One of the most notable impacts is observed in the enhancement of diagnostic capabilities and the interpretation of medical data. The paper effectively demonstrates how deep learning techniques have the capacity to revolutionize healthcare practices, particularly by improving the accuracy and efficacy of disease detection and diagnosis processes.

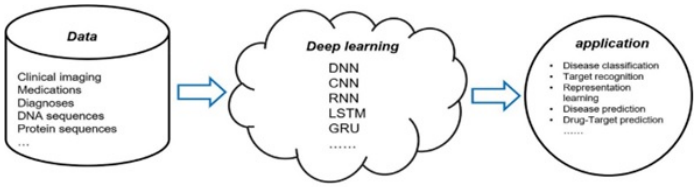

Figure 1 Deep learning applications in computational medicine (Yang *et al.* 2021)

CONVOLUTIONAL NEURAL NETWORK

Deep architectural models encompass various neural networks, with one prominent example being the feed-forward artificial neural network known as the Convolutional Neural Network(CNN).The CNN comprises an input layer, an output layer, and numerous hidden layers, making it a highly acclaimed and potent algorithm within the domain of computer vision.Among the diverse range of deep learning algorithms, the CNN stands out. In the subsequent discussion,the functions and significance of each layer within the CNN framework will be thoroughly elucidated.

Convolution Layer

The Convolutional Neural Network (CNN) serves as the central neural network architecture in the field of Deep Learning,specifically designed for computer vision tasks. This network stands out for its exclusive use of convolutional layers, each comprised of multiple filters with arbitrary weights. These layers extract information and discern patterns from input data via convolutional operations.The core principle of convolutional operations involves the meticulous computation of dot products between the filters and discrete regions of input images,which are referred to as "receptive fields". The filters systematically traverse the input images,scanning from the rightmost edge to the left and descending from the topmost to the bottom. This meticulously orchestrated process yields intricate feature maps while simultaneously reducing the complexity of the network through a process of weight diminishment. This weight reduction proves particularly advantageous during training, as it aids in effectively training the network even when working with limited datasets. For better understanding, the visual depiction of the convolution operation is shown in Figure 2.

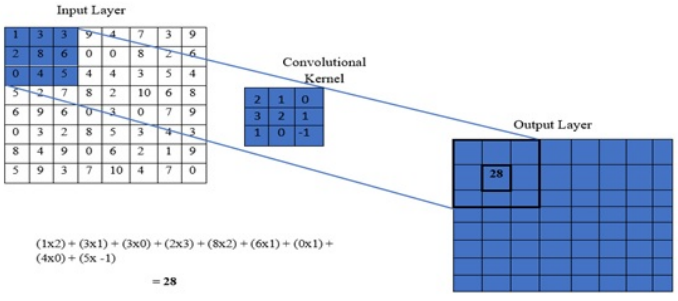

Figure 2 Convolution Operation

Weight Sharing

Within convolutional neural networks (CNNs), weights are not allocated to individual pairs of neurons in adjacent layers.Instead, each weight operates across the entirety of the input array, spanning every pixel. This obviates the need for procuring supplementary weights for every neuron, resulting in a substantial reduction in both training time and associated expenses. The acquisition of a singular set of weights for all inputs streamlines the training process, yielding significant efficiency gains.

Sparse Connectivity

The sparse connectivity nature of CNNs leads to each neuron having a restricted number of connections to other neurons.As a result, the abundance of weights and connections required in a fully-connected layer characterized by dense connectivity (as depicted in Figure 4) is noticeably reduced as illustrated in Figure 3. Storing these weights in memory does not consume a substantial amount of space due to this configuration.This specific characteristic makes the approach highly memory efficient.

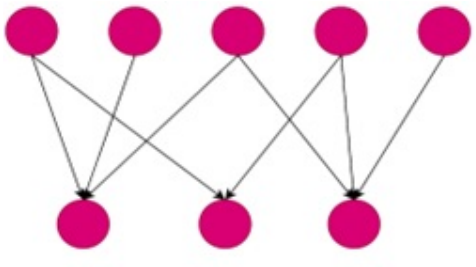

Figure 3 Sparse Connectivity

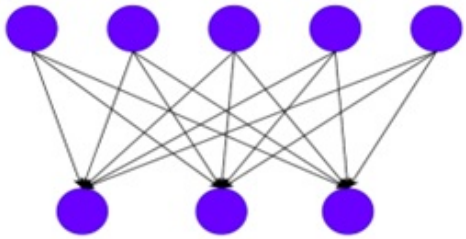

Figure 4 Dense Connectivity

Pooling Operation

Pooling layers receive convoluted feature maps as input,typically positioned between convolutional layers within a neural network architecture. This pivotal layer functions by combining neuron clusters from the preceding layer with those of the subsequent layer. This process enables the selective extraction of crucial information from input images, while concurrently discarding extraneous or irrelevant features. A range of pooling techniques exists, encompassing global average pooling (GAP), global maximum pooling, minimum pooling, maximum pooling, and average pooling (Alzubaidi *et al.* 2021). Among these varied techniques, the preeminent and widely adopted techniques include maximum pooling, minimum pooling, and Global Average pooling. The illustration of these techniques is visually depicted in Figure 5.

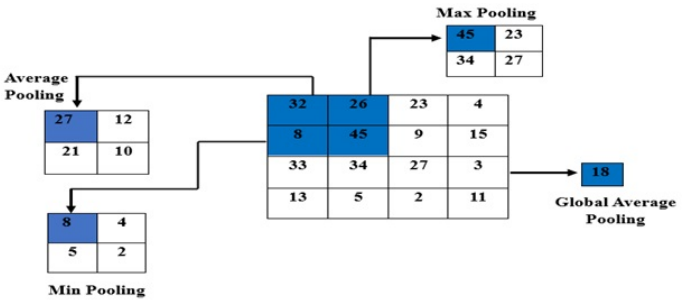

Figure 5 Visual Depiction of Pooling Operations

Fully Connected Layer

After subjecting the input images to a sequence of convolutional and pooling layers, the features extracted as a result then undergo a flattening process.Following this,these features are introduced into the fully connected layer (FCL), which generates probabilities corresponding to each label and thus predicts the final output. The subsequent step involves the utilization of a loss function to compare the outcomes produced by the fully connected layer with the original data (Liu *et al.* 2023). The objective here is to reduce this loss function, thereby enhancing the efficiency of the network. In cases where the actual outcome deviates from the anticipated result, the loss function comes into play, adjusting the elements within the matrix to diminish errors. This iterative process persists until the model's performance reaches a plateau.As the loss function's value decreases, the overall performance of the model improves,and conversely, an increase in the loss value corresponds to a decrease in performance.However, given the substantial number of parameters intrinsic to the fully connected layer, a potential issue of overfitting arises. To counteract this concern, a strategy known as the dropout approach (Albarqouni *et al.* 2016) is usually employed.This approach involves randomly deactivating specific neurons during the training process, effectively preventing intricate co-adaptations of data that could potentially lead to overfitting and thus maintaining the generalization ability of the model.

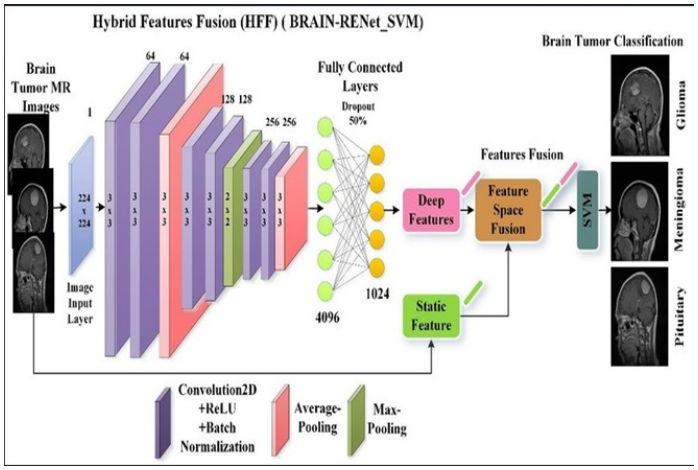

Figure 6 BRAIN-RENet deep CNN for Brain Tumor (Zahoor *et al.* 2022)

CLASSIFICATION OF DEEP LEARNING APPROACHES

The three categories of deep learning techniques are supervised,unsupervised, and semi-supervised.

Supervised Learning

Supervised learning stands as a robust methodology that relies on labeled data to establish a relationship between a set of input variables (denoted as 'x') and their corresponding output variables (denoted as 'y'). This method harnesses the power of this established relationship to predict outcomes for entirely new and unseen data instances. Throughout the process of learning,models are trained to produce the intended outcomes by utilizing a dependable training dataset composed of both input instances and their corresponding outputs (Gulshan *et al.* 2016; Rajpurkar *et al.* 2018). This contributes to the algorithm's long-term development.

To ascertain the efficacy of these trained models, a crutial tool comes into play –the loss function.This function quantifies the disparity between the model's predictions and the actual outputs, providing a metric for the model's performance. The algorithm then undertakes a dynamic self-improvement process, iteratively adjusting its internal parameters until the discrepancy between predictions and actual outcomes is effectively minimized.This iterative refinement process captures the essence of supervised learning, results in models that possess the capability to generate predictions of remarkably high accuracy.

When working with image data, deep learning employs supervised learning techniques such as convolutional neural networks (CNNs)(Pereira *et al.* 2016; Vorontsov *et al.* 2019), artificial neural networks(ANNs), recurrent neural networks (RNNs) (Lipton *et al.* 2015), and deep neural networks (DNNs)(Chen and Mak 2015). In healthcare, supervised learning empowers predictions and diagnoses. Notably in medical imaging, like X-rays, CNNs excel, recognizing patterns and improving diagnostics. This synergy advances healthcare, enhancing precision, prognostics, and patient outcomes.One advantage of deep supervised learning is its ability to produce outputs based on prior knowledge and expertise.However, a drawback of this approach is its heavy reliance on properly labeled data. If the data is not appropriately labeled, the algorithms may fail to generate accurate results. Additionally, training the algorithms with irrelevant input features can lead to inaccurate outcomes.

Unsupervised Learning

This method standardizes the learning procedure by removing the necessity for labels, making it applicable even when labeled data is absent. In this context, the algorithm uncovers essential features necessary for detecting patterns within the input data that were previously unnoticed (Miotto *et al.* 2016). Various sophisticated deep learning techniques, including autoencoders, restricted Boltzmann machines,and Generative Adversarial Networks(GANs),have demonstrated impressive performance in tasks involving nonlinear dimensionality reduction and classification(Esteban *et al.* 2017; Du *et al.* 2017). Furthermore,the utilization of recurrent neural networks in unsupervised learning across diverse applications, incorporating methods like Gated Linear Units and extended shortterm memory networks, has yielded promising results. In the field of healthcare,this strategy holds great potential due to the complexities associated with processing vast medical data.Unsupervised learning, circumventing the need for manual labeling, extracts patterns directly from the data.This aids in diagnosis, trend recognition,and adaptation to evolving medical knowledge, ultimately enhancing patient care. One of the primary advantages of unsupervised learning lies in its ability to efficiently reduce data dimensions without heavy reliance on manual labeling—an often time-consuming and expertise demanding task. Instead, unsupervised learning gleans insights directly from the data and categorizes it without explicit labels.This learning approach progressively improves its results as it computes outcomes, sharing certain resemblances with elements of human intelligence.

Semi-Supervised Learning

Semi-supervised learning occupies a significant position that bridges the gap between supervised and unsupervised learning methodologies. It presents a valuable technique for analyzing datasets that are partially labeled, yet predominantly unlabeled, which finds relevance in the medical domain as well (Liu *et al.* 2020). In the domain of deep learning, the utilization of techniques such as Generative Adversarial Networks (GANs) and Recurrent Neural Networks has proven effective for semi-supervised learning in the medical field as well(Saba *et al.* 2020).Especially within the context of medical applications like DNA segment analysis, where human involvement remains crucial due to the complexity of longer sequences, the development and deployment of semi-supervised approaches have garnered notable attention. A key advantage of this approach lies in its capacity to enhance algorithmic efficiency and generalizability, a boon particularly valuable when working with a limited number of labeled examples alongside a substantial volume of unlabeled data.However, it's worth noting that a potential limitation of this method is the risk of making erroneous decisions if insignificant input features find their way into the training data.

MEDICAL IMAGE PROCESSING STEPS

Pre-Processing

The preprocessing of medical images constitutes a foundational step that plays a crucial role in improving the quality and reliability of diagnostic and analytical procedures.This initial stage involves a series of essential steps aimed at optimizing raw medical image data for subsequent analysis. The process begins with image acquisition, where modalities such as X-rays, MRIs, CT scans, and ultrasounds capture anatomical or physiological information. However, these images often contain noise, artifacts, and inconsistencies.Various preprocessing techniques including noise reduction, image intensity normalization, and artifact removal, are implemented to address challenges related to image quality and variability (Abiwinanda *et al.* 2019). Specifically, intensity normalization is applied to standardize pixel values across images, ensuring uniform measurements and facilitating more reliable analysis in the medical domain.Subsequently, image registration, which is an another preprocessing step, aligns multiple images from different modalities or time points,facilitating accurate comparisons and overlays. This systematic process enhances image quality, ultimately contributing to improved diagnostic accuracy. Consequently, it aids healthcare professionals, researchers, and computer algorithms in conducting more effective analyses.

Segmentation

Image segmentation serves as a pivotal technique used to divide images into distinct regions based on similar characteristics, including grey level, texture, color, luminosity, and contrast Sharma and Aggarwal (2010). In healthcare sector,specifically in medical image segmentation, the goals encompass the analysis of the skeletal system, identification of the region of interest,

assessment of tumor growth, and measurement of tissue volume, among other objectives.The field of artificial intelligence (AI) has produced methodologies for automated segmentation, broadly categorized into three primary approaches: supervised, unsupervised, and semi-supervised methodologies.

Classification

For image classification,particularly in the medical domain, CNN-based deep neural networks are commonly utilized. CNNs prove to be effective in extracting features, facilitating the efficient categorization of medical images without the need for intricate and costly feature engineering.In the context of classifying patches depicting lung ailments, a tailored CNN with a shallow ConvLayer was introduced by (Li *et al.* 2014). This approach has demonstrated effectiveness. Additionally, separate studies emphasize the notable improvements in accuracy and sensitivity achieved by employing a CNN-based algorithm on extensive chest X-ray film datasets (Sharma and Aggarwal 2010).

Post-processing

The primary aim of postprocessing in medical imaging is to standardize and enhance the visual representation of images, thereby enabling more accurate diagnostic analysis. Post-processing techniques serve a multitude of purposes, encompassing image enhancement, restoration, analysis, and compression. One such method, Connected-Component Labeling, frequently employed in computer vision, aids in the analysis and segmentation of images by considering pixel interactions. This approach enables the identification of interconnected regions within the image, effectively grouping similar pixels together (Mimboro *et al.* 2021). Consequently, pixels belonging to the same component are linked and display comparable intensity values. This process proves instrumental in eliminating unwanted pixels or noise that may be present in the image due to various factors, including the imaging process itself.

MEDICAL IMAGERY WITH STATE-OF-THE-ART DEEP LEARNING

Medical imagery has undergone a profound transformation through the integration of state-of-the-art deep learning techniques. This convergence has brought about a revolution in diagnostic accuracy and treatment planning by enabling the automated detection of subtle patterns and anomalies within medical images. Utilizing advanced neural networks such as convolutional neural networks (CNNs) and their variants like U-Net, ResNet, and other novel architectures, these technologies excel in identifying intricate details in X-rays, MRIs, CT scans, and more.This fusion of medical expertise and deep learning capabilities stands as a cornerstone in modern healthcare, providing clinicians with powerful tools to make faster and more informed decisions, ultimately leading to improved patient care.

(Ahuja *et al.* 2022) introduced Darknet models for brain tumor classification.The method automates identification,localization, and segmentation of tumor from the TIW-CE MRI dataset. To address overfitting, the training dataset was augmented through geometrical methods and 2-level wavelet decomposition. Darknet models pretrained for brain tumor classification were adopted, along with a 2D superpixel segmentation approach for segmentation. Impressive results were achieved, with training accuracy reaching 0.99 and validation accuracy at 0.98.Notably, the proposed approach demonstrated superior performance compared to state-of-the-art techniques when evaluated on the T1W-CE MRI dataset.

(Sreng *et al.* 2020) introduced an automated two-phase system for glaucoma screening using deep learning.In the initial phase, the authors employed the DeepLabv3+ architecture to accurately segment the optic disc region.Subsequently,they leveraged pretrained deep convolutional neural networks for precise glaucoma classification.The authors meticulously assessed their methodologies using five distinct datasets,encompassing a total of 2787 retinal images.The results of their study showcased that the most effective approach for optic disc segmentation entailed a fusion of the DeepLabv3+ and MobileNet architectures. In terms of glaucoma classification, the combination of techniques outperformed conventional methods across various datasets,including Rim-one, Origa, Drishti-gs1, and Acrima.Impressively, the achieved Area Under Curve (AUC) scores were as follows: 100 percent for rim-one, 0.99 for acrima, 0.91 for drishti-gs1, and 0.92 for origa.The system's performance closely paralleled that of Cuhkmed, the leading team in the refuge challenge, on the refuge dataset. Specifically,they achieved an accuracy of 0.95 percent.

(Zhu *et al.* 2021) introduced a dual-attention multi-instance deep neural network designed for the early detection of Alzheimer's disease and its preliminary stages. This network comprises three key components. Firstly, they employ spatially focused patch-nets with attention to enhance the features of aberrantly altered micro-structures within the cerebral cortex. This enhancement enables the extraction of distinct characteristics within each sMRI patch. To ensure equitable input from all patches and to generate a comprehensive weighted representation of the entire brain structure,they adopt an attention based multi-instance learning pooling technique. Lastly,the authors employ a global classifier endowed with attentional awareness.This classifier is tasked with learning additional pivotal features and categorizing data related to Alzheimer's disease. The proposed model's efficacy is evaluated using initial sMRI images obtained from 1689 individuals in two distinct datasets. The experimental outcomes underscore the superiority of their approach compared to other state-of-the-art techniques. Their method excels in accurately identifying specific affected areas and achieving improved classification performance. This is characterized by better generalizability and overall accuracy.

(Saba *et al.* 2020) proposed a new approach for identifying tumors utilized the grab-cut method to accurately distinguish the symptoms of real lesions. Deep learning and manually created features were retrieved from the segmented images and subsequently optimized using entropy. A serial fusion approach was employed to combine the optimized features into a unified feature vector, enabling the identification of gliomas or normal images.To assess the efficiency of the suggested approach, specific benchmark datasets from 2015 to 2017 were employed. Ultimately, various classifiers were applied to ascertain whether the images were indicative of normalcy or disease. Notably, the proposed method yielded the most favorable testing outcomes on the BRATS 2015 dataset, achieving a Dice Similarity Coefficient(DSC) of 0.9636 and an accuracy of 0.9878.

(Feng *et al.* 2019) introduced an innovative deep learning architecture, aimed at detecting Alzheimer's disease. The proposed methodology amalgamated a fully layered bidirectional long short-term memory (FSBi-LSTM) with a three-dimensional Convolutional Neural Network(3D CNN). Initially, the researchers

extracted prominent characteristics from MRI and PET scan images.To augment the model's performance, they employed the FSBi-LSTM technique to process latent information extracted from the deeper feature maps. To substantiate their approach, they conducted experiments employing data from the Alzheimer's Disease Brain Imaging Initiative dataset. The findings exhibited mean accuracies of 0.86, 0.94, and 0.65 for discerning progressive mild cognitive impairment from normal control, distinguishing Alzheimer's disease from normal control, and identifying stable mild cognitive impairment from normal control, respectively.

(Albarqouni *et al.* 2016) introduced AggNet,a sophisticated deep learning system aimed at the identification of mitosis in histology images related to breast cancer. Leveraging advanced deep learning techniques, the researchers devised a strategy for achieving precise labeling by harnessing the power of crowd-sourced mass annotation within the domain of biomedicine.Their innovative approach encompassed the integration of deep learning principles into the very fabric of data collection, constituting an integral facet of the learning process. This unique methodology incorporated an additional layer of crowdsourcing, further enhancing the efficacy of their multiscale Convolutional Neural Network (CNN). To facilitate comprehensive training and robust evaluation, the researchers harnessed the complete AMIDA13 dataset. The outcomes of their investigation yielded invaluable insights into the potency of deep CNN learning when coupled with mass annotations.The study's findings underscored the pivotal role played by data aggregation in the amalgamation process, emphasizing its profound significance in the realm of deep learning for biomedical image analysis.

(Liu *et al.* 2018) suggested a novel deep learning approach for analyzing breast cancer tissue microarrays.Their method aims to predict the H-Score autonomously. To achieve this objective, they leveraged the H-Score dataset for experimentation, drawing inspiration from the H-Score asassessment routinely performed by medical professionals.In the H-Score assessment procedure, various factors such as the total cell count,the quantity of tumor-associated cells, and the categorization of cells based on the intensity of positive marks are evaluated. The authors employed a single fully convolutional network (FCN) to extract nucleus areas from both tumor and healthy tissues. Additionally, they utilized an extra FCN to specifically isolate the nuclei area pertaining to the tumor cells.To further enhance their approach, the authors designed a multi-column convolutional neural network(CNN). This CNN utilizes the outputs from the initial FCNs, as well as the image containing details about stain intensities,as its input. The CNN functions as an advanced decision-making system,directly generating the H-Score for the original tissue microarray image source.

(Lian *et al.* 2018) presented a hierarchical fully convolutional network (H-FCN) aimed at automating the identification of specific local patches and regions within brain structural MRI (sMRI) scans.The primary objective was the identification of Alzheimer's disease. The H-FCN model effectively facilitated the acquisition and fusion of multi-scale feature representations, enabling the construction of hierarchical classification frameworks. To gauge the efficacy of their proposed methodology, comprehensive testing was conducted on a diverse cohort sourced from two distinct datasets: ADNI-1 and ADNI-2. The results underscored the effectiveness of the H-FCN approach,showcasing its proficiency in pinpointing localized degenerative patterns and diagnosing cerebral disorders.

(Wu *et al.* 2019) introduced a novel approach that utilizes deep convolutional neural networks for breast cancer scans classification. The authors employed a patch-level framework with a large capacity, enabling the network to learn from pixel-level labels effectively. Additionally, they incorporated a two-stage design and training process that allowed the network to learn from large breast-level labels, specifically optimized for high-resolution healthcare images in terms of breadth and width. To pretrain the network, they utilized BI-RADS classification screening, a similar task with labels that are more susceptible to noise. Among various options,the authors combined multiple input viewpoints optimally. The training and evaluation of the proposed model involved over 200,000 tests. For model validation, a reader study was conducted, involving fourteen readers who examined 720 diagnostic mammograms. The results demonstrated that, when provided with the same information,the model's reliability was comparable to that of expert radiologists. However, the authors acknowledged the need for additional clinical validation due to the relatively limited test set used in their experiments, despite the encouraging findings.The proposed network achieved successful prediction of breast cancer presence, with an AUC (Area Under the Curve) value of 0.895.

(Liu *et al.* 2021) introduced a novel three-dimensional technique known as the Context-Aware Network (CANet) for segmenting gliomas. Their approach involved a combination of deep supervised learning and graph convolution contexts within a hybrid feature extractor.To enhance the segmentation process by capturing pertinent features, the authors employed simple feature fusion methods, such as element-wise summation, synergizing with conditional random fields. Furthermore,the authors integrated a context-guided attention-CRF's mean-field estimate as a convolutional procedure into the segmentation network, enabling holistic end-to-end training. The effectiveness of their method was assessed using the BRATS 2017-2019 datasets, showcasing CANet's supremacy in various evaluation measures. In their future work, the authors intend to merge the proposed network with new training strategies to further enhance its efficacy.

(Sarraf and Tofighi 2016) introduced a Convolutional Neural Network(CNN) as a technique to differentiate between brain scans of people with Alzheimer's disease and those of healthy individuals. They employed CNN and LeNet-5 models to effectively differentiate functional MRI scans of Alzheimer's patients from those of normal individuals. The study utilized the ADNI dataset for both training and testing, achieving an impressive accuracy of 0.96.This research suggests that the most effective approach for distinguishing patient information from healthy data obtained from fMRI scans involves harnessing the shift and scale invariant characteristics provided by CNNs, in conjunction with deep learning classification.

(Zeineldin *et al.* 2020) introduced the DeepSeg framework, which serves as a completely automated approach designed for the detection and delineation of brain tumors using FLAIR MRI data.The DeepSeg architecture proposed by the authors is modular, emphasizing the connection between encoding and decoding through two interconnected core components.Spatial data retrieval is achieved through the utilization of convolutional neural networks (CNNs) in the encoder part. The decoder component takes the generated semantic map, aggregates it, and produces the full-resolution likelihood map.The authors utilize different CNN architectures, including dense convolutional networks, residual neural networks, and NAS-Net.These architectures are based upon a modified U-Net design. The proposed architectures are

Table 1 Key Features and Characteristics of Deep Learning Models

Model Architecture	Short Description	Key Features
Recurrent Neural Network	• An artificial neural network called a recurrent neural network (RNN) is one type of such network that utilizes sequential input or time series input. • Any length of input may be analyzed by RNN. • Extensively employed in natural language processing and speech recognition.	Merit: An RNN's internal memory allows it to retain previous input. Demerits: Recurrent neural network's computation is slow. It has problems like Vanishing Gradient or Exploding Gradient.
Deep Auto-Encoder	• The essential use of an autoencoder includes illness detection, denoising of images, and compression of images. • It is a method of unsupervised learning. • In an autoencoder neural network, the amount of units in the output layer matches that of the input layer.	Merit: The widely used autoencoder achieves a high success rate in many fields and reduces the complexity of the network by lowering the dataset dimensions. Demerit: Their rate of learning is very sluggish.
Deep Boltzmann Machine	• The deep Boltzmann machine is a powerful and effective computational tool for compressing any distribution. • It is an unsupervised deep learning model. • Each node between levels of the network is connected to every other node.	Merit: Top-down feedback is integrated for strong conclusions on indefinite basics. Demerit: For big datasets, parameter optimization is time-consuming.
Deep Belief Network	• Deep Belief Network (DBN) is particularly strong in its classification. • The same neural network methodology used in DBN can be applied to various applications and data formats. • It supports both unsupervised as well as supervised learning.	Merits: • In addition to voice recognition, Deep Belief Networks can be used for picture recognition, capturing motion data, and more. • They are a computationally effective variant of feedforward neural networks. • Directly increasing the probability of results. Demerits: • To outperform alternative methods, DBN needs a lot of data. • Due to its complex data models, DBN is expensive to train, often requiring multiple machines. • DBN is challenging for people with less experience.

Deep Neural Network	• A Deep Neural Network (DNN) is an artificial neural network that includes additional layers of neurons between its input and output layers. • DNNs are extremely scalable, allowing them to address problems of any scale. • DNNs are frequently employed to extract high-level abstract features because they perform better than conventional models. • They have more than two hidden layers.	Merit: Recognizes appropriate characteristics instantly without human assistance. Demerits: • Computation of DNNs is quite resource-intensive. • Necessitates a lot of memory and processing power. • Enormous amounts of data and training are needed to achieve desired goals.
Generative Adversarial Networks	• The generation network and the discriminator are the two artificial neural networks which make up a Generative Adversarial Network. In which the generator serves as convolutional neural network. while as, discriminator serves as deconvolutional neural network.	Merit GANs can produce synthetic data that matches the distribution of real data. Demerit: To achieve effective results, GANs frequently require plenty of training data.
Convolutional Neural Networks	• Convolutional neural networks are created using the behavior of neurons of the human brain. • Convolutional neural networks are constructed from several building blocks, including layers of convolution, layers of pooling, and fully connected layers.	Merit: Using a backpropagation algorithm, convolutional neural networks are designed to acquire a spatial hierarchy of characteristic patterns automatically and adaptively. Demerits: • The CNN cannot function without a significant quantity of data related to training. • Because of MaxPooling operations, CNNs often run substantially slower.

evaluated using the 2019 BraTS competition dataset for brain tumor segmentation.The obtained segmentation results show Dice and Hausdorff distance values ranging from 0.81 to 0.84 percent and 9.8 to 19.7, respectively.

Costanzo *et al.* (2023) introduced a prompt and precise machine learning technique for microwave-based medical imaging in cancer identification.Authors utilized an innovative architecture that combines U-Net and ResNet-18, leveraging ResNet-18's residual connections and pre-trained weights.This fusion yields highly accurate segmentations at a reduced computational cost. The study employed a dataset of 1500 breast images containing randomly situated tumors. For each proposed network, they generated training and validation samples. The authors conducted comprehensive quantitative assessments using diverse breast models, including instances of abnormal lesions, to validate their machine learning approach's efficacy. To demonstrate the deep neural network-based inversion and segmentation strategy's performance in breast imaging,the authors presented three numerical scenarios. The evaluation metrics encompassed Percentage Reconstruction Relative Error, Root Mean Square Error, and the Coefficient of Determination.The study covered sixty distinct images separate from the training set, considering both noise free images and those with added Gaussian noise. Moreover, the study featured a meticulous comparison of computational costs and image reconstruction precision.The results of numerical tests conducted in both noisy and noise-free environments demonstrated the proposed method's effectiveness in reconstructing the distribution of dielectric properties for breast imaging.Proposed method exhibited exceptional capability in detecting abnormal scatterers, such as tumors.

Tang *et al.* (2020) introduced a new method that utilizes deep learning to examine pre-operative multimodal MRI brain data in individuals with glioblastoma. Their approach focuses on extracting tumor genotype related features and their seamless integration into the prediction of Overall Survival.To evaluate the effectiveness of their approach, the authors utilized a dataset comprising brain MRI scans from 120 glioblastoma patients, along with up to four different genotypic/molecular indicators.When compared to other cutting-edge approaches, suggested method exhibited the highest accuracy in forecasting overall survival.

Awotunde *et al.* (2022) introduced an advanced approach to fuzzy elephant herding optimization (EFEHO). This technique, referred to as EFEHO-OTSU, was specifically developed to enhance OTSU segmentation. Its primary goal was to achieve precise identification of optimal segmentation. Following this, authors implemented a dual-attention multi-instance deep neural network for the purpose of Alzheimer's disease detection,including its early stage characterized as moderate cognitive decline. The evaluation was conducted using the ADNI AIBL datasets, resulting in a remarkable accuracy score of 0.942, the highest among all achieved within the ADNI dataset.

Shubham *et al.* (2023) introduced a deep learning-driven approach to identify glomeruli within pictures of human kidney tissue. The segmentation architecture utilized was U-Net, with EfficientNet B4 serving as the underlying backbone.Training and evaluation utilized the HuBMAP dataset, which comprises eight training sets and five public test sets. The optimization algorithm employed was Adam.The training was conducted over four K-folds, with each fold undergoing a 100 epoch process.Within each epoch,300 iterations were performed, and a batch size of six patches was utilized.The selected loss function was binary cross-entropy. Importantly, the training dataset included eleven newly frozen as well as nine Formalin-fixed Paraffin-Embedded

Table 2 Evaluation of Deep Learning Techniques in Healthcare Applications

Author	Purpose	Approach	Dataset	Results
(Dominguez-Morales *et al.* 2017)	Detection and Classification of Cardiac murmurs	CNN employing Neuromorphic Hearing Sensors	Sonogram Images	Accuracy:0.97, Specificity:0.95, Sensitivity:0.93, PhysioNet score: 0.9416
(Dai *et al.* 2018)	Detection of retinal microaneurysms	Multiple-Sieve CNN	DIARETDB1 Dataset	Precision: 0.99 and Recall: 0.87, Accuracy:0.96, F1 score:0.934
(Fu *et al.* 2018)	Ocular Disc and Cup Segmentation from Fundus Images	Deep learning-based M-Net	ORIGA dataset and Singapore Chinese Eye Study (SCES) dataset	ORIGA Dataset:CDR: 0.80, RDAR: 0.79 SCES Dataset:CDR:0.83, RDAR:0.82
(Ahuja *et al.* 2022)	Brain tumors segmentation and classification	DarkNet-53 models, 2d-superpixel segmentation approachs	TIW-CE MRI Dataset	Accuracy:98.54, Area under curve:0.99, Average Dice Index:0.94±2.6
(Saba *et al.* 2020)	Identify gliomas or normal images	Grab cut method	BRATS 2015,2016,2017 datasets	BRATS2015:0.99(DSC), BRATS2016:1.00(DSC), BRATS2017:0.99(DSC)
(Vorontsov *et al.* 2019)	Colorectal Liver Metastases	Convolutional Network	Training and Validation: LiTS challenge dataset,Testing:26 CT images.	Total per-lesion DSC:0.14-0.68
(Shen *et al.* 2020)	Diagnosis of Breast Cancer	Deep Learning and fuzzy learning	INbreast Dataset, Private Dataset.	Accuracy:0.82. Average Recall:0.78,Average Specificity:0.78, Average Precision:0.84,Average F1-score:0.79
(Pereira *et al.* 2016)	Brain Tumor Segmentation	Convolutional Neural Network	BRATS2013,BRATS2015	BRATS2013:WT:0.88, CT:0.83,ET:0.77, BRATS2015:WT:0.78, CT:0.65, ET:0.75.
(Costanzo *et al.* 2023)	Cancer Detection	UNet and ResNet Models	Breast Imaging Dataset	In noise-free settings, U-Net 1, U-Net 2, and U-Net 3 achieved mean IoU scores of 0.995, 0.996, and 0.994, respectively.
(Chen *et al.* 2021)	Diagnosis of Breast Cancer	3D CNN	Breast-CEUS Dataset	Sensitivity:0.97, Accuracy: 0.86
(Sreng *et al.* 2020)	Identifying glaucoma through optic disc segmentation in retinal images	Combination of DeepLabv3+ and MobileNet for optic disc segmentation and deep CNN for glaucoma classification	ACRIMA, DRISHTI-GS1, RIM-ONE, REFUGE and ORIGA.	Accuracy: 0.99(ACRIMA), 0.86(DRISHTI-GS1),0.95(RIM-ONE),0.97(ORIGA).
(Shubham *et al.* 2023)	Detection of glomeruli within human kidney tissue	UNet for segmentation with EfficientNetB4 as its backbone	HuBMAP Dataset	Accuracy: 0.99, and Dice Coefficient:0.90.

(Bhattacharjee *et al.* 2023)	Segmentation of Pulmonary Nodules	ResiU-Net	Dataset of lung cancer CT scans from National Center for Cancer Diseases (IQ-OTH/NCCD)	F score of 97.44, an intersection over union score of 95.02, a dice score of 94.87, a binary cross-entropy loss of 0.34, along with a combined dice coefficient and binary focal loss of 0.7585.
(Zhao *et al.* 2023)	Segmentation and classification of kidney masses	3D U-Net and ResNet	Utilized an institutional CT image dataset for training and evaluated on the kidney tumor segmentation (KiTS21) Challenge Dataset	Achieved a 0.99 DSC for bilateral kidney boundary segmentation, alongside 0.86 accuracy for <5 mm masses and 0.91 accuracy for 5 mm masses
(Li *et al.* 2023)	Transcranial Brain Hemorrhage Detection	Residual attention U-Net	Employed a simulation approach to construct training datasets, utilized images generated through conventional imaging algorithms as network input.	Employed two synthetic samples: the first showcased enhanced visibility of a 10-mm hemorrhage spot, while the second accurately reconstructed a barely visible 5-mm hemorrhage spot using the trained network.
(Zhu *et al.* 2023)	Predicting the survival time of glioblastoma multiforme patients using non-invasive methods	Modified 3D-UNet	BraTS2018,BraTS2019, BraTS2020	DSC of BraTS2018-0.83(WT),0.75(CT),0.66(ET), BraTS2019-0.79(WT), 0.72(CT),0.75(ET),Brats2020-0.83(WT),0.72(CT),0.69(ET).
(Rajput *et al.* 2023)	Survival prediction for brain tumor patients using interpretable ML	3D-UNet	BraTS2020	Survival Prediction accuracy-0.55, MSE-79826.24, medianSE-14148.89, SpearmanR-0.711

(FFPE) PAS kidney images. These images featured histological stains designed to enhance resolution and precision during model training. The proposed method attained an impressive accuracy level of 0.99, along with a Dice coefficient measuring 0.9060.

Rajput *et al.* (2023) introduced an end-to-end AI approach to forecast survival days (SD) in glioblastoma multiforme(GBM) brain tumor patients. Proposed method employs MRI-derived features and patient data, encompassing shape, location, and radiomics aspects.Feature selection involves recursive elimination, permutation importance, and correlation analysis, revealing 29 key features, notably age, location, and radiomics parameters,influencing SD prognosis. The model's predictions are corroborated through post-hoc interpretability techniques, confirming alignment with established medical knowledge and showcasing a 33 percent SD prediction enhancement over prior methods.

Zhao *et al.* (2023) presented an innovative deep learning method that enables the complete automation of segmenting and categorizing renal masses in CT images. Their method employs a two-step process involving a cascade architecture that combines a 3D U- Net and ResNet. This combination effectively achieves precise segmentation and classification of focal renal lesions. Initially,they employ a 3D U-Net-driven technique to define kidney boundaries within CT images, creating a region of interest for identifying renal masses. Subsequently, an ensemble learning model utilizing the 3D U-Net detects and segments these masses,followed by classification using a ResNet algorithm. The algorithm demonstrated impressive performance with a high Dice similarity coefficient (DSC) for delineating bilateral kidney boundaries and renal masses. The effectiveness of this proposed technique was confirmed through assessment with an independent validation dataset and the Kidney Tumor Segmentation (KiTS21) challenge dataset. The outcomes underscore the method's potential to precisely localize and categorize renal masses.

Bhattacharjee *et al.* (2023) put forward an innovative segmentation framework that refines dual skip connections.The novel framework combines a pre-trained Residual Neural Network(ResNet) 152 with the U-Net architecture, resulting in what they term ResiU-Net. Their research encompassed the comparison of nine different pretrained and fine-tuned encoder backbones. These included ResNet18, ResNet 34, ResNet 50, ResNet 101, ResNet 152, SEResNet18,ResNext 101, SE-ResNet34, and ResNext 50. The findings indicated that the proposed ResiU-Net approach outperformed the alternatives. For Training and evaluation, authors utilized the HuBMAP dataset, which comprises eight

training sets and five public test sets. The optimization algorithm employed was Adam. The suggested approach attains a Fscore of 97.44, an intersection over union score of 95.02, a dice score of 94.87 percent, a binary cross-entropy loss of 0.34, and a combined dice coefficient and binary focal loss of 0.7585. The ResiU-Net proposed in this study surpasses existing methods, yielding superior evaluation metrics. The model's training duration was 43 minutes, underscoring its rapid yet precise segmentation capability

Li *et al.* (2023) introduced an innovative deep learning approach designed to detect transcranial brain hemorrhages and address other transcranial brain imaging needs. Proposed methodology employs an attention-guided mechanism to emphasize important features as they pass through skip connections. The researchers conducted two separate ex-vivo experiments using artificially created samples to generate testing data.In the first image, they notably improved image contrast and significantly reduced artifacts, leading to a clear distinction of the hemorrhage spot.Proposed approach also accurately reconstructed the spot's boundaries, size, and shape. In the second sample, a hemorrhage spot with a diameter of 5 millimeters was hardly discernible using the delay-and-sum (DAS) approach. Nevertheless, the proposed method achieved a high level of accuracy in detecting the aforementioned spot.

Zhu *et al.* (2023) introduced a novel approach for the non-invasive prediction of overall survival time in patients with glioblastoma multiforme. The proposed approach is based on utilizing multimodal MRI radiomics.The methodology involves segmenting distinct tumor subregions, namely the Whole Tumor (WT), Enhancing Tumor (ET), and Core Tumor (CT), for comprehensive assessment. The model's performance was truly remarkable, as evidenced by the evaluation metrics.Notably, the specificity index of 0.999 underscores its remarkable accuracy in effectively identifying normal tissue regions.To validate its effectiveness, the proposed model underwent evaluation on three significant datasets: BraTS2020, BraTS2019, and BraTS2018. The validation subsets within these datasets consisted of 125 cases for BraTS2020 and BraTS2019, and 66 cases for BraTS2018, respectively. Across all three datasets,the model consistently demonstrated outstanding performance, reinforcing its reliability and applicability.While the proposed model excelled at accurately segmenting the subregions of brain tumors,however some fine details along the edges were slightly blurred due to the absence of distinct features.

Table 2 compiles the summarized outcomes of diverse deep learning techniques within the healthcare domain.

CRITICAL OBSERVATIONS

Deep learning technology, as highlighted by authors such as (Rajkomar *et al.* 2018) and (Esteva *et al.* 2017), has made significant contributions to the healthcare sector and has demonstrated remarkable effectiveness in medical image analysis. Pioneering research conducted by (Rajpurkar *et al.* 2018) and (Gulshan *et al.* 2016) showcases the accuracy of deep learning in detecting diseases, including cancer and brain tumors. Convolutional Neural Networks (CNNs), studied by researchers including (Lipton *et al.* 2015) and (Shin *et al.* 2016), have played a key role in improving medical image classification.The benefits of deep learning in healthcare, such as faster evaluation and handling large datasets, have been emphasized by authors such as (Miotto *et al.* 2016). However, challenges related to data quality, interpretability, and biases, as discussed by (Cheplygina *et al.* 2019), necessitate ongoing research and collaboration to fully leverage deep learning's potential in healthcare.

CONCLUSION

Recent advancements in deep learning have introduced novel perspectives for the analysis of medical images, revolutionizing the identification of disease patterns within these images. This paper presents a comprehensive review and synthesis of cutting-edge deep learning applications in medical image analysis, with a primary focus on disease detection, segmentation, and classification. We elucidate the strengths and limitations of these approaches, the utilized datasets, assessment metrics, methodologies, with a particular emphasis on convolutional neural networks (CNNs) as a prominent deep learning application for computer vision tasks. Additionally,we underscore deep learning-based classification techniques, encompassing supervised, unsupervised, and semi-supervised methods, as well as their integration into medical image processing procedures. Despite the remarkable efficiency achieved by deep learning techniques across diverse medical applications, there remains an evident scope for enhancement due to inherent challenges linked to healthcare data. These challenges and outline potential future directions are discussed as under:

Enhanced Accuracy and Early Detection

Deep learning algorithms possess the capacity to enhance the accuracy of disease detection and diagnosis (Zheng *et al.* 2020). Future developments may focus on refining existing models and creating new ones that are even more adept at identifying subtle patterns in medical images,leading to earlier and more accurate diagnoses.

Multi-Modal Fusion

Combining information from various medical imaging modalities (such as MRI, CT, PET, Ultrasound, etc.) can offer a more holistic perspective of a patient's state. This approach enhances diagnostic accuracy by assessing various health facets (Zhang *et al.* 2021). Future research might focus on developing optimized deep learning techniques that effectively integrate and analyze data from multiple modalities for improved diagnostic accuracy.

Interpretable and Explainable Models

Deep learning models often operate as black boxes, complicating the comprehension of their predictions (Rajput *et al.* 2023). In medical settings, interpretability is paramount for fostering trust and elucidating decision-making processes to clinicians. The path ahead involves designing models that offer clear insights into their decision logic.Incorporating attention mechanisms, feature visualization, and saliency mapping can provide visibility into what the model focuses on during analysis.Integrating medical knowledge into model architectures and utilizing explainable AI techniques like rule-based systems or gradient-based explanations can further enhance interpretability. As the field progresses, these efforts will promote greater trust in AI-driven medical diagnostics and treatment planning.

Data Augmentation and Synthesis

Since medical datasets are often limited, techniques that effectively generate synthetic medical images could play a crucial role in training more robust deep learning models and addressing data scarcit (Mumuni and Mumuni 2022). Addressing limited medical

datasets involves refining Generative Adversarial Networks and transferring pre-trained models for improved synthetic image generation. Domain adaptation, semi-supervised, and active learning strategies optimize data use,while collaborative sharing expands resources. Multi-modal integration and tailored image augmentation further enrich datasets. Embracing these approaches and interdisciplinary collaboration can effectively tackle data augmentation challenges, revolutionizing healthcare diagnostics through advanced machine learning solutions.

Knowledge Transfer and Few-shot Learning

Developing deep learning models with the ability to transfer knowledge across different medical domains or learn from only a few examples is a significant challenge (Li *et al.* 2019). This challenge becomes crucial in scenarios involving rare diseases or situations where there is limited available data for training. The future direction in addressing this challenge involves the advancement of cross-domain adaptation techniques and few-shot learning methods.Domain adaptation techniques can facilitate the effective generalization of models trained in one medical domain to another.

Class Imbalance

In the field of deep learning for medical image analysis, class imbalance presents a significant challenge (Johnson and Khoshgoftaar 2019). This issue is particularly apparent in datasets like BraTS for brain tumor segmentation.To overcome this, the future trajectory involves innovative data augmentation, strategic re-sampling methods, and advanced algorithms. These endeavors hold the potential to bolster accuracy and clinical utility, ensuring robust diagnostics and well-informed healthcare decisions.

Lack of Standardization in Medical Imaging

The variability in resolutions, orientations, and acquisition protocols of medical imaging modalities like MRI and CT poses a challenge in ensuring consistent preprocessing and analysis of diverse datasets (Cobo *et al.* 2023). To address this, the future direction involves devising standardized protocols for data acquisition and preprocessing, defining uniform imaging practices and resolution standards, as well as exploring advanced techniques beyond normalization and registration to enhance the reliability and accuracy of deep learning-based medical image analysis.

Small Anomalies Detection

Detecting subtle anomalies or abnormalities that could signal a disease poses a difficulty, particularly when these irregularities are small and blend with healthy tissues.To overcome the hurdle of identifying tiny anomalies within medical images (Pang *et al.* 2021), the future lies in refining algorithms for improved sensitivity.Embracing multi-modal analysis and leveraging contextual cues can enhance the ability to spot minute irregularities.Integrating deep generative models and leveraging self-supervised learning strategies can empower the system to recognize intricate patterns.By relentlessly pursuing these avenues, the field aims to bolster the accuracy of medical image analysis and pave the way for more effective disease detection.

Data Privacy and Security

Medical data,being sensitive and governed by privacy regulations, presents a substantial challenge in devising methods that balance patient data protection with effective analysis (Ramzan *et al.* 2022). The future entails the development of privacy-preserving techniques that enable meaningful analysis while upholding confidentiality. Differential privacy, federated learning, and homomorphic encryption are promising avenues. Additionally, exploring decentralized data sharing models and blockchain-based solutions can enhance security.By integrating these strategies, the field aims to achieve a harmonious equilibrium between robust data analysis and stringent privacy considerations, ensuring trust and compliance in healthcare applications.

Longer Training Time

A significant challenge in medical imaging's deep learning is extended model training due to complex structures (Ahmad *et al.* 2020). To optimize training, researchers explore transfer learning, leveraging pretrained models and hardware advancements like GPUs. Additionally, model compression techniques and generative adversarial networks for data augmentation show promise. This convergence of strategies holds potential for curtailing training time, expediting model development and real world deployment.

Limited Annotation and Ground Truth

Obtaining accurate annotations and ground truth labels for medical images can pose a considerable difficulty due to the need for expert clinicians and time-consuming manual labeling, especially for complex structures and rare conditions (Zhang *et al.* 2020). Future direction involves exploring semi-supervised learning techniques, which leverage a smaller set of fully labeled data alongside a larger pool of unlabeled data. Additionally, weakly supervised learning approaches, where models are trained with less detailed annotations like image-level labels, hold potential. These methods aim to alleviate the burden of meticulous manual annotation while maintaining high accuracy, thus optimizing the use of expert resources and enhancing the efficiency of medical image analysis.

Availability of data and material

Not applicable.

Conflicts of interest

The authors declare that there is no conflict of interest regarding the publication of this paper.

Ethical standard

The authors have no relevant financial or non-financial interests to disclose.

LITERATURE CITED

Abiwinanda, N., M. Hanif, S. T. Hesaputra, A. Handayani, and T. R. Mengko, 2019 Brain tumor classification using convolutional neural network. In *World Congress on Medical Physics and Biomedical Engineering 2018: June 3-8, 2018, Prague, Czech Republic (Vol. 1)*, pp. 183–189, Springer.

Ahmad, H. M., M. J. Khan, A. Yousaf, S. Ghuffar, and K. Khurshid, 2020 Deep learning: a breakthrough in medical imaging. Current Medical Imaging **16**: 946–956.

Ahuja, S., B. K. Panigrahi, and T. K. Gandhi, 2022 Enhanced performance of dark-nets for brain tumor classification and segmentation using colormap-based superpixel techniques. Machine Learning with Applications **7**: 100212.

Albarqouni, S., C. Baur, F. Achilles, V. Belagiannis, S. Demirci, *et al.*, 2016 Aggnet: deep learning from crowds for mitosis detection in breast cancer histology images. IEEE transactions on medical imaging **35**: 1313–1321.

Alwzwazy, H. A., H. M. Albehadili, Y. S. Alwan, and N. E. Islam, 2016 Handwritten digit recognition using convolutional neural networks. International Journal of Innovative Research in Computer and Communication Engineering **4**: 1101–1106.

Alzubaidi, L., J. Zhang, A. J. Humaidi, A. Al-Dujaili, Y. Duan, *et al.*, 2021 Review of deep learning: Concepts, cnn architectures, challenges, applications, future directions. Journal of big Data **8**: 1–74.

Arif, M., F. Ajesh, S. Shamsudheen, O. Geman, D. Izdrui, *et al.*, 2022 Brain tumor detection and classification by mri using biologically inspired orthogonal wavelet transform and deep learning techniques. Journal of Healthcare Engineering **2022**.

Awotunde, J. B., N. S. Sur, A. L. Imoize, S. Misra, and T. Gaber, 2022 An enhanced residual networks based framework for early alzheimer's disease classification and diagnosis. In *International Conference on Communication, Devices and Networking*, pp. 335–348, Springer.

Bhattacharjee, A., R. Murugan, T. Goel, and S. Mirjalili, 2023 Pulmonary nodule segmentation framework based on fine-tuned and pretrained deep neural network using ct images. IEEE Transactions on Radiation and Plasma Medical Sciences **7**: 394–409.

Chen, C., Y. Wang, J. Niu, X. Liu, Q. Li, *et al.*, 2021 Domain knowledge powered deep learning for breast cancer diagnosis based on contrast-enhanced ultrasound videos. IEEE Transactions on Medical Imaging **40**: 2439–2451.

Chen, D. and B. K.-W. Mak, 2015 Multitask learning of deep neural networks for low-resource speech recognition. IEEE/ACM Transactions on Audio, Speech, and Language Processing **23**: 1172–1183.

Cheplygina, V., M. de Bruijne, and J. P. Pluim, 2019 Not-so-supervised: a survey of semi-supervised, multi-instance, and transfer learning in medical image analysis. Medical image analysis **54**: 280–296.

Cobo, M., P. Menéndez Fernández-Miranda, G. Bastarrika, and L. Lloret Iglesias, 2023 Enhancing radiomics and deep learning systems through the standardization of medical imaging workflows. Scientific Data **10**: 732.

Costanzo, S., A. Flores, and G. Buonanno, 2023 Fast and accurate cnn-based machine learning approach for microwave medical imaging in cancer detection. IEEE Access .

Dai, L., R. Fang, H. Li, X. Hou, B. Sheng, *et al.*, 2018 Clinical report guided retinal microaneurysm detection with multi-sieving deep learning. IEEE transactions on medical imaging **37**: 1149–1161.

Dominguez-Morales, J. P., A. F. Jimenez-Fernandez, M. J. Dominguez-Morales, and G. Jimenez-Moreno, 2017 Deep neural networks for the recognition and classification of heart murmurs using neuromorphic auditory sensors. IEEE transactions on biomedical circuits and systems **12**: 24–34.

Dong, H., G. Yang, F. Liu, Y. Mo, and Y. Guo, 2017 Automatic brain tumor detection and segmentation using u-net based fully convolutional networks. In *Medical Image Understanding and Analysis: 21st Annual Conference, MIUA 2017, Edinburgh, UK, July 11–13, 2017, Proceedings 21*, pp. 506–517, Springer.

Du, M., F. Li, G. Zheng, and V. Srikumar, 2017 Deeplog: Anomaly detection and diagnosis from system logs through deep learning. In *Proceedings of the 2017 ACM SIGSAC conference on computer and communications security*, pp. 1285–1298.

Esteban, C., S. L. Hyland, and G. Rätsch, 2017 Real-valued (medical) time series generation with recurrent conditional gans. arXiv preprint arXiv:1706.02633 .

Esteva, A., B. Kuprel, R. A. Novoa, J. Ko, S. M. Swetter, *et al.*, 2017 Dermatologist-level classification of skin cancer with deep neural networks. nature **542**: 115–118.

Feng, C., A. Elazab, P. Yang, T. Wang, F. Zhou, *et al.*, 2019 Deep learning framework for alzheimer's disease diagnosis via 3d-cnn and fsbi-lstm. IEEE Access **7**: 63605–63618.

Fu, H., J. Cheng, Y. Xu, D. W. K. Wong, J. Liu, *et al.*, 2018 Joint optic disc and cup segmentation based on multi-label deep network and polar transformation. IEEE transactions on medical imaging **37**: 1597–1605.

Gulshan, V., L. Peng, M. Coram, M. C. Stumpe, D. Wu, *et al.*, 2016 Development and validation of a deep learning algorithm for detection of diabetic retinopathy in retinal fundus photographs. jama **316**: 2402–2410.

Islam, J. and Y. Zhang, 2018 Brain mri analysis for alzheimer's disease diagnosis using an ensemble system of deep convolutional neural networks. Brain informatics **5**: 1–14.

Johnson, J. M. and T. M. Khoshgoftaar, 2019 Survey on deep learning with class imbalance. Journal of Big Data **6**: 1–54.

LeCun, Y., Y. Bengio, and G. Hinton, 2015 Deep learning. nature **521**: 436–444.

Li, A., T. Luo, Z. Lu, T. Xiang, and L. Wang, 2019 Large-scale few-shot learning: Knowledge transfer with class hierarchy. In *Proceedings of the ieee/cvf conference on computer vision and pattern recognition*, pp. 7212–7220.

Li, C., Z. Xi, G. Jin, W. Jiang, B. Wang, *et al.*, 2023 Deep-learning-enabled microwave-induced thermoacoustic tomography based on resattu-net for transcranial brain hemorrhage detection. IEEE Transactions on Biomedical Engineering .

Li, Q., W. Cai, X. Wang, Y. Zhou, D. D. Feng, *et al.*, 2014 Medical image classification with convolutional neural network. In *2014 13th international conference on control automation robotics & vision (ICARCV)*, pp. 844–848, IEEE.

Lian, C., M. Liu, J. Zhang, and D. Shen, 2018 Hierarchical fully convolutional network for joint atrophy localization and alzheimer's disease diagnosis using structural mri. IEEE transactions on pattern analysis and machine intelligence **42**: 880–893.

Lipton, Z. C., D. C. Kale, C. Elkan, and R. Wetzel, 2015 Learning to diagnose with lstm recurrent neural networks. arXiv preprint arXiv:1511.03677 .

Liu, J., B. Xu, C. Zheng, Y. Gong, J. Garibaldi, *et al.*, 2018 An end-to-end deep learning histochemical scoring system for breast cancer tma. IEEE transactions on medical imaging **38**: 617–628.

Liu, M., M. Zhou, T. Zhang, and N. Xiong, 2020 Semi-supervised learning quantization algorithm with deep features for motor imagery eeg recognition in smart healthcare application. Applied Soft Computing **89**: 106071.

Liu, Z., L. Tong, L. Chen, Z. Jiang, F. Zhou, *et al.*, 2023 Deep learning based brain tumor segmentation: a survey. Complex & intelligent systems **9**: 1001–1026.

Liu, Z., L. Tong, L. Chen, F. Zhou, Z. Jiang, *et al.*, 2021 Canet: Context aware network for brain glioma segmentation. IEEE Transactions on Medical Imaging **40**: 1763–1777.

Meena, T. and S. Roy, 2022 Bone fracture detection using deep supervised learning from radiological images: A paradigm shift. Diagnostics **12**: 2420.

Mimboro, P., A. Sunyoto, and R. S. Kharisma, 2021 Segmentation of brain tumor objects in magnetic resonance imaging (mri) image using connected component label algorithm. In *2021 International Conference on Advanced Mechatronics, Intelligent Manufacture and Industrial Automation (ICAMIMIA)*, pp. 195–198, IEEE.

Miotto, R., L. Li, B. A. Kidd, and J. T. Dudley, 2016 Deep patient: an unsupervised representation to predict the future of patients from the electronic health records. Scientific reports **6**: 1–10.

Muhammad, K., S. Khan, J. Del Ser, and V. H. C. De Albuquerque, 2020 Deep learning for multigrade brain tumor classification in smart healthcare systems: A prospective survey. IEEE Transactions on Neural Networks and Learning Systems **32**: 507–522.

Mumuni, A. and F. Mumuni, 2022 Data augmentation: A comprehensive survey of modern approaches. Array p. 100258.

Pang, G., C. Shen, L. Cao, and A. V. D. Hengel, 2021 Deep learning for anomaly detection: A review. ACM computing surveys (CSUR) **54**: 1–38.

Pereira, S., A. Pinto, V. Alves, and C. A. Silva, 2016 Brain tumor segmentation using convolutional neural networks in mri images. IEEE transactions on medical imaging **35**: 1240–1251.

Rajkomar, A., E. Oren, K. Chen, A. M. Dai, N. Hajaj, *et al.*, 2018 Scalable and accurate deep learning with electronic health records. NPJ digital medicine **1**: 18.

Rajpurkar, P., J. Irvin, R. L. Ball, K. Zhu, B. Yang, *et al.*, 2018 Deep learning for chest radiograph diagnosis: A retrospective comparison of the chexnext algorithm to practicing radiologists. PLoS medicine **15**: e1002686.

Rajput, S., R. A. Kapdi, M. S. Raval, and M. Roy, 2023 Interpretable machine learning model to predict survival days of malignant brain tumor patients. Machine Learning: Science and Technology **4**: 025025.

Ramzan, M., M. Habib, and S. A. Khan, 2022 Secure and efficient privacy protection system for medical records. Sustainable Computing: Informatics and Systems **35**: 100717.

Rasool, N. and J. I. Bhat, 2023 Glioma brain tumor segmentation using deep learning: A review. In *2023 10th International Conference on Computing for Sustainable Global Development (INDIACom)*, pp. 484–489, IEEE.

Saba, T., A. S. Mohamed, M. El-Affendi, J. Amin, and M. Sharif, 2020 Brain tumor detection using fusion of hand crafted and deep learning features. Cognitive Systems Research **59**: 221–230.

Sarraf, S. and G. Tofighi, 2016 Deep learning-based pipeline to recognize alzheimer's disease using fmri data. In *2016 future technologies conference (FTC)*, pp. 816–820, IEEE.

Sharma, N. and L. M. Aggarwal, 2010 Automated medical image segmentation techniques.

Shen, T., J. Wang, C. Gou, and F.-Y. Wang, 2020 Hierarchical fused model with deep learning and type-2 fuzzy learning for breast cancer diagnosis. IEEE Transactions on Fuzzy Systems **28**: 3204–3218.

Shin, H.-C., K. Roberts, L. Lu, D. Demner-Fushman, J. Yao, *et al.*, 2016 Learning to read chest x-rays: Recurrent neural cascade model for automated image annotation. In *Proceedings of the IEEE conference on computer vision and pattern recognition*, pp. 2497–2506.

Shubham, S., N. Jain, V. Gupta, S. Mohan, M. M. Ariffin, *et al.*, 2023 Identify glomeruli in human kidney tissue images using a deep learning approach. Soft Computing **27**: 2705–2716.

Sreng, S., N. Maneerat, K. Hamamoto, and K. Y. Win, 2020 Deep learning for optic disc segmentation and glaucoma diagnosis on retinal images. Applied Sciences **10**: 4916.

Tan, C., F. Sun, T. Kong, W. Zhang, C. Yang, *et al.*, 2018 A survey on deep transfer learning. In *Artificial Neural Networks and Machine Learning–ICANN 2018: 27th International Conference on Artificial Neural Networks, Rhodes, Greece, October 4-7, 2018, Proceedings, Part III 27*, pp. 270–279, Springer.

Tang, Z., Y. Xu, L. Jin, A. Aibaidula, J. Lu, *et al.*, 2020 Deep learning of imaging phenotype and genotype for predicting overall survival time of glioblastoma patients. IEEE transactions on medical imaging **39**: 2100–2109.

Trajanovski, S., C. Shan, P. J. Weijtmans, S. G. B. de Koning, and T. J. Ruers, 2020 Tongue tumor detection in hyperspectral images using deep learning semantic segmentation. IEEE transactions on biomedical engineering **68**: 1330–1340.

Vorontsov, E., M. Cerny, P. Régnier, L. Di Jorio, C. J. Pal, *et al.*, 2019 Deep learning for automated segmentation of liver lesions at ct in patients with colorectal cancer liver metastases. Radiology: Artificial Intelligence **1**: 180014.

Wang, H. and B. Raj, 2017 On the origin of deep learning. arXiv preprint arXiv:1702.07800 .

Wu, N., J. Phang, J. Park, Y. Shen, Z. Huang, *et al.*, 2019 Deep neural networks improve radiologists' performance in breast cancer screening. IEEE transactions on medical imaging **39**: 1184–1194.

Yang, S., F. Zhu, X. Ling, Q. Liu, and P. Zhao, 2021 Intelligent health care: Applications of deep learning in computational medicine. Frontiers in Genetics **12**: 607471.

Zahoor, M. M., S. A. Qureshi, S. Bibi, S. H. Khan, A. Khan, *et al.*, 2022 A new deep hybrid boosted and ensemble learning-based brain tumor analysis using mri. Sensors **22**: 2726.

Zeineldin, R. A., M. E. Karar, J. Coburger, C. R. Wirtz, and O. Burgert, 2020 Deepseg: deep neural network framework for automatic brain tumor segmentation using magnetic resonance flair images. International journal of computer assisted radiology and surgery **15**: 909–920.

Zhang, D., G. Huang, Q. Zhang, J. Han, J. Han, *et al.*, 2020 Exploring task structure for brain tumor segmentation from multi-modality mr images. IEEE Transactions on Image Processing **29**: 9032–9043.

Zhang, Y., D. Sidibé, O. Morel, and F. Mériaudeau, 2021 Deep multimodal fusion for semantic image segmentation: A survey. Image and Vision Computing **105**: 104042.

Zhao, T., Z. Sun, Y. Guo, Y. Sun, Y. Zhang, *et al.*, 2023 Automatic renal mass segmentation and classification on ct images based on 3d u-net and resnet algorithms. Frontiers in Oncology **13**: 1169922.

Zheng, J., D. Lin, Z. Gao, S. Wang, M. He, *et al.*, 2020 Deep learning assisted efficient adaboost algorithm for breast cancer detection and early diagnosis. IEEE Access **8**: 96946–96954.

Zhu, J., J. Ye, L. Dong, X. Ma, N. Tang, *et al.*, 2023 Non-invasive prediction of overall survival time for glioblastoma multiforme patients based on multimodal mri radiomics. International Journal of Imaging Systems and Technology .

Zhu, W., L. Sun, J. Huang, L. Han, and D. Zhang, 2021 Dual attention multi-instance deep learning for alzheimer's disease diagnosis with structural mri. IEEE Transactions on Medical Imaging **40**: 2354–2366.

How to cite this article: Rasool, N., and Bhat, J. I. Unveiling the Complexity of Medical Imaging through Deep Learning Approaches. *Chaos Theory and Applications*, 5(4), 267-280, 2023.

CHAOS
Theory and Applications
in Applied Sciences and Engineering

e-ISSN: 2687-4539
RESEARCH ARTICLE
Vol.5 / No.4 / 2023 / pp.281-285
Special Issue
https://doi.org/10.51537/chaos.1322939

Novel Traveling Wave Solutions of Jaulent-Miodek Equations and Coupled Konno-Oono Systems and Their Dynamics

Raj Kumar [α,1], **Kripa Shankar Pandey** [α,2], **Avneesh Kumar** [α,3] **and Anshu Kumar** [β,4]

[α] Department of Mathematics, Faculty of Engineering and Technology, V. B. S. Purvanchal University, Jaunpur–222003, India, [β]Department of Mathematics, Sharda University, Knowledge Park III, Greater Noida–201310, India.

ABSTRACT This research article deals with analytical solutions to two problems. The first is the (1+1)-coupled Jaulent-Miodek system of equations, which is associated with the energy-dependent Schrödinger potential, whereas the second problem, the system of coupled Konno-Oono equations relates to complexity and chaos in electromagnetic fields. Similarity reductions via Lie-symmetry analysis is performed for the systems to derive their analytical solutions. Since Lie symmetry involves arbitrary constants in the infinitesimals, this opens up more possibilities for getting a rich variety of analytical solutions for both real-life problems. The analytical solutions are supplemented graphically to understand them in a better way. Traveling wave profiles are obtained eventually. Solution for CKOEs are different from the earlier research (Kumar and Kumar 2022a; Kumar *et al.* 2022) as far as the authors are aware.

KEYWORDS
CKOEs
JMEs
Lie-symmetry analysis
Traveling wave solutions
Chaos

INTRODUCTION

During the last few decades, interest in solving nonlinear systems of partial differential equations has increased. Nonlinear partial differential equations (NPDEs) are used in many different scientific disciplines to describe the motion of specific waveforms. In physics, for example, NPDEs can be used to study complexity in electromagnetic fields, chaos theory (Karaca and Baleanu 2022; Karaca 2023) shallow-water wave propagation, oceanic research and engineering, material science, optics, and many other fields. The appearance of NPDEs is cause for serious concern when research numerical results are physically defined. The energy-dependent Schrödinger potential and electromagnetic fields have a connection to this occurrence.

An adequate literature review (Jaulent and Miodek 1976; Zhou 1997; Özer and Salihoğlu 2007; Xu *et al.* 2014) that includes historical context, various sorts of solutions, and employed methodologies is presented for the following form of Jaulent-Miodek equations (JMEs).

$$3u\frac{\partial u}{\partial x}+\frac{\partial u}{\partial t}-2\frac{\partial v}{\partial x}=0,\ \text{and}\ 4v\frac{\partial u}{\partial x}-2u\frac{\partial v}{\partial x}-\frac{\partial^3 u}{\partial x^3}+2\frac{\partial v}{\partial t}=0, \tag{1}$$

where the wave components in space are denoted by the variables $u(x,t)$ and $v(x,t)$, and both of these variables depend on time t as well. Another form of JMEs is as follows:

$$\frac{\partial u}{\partial t}+\frac{\partial^3 u}{\partial x^3}+\frac{3}{2}v\frac{\partial^3 v}{\partial x^3}+\frac{9}{2}\frac{\partial v}{\partial x}\frac{\partial^2 v}{\partial x^2}-6u\frac{\partial u}{\partial x}-6uv\frac{\partial v}{\partial x}-\frac{3}{2}v^2\frac{\partial u}{\partial x}=0,$$
$$\text{and}\ \frac{\partial v}{\partial t}+\frac{\partial^3 v}{\partial x^3}-6v\frac{\partial u}{\partial x}-6u\frac{\partial v}{\partial x}-\frac{15}{2}v^2\frac{\partial v}{\partial x}=0. \tag{2}$$

This form of JMEs was also tried by the authors to be solved analytically by using Lie symmetry, but its reduction could not be further solved. It opens the door for further research in this field.

Some more literature review for the JMEs (1) is also presented. The JMEs (1) were first introduced by (Jaulent and Miodek 1976) using the inverse scattering transform, which associates with the energy-dependent Scrödinger potential (Özer and Salihoğlu 2007). The finite-band solution of the JMEs (1) can be obtained through nonlinearization of the Lax pair (Zhou 1997). Darboux transformation (Xu *et al.* 2014) for the JMEs (1) yields some accurate solutions like a kink- and bell-type solitons. These results are based on the Lax pair of the JMEs spectral issue.

Manuscript received: 5 July 2023,
Revised: 23 August 2023,
Accepted: 27 August 2023.

[1]rsoniraj2@gmail.com
[2]kripa5881@gmail.com
[3]avnee2864@gmail.com
[4]anshu.kumar@sharda.ac.in (**Corresponding author**)

In this research, second problem *i.e.* coupled Konno-Oono Equations (CKOEs) is also solved by employing Lie-symmetry analysis (Konno and Oono 1994). The general form of the CKOEs is represented by

$$\begin{aligned}
&\frac{\partial^2 u}{\partial x \partial t} - (2\alpha u - \gamma w)\frac{\partial v}{\partial x} - (2\beta u - \gamma v)\frac{\partial w}{\partial x} = 0,\\
&\frac{\partial^2 v}{\partial x \partial t} + 2(2\beta u - \gamma u)\frac{\partial u}{\partial x} - 2(\alpha v - \beta w)\frac{\partial v}{\partial x} = 0, \text{ and}\\
&\frac{\partial^2 w}{\partial x \partial t} + 2(2\alpha u - \gamma w)\frac{\partial u}{\partial x} + 2(\alpha v - \beta w)\frac{\partial w}{\partial x} = 0.
\end{aligned} \tag{3}$$

where the wave components in space are denoted by the variables $u(x,t)$, $v(x,t)$ and $w(x,t)$, all of these variables depend on x and time t, while α, β and γ are parameters. The CKOEs are classified as Coupled Integrable Dispersionless (CID) equations (Pan and Yan 2010; Souleymanou *et al.* 2012). The CKOEs describe how a string moves in a three-dimensional space when interacting with a magnetic field surrounding it. Each point on the curve along the time direction appears to be transiting in parallel in a magnetic-field (Konno and Oono 1994; Konno and Kakuhata 1995; Souleymanou *et al.* 2012).

Another particular forms of the CKOEs (3) are discussed in (Pan and Yan 2010; Souleymanou *et al.* 2012; Konno and Kakuhata 1995) and derived assuming particular values of α and β as zero while $\gamma = 1$ and recasts as:

$$\begin{aligned}
&\frac{\partial^2 u}{\partial x \partial t} + w\frac{\partial v}{\partial x} + v\frac{\partial w}{\partial x} = 0, \ \frac{\partial^2 v}{\partial x \partial t} - 2v\frac{\partial u}{\partial x} = 0, \text{ and}\\
&\frac{\partial^2 w}{\partial x \partial t} - 2\gamma w\frac{\partial u}{\partial x} = 0.
\end{aligned} \tag{4}$$

Under the conditions u takes value u_0 when v tends to 0 and $|x|$ tends to ∞, this kind of CKOEs can be resolved by the inverse scattering method (ISM) and satisfies the conservation law (Konno and Oono 1994; Kakuhata and Konno 1996; Konno and Kakuhata 1996). As these requirements are satisfied with the proper conversion in (5), the solution of CKOEs gradually resembles as Sine-Gordon's solutions and Pohlmeyer-Lund-Regge equations (Pan and Yan 2010; Konno and Kakuhata 1996; Hirota and Tsujimoto 1994).

Furthermore, a form of CKOEs in which only u and v appears can be discussed as

$$\frac{\partial u}{\partial t} + 2v\frac{\partial v}{\partial x} = 0, \text{ and } \frac{\partial^2 v}{\partial x \partial t} - 2uv = 0, \tag{5}$$

Konno and Oono (1994) derived the system (5) after replacing R_x, S, T, α, β and γ by $-iu, iv, iv, 0, 0, 1$ respectively into the following integrable PDEs

$$\begin{aligned}
&i\frac{\partial^2 R}{\partial x \partial t} + (2\alpha R + \gamma T)\frac{\partial S}{\partial x} + (2\beta + \gamma)S\frac{\partial T}{\partial x} = 0,\\
&i\frac{\partial^2 S}{\partial x \partial t} + 2(2\beta R + \gamma B)\frac{\partial R}{\partial x} - 2(\alpha S - \beta T)\frac{\partial S}{\partial x} = 0, \text{ and}\\
&i\frac{\partial^2 T}{\partial x \partial t} + 2(2\beta R + \gamma T)\frac{\partial R}{\partial x} - 2(\alpha T - \beta S)\frac{\partial T}{\partial x} = 0.
\end{aligned} \tag{6}$$

Furthermore, the stochastic form of CKOEs (Mohammed *et al.* 2021) is given by

$$\frac{\partial u}{\partial t} + 2v\frac{\partial v}{\partial x} = 0, \text{ and } \frac{\partial^2 v}{\partial x \partial t} - 2uv = \sigma F(\nu), \tag{7}$$

where the noise term, $F(\nu)$ is a function of strength (σ) of noise. CKOEs (5) can be obtained by Eq. (7) if σ vanishes.

Some tools/methods such as ISM (Konno and Oono 1994; Kakuhata and Konno 1996), classical Lie-symmetry (Khalique 2012), G'/G-expansion and tanh (Abdullah *et al.* 2023), and some others (Khan and Akbar 2013; Alam and Belgacem 2016; Yel *et al.* 2017; Mohammed *et al.* 2021) are used for solving CKOEs (3) in their various forms.

Khalique (2012) used similarity reduction to solve the CKOEs (3), and obtained kink type solutions. Abdullah *et al.* (2023) derived rational, trigonometric and hyperbolic solutions. Zahran and Bekir (2023) got W-shaped, singular dark solitons type solutions. Mohammed *et al.* (2021) and Wang and Liu (2022) obtained solitary wave type solutions, whereas in our previous contributions (Kumar and Kumar 2022a; Kumar *et al.* 2022) optimal sub-algebra utilizing killing form is exploited and derived some initial traveling wave solutions for the same form of the CKOEs (3). Besides the work of (Khalique 2012), and authors (Kumar *et al.* 2022) a group of researchers (Bashar *et al.* 2016; Khan and Akbar 2013) has solved some specific forms of the CKOEs (5) and obtained more traveling wave solutions.

The research conducted by Torvattanabun *et al.* (2018) derived both trigonometric and hyperbolic solutions. The hyperbolic, trigonometric, and rational types were obtained by Alam and Belgacem (2016), whereas Khater *et al.* (2018) derived travelling and solitary wave type solutions. The hyperbolic and trigonometric wave types were derived by Mirhosseini-Alizamini *et al.* (2020). The results of Manafian *et al.* (2018) were hyperbolic, elliptic, and solitons. Solitons were obtained by Yel *et al.* (2017), whilst solutions in the form of travelling waves were obtained by Koçak *et al.* (2016). In addition, CKOEs (5) are solved by Abdelrahman and Alkhidhr (2020) that contain solitary type solutions.

Above reviews motivate to derive some novel variety of solutions for JMEs (1), and CKOEs (3).

INFINITESIMALS *VIA* LIE-SYMMETRY ANALYSIS

In this section, infinitesimals of the JMEs (1) and CKOEs (3) are derived by using one parameter Lie group similarity transformations method (STM). Such transformations can be treated as:

$$\begin{aligned}
&x^* \to x + \epsilon\,\xi(\Xi) + o(\epsilon^2),\ t^* \to t + \epsilon\,\tau(\Xi) + o(\epsilon^2),\\
&u^* \to u + \epsilon\,\eta^{(u)}(\Xi) + o(\epsilon^2),\ v^* \to v + \epsilon\,\eta^{(v)}(\Xi) + o(\epsilon^2), \text{ and}\\
&\frac{\partial u^*}{\partial x^*} \to \frac{\partial u}{\partial x} + \epsilon\,[\eta_x^{(u)}] + o(\epsilon^2) \text{ etc.}
\end{aligned} \tag{8}$$

where ξ, τ, $\eta^{(u)}$ and $\eta^{(v)}$ are the infinitesimals for x, t, u and v respectively and $(\Xi) \equiv (u, v, x, t)$.

Let $u = \theta^{(u)}(x,t)$, and $v = \theta^{(v)}(x,t)$ be the solutions for JMEs (1), then its invariance conditions are

$$\begin{aligned}
&[\eta_t^{(u)}] + 3\theta_x^{(u)}\,\theta^{(u)} + 3\,u\,[\eta_x^{(u)}] - 2[\eta_x^{(v)}] = 0, \text{ and}\\
&2[\eta_t^{(v)}] + 4\theta_x^{(u)}\,\theta^{(v)} + 4v\,[\eta_x^{(u)}] - 2\theta_x^{(v)}\,\theta^{(u)} - 2u\,[\eta_x^{(v)}] - [\eta_{xxx}^{(u)}] = 0.
\end{aligned} \tag{9}$$

One can follow the textbooks (Bluman and Cole 1974; Olver 1993) and research articles (Kumar and Kumar 2022a,b; Kumar *et al.* 2023) for getting the values of the extensions $[\eta_x^{(1)}]$, $[\eta_{xx}^{(1)}]$, and $[\eta_{xxx}^{(1)}]$ etc. Making use of Eq. (1) into Eq. (9) which gives

$$\begin{aligned}
&\tau_u = \tau_v = \tau_x = 0,\ \tau_{tt} = 0,\ \xi_u = \xi_v = \xi_t = 0,\ 2\xi_x = \tau_t, \xi_{xx} = 0,\\
&2\eta_u^{(1)} = -u\tau_t, \text{ and } \eta_v^{(2)} = -v\tau_t.
\end{aligned} \tag{10}$$

The resulting infinitesimal generators for Eq. (1) can be derived by solving the above determining Eqs. (10).

$$\xi = a_1 x + a_2,\ \tau = 2a_1 t + a_3,\ \eta^{(u)} = -a_1 u, \text{ and } \eta^{(v)} = -2a_1 v. \tag{11}$$

where all $a_i's$ are arbitrary constants.

Similarly for CKOEs (3), the infinitesimals are as follows:

$$\xi = 2c_1 x + c_2,\ \tau = -c_1 t + c_3,\ \eta^{(u)} = c_1 u,\ \eta^{(v)} = c_1 v,\ \text{and}$$
$$\eta^{(w)} = c_1 w. \tag{12}$$

where $c_i's$ are arbitrary constants.

SIMILARITY REDUCTIONS AND INVARIANT SOLUTIONS

Jaulent-Miodek equations

Case 1: For $a_1 \neq 0$, the Eq. (11) provides,

$$\frac{dx}{x + A_1} = \frac{dt}{2t + A_2} = -\frac{du}{u} = -\frac{dv}{2v}, \tag{13}$$

On solving above, similarity variable is given as $X_1 = (x + A_1)(2t + A_2)^{-\frac{1}{2}}$ and similarity functions $u = (2t + A_2)^{-\frac{1}{2}} F_1(X_1)$, and $v = (2t + A_2)^{-1} G_1(X_1)$, where $A_1 = \frac{a_2}{a_1}$, and $A_2 = \frac{a_3}{a_1}$. Treating $G_1 = F_1$, similarity reduction of JMEs (1) yield the following ODE:

$$\bar{\bar{\bar{F}}}_1 - 6F_1^2 \bar{F}_1 + 9X_1 F_1 \bar{F}_1 + F_1^2 - 2X_1^2 \bar{F}_1 - 2X_1 F_1 - 4C_1 \bar{F}_1 = 4C_1, \tag{14}$$

where C_1 is an integration constant.

On solving Eq. (14), one can find

$$F_1 = X_1 \pm \sqrt{X_1^2 + 4C_1}, \tag{15}$$

So, the first solution of JMEs (1) is

$$u_1 = \frac{1}{(2t + A_2)}\left[(x + A_1) \pm \sqrt{(x + A_1)^2 + 4C_1(2t + A_2)}\right], \text{and}$$
$$v_1 = \frac{(x + A_1)}{2(2t + A_2)^2}\left[(x + A_1) + \sqrt{(x + A_1)^2 + 4C_1(2t + A_2)}\right]$$
$$+ \frac{4C_1}{(2t + A_2)}. \tag{16}$$

Case 2: For $a_1 = 0$ and $a_3 \neq 0$, Lagrange's characteristic equations for the Eq. (11) recasts as

$$\frac{dx}{B} = \frac{dt}{1} = \frac{du}{0} = \frac{dv}{0}, \tag{17}$$

where $B = \frac{a_2}{a_3}$. On integrating, one can get similarity forms as $X_2 = \frac{1}{B}(x - t)$ and $u = F_2(X_2)$, and $v = G_2(X_2)$.

Hence, similarity reduction of JMEs (1) is represented by the following ODE (for $F_2 = G_2$).

$$\bar{\bar{\bar{F}}}_2 - B^4 \bar{F}_2 + 6B^3 F_2 \bar{F}_2 - 6B^2 F_2^2 \bar{F}_2 - 2B^2 C_2 F_2 = 0, \tag{18}$$

where integration constant is C_2.

Eq. (18) is satified by

$$F_2 = \frac{1}{2}B \pm \frac{1}{2}\sqrt{B^2 - 4C_2}\tanh\left(\pm C_3 + \frac{1}{2}\sqrt{B^2 - 4C_2}\, BX_2\right). \tag{19}$$

So, another solution of JMEs (1) is given by

$$u_2 = \frac{1}{2}B \pm \frac{1}{2}\sqrt{B^2 - 4C_2}\tanh\left(\pm C_3 + \frac{1}{2}\sqrt{B^2 - 4C_2}\, BX_2\right) \text{ and}$$
$$v_2 = -\frac{9}{16}B^2 + \frac{3}{16}(B^2 - 4C_2)\tanh^2\left(\pm C_3 + \frac{1}{2}\sqrt{B^2 - 4C_2}\, BX_2\right)$$
$$- \frac{3}{8}B\sqrt{B^2 - 4C_2}\tanh\left(\pm C_3 + \frac{1}{2}\sqrt{B^2 - 4C_2}\, BX_2\right) + C_3. \tag{20}$$

where C_3 is an integration constant.

Coupled Konno-Oono equations

The Lie algebra L^3 can be generated by L_is $(1 \leq i \leq 3)$ in which $L_1 = \frac{\partial}{\partial x}$, $L_2 = \frac{\partial}{\partial t}$, and $L_3 = 2x\frac{\partial}{\partial x} - t\frac{\partial}{\partial t} + u\frac{\partial}{\partial u} + v\frac{\partial}{\partial v} + w\frac{\partial}{\partial w}$. Thus symmetry reductions of the CKOEs (3) are as follows.

Case 1: The symmetry generator $\mu_1 L_1 + L_2$ gives rise to the group-invariant solution $u = U(X), v = V(X)$, and $w = W(X)$; in which $X = x - \mu_1 t$ is an invariant of the symmetry $\mu_1 L_1 + L_2$, where μ_1 is an arbitrary constant. Substituting these values into (3) yields the system of ODEs as

$$\mu_1 U'' + 2\alpha V' U + 2\beta W' U - \gamma V' W - \gamma W' V = 0,$$
$$\mu_1 V'' + 2\alpha V' V - 4\beta U' U - 2\beta V' W + 2\gamma U' V = 0, \text{ and}$$
$$\mu_1 W'' - 4\alpha U' U - 2\alpha W' V + 2\beta W' W + 2\gamma U' W = 0. \tag{21}$$

After solving the above system of reduction, following variety of solutions can be obtained

$$u_1 = 0,\ v_1 = \tanh C_1\alpha(x - \mu_1 t),\ w_1 = 0. \tag{22}$$

$$u_2 = \frac{\gamma}{2\alpha}\Big(C_1(x - \mu_1 t) + C_2\Big),\ v_2 = \frac{\beta}{\alpha}\Big(C_1(x - \mu_1 t) + C_2\Big),$$
$$w_2 = C_1(x - \mu_1 t) + C_2. \tag{23}$$

$$u_3 = \frac{\gamma}{\mu_1\alpha^2(\gamma^2 + 4\alpha\beta)}\tanh\Big(\frac{1}{2}C_3(x - \mu_1 t) + C_2\Big)C_3,$$
$$v_3 = -\frac{1}{2}\frac{\gamma^2}{\mu_1\alpha^2(\gamma^2 + 4\alpha\beta)}\tanh\Big(\frac{1}{2}C_3(x - \mu_1 t) + C_2\Big)C_3,$$
$$w_3 = \frac{2}{\mu_1\alpha(\gamma^2 + 4\alpha\beta)}\tanh\Big(\frac{1}{2}C_3(x - \mu_1 t) + C_2\Big)C_3. \tag{24}$$

Case 2: The symmetry operator $\mu_2 L_1 + L_2 + \mu_3 L_3$ (where μ_2 and μ_3 are arbitrary constants) provides group-invariant solution of the form $u = U(X) + \mu_3\gamma t$, $v = V(X) + 2\mu_3\beta t$, $w = W(X) + 2\mu_3\alpha t$ where $X = x - \mu_2 t$ is an invariant of $\mu_2 H_1 + H_2 + \mu_3 H_3$ and the functions U, V and W satisfy the same reductions as given in Eq. (21), but solutions are different due to different similarity forms.

So, solution is given by

$$u_4 = 0,\ v_4 = \tanh(x - \mu_2 t)C_1\alpha + 2\mu_2\gamma t,\ w_4 = 0. \tag{25}$$

$$u_5 = \frac{\gamma C_1}{2\alpha} + \mu_t\gamma t,\ v_5 = C_1 + 2\mu_2\beta t,\ w_5 = C_1 + 2\mu_2\alpha t. \tag{26}$$

$$u_6 = \frac{\gamma}{2\alpha}\{C_1(x - \mu_2 t) + C_2\} + 2\mu_2\alpha t,$$
$$v_6 = \frac{\beta}{\alpha}\{C_1(x - \mu_2 t) + C_2\} + 2\mu_2\beta t,$$
$$w_6 = C_1(x - \mu_2 t) + C_2 + \mu_2\gamma t. \tag{27}$$

$$u_7 = \frac{\gamma}{\mu_2\alpha^2(\gamma^2 + 4\alpha\beta)}\tanh\Big(\frac{1}{2}C_3(x - \mu_2 t) + C_2\Big)C_3 + \mu_2\gamma t,$$
$$v_7 = -\frac{\gamma^2}{2\mu_2\alpha^2(\gamma^2 + 4\alpha\beta)}\tanh\Big(\frac{1}{2}C_3(x - \mu_2 t) + C_2\Big)C_3 + 2\mu_2\beta t,$$
$$w_7 = \frac{2}{\mu_2\alpha(\gamma^2 + 4\alpha\beta)}\tanh\Big(\frac{1}{2}C_3(x - \mu_2 t) + C_2\Big)C_3 + 2\mu_2\alpha t. \tag{28}$$

PHYSICAL ANALYSIS AND DISCUSSION

Two analytic solutions for the JMEs (1) are represented by the expressions (16) and (20) while seven analytic solutions for the CKOEs (3) are expressed by Eqs. (22)–(28). The solution profiles are shown which have different animation behaviour. The stationary-progressive profile of the JMEs is shown via the Figs. (1) and progressive, traveling and stationary-progressive profiles for the CKOEs (3) are given by Figs. (2)-(4). A progressive wave is a wave that conveys energy and momentum from one region of space to another. The numerical simulation is performed with the help of MATLAB. The space and the time ranges are taken as $-25 \geq x \leq 25$ and $0 < t \leq 50$ respectively for each profile. For all profiles of the CKOEs (3), the arbitrary constants involved in the solutions are chosen as $C = C_1 = C_2 = C_3 = \mu_1 = \mu_2 = 1.25$ and $\alpha = 0.95$, and $\beta = \gamma = 1.50$. For all the JMEs profiles, the arbitrary constants are taken as $a_1 = 0.4387, a_2 = 0.3816, a_3 = 0.7655$, and $A_1 = 0.3804$, $A_2 = 0.4217$ and $A_3 = 0.7537$.

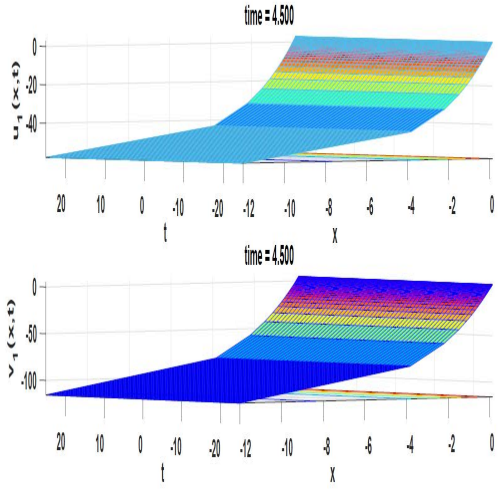

Figure 1 Stationary-progressive profile for the solution (16)

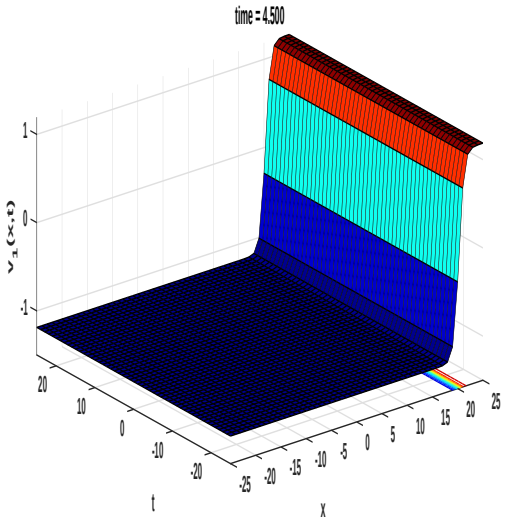

Figure 2 Progressive profile for the solution (22)

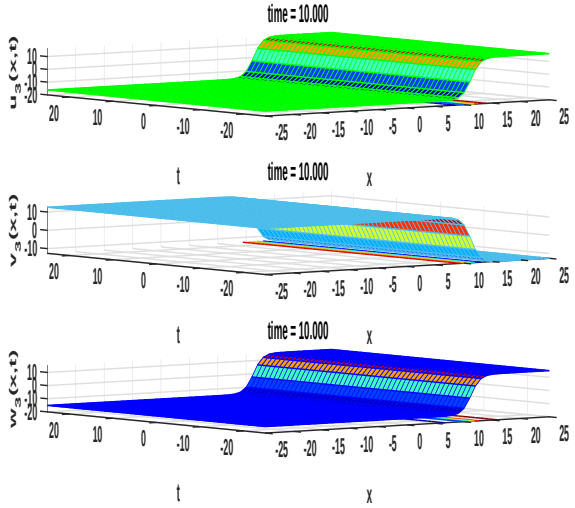

Figure 3 Traveling wave profile for the solution (25)

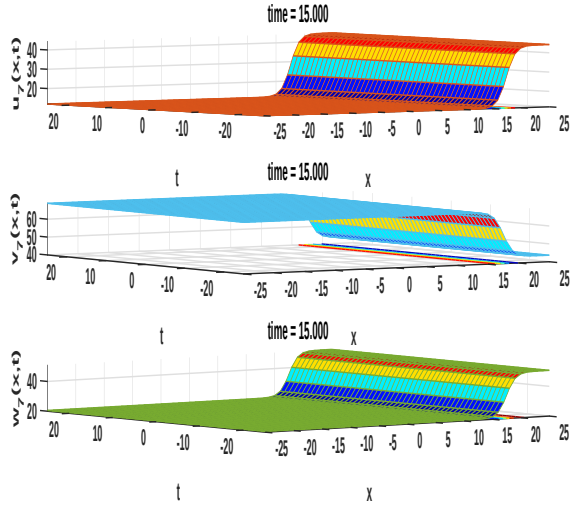

Figure 4 Stationary-progressive profile for the solution (28)

CONCLUSION

The Lie-symmetry analysis is successfully explored to obtain seven analytic solutions for the CKOEs (3) and two analytic solutions for the JMEs (1). Solutions of JMEs are given by Eqs. (16) and (20), while solutions to CKOEs (3) are represented by Eqs. (22)- (28). Mathematical expressions are explored physically as stationary-progressive and progressive profiles for the solutions (16) and (20) are depicted in Figure 1 and Figure 2 respectively. The progressive, traveling and stationary-progressive profiles for the CKOEs (3) are given by Figures (2)-(4). The solutions established here can explore some more applications in the fields of chaos and the complexities of the magnetic field since they provide a realistic perspective.

Acknowledgments

Authors convey sincere thanks to accept this research in the proceedings of the conference ICAIM-2023 organised by Sharda University, Grater Noida, India and exploring this research in the field of Chaos, theory and their applications.

Availability of data and material

Not applicable.

Conflicts of interest

The authors declare that there are no competing interests in the publication of this research.

LITERATURE CITED

Abdelrahman, M. and H. Alkhidhr, 2020 Fundamental solutions for the new coupled Konno-Oono equation in magnetic field. Results Phys. **19**: 103445.

Abdullah, F. A., M. T. Islam, J. F. Gómez-Aguilar, and M. A. Akbar, 2023 Impressive and innovative soliton shapes for nonlinear Konno–Oono system relating to electromagnetic field. Opt. Quantum Electron. **55**: 69.

Alam, M. N. and F. B. M. Belgacem, 2016 New generalized (G′/G)-expansion method applications to coupled Konno-Oono equation. Adv. Pure Math. **06**: 168–179.

Bashar, M. A., G. Mondal, K. Khan, and A. Bekir, 2016 Traveling wave solutions of new coupled konno-oono equation. New Trends in Mathematical Sciences **4**: 296–303.

Bluman, G. and J. Cole, 1974 *Similarity Methods for Differential Equations*. Springer New York.

Hirota, R. and S. Tsujimoto, 1994 Note on "new coupled integrable dispersionless equations". J. Phys. Soc. Japan **63**: 3533–3533.

Jaulent, M. and I. Miodek, 1976 Nonlinear evolution equations associated with energy dependent schrödinger potentials. Lett. Math. Phys. **1**: 243–250.

Kakuhata, H. and K. Konno, 1996 A Generalization of Coupled Integrable, Dispersionless System. J. Phys. Soc. Japan **65**: 340–341.

Karaca, Y., 2023 Computational complexity-based fractional-order neural network models for the diagnostic treatments and predictive transdifferentiability of heterogeneous cancer cell propensity. Chaos Theory and Applications **5**: 34–51.

Karaca, Y. and D. Baleanu, 2022 Evolutionary mathematical science, fractional modeling and artificial intelligence of nonlinear dynamics in complex systems. Chaos Theory and Applications **4**: 111–118.

Khalique, M., 2012 Exact solutions and conservation laws of a coupled integrable dispersionless system. Filomat **26**: 957–964.

Khan, K. and M. A. Akbar, 2013 Traveling Wave Solutions of Some Coupled Nonlinear Evolution Equations. ISRN Math. Phys. **2013**: 1–8.

Khater, M. M., A. R. Seadawy, and D. Lu, 2018 Dispersive solitary wave solutions of new coupled Konno-Oono, Higgs field and Maccari equations and their applications. J. King Saud Univ. - Sci. **30**: 417–423.

Koçak, Z. F., H. Bulut, D. A. Koc, and H. M. Baskonus, 2016 Prototype traveling wave solutions of new coupled Konno-Oono equation. Optik (Stuttg). **127**: 10786–10794.

Konno, K. and H. Kakuhata, 1995 Interaction Among Growing, Decaying and Stationary Solitons for Coupled Integrable Dispersionless Equations. J. Phys. Soc. Japan **64**: 2707–2709.

Konno, K. and H. Kakuhata, 1996 Novel solitonic evolutions in a coupled integrable, dispersionless system. J. Phys. Soc. Japan **65**: 713–721.

Konno, K. and H. Oono, 1994 New Coupled Integrable Dispersionless Equations. J. Phys. Soc. Japan **63**: 377–378.

Kumar, R. and A. Kumar, 2022a Dynamical behavior of similarity solutions of CKOEs with conservation law. Appl. Math. Comput. **422**: 126976.

Kumar, R. and A. Kumar, 2022b Some invariant solutions of coupled Konno-Oono equations arising in electromagnetic and quantum fields. Phys. Scr. **97**: 075501.

Kumar, R., K. Pandey, and A. Kumar, 2022 Dynamical Behavior of the Solutions of Coupled Boussinesq–Burgers Equations Occurring at the Seaside Beaches. Brazilian J. Phys. **52**: 201.

Kumar, R., R. Verma, and A. Tiwari, 2023 On similarity solutions to (2+1)-dispersive long-wave equations. J. Ocean Eng. Sci. **8**: 111–123.

Manafian, J., I. Zamanpour, and A. Ranjbaran, 2018 On some new analytical solutions for new coupled Konno–Oono equation by the external trial equation method. J. Phys. Commun. **2**: 015023.

Mirhosseini-Alizamini, S. M., H. Rezazadeh, K. Srinivasa, and A. Bekir, 2020 New closed form solutions of the new coupled Konno–Oono equation using the new extended direct algebraic method. Pramana **94**: 52.

Mohammed, W. W., N. Iqbal, A. Ali, and M. El-Morshedy, 2021 Exact solutions of the stochastic new coupled Konno-Oono equation. Results Phys. **21**: 103830.

Olver, P., 1993 *Applications of Lie groups to differential equations*, volume 107. Springer Science & Business Media.

Özer, H. and S. Salihoğlu, 2007 Nonlinear Schrödinger equations and N=1 superconformal algebra. Chaos, Solitons & Fractals **33**: 1417–1423.

Pan, B. T. L. W. Q. Q.-X., W. and J. Yan, 2010 Conservation laws and analytic soliton solutions for coupled integrable dispersionless equations with symbolic computation. Commun. Theor. Phys. **54**: 687–696.

Souleymanou, A., V. K. Kuetche, T. B. Bouetou, and T. C. Kofane, 2012 Traveling Wave-Guide Channels of a New Coupled Integrable Dispersionless System. Commun. Theor. Phys. **57**: 10–14.

Torvattanabun, M., P. Juntakud, A. Saiyun, and N. Khansai, 2018 The new exact solutions of the new coupled Konno-Oono equation by using extended simplest equation method. Appl. Math. Sci. **12**: 293–301.

Wang, K.-J. and J.-H. Liu, 2022 Study on abundant analytical solutions of the new coupled Konno–Oono equation in the magnetic field. Open Phys. **20**: 390–401.

Xu, G. *et al.*, 2014 N-fold darboux transformation of the jaulent-miodek equation. Applied Mathematics **5**: 2657.

Yel, G., H. M. Baskonus, and H. Bulut, 2017 Novel archetypes of new coupled Konno–Oono equation by using sine–Gordon expansion method. Opt. Quantum Electron. **49**: 285.

Zahran, E. and A. Bekir, 2023 New diverse soliton solutions for the coupled konno-oono equations. Optical and Quantum Electronics **55**: 1–12.

Zhou, R., 1997 The finite-band solution of the Jaulent–Miodek equation. J. Math. Phys. **38**: 2535–2546.

How to cite this article: Kumar, R., Pandey, K. S., Kumar, A., and Kumar, A. Novel Traveling Wave Solutions of Jaulent-Miodek Equations and Coupled Konno-Oono Systems and Their Dynamics. *Chaos Theory and Applications*, 5(4), 281-285, 2023.

CHAOS
Theory and Applications
in Applied Sciences and Engineering

e-ISSN: 2687-4539
RESEARCH ARTICLE
Vol.5 / No.4 / 2023 / pp.286-292
Special Issue
https://doi.org/10.51537/chaos.1320430

Study of Fixed Points and Chaos in Wave Propagation for the Generalized Damped Forced Korteweg-de Vries Equation using Bifurcation Analysis

Shruti Tomar *,1 **and Naresh M. Chadha** *,2
*School of Physical Sciences, DIT University, Dehradun, Uttarakhand, India.

ABSTRACT In this article, we consider the Generalized Damped Forced Korteweg-de Vries (GDFKdV) equation. The forcing term considered is of the form $F(U) = U(U - v_1)(U - v_2)$, where v_1 and v_2 are free parameters. We investigate the behaviour of fixed points evaluated for the corresponding dynamical system of our model problem. With respect to these fixed points, we investigate the effects of a few significant parameters involved in the model, namely, the free parameters v_1 and v_2, the nonlinear, dispersion and damping coefficients using the tools from bifurcation analysis. We also obtain the wave plots for the critical values of the nonlinear and dispersion coefficients for which the system becomes unstable and exhibit chaotic behaviour. We confirm the chaos in our dynamical system under various conditions with the help of Lyapunov exponents.

KEYWORDS
GDFKdV equation
Nonlinear dynamics
Chaos
Wave propagation
Lyapunov exponent
Phase portraits

INTRODUCTION

In dispersive media, weakly non-linear long wave propagation is described by the universal mathematical model KdV. It is also used as a model to examine several quantum mechanics-related phenomena in theoretical physics. In many real-world applications, it is recognized that higher-order non-linearity should be included in the KdV equation in order to explain the physical phenomenon, which leads to a more generalised KdV equation. This equation accounts for the wide range of applicability; Shallow-water gravity waves, ion-acoustic waves in collisionless plasma, internal waves in the atmosphere and ocean, and waves in bubbly fluids are only a few examples of the physical uses of the generalized KdV equation (Stuhlmeier 2009; Khater 2022; Vasavi *et al.* 2021; Crighton 1995).

In this article, we study the Generalized Korteweg-de Vries (GKdV) equation with damping and external force of the following form

$$U_t + PU^n U_x + QU_{xxx} + SU = \gamma F(U, x, t, v_i), \tag{1}$$

where U denotes the excitation, t, x denote time, and space coordinates, respectively. P, Q, and S denote coefficients of nonlinearity, dispersion, damping, respectively; n is the exponent which controls the non-linearity. The coefficients P and Q, which can either be constants or functions of x and t, are determined by the characteristics of the medium. The Generalized KdV equation describes the combined effect of the basic long wave dispersion (U_{xxx}) and, ($U^n U_x, n > 0$) which has the same form as that in the KdV or 1-dimensional Navier-Stokes equations, stabilizes by transferring energy between large and small scales (Alshenawy *et al.* 2020; Zhang 2014; El 2007). In equation 1, the function F denotes an additional forcing term. The parameter γ is the force coefficient. The range of γ governs the strength of the force field. For instance, for $\gamma > 1$, $\gamma \approx 1$, and $\gamma \ll 1$ the force field can be considered strong, weak or very weak.

In this study, we consider $F(U, x, t, v_i) \equiv F(U) = U(U - v_1)(U - v_2)$. The roots of the polynomial $F(U) = 0$ are $U = 0, v_1$ and v_2. The parameters v_1 and v_2 are referred to as forcing parameters. Under certain conditions imposed on these parameters, the forcing term in its present form may act as an attenuator or amplifier for the solitary waves (Engelbrecht and Peipman 1992). Such forcing terms have been used to study the wave propagation in different media within the framework of a perturbed KdV equation (see for example (Engelbrecht and Khamidullin 1988; Engelbrecht and Peipman 1992; Engelbrecht 1991). See also (Peterson and Salupere 1997; Peterson 1997) for the numerical treatment of the KdV equation with forcing term in cubic polynomial form with periodic boundary conditions and the harmonic initial condition. It is important to

Manuscript received: 27 June 2023,
Revised: 2 September 2023,
Accepted: 3 September 2023.

[1]tomer05shruti@gmail.com
[2]nareshmchadha@gmail.com (**Corresponding author**)

note that due to the presence of the forcing term in the model equation 1 does not satisfy the conservation laws.

For $n = 1, 2$, the well-developed techniques are available to obtain the analytical solutions of KdV equation and its variants without forcing term in the right hand side, refer to (Wazwaz 2004; Zuo and Zhang 2011) and references therein. However, for $n \geq 3$, the generalized KdV equation becomes non-integrable. According to (Merle 2001; Bona *et al.* 1987; Hereman and Takaoka 1990; Zabusky 1967), the solutions of GKdV are stable for $n \leq 4$, unstable for $n \geq 6$ and conditionally stable for $n = 5$. Even for the numerical treatment of generalized KdV equation for $n \geq 5$, one has to take a very small mesh width in space or time step in order to obtain an acceptable computed solution. The problem becomes more challenging when $P >> Q$ (Alvarado and Omel'yanov 2012). This poses serious limitations on the conventional analytical and numerical methods. To analyse such intricate non-linear systems, it is desirable to employ tools available in the bifurcation analysis (Guckenheimer and Holmes 2013). Bifurcation analysis is a mathematical framework to study qualitative changes to investigate the unexpected appearance, disappearance, or change in the stability of equilibrium points with respect to certain parameters or perturbations. Bifurcation analysis has long been used to investigate dynamical systems emerging from varied real world problems, refer to (Hilborn *et al.* 2000) and references therein.

Many authors have studied the KdV equation and its variants using bifurcation analysis. Zao Li *et.el*. (Li *et al.* 2021) studied the fractional generalized Hirota–Satsuma coupled KdV equations with the help of bifurcation theory. Yiren Chen and Shaoyong Li (Chen and Li 2021) investigated the generalized KdV-mKdV-like equation with the help of bifurcation analysis; see also (Saha and Chatterjee 2014; Tamang and Saha 2020) for similar studies. To the best of our knowledge in most of these studies, the authors have considered fixed values of the parameters involved in the equations. The novelty of this work presented here is that we have not put any restriction on the range of any of these parameters and investigated the nature of the dynamical system corresponding to the generalized damped forced KdV equation given by equation 1 with respect to all the equilibrium points. In view of the facts mentioned above, we analyse our model problem for $n \geq 3$, $P >> Q$ and various values of S using bifurcation tools. The authors (Chadha *et al.* 2023; Tomar *et al.* 2023; Chen and Li 2021) used bifurcation analysis to study the behaviour of the dynamical system for the equilibrium points and found chaotic behaviours in the Damped Forced KdV and Generalized KdV equations under certain conditions on the parameters involved. The interested reader may also refer to (Haidong *et al.* 2023; Sami *et al.* 2022; Xu *et al.* 2022) for some recent work on fractional order dynamical systems and their applications where the authors have used phase portraits, time series plots, the Lyapunov spectrum and other related tools from the bifurcation analysis to study the chaotic behaviour of the systems.

The organization of this study is as follows: First, we evaluate three different equilibrium points obtained from a three-dimensional dynamical system corresponding to the generalized DFKdV equation. We study the behaviour of these equilibrium points and wave propagation in the dynamical system using the bifurcation analysis. For the first equilibrium point, we investigate the system with respect to the free parameters v_1, v_2, and S. It is important to mention that the other two equilibrium points have locational dependence on v_1, v_2, and S, which further complicates the problem. For these equilibrium points, we investigate the system for $n = 5$ and P and Q ratio up to 10^4. The system exhibits chaotic behaviour. These theoretical findings are confirmed by the wave propagation plots and the Lyapunov exponents. We conclude with our major findings in this study.

BIFURCATION ANALYSIS OF GDFKDV EQUATION

In this section, we investigate the dynamical behaviour of the generalized damped forced KdV equation 1 with forcing term $F(U) = U(U - v_1)(U - v_2)$ and $\gamma = 1$ with respect to the different equilibrium points.

The Generalized DFKdV equation is

$$U_t + PU^n U_x + QU_{xxx} + SU = F(U). \tag{2}$$

Consider a wave transformation,

$$U(x,t) = U(z),\ z = (x - ct). \tag{3}$$

Using the wave transformation in equation 2, we get the ordinary differential equation:

$$-cU_z + PU^n U_z + QU_{zzz} + SU = F(U). \tag{4}$$

Equation 4 can be rewritten as follows

$$\begin{aligned} U' &= V, \\ V' &= W, \\ W' &= \frac{1}{Q}(cV - PU^n V - SU + U(U - v_1)(U - v_2)). \end{aligned} \tag{5}$$

By solving this system of equation, we obtain the equilibrium points $(0,0,0)$, $(h,0,0)$ and $(k,0,0)$, here $h,k = \frac{1}{2}(v_1 + v_2 \mp ((v_1 - v_2)^2 + 4S)^{1/2})$.

For the dynamical system equation 5, the Jacobian matrix is

$$J = \begin{bmatrix} 0 & 1 & 0 \\ 0 & 0 & 1 \\ \frac{-nPU^{n-1}V - S + 3U^2 - 2(v_1+v_2)U + v_1v_2}{Qw_0^2} & \frac{c - PU^n}{Qw_0^2} & 0 \end{bmatrix}$$

Corresponding characteristic equation is

$$\begin{aligned} &\frac{-1}{Q}(QE^3 + (PU^n - c)E + \\ &(S + 2U(v_1 + v_2) - 3U^2 - v_1v_2 + PU^{n-1}V^n) = 0. \end{aligned} \tag{6}$$

The eigenvalues for this system are

$$\begin{aligned} E_1 &= T + \frac{Uc - PUU^n}{3QUT}, \\ E_{2,3} &= -\left(\frac{T}{2} + \frac{Uc - PUU^n}{6QUT}\right) \pm \frac{\sqrt{3}i}{2}\left(T - \frac{Uc - PUU^n}{3QUT}\right). \end{aligned} \tag{7}$$

Here,

$$\begin{aligned} T &= \left(\left(\frac{A}{4Q^2U^2} - \frac{(Uc - PUU^n)^3}{27Q^3U^3}\right)^{1/2} - \frac{A}{2Q^2U^2}\right)^{1/3}, \\ A &= (SU + 2U^2v_1 + 2U^2v_2 + 3U^3 - Uv_1v_2 + PU^nVn)^2. \end{aligned}$$

To study the behaviour of the dynamical system equation 5, it is important to investigate the nature of the eigenvalues for all the equilibrium points.

For a three dimensional system: $(E_1, E_2, E_3) = (-,-,-)$ corresponds to fixed point, $(E_1, E_2, E_3) = (0,0,-)$ corresponds to limit cycle, $(E_1, E_2, E_3) = (0,0,-)$ corresponds to two dimensional annulus, $(E_1, E_2, E_3) = (+,+,-)$ correspond to unstable limit cycle, $(E_1, E_2, E_3) = (+,0,-)$ correspond to strange attractor, $(E_1, E_2, E_3) = (+,0,0)$ corresponds to strange attractor, (Layek *et al.* 2015).

For study of these equilibrium points, this investigation is divided into two sections: at first equilibrium point $(0,0,0)$ and second equilibrium point $(h,0,0)$ and third equilibrium point $(k,0,0)$.

At equilibrium point $(0,0,0)$**:**

The first equilibrium point $(0,0,0)$ is independent of the parameters. In this case, we are investigating the effect of the damping parameter S and the forcing parameters v_1, and v_2. Exactly at the equilibrium point, we could not find any interesting feature worth reporting. So, we take a point $(1e-5, 1e-5, 1e-5)$ which is in the close vicinity of the equilibrium point.

In Figure 1, we have generated the phase portraits which show the quasi-periodic movement in trajectories for the constant value of the parameters $c = 0.7; P = 2; Q = 0.2; v_1 = 0.2; v_2 = 0.5; n = 3$, and $S = 0.15$ in the time interval $0 : \pi/1000 : 6\pi$. The projections in $U-V$, $V-W$, and $U-W$ planes are shown in Figure 1 (a), (b), (c), respectively.

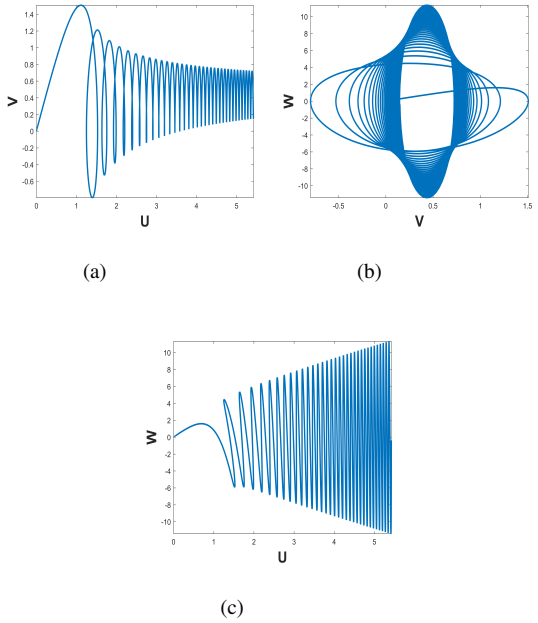

Figure 1 Phase portraits of the dynamical system equation 5 with respect to first equilibrium point $(1e-5, 1e-5, 1e-5)$. Parameters are $c = 0.7; P = 2; Q = 0.2; v_1 = 0.2; v_2 = 0.5; n = 3$, and $S = 0.15$. Time interval is $0 : \pi/1000 : 6\pi$.

Figure 2 $(a), (b)$, and (c) exhibit the quasi-periodic behaviour of two trajectories for the range of parameter $v_1 \in [0.1, 0.97]$; $v_1 = 1.1$ is the break point for the system. These figures are generated for the four representing values from this range, $v_1 = [0.1, 0.8, 0.95, 0.97]$ to show the complete behaviour for the defined range. The value of other parameters are $c = 0.7; P = 2; Q = 0.2; v_2 = 0.5; n = 3$, and $S = 0.15$; time interval considered is $0 : \pi/1000 : 6\pi$. This behaviour of the dynamical system can be justified by the eigenvalues for this equilibrium point, which are given in Table 1. We observe that we have two negative and one positive eigenvalues. Since one of the eigenvalue is always possible for this range of v_1, the equilibrium point will be unstable and system will be weak chaotic. In this forcing term, we have one more parameter v_2 for which we found almost identical behaviour corresponding to v_1. Thus, plots for v_2 are not presented here.

For the damping parameter S, we have investigated the nature of the trajectories for the four representing values from the range of $S \in [0.1, 0.48]$. From Figure 3 $(a), (b)$, and (c), it is evident that the movement of trajectories is quasi-periodic and $S = 0.48$ is the break-point which can be seen in Figure 3 (d). The corresponding behaviour of

Table 1 Eigenvalues of the Jacobian matrix with respect to equilibrium points $(1e-5, 1e-5, 1e-5)$ for $v_1 \in [0.1, 0.97]$. Other parameters are $c = 0.7; P = 2; Q = 0.2; v_2 = 0.5; n = 3$, and $S = 0.15$.

v_1	E_1	E_2	E_3
0.1	1.7948	0.1437	−1.9385
0.8	2.0288	−0.3718	−1.6570
0.95	2.0700	−0.5000	−1.5701
0.97	2.0753	−0.5183	−1.5570

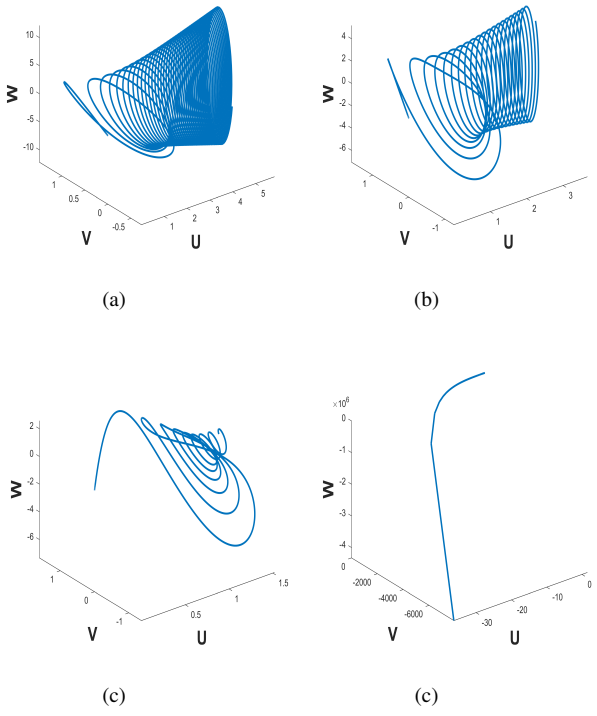

Figure 2 Three dimensional phase portraits of the dynamical system equation 5 with respect to the range value of parameter $v_1 = [0.1, 0.8, 0.95, 0.97]$ are shown for first equilibrium point $(1e-5, 1e-5, 1e-5)$. Parameters are $c = 0.7; P = 2; Q = 0.2; v_2 = 0.5; n = 3$, and $S = 0.15$. Time interval is $0 : \pi/1000 : 6\pi$.

the dynamical system is strongly chaotic, which can be justified by the nature of the eigenvalues shown in Table 2.

Table 2 Eigenvalues of the Jacobian matrix with respect to equilibrium points $(1e-5, 1e-5, 1e-5)$ for $S \in [0.1, 0.48]$. Other parameters are $c = 0.7; P = 2; Q = 0.2; v_2 = 0.5; n = 3$, and $v_1 = 0.2$.

S	E_1	E_2	E_3
0.1	1.7948	0.1437	−1.9385
0.3	1.6009	0.4556	−2.0565
0.45	1.3573	0.7768	−2.1341
0.48	1.2674	0.8813	−2.1487

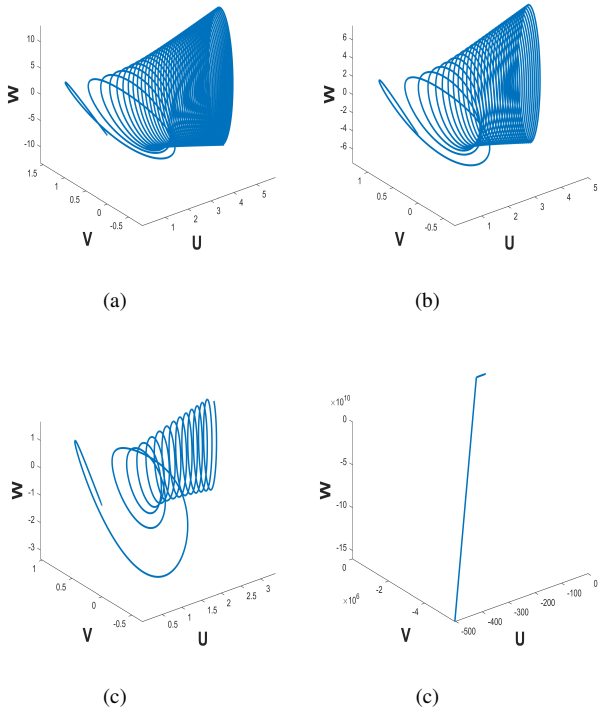

Figure 3 Three dimensional phase portraits of the dynamical system equation 5 with respect to the range value of parameter $S = [0.1, 0.3, 0.45, 0.48]$ are shown for first equilibrium point $(1e-5, 1e-5, 1e-5)$. Parameters are $c = 0.7; P = 2; Q = 0.2; v_2 = 0.5; n = 3$, and $S = 0.15$. Time interval is $0 : \pi/1000 : 6\pi$.

Study of the second equilibrium point $(h,0,0)$ and third equilibrium point $(k,0,0)$ here, $(h,k) \equiv (\frac{1}{2}(v_1 + v_2 \mp ((v_1 - v_2)^2 + 4S)^{1/2})$:

In this case, we investigate the behaviour of the dynamical system equation 5 with respect to the second $(h,0,0)$, and third equilibrium points $(k,0,0)$. These equilibrium points involve other three parameters v_1, v_2, and S. The location of these equilibrium points may vary depending on the range of these parameters.

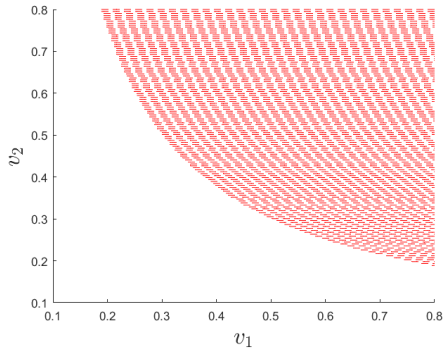

Figure 4 Behaviour of the second equilibrium point of the dynamical system equation 5 for the range the parameters v_1, and v_2. Here $v_1 \in (0.1, 0.8), v_2 \in (0.1, 0.8)$, and $S = 0.5$.

In Figure 4, the coloured portion depicts the nature of the second equilibrium point. Here the boundary of the shaded region shows the conversion of the nature of the equilibrium point from negative to positive. Below the boundary, the value of the equilibrium point is negative and it is positive in the shaded region. From this figure, we get three different ranges for the parameters v_1, and v_2 for which the nature of the second equilibrium point changes from negative to positive and tends to zero at the boundary.

To see the behaviour of the dynamical system for these equilibrium points, we have generated the phase portraits. The Figure $5(a), (b)$, and (c) show the movement of the trajectories in $U-V$, $V-W$, and $U-W$ planes, respectively for the equilibrium point $(h,0,0)$. The values of the parameters involved are as follows: $c = 0.7; P = 2; Q = 0.2; v_1 = 0.01; v_2 = 0.5; n = 3$, and $S = 2$ and taken time interval is $0 : \pi/1000 : 6\pi$.

For the comparison purpose, while studying the nature of the third equilibrium point $(k,0,0)$, we have considered the same parameter values as for the second equilibrium point $(h,0,0)$ and generated few phase portraits. For these same value of the parameters, the behaviour of both the equilibrium points is the same but the location of both the equilibrium points is different. On this basis, the movement in the trajectories is totally different. They are depicted by the phase portraits shown in Figure $6(a), (b)$, and (c).

This generalized DFKdV equation is having two more important parameters: one is the non-linear parameter P and the other one is the dispersion parameter Q. The ratio of these two parameters may significantly affect the nature of the wave propagation for this dynamical system. To see the effect of the ratio of these parameters, we present some wave propagation plots shown in Figure 7 and Figure 8. For the second equilibrium point, the nature of the wave is quasi-periodic for $\frac{P}{Q} = 10^2$, refer to Figure $7(a)$. But when we increase the ratio $\frac{P}{Q} = 10^4$, the oscillations are significantly increased in the waves, and the system becomes chaotic; this is clearly visible in Figure $7(c)$. The value of the parameters considered to generate these plots are as follows: $c = 0.7, v_1 = 0.2; v_2 = 0.5; n = 5$, and $S = 0.5$. Time interval is $0 : \pi/100 : 2\pi$.

For the third equilibrium point, for the same value of the parameters considered for the second equilibrium point, the wave propagation is quasi-periodic; refer to Figure $8(a)$. For a higher ratio of P, and Q, the oscillations become more complex, shown in Figure $8(b)$, and (c). This suggests that the system may be a chaotic system. To confirm this, we use the Lyapunov exponents (Hilborn *et al.* 2000). From Figure $7(d), (e)$, and (f) and Figure $8(d), (e)$, and (f), it is clearly visible that one of the Lyapunov exponent is always positive. This confirms that the system is chaotic.

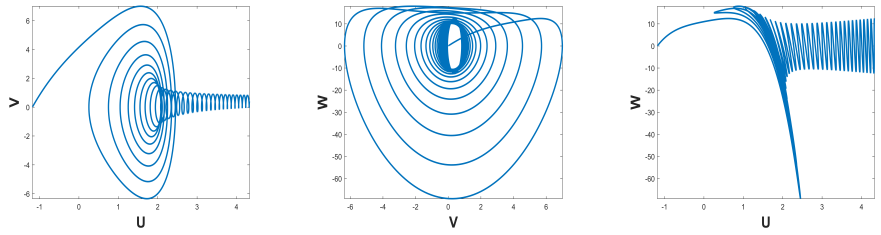

(a) (b) (c)

Figure 5 Phase portraits of the dynamical system equation 5 with respect second equilibrium point $(h, 0, 0)$. Parameters are $c = 0.7; P = 2; Q = 0.2; v_1 = 0.01; v_2 = 0.5; n = 3$, and $S = 2$. Time interval is $0 : \pi/1000 : 6\pi$.

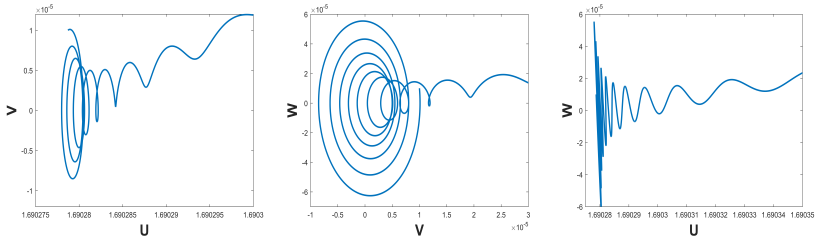

(a) (b) (c)

Figure 6 Phase portraits of the dynamical system equation 5 with the third equilibrium point $(k, 0, 0)$. Corresponding parameters are same as in Figure 5.

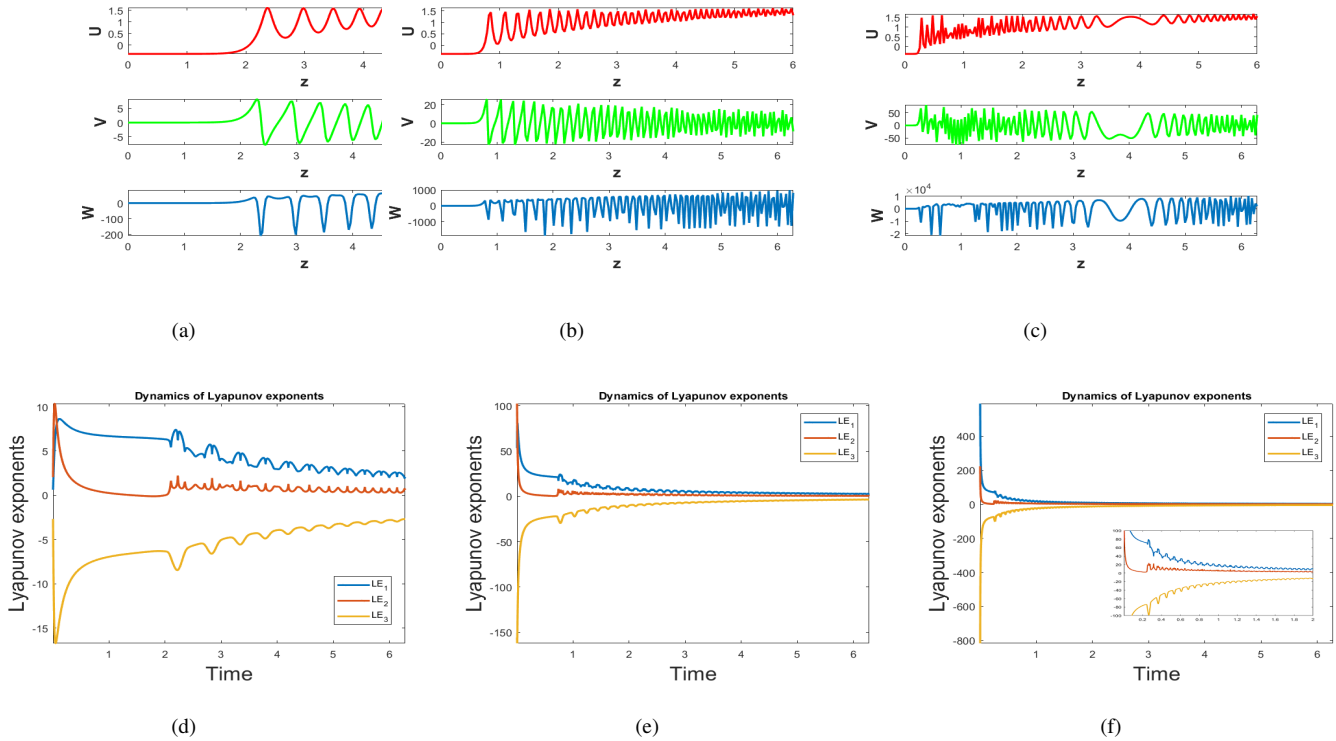

(a) (b) (c)

(d) (e) (f)

Figure 7 Wave propagation and the Lyapunov exponent plots of the dynamical system equation 5 with respect to second equilibrium point $(h, 1e-5, 1e-5)$ for the ratio between non-linear and dispersion parameters. Parameters are $c = 0.7; P = 2; Q = 2 * [1e-2, 1e-3, 1e-4]; v_1 = 0.2; v_2 = 0.5; n = 5$, and $S = 0.5$. Time interval is $0 : \pi/1000 : 2\pi$.

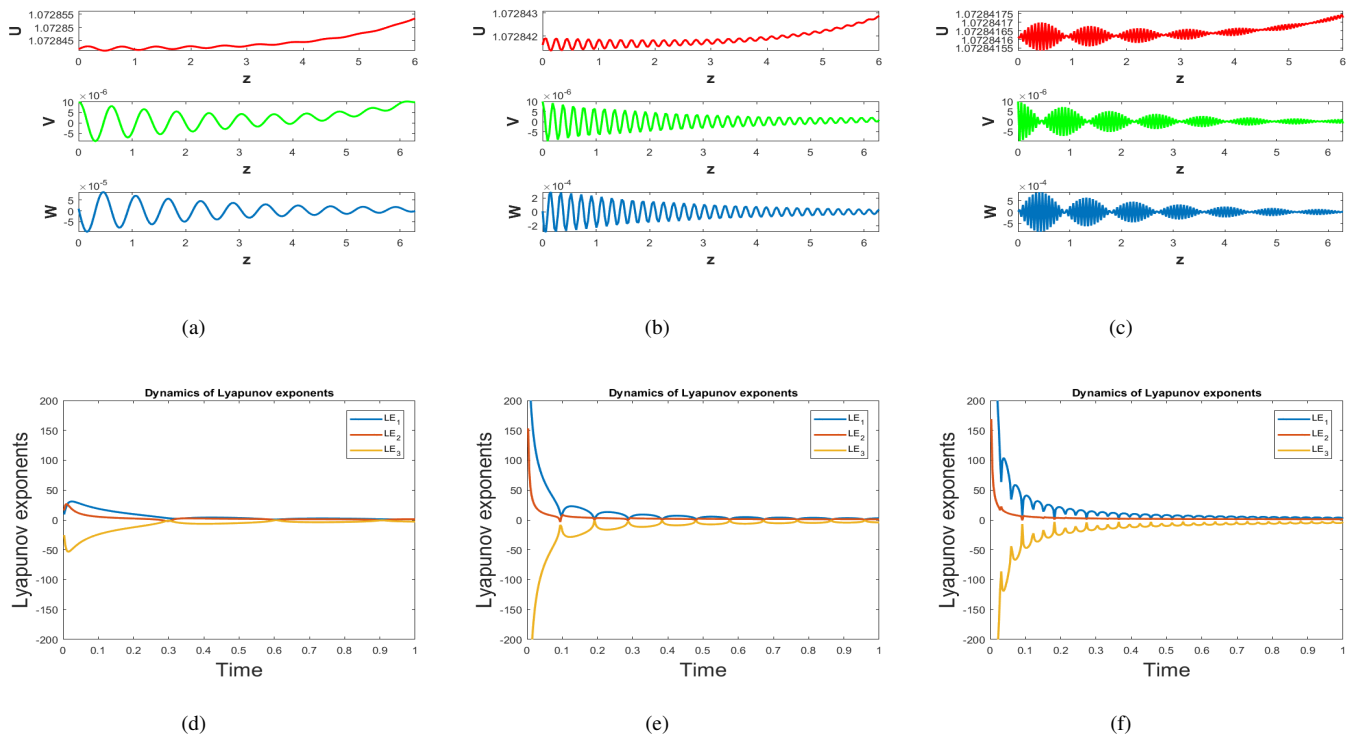

Figure 8 Wave propagation and the Lyapunov exponent plots of the dynamical system equation 5 with respect to third equilibrium point $(k, 1e-5, 1e-5)$ for the ratio between non-linear and dispersion parameters. Parameters are $c = 0.7; P = 2; Q = 2 * [1e-2, 1e-3, 1e-4]; v_1 = 0.2; v_2 = 0.5; n = 5$, and $S = 0.5$. Time interval is $0 : \pi/1000 : 2\pi$.

CONCLUSION

In this study, we studied a higher-order non-linear generalized damped forced KdV equation by employing the tools available in the bifurcation analysis such as phase portraits, time-series plots, Lyapunov exponents etc. The model equation was converted into a three dimensional dynamical system which was investigated for certain parameters involved, namely, P, Q, S which denote the coefficients of non-linearity, dispersion, and damping respectively. Furthermore, the dynamical system was investigated for two forcing parameters v_1, and v_2 which appear in the forcing term appearing in the right hand side of our model problem.

For the first equilibrium point, we can conclude that the dynamical system exhibits the unstable limit cyclic behaviour with respect to the damping parameter S and the forcing parameter v_1. The location of the second and third equilibrium points further depend on the parameters. Thus, the dynamical system exhibited different behaviour at these points. One noteworthy point here is that the behaviour of the system is significantly affected by the ratio of P, and Q. With the help of phase portraits, wave propagation plots and Lyapunov exponents, we showed that the system changes its behaviour from being quasi-periodic to become chaotic for an increased ratio. It is well known that for a highly non-linear Generalized KdV equation with a forcing term in the right hand side such as our model problem considered here, the conventional analytical and numerical methods may not produce acceptable results. In particular a higher ratio of P, and Q may pose a serious challenge for conventional numerical methods. In view of the results presented here regarding the range of the parameters and their corresponding effect on the dynamical system, the investigation may be helpful to devise advance analytical and numerical methods.

Availability of data and material

Not applicable.

Conflicts of interest

The authors declare that there are no competing interests in the publication of this research.

Ethical standard

The authors have no relevant financial or non-financial interests to disclose.

LITERATURE CITED

Alshenawy, R., A. Al-alwan, and A. Elmandouh, 2020 Generalized kdv equation involving riesz time-fractional derivatives: constructing and solution utilizing variational methods. Journal of Taibah University for Science **14**: 314–321.

Alvarado, M. G. G. and G. A. Omel'yanov, 2012 Interaction of solitary waves for the generalized kdv equation. Communications in Nonlinear Science and Numerical Simulation **17**: 3204–3218.

Bona, J. L., P. E. Souganidis, and W. A. Strauss, 1987 Stability and instability of solitary waves of korteweg-de vries type. Proceedings of the Royal Society of London. A. Mathematical and Physical Sciences **411**: 395–412.

Chadha, N. M., S. Tomar, and S. Raut, 2023 Parametric analysis of dust ion acoustic waves in superthermal plasmas through non-autonomous kdv framework. Communications in Nonlinear Science and Numerical Simulation **123**: 107269.

Chen, Y. and S. Li, 2021 New traveling wave solutions and interesting bifurcation phenomena of generalized kdv-mkdv-like equation. Advances in Mathematical Physics **2021**: 1–6.

Crighton, D., 1995 Applications of kdv. In *KdV'95: Proceedings of the International Symposium held in Amsterdam, The Netherlands, April 23–26, 1995, to commemorate the centennial of the publication of the equation by and named after Korteweg and de Vries*, pp. 39–67, Springer.

El, G., 2007 Korteweg–de vries equation: solitons and undular bores. WIT Transactions on State-of-the-art in Science and Engineering **9**.

Engelbrecht, J., 1991 Solutions to the perturbed kdv equation. Wave Motion **14**: 85–92.

Engelbrecht, J. and Y. Khamidullin, 1988 On the possible amplification of nonlinear seismic waves. Physics of the earth and planetary interiors **50**: 39–45.

Engelbrecht, J. and T. Peipman, 1992 Nonlinear waves in a layer with energy influx. Wave Motion **16**: 173–181.

Guckenheimer, J. and P. Holmes, 2013 *Nonlinear oscillations, dynamical systems, and bifurcations of vector fields*, volume 42. Springer Science & Business Media.

Haidong, Q., M. ur Rahman, S. E. Al Hazmi, M. F. Yassen, S. Salahshour, *et al.*, 2023 Analysis of non-equilibrium 4d dynamical system with fractal fractional mittag–leffler kernel. Engineering Science and Technology, an International Journal **37**: 101319.

Hereman, W. and M. Takaoka, 1990 Solitary wave solutions of nonlinear evolution and wave equations using a direct method and macsyma. Journal of Physics A: Mathematical and General **23**: 4805.

Hilborn, R. C. *et al.*, 2000 *Chaos and nonlinear dynamics: an introduction for scientists and engineers*. Oxford University Press on Demand.

Khater, M., 2022 Analytical and numerical-simulation studies on a combined mkdv–kdv system in the plasma and solid physics. The European Physical Journal Plus **137**: 1–9.

Layek, G. *et al.*, 2015 *An introduction to dynamical systems and chaos*, volume 449. Springer.

Li, Z., P. Li, and T. Han, 2021 Bifurcation, traveling wave solutions, and stability analysis of the fractional generalized hirota–satsuma coupled kdv equations. Discrete Dynamics in Nature and Society **2021**: 1–6.

Merle, F., 2001 Existence of blow-up solutions in the energy space for the critical generalized kdv equation. Journal of the American Mathematical Society **14**: 555–578.

Peterson, P., 1997 Travelling waves in nonconservative media with dispersion. Master's thesis, Tallinn Technical University .

Peterson, P. and A. Salupere, 1997 Solitons in a perturbed korteweg-de vries system. Proc. Estonian Acad. Sci. Phys. Math **46**: 102–110.

Saha, A. and P. Chatterjee, 2014 Bifurcations of electron acoustic traveling waves in an unmagnetized quantum plasma with cold and hot electrons. Astrophysics and Space Science **349**: 239–244.

Sami, A., S. Saifullah, A. Ali, and M. ur Rahman, 2022 Chaotic dynamics in tritrophic interaction with volatile compounds in plants with power law kernel. Physica Scripta **97**: 124004.

Stuhlmeier, R., 2009 Kdv theory and the chilean tsunami of 1960. Discrete Contin. Dyn. Syst. Ser. B **12**: 623–632.

Tamang, J. and A. Saha, 2020 Bifurcations of small-amplitude supernonlinear waves of the mkdv and modified gardner equations in a three-component electron-ion plasma. Physics of Plasmas **27**: 012105.

Tomar, S., N. M. Chadha, and S. Raut, 2023 Generalized solitary wave approximate analytical and numerical solutions for generalized damped forced kdv and generalized damped forced mkdv equations. In *Advances in Mathematical Modelling, Applied Analysis and Computation: Proceedings of ICMMAAC 2022*, pp. 177–194, Springer.

Vasavi, S., C. Divya, and A. S. Sarma, 2021 Detection of solitary ocean internal waves from sar images by using u-net and kdv solver technique. Global Transitions Proceedings **2**: 145–151.

Wazwaz, A.-M., 2004 A sine-cosine method for handlingnonlinear wave equations. Mathematical and Computer modelling **40**: 499–508.

Xu, C., M. Ur Rahman, B. Fatima, and Y. Karaca, 2022 Theoretical and numerical investigation of complexities in fractional-order chaotic system having torus attractors. Fractals **30**: 2250164.

Zabusky, N. J., 1967 A synergetic approach to problems of nonlinear dispersive wave propagation and interaction. In *Nonlinear partial differential equations*, pp. 223–258, Elsevier.

Zhang, Y., 2014 Formulation and solution to time-fractional generalized korteweg-de vries equation via variational methods. Advances in Difference Equations **2014**: 1–12.

Zuo, J.-M. and Y.-M. Zhang, 2011 The hirota bilinear method for the coupled burgers equation and the high-order boussinesq—burgers equation. Chinese Physics B **20**: 010205.

How to cite this article: Tomar, S., and Chadha, N. M. Study of Fixed Points and Chaos in Wave Propagation for the Generalized Damped Forced Korteweg-de Vries Equation using Bifurcation Analysis. *Chaos Theory and Applications*, 5(4), 286-292, 2023.

CHAOS
Theory and Applications
in Applied Sciences and Engineering

e-ISSN: 2687-4539
RESEARCH ARTICLE
Vol.5 / No.4 / 2023 / pp.293-299
Special Issue
https://doi.org/10.51537/chaos.1320442

Different Variants of Bernstein Kantorovich Operators and Their Applications in Sciences and Engineering Field

Parveen Bawa *,1, **Neha Bhardwaj** β,2 **and Sumit Kaur Bhatia** *,3

*Department of Mathematics,Amity Institute of Applied Sciences, Amity University Uttar Pradesh, India, βDepartment of Mathematics, Sharda School of Basic Sciences and Research, Sharda University, Greater Noida, India.

ABSTRACT In this article, we investigate various Bernstein-Kantorovich variants together with their approximation properties. Nowadays, these variants of Bernstein-Kantorovich operators have been a source of inspiration for researchers as it helps to approximate integral functions also which is not feasible in the case of discrete operators. Chaos theory has also been referred to as complexity theory. Using chaos theory complexity is also reduced as in approximation theory. Thus in order to reduce complexity and to have better understanding of images in sciences and engineering field, sampling Kantorovich operators of approximation theory are widely used in this regard for enhancement of images. Thus, we discuss the important applications of Kantorovich operators depicting pragmatic and theoretical aspects of approximation theory.

KEYWORDS
Bernstein Kantorovich operators
q-calculus
Lupas-Stancu operators
Polya distribution

INTRODUCTION

The objective of this paper is to highlight the different variants of Bernstein-Kantorovich operators which are widely used for approximation of functions in L^p spaces. The advantage of using Kantorovich variants over discrete operators is that discrete operators are not suitable for approximating functions which are not continuous, therefore these operators were generalized into operators of integral type and one such technique is Kantorovich which helps to approximate integral functions and thus Kantorovich variant of various linear positive operators have been a source of inspiration for many scholars.

Approximation theory is an area of mathematical analysis which is mainly concerned with approximation of complicated quantities by simpler functions. This unique feature of approximation theory forces us to study this field alongwith the study of some ideas of functional anaysis. In (Rashid *et al.* 2022), discrete proportional fraction operators are used to contribute to the major effects of some innovative variants of reverse Minkowski and related H-older-type inequalities. Approximation theory gained popularity with the emergence of Weierstrass theorem (1885). Karl Weierstrass prsesented the first proof of his fundamental theorem on approximation by algebraic and trignometric polynomials but the complications in proof provoked many famous mathematicians to work on this fundamental theorem of approximation theory. Most commonly used proofs of Weierstrass theorem are of Fejer (1900) and Bernstein (1912) as proofs given by other famous mathematicians were not very productive and satisfactory (see e.g. (Bartle 1976; Cheney 1966; Lubinsky 1995; Pinkus 2000). S.N Bernstein (Bernšteın 1912) gave the most simplest and constructive proof of Weierstrass theorem using Bernstein operators $E_\Theta : \check{c}[0,1] \to \check{c}[0,1]$ defined in (Bernšteın 1912) as follows:

$$E_\Theta(\mathfrak{g}';\varkappa) = \sum_{\mathfrak{l}=0}^{\Theta} \binom{\Theta}{\mathfrak{l}} \mathfrak{e}_{\Theta,\mathfrak{l}}(\varkappa)\, \mathfrak{g}'\left(\frac{\mathfrak{l}}{\Theta}\right), \tag{1}$$

where $\mathfrak{e}_{\Theta,\mathfrak{l}}(\varkappa) = \binom{\Theta}{\mathfrak{l}} \varkappa^{\mathfrak{l}}(1-\varkappa)^{\Theta-\mathfrak{l}}$, $\mathfrak{g}' \in \check{c}[0,1], \Theta \geq 1$ and $0 \leq \varkappa \leq 1$.

Bernstein operators are considered as foundational operators due to its immense contribution in the field of approximation theory. These operators occupy prominent position among all linear positive operators because of their efficent and noteable approxi-

Manuscript received: 27 June 2023,
Revised: 25 August 2023,
Accepted: 4 September 2023.

[1]parveen.bawa@s.amity.edu
[2]nehabhr1807@gmail.com (**Corresponding author**)
[3]sumit2212@gmail.com

mation properties but its favourable properties gets overshadowed because of slow rate of convergence. Keeping in view these drawbacks, various modifications has been made to these operators using bezier basis (Agrawal *et al.* 2022). These operators cannot be used to approximate the function in integral metrics. In order to overcome this problem, Kantorovich made small modification of Bernstein operators in 1930 (see (Kantorovich 1930)). In that paper the author L.V Kantorovich, introduces modified operators known as nth Bernstein-Kantorovich operators $L_\Theta : L^1([0,1]) \to \check{c}[0,1]$ defined by

$$L_\Theta(\mathfrak{g}';\varkappa) = \sum_{\mathfrak{l}=0}^{\Theta} (\Theta+1) \left(\int_{\frac{\mathfrak{l}}{\Theta+1}}^{\frac{\mathfrak{l}+1}{\Theta+1}} \mathfrak{g}'(t)\, dt \right) \binom{\Theta}{\mathfrak{l}} \varkappa^{\mathfrak{l}} (1-\varkappa)^{\Theta-\mathfrak{l}}, \tag{2}$$

where $\mathfrak{g}' \in L^1([0,1])$ and $\varkappa \in [0,1]$.

Study of Lebesgue integrable functions in L^1 space became possible due to modification of Bernstein operators by Kantorovich. Moreover, Altomare et al. (Altomare and Campiti 2011), established the approximation properties using Korovkin theorem and investigate the rate of convergence associated with these operators. The idea of Kantorovich modifications of sequence of linear positive operators inspires many other mathematicians to investigate some new operators within approximation theory. Many authors constructed and studied the Kantorovich type modification of some various operators (see e.g. (Agratini 2001; Barbosu 2004; Dogru and Ozalp 2001; Duman *et al.* 2006; Özarslan *et al.* 2008; Kac and Cheung 2001; Karaca 2022)

In this article, we try to give some important information about different variants of Bernstein-Kantorovich operators, hoping that this will act as a beneficial tool for all those reserachers that work in approximation theory and intend to apply Kantorovich technique in order to modify various linear positive operators.

LITERATURE REVIEW

In this section, we review some variants of Bernstein-Kantorovich operators which are being very popularly used in approximation theory. We refer readers to some papers such as (Acu 2015; Agrawal *et al.* 2015; Altomare *et al.* 2013; Barbosu 2004; Bardaro *et al.* 2007; de la Cal and Valle 2000; Deo *et al.* 2016; Gonska *et al.* 2011; Igoz 2012) for generalization of these operators in Kantorovich form.

Let us recall some notations. Throughout this paper, $\check{c}[a,b]$ is the space of all continuous real valued functions on $[a,b]$, $L^p_{[0,1]}$ is the class of all p power integrable functions on the interval $[0,1]$. For basic definitions and results regarding Banach spaces with the proof as well as applications, one may refer (Karaca 2022).

Kantorovich's idea has been applied also to Bernstein operators involving q-calculus. For definition and notations from q-calculus, we refer readers to (Andrews *et al.* 1999; Kac and Cheung 2001). In (Lupas 1987) Lupas introduced modified form of Bernstein operators using q-calculus and explored its approximation and shape-preserving properties. Subsequently, philips in (Phillips 2003) has done q-generalization of Bernstein operators known as Bernstein operators in q-calculus (q-Bernstein operators) defined, for every positive integer Θ and $\mathfrak{g}' \in [0,1]$, by

$$B_\Theta(\mathfrak{g}';q;\varkappa) = \sum_{\mathfrak{l}=0}^{\Theta} \mathfrak{g}'\left(\frac{[\mathfrak{l}]}{[\Theta]}\right) \begin{bmatrix}\Theta\\ \mathfrak{l}\end{bmatrix} \varkappa^{\mathfrak{l}} \prod_{s=0}^{\Theta-\mathfrak{l}-1} (1-q^s\varkappa). \tag{3}$$

and also studied various results including the theorem confirming uniform convergence (korovkin theorem), order of convergence and asymptotic expansion of these operators given by voronovskaya theorem. See (Ostrovska 2016) for similarities and distinctions of operators given by Lupas and Philips.

In (Dalmanoğlu 2007) modification of Bernstein operators in q-calculus using Kantorovich technique is instigated and its approximation properties are satisfied, while in (Radu 2008) Bernstein-Kantorovich operators in q-calculus are extended and their statistical convergence propertis are prepensed.

In (Dalmanoğlu 2007; Radu 2008), the another modification of the Bernstein operators using Kantorovich technique is elucidate in q-calculus, for every $\Theta \in \mathbb{N}$, $\varkappa \in [0,1]$ and $0 < q < 1$, by

$$K_\Theta(\mathfrak{g}';q;\varkappa) = [\Theta+1] \sum_{\mathfrak{l}=0}^{\Theta} \begin{bmatrix}\Theta\\ \mathfrak{l}\end{bmatrix} \left(\frac{\varkappa}{q}\right)^{\mathfrak{l}} \prod_{s=0}^{\Theta-\mathfrak{l}-1} (1-q^s\varkappa) \times \int_{\frac{[\mathfrak{l}]}{[\Theta+1]}}^{\frac{[\mathfrak{l}+1]}{[\Theta+1]}} \mathfrak{g}'(t)\, d_q t. \tag{4}$$

Subsequently, the study of operators has been intensified by Dalmanog et al. in (Dalmanog *et al.* 2010), where they reconceive the Kantorovich variant of Bernstein operators in q-calculus using the definition of q-integral of Riemann type (see (Marinković *et al.* 2008)) into the operator instead of general q-integral as:

$$B^*_\Theta(\mathfrak{g}';q;\varkappa) = [\Theta+1] \sum_{\mathfrak{l}=0}^{\Theta} q^{-\mathfrak{l}} \begin{bmatrix}\Theta\\ \mathfrak{l}\end{bmatrix} \prod_{s=0}^{\Theta-\mathfrak{l}-1} (1-q^s\varkappa) \int_{\frac{[\mathfrak{l}]}{[\Theta+1]}}^{\frac{[\mathfrak{l}+1]}{[\Theta+1]}} \mathfrak{g}'(t)\, d_q^{\mathfrak{r}} t. \tag{5}$$

The need of redefining the operators arises because the study of statistical convergence of operators $K_\Theta(\mathfrak{g}';q;\varkappa)$ to the function $\mathfrak{g}'$ is problematical with the usage of classical q-integral.

Stancu operators are instead object of a modification for various researchers. In (Gadjiev and Ghorbanalizadeh 2010) Gadjiev et al. introduced Bernstein-Stancu type polynomials with shifted knots:

$$S_{\Theta,\alpha,\beta}(\mathfrak{g}';\varkappa) = \left(\frac{\Theta+\beta_2}{\Theta}\right)^{\Theta} \sum_{\mathfrak{r}=0}^{\Theta} \mathfrak{g}'\left(\frac{\mathfrak{r}+\alpha_1}{\Theta+\beta_1}\right) \binom{\Theta}{\mathfrak{r}} \left(\varkappa - \frac{\alpha_2}{\Theta+\beta_2}\right)^{\mathfrak{r}} \left(\frac{\Theta+\alpha_2}{\Theta+\beta_2} - \varkappa\right)^{\Theta-\mathfrak{r}}, \tag{6}$$

where $\frac{\alpha_2}{\Theta+\beta_2} \le \varkappa \le \frac{\Theta+\alpha_2}{\Theta+\beta_2}$ and $\alpha_{\mathfrak{l}}, \beta_{\mathfrak{l}}\ (\mathfrak{l}=1,2)$ are such that $0 \le \alpha_1 \le \alpha_2 \le \beta_1 \le \beta_2$.

Motivated by above operators, *İçöz* in (İçöz 2012) designate a generalized form of Bernstein-Stancu operators using Kantorovich technique under same assumptions as:

$$S^*_{\Theta,\alpha,\beta}(\mathfrak{g}';\varkappa) = (\Theta+\beta_1+1)\left(\frac{\Theta+\beta_2}{\Theta}\right)^{\Theta} \sum_{\mathfrak{r}=0}^{\Theta} \binom{\Theta}{\mathfrak{r}} \left(\varkappa - \frac{\alpha_2}{\Theta+\beta_2}\right)^{\mathfrak{r}} \left(\frac{\Theta+\alpha_2}{\Theta+\beta_2} - \varkappa\right)^{\Theta-\mathfrak{r}} \int_{\frac{\mathfrak{r}+\alpha_1}{\Theta+\beta_1+1}}^{\frac{\mathfrak{r}+\alpha_1+1}{\Theta+\beta_1+1}} \mathfrak{g}'(s)\, ds. \tag{7}$$

To show the extend of research in direction of q-calculus, we mention the work done by Muraru in (Muraru 2011). She bring

forward the q analogue of Bernstein-Schurer operators that are given by

$$E_{\Theta,p}\left(\mathfrak{g}';q,\varkappa\right)=\sum_{\mathfrak{l}=0}^{\Theta+p}p_{\Theta,\mathfrak{l}}\left(q,\varkappa\right)\mathfrak{g}'\left(\frac{[\mathfrak{l}]_q}{[\Theta]_q}\right), \tag{8}$$

where $p_{\Theta,\mathfrak{l}}\left(q,\varkappa\right)=\begin{bmatrix}\Theta+p\\ \mathfrak{l}\end{bmatrix}\varkappa^{\mathfrak{l}}\left(1-\varkappa\right)_q^{\Theta+p-\mathfrak{l}},\varkappa\in[0,1]$ and prepense various results involving necessary and sufficient condition for convergence of operators given by the Korovkin and Voronovskaja theorem concerning asymptotic convergence of linear positive operators.

Kantorovich modification of the operators (8) have been introduced by Ozarsland et al. in (Özarslan and Vedi 2013) defined, for every $\mathfrak{g}'\in\mathfrak{C}\left[0,p+1\right],0<q<1$ and $p\in\Theta_0=\{0,1,2,...\}$, by

$$K_{\Theta}^{p}\left(\mathfrak{g}';q;\varkappa\right)=\sum_{\mathfrak{r}=0}^{\Theta+p}\begin{bmatrix}\Theta+p\\ \mathfrak{r}\end{bmatrix}\varkappa^{\mathfrak{r}}\prod_{s=0}^{\Theta+p-\mathfrak{r}-1}\left(1-q^s\varkappa\right)\times$$
$$\int_0^1\mathfrak{g}'\left(\frac{[\mathfrak{r}]}{[\Theta+1]}+\frac{1+(q-1)[\mathfrak{r}]}{[\Theta+1]}t\right)d_qt. \tag{9}$$

Ren et al. modified the operators (8) in (Ren and Zeng 2013). A new variant of Bernstein-Schurer operators in q-calculus are given by

$$\widetilde{\mathfrak{e}}_{\Theta,p}\left(\mathfrak{g}';q;\varkappa\right)=\sum_{\mathfrak{l}=0}^{\Theta+p}\widetilde{p}_{\Theta,\mathfrak{l}}^{*}\left(q,\varkappa\right)\mathfrak{g}'\left(\frac{[\mathfrak{l}]_q}{[\Theta]_q}\right), \tag{10}$$

where $\widetilde{p}_{\Theta,\mathfrak{l}}^{*}\left(q,\varkappa\right)=\frac{[\Theta]_q^{\Theta+p}}{[\Theta+p]_q^{\Theta+p}}\begin{bmatrix}\Theta+p\\ \mathfrak{l}\end{bmatrix}_q\varkappa^{\mathfrak{l}}\left(\frac{[\Theta+p]_q}{[\Theta]_q}-\varkappa\right)_q^{\Theta+p-\mathfrak{l}}$ and $\varkappa\in[0,1]$.

Authors investigated compulsory Korovkin type statistical convergence theorem for uniform convergence, Voronovskaja theorem concerning asymptotic convergence, the rate of statistical convergence using various tools such as modulus of continuity and a Lipschitz function for the operators in (Ren and Zeng 2013).

Agrawal et al. in (Agrawal *et al.* 2015) present a stancu variant of operators (8) using Kantorovich technique defined, for every $\mathfrak{g}'\in C\left[0,1+p\right]$ endowed with the norm $\|\mathfrak{g}'\|=\sup_{\varkappa\in[0,1]}\left|\mathfrak{g}'\left(\varkappa\right)\right|,\alpha,\beta\in\mathbb{R}$ such that $0\leq\alpha\leq\beta$ and $0<q<1$, by

$$\kappa_{\Theta,p}^{(\alpha,\beta)}\left(\mathfrak{g}';q;\varkappa\right)=\sum_{\mathfrak{l}=0}^{\Theta+p}\widetilde{p}_{\Theta,\mathfrak{l}}^{*}\left(q,\varkappa\right)\int_0^1\mathfrak{g}'\left(\frac{[\mathfrak{l}]_q+q^{\mathfrak{l}}t+\alpha}{[\Theta+1]_q+\beta}\right)d_qt. \tag{11}$$

Kantorovich (Kantorovich 1930) gave the integral modification of Bernstein operators so as to approximate integrable functions defined on $[0,1]$. In (Ozarslan and Duman 2016) Özarslan et al. introduced modified Kantorovich operators based on non-negative parameter ρ as:

$$K_{\Theta,\rho}\left(\mathfrak{g}';\varkappa\right)=\sum_{\mathfrak{l}=0}^{\Theta}\mathfrak{e}_{\Theta,\mathfrak{l}}\left(\varkappa\right)\int_0^1\mathfrak{g}'\left(\frac{\mathfrak{l}+t^{\rho}}{\Theta+1}\right)dt. \tag{12}$$

and investigated the order of convergence and various approximation properties of these operators using various mathematical tools concerning smoothness of operators. In that paper, authors also showed that modified Kantorovich operators based on non-negative parameter ρ depicts faster rate of convergence to a function than that of Kantorovich operators in classical form.

Another new general approach is considered by Mursaleen et al. (Mursaleen *et al.* 2015). In that paper authors prepensed another modified form of Bernstein operators in ((p,q)-calculus) known as (p,q)-Bernstein operators defined, for every $\varkappa\in[0,1],0<p<q\leq1$, by

$$B_{\Theta,p,q}\left(\mathfrak{g}';\varkappa\right)=\sum_{\mathfrak{l}=0}^{\Theta}\begin{bmatrix}\Theta\\ \mathfrak{l}\end{bmatrix}_{p,q}\varkappa^{\mathfrak{l}}\prod_{s=0}^{\Theta-\mathfrak{l}-1}\left(p^s-q^s\varkappa\right)\mathfrak{g}'\left(\frac{[\mathfrak{l}]_{p,q}}{[\Theta]_{p,q}}\right). \tag{13}$$

These operators turned into classical Bernstein operators in q-calculus for p=1.

For notations used in operators (13), we refer reader to (Mursaleen *et al.* 2015). Also details on (p,q)-calculus can be found in (Hounkonnou *et al.* 2013; Katriel and Kibler 1992; Sahai and Yadav 2007).

Afterward, Mursaleen et al. (Mursaleen *et al.* 2016) constructed of Bernstein-Kantorovich operators in ((p,q)-calculus) as:

$$K_{\Theta}^{(p,q)}\left(\mathfrak{g}';\varkappa\right)=\frac{[\Theta]_{p,q}}{p^{\frac{\Theta(\Theta-1)}{2}}}\sum_{\mathfrak{l}=0}^{\Theta}\frac{b_{\Theta,\mathfrak{l}}^{(p,q)}\left(\varkappa\right)}{p^{\Theta-\mathfrak{l}}q^{\mathfrak{l}}}\int_{\frac{[\mathfrak{l}]_{p,q}}{p^{\mathfrak{l}-\Theta-1}[\Theta]_{p,q}}}^{\frac{[\mathfrak{l}+1]_{p,q}}{p^{\mathfrak{l}-\Theta}[\Theta]_{p,q}}}\mathfrak{g}'\left(t\right)d_pt, \tag{14}$$

where $\varkappa\in[0,1],b_{\Theta,\mathfrak{l}}^{(p,q)}\left(\varkappa\right)=\begin{bmatrix}\Theta\\ \mathfrak{l}\end{bmatrix}_{p,q}\left(\varkappa\right)_{p,q}^{\mathfrak{l}}\left(1-\varkappa\right)_{p,q}^{\Theta-\mathfrak{l}}$ and $\left(\varkappa\right)_{p,q}^{\mathfrak{l}}=\varkappa\left(px\right)\left(p^2\varkappa\right).....\left(p^{\mathfrak{l}-1}\varkappa\right)=p^{\frac{\mathfrak{l}(\mathfrak{l}-1)}{2}}\varkappa^{\mathfrak{l}}$.

Moreover, authors study the local approximation property of $K_{\Theta}^{(p,q)}\left(\mathfrak{g}';\varkappa\right)$ and obtain faster rate of convergence and better error estimates of operators as compared to Bernstein-Kantorovich operators in q-calculus.

Realising the essentials of Bernstein-Stancu, Mursaleen el at. in (Mursaleen *et al.* 2017) introduce another variant of Bernstein-Stancu in q-calculus using Kantorovich technique as follows:

$$K_{\Theta,q}^{(\alpha,\beta)}=\left(\frac{[\Theta]+\beta_2}{[\Theta]}\right)^{\Theta}\sum_{\mathfrak{l}=0}^{\Theta}\begin{bmatrix}\Theta\\ \mathfrak{l}\end{bmatrix}\left(\varkappa-\frac{\alpha_2}{[\Theta]+\beta_2}\right)_q^{\mathfrak{l}}$$
$$\times\left(\frac{[\Theta]+\alpha_2}{[\Theta]+\beta_2}-\varkappa\right)_q^{\Theta-\mathfrak{l}}\int_0^1\mathfrak{g}'\left(\frac{[\mathfrak{l}]q^{\mathfrak{l}}t+\alpha_1}{[\Theta+1]+\beta_1}\right)d_qt. \tag{15}$$

New Kantorovich-type operators based on Pòlya-Eggenberger distribution (Eggenberger and Pólya 1923) are introduced by Kajla et al. in (Kajla and Araci 2017) as:

$$K_{\Theta,\rho}^{[\alpha]}\left(\mathfrak{g}';\varkappa\right)=\sum_{\mathfrak{l}=0}^{\Theta}p_{\Theta,\mathfrak{l}}^{[\alpha]}\left(\varkappa\right)\int_0^1\mathfrak{g}'\left(\frac{\mathfrak{l}+t^{\rho}}{\Theta+1}\right)dt, \tag{16}$$

where $\rho>0$ and $p_{\Theta,\mathfrak{l}}^{[\alpha]}\left(\varkappa\right)=\binom{\Theta}{\mathfrak{l}}\frac{1}{1^{[\Theta,-\alpha]}}\chi^{\mathfrak{l},-\alpha}\left(1-\chi\right)^{[\Theta-\mathfrak{l},-\alpha]}$.

In (Acu *et al.* 2018) Acu et al. study a new type of Bernstein operators depending on the parameter $\lambda\in[-1,1]$ proposed by Cai et al. (Cai *et al.* 2018) as follows:

$$B_{\Theta,\lambda}\left(\mathfrak{g}';\varkappa\right)=\sum_{\mathfrak{l}=0}^{\Theta}\widetilde{\mathfrak{e}}_{\Theta,\mathfrak{l}}\left(\lambda;\varkappa\right)\mathfrak{g}'\left(\frac{\mathfrak{l}}{\Theta}\right), \tag{17}$$

where $\widetilde{\mathfrak{e}}_{\Theta,0}\left(\lambda;\varkappa\right),\mathfrak{l}=0,1,2,3.....$, are defined as:

$$\widetilde{\mathfrak{e}}_{\Theta,0}\left(\lambda;\varkappa\right)=\mathfrak{e}_{\Theta,0}\left(\varkappa\right)-\frac{\lambda}{\Theta+1}\mathfrak{e}_{\Theta+1,1}\left(\varkappa\right),$$

$$\widetilde{\mathfrak{e}}_{\Theta,\mathfrak{l}}(\lambda;\varkappa)=\mathfrak{e}_{\Theta,\mathfrak{l}}(\varkappa)$$
$$+\lambda\left(\frac{\Theta-2k+1}{\Theta^2-1}\mathfrak{e}_{\Theta+1,\mathfrak{l}}(\varkappa)-\frac{\Theta-2k-1}{\Theta^2-1}\mathfrak{e}_{\Theta+1,\mathfrak{l}+1}(\varkappa)\right)$$
$$\widetilde{\mathfrak{e}}_{\Theta,\Theta}(\lambda;\varkappa)=\mathfrak{e}_{\Theta,\Theta}(\varkappa)-\frac{\lambda}{\Theta+1}\mathfrak{e}_{\Theta+1,\Theta}(\varkappa).$$

Moreover, Ana et al. considered a Kantorovich modification of λ-Bernstein operators, namely

$$K_{\Theta,\lambda}(\mathfrak{g}';\varkappa)=(\Theta+1)\sum_{\mathfrak{l}=0}^{\Theta}\widetilde{\mathfrak{e}}_{\Theta,\mathfrak{l}}(\varkappa)\int_{\frac{\mathfrak{l}}{\Theta+1}}^{\frac{\mathfrak{l}+1}{\Theta+1}}\mathfrak{g}'(t)\,dt. \tag{18}$$

In particular, in (Acu *et al.* 2018) (see Example 4) authors obtained better error estimate for λ-Bernstein operators as compared to classical Kantorovich operators.

In (Chen *et al.* 2017) Chen et al. studied another modification of Bernstein operators, depending on a non-negative real parameter α (α-Bernstein operators) defined, for every $\mathfrak{g}'\in\mathfrak{C}[0,1]$, $\Theta\geq 2$ and $0\leq\varkappa\leq 1$, by

$$T_{\Theta}^{\alpha}(\mathfrak{g}';\varkappa)=\sum_{\mathfrak{l}=0}^{\Theta}p_{\Theta,\mathfrak{l}}^{(\alpha)}(\varkappa)\,\mathfrak{g}'\left(\frac{\mathfrak{l}}{\Theta}\right), \tag{19}$$

where

$$p_{\Theta,\mathfrak{l}}^{(\alpha)}(\varkappa)=\left[\binom{\Theta-2}{\mathfrak{l}}(1-\alpha)\varkappa+\binom{\Theta-2}{\mathfrak{l}-2}(1-\alpha)(1-\varkappa)\right.$$
$$\left.+\binom{\Theta}{\mathfrak{l}}\alpha\varkappa(1-\varkappa)\right]\varkappa^{\mathfrak{l}-1}(1-\varkappa)^{\Theta-\mathfrak{l}-1}$$

The authors also proved the degree of convergence, Voronovskaja theorem concerning asymptotic formula and shape preserving properties for operator(19).

In (Mohiuddine *et al.* 2017) Mohiuddine et al. proposed and investigated the kantorovich type modification of operators (19) defined, for for every $\mathfrak{g}'\in\mathfrak{C}[0,1]$, $\Theta\geq 2$ and $0\leq\varkappa\leq 1$, by

$$\widehat{\mathfrak{l}}_{\Theta,\alpha}(\mathfrak{g}';\varkappa)=(\Theta+1)\sum_{s=0}^{\Theta}p_{\Theta,s}^{(\alpha)}\int_{\frac{s}{\Theta+1}}^{\frac{s+1}{\Theta+1}}\mathfrak{g}'(t)\,dt. \tag{20}$$

Araci et al. also proved various approximation properties with the help of Bohman-Korovkin's principle which is necessary and sufficient criteria for uniform convergence and used various tools such as the modulus of smoothness and Lipschitz type function to study the approximation rate of operators. They also derived Voronovskaja type asymptotic convergence theorem and Korovkin type A-statistical approximation theorem of these operators.

A short time ago, the Kantorovich modification of the operators (19) by Araci et al. is defined in (Araci *et al.* 2019), for every $\mathfrak{g}'\in\mathfrak{C}[0,1]$, $\alpha>0$ and $\rho>0$, by

$$\kappa_{m,\rho}^{\alpha,a}(\mathfrak{g}';\varkappa)=\sum_{\mathfrak{l}=0}^{\Theta}p_{\Theta,\mathfrak{l}}^{(\alpha)}(\varkappa)\int_0^1 f\left(\frac{\mathfrak{l}+at^{\rho}}{\Theta+a}\right)dt, \tag{21}$$

where $\varkappa\in[0,1]$ and $p_{\Theta,\mathfrak{l}}^{(\alpha)}$ is defined above.

Afterward, α, q-Bernstein operators by Cai et al. in (Cai and Xu 2018) are presented as:

$$\mathfrak{T}_{\Theta,q,\alpha}(\mathfrak{g}';\varkappa)=\sum_{\mathfrak{k}=0}^{\Theta}p_{\Theta,q,\mathfrak{k}}^{(\alpha)}f\left(\frac{[\mathfrak{k}]_q}{[\Theta]_q}\right), \tag{22}$$

where $\alpha\in[0,1]$, $q\in(0,1]$, $\varkappa\in[0,1]$, $\mathfrak{g}'\in\mathfrak{C}[0,1]$ and

$$p_{1,q,0}^{(\alpha)}(\varkappa)=1-\varkappa,\ p_{1,q,1}^{(\alpha)}(\varkappa)=\varkappa,$$
$$p_{\Theta,q,\mathfrak{k}}^{(\alpha)}(\varkappa)=\left(\begin{bmatrix}\Theta-2\\ \mathfrak{l}\end{bmatrix}_q(1-\alpha)\varkappa+\begin{bmatrix}\Theta-2\\ \mathfrak{l}-2\end{bmatrix}_q\right.$$
$$(1-\alpha)q^{\Theta-\mathfrak{k}-2}\left(1-q^{\Theta-\mathfrak{k}-1}\varkappa\right)+\begin{bmatrix}\Theta\\ \mathfrak{l}\end{bmatrix}_q\times$$
$$\left.\alpha\varkappa\left(1-q^{\Theta-\mathfrak{k}-1}\varkappa\right)\right)\varkappa^{\mathfrak{l}-1}(1-\varkappa)_q^{\Theta-\mathfrak{l}-1},\Theta\geq 2$$

Subsequently, Cai et al. establish a more general approach to Kantorovich operators known as bivariate α, q-Bernstein-Kantorovich operators in (Cai *et al.* 2019) as:

$$\kappa_{\mathfrak{m}_1,\mathfrak{m}_2,q_1,q_2}^{(\alpha_1,\alpha_2)}(\mathfrak{g}';\varkappa;\mathfrak{s})=[\Theta_1+1]_{q_1}[\Theta_2+1]_{q_2}$$
$$\times\sum_{\mathfrak{k}_1=0}^{\Theta_1}\sum_{\mathfrak{k}_2=0}^{\Theta_2}p_{\Theta_1,q_1,\mathfrak{k}_1}^{(\alpha_1)}(\varkappa)\,p_{\Theta_2,q_2,\mathfrak{k}_2}^{(\alpha_2)}(\mathfrak{s})\,q_1^{-\mathfrak{k}_1}q_1^{-\mathfrak{k}_2}$$
$$\times\int_{\frac{[\mathfrak{k}_1]_{q_1}}{[\Theta_1+1]_{q_1}}}^{\frac{[\mathfrak{k}_1+1]_{q_1}}{[\Theta_1+1]_{q_1}}}\int_{\frac{[\mathfrak{k}_2]_{q_2}}{[\Theta_2+1]_{q_2}}}^{\frac{[\mathfrak{k}_2+1]_{q_2}}{[\Theta_2+1]_{q_2}}}\mathfrak{g}'(t;u)\,dq_1t dq_2u,$$

where $\varkappa,\mathfrak{s}\in[0,1]$, $\mathfrak{g}'\in\mathfrak{C}([0,1]\times[0,1])$, $0<q_1<q_2<1$ and $\alpha_1,\alpha_2\in[0,1]$.

APPLICATIONS

Approximation Theory is rigorous branch of study, developed in different directions by mathematicians. It's centrality in the development of many area of mathematics and its diverse application in Sciences and Engineering field makes it attractive field of study and research. Approximation Theory has two aspects:

- Pragmatic: Which is concerned largely with computational practicalities.
- Theoretical: Which is more concerned with applications to theoretical issues.

Sampling Kantorovich operators are concerned more with pragmatic aspects. In (Bardaro *et al.* 2007) the authors introduced the sampling Kantorovich operators and studied their convergence in the general setting of orlicz spaces in the one-dimensional space. Afterward, the results to multivariate setting have been extended in (Costarelli and Vinti 2011), to the nonlinear case in (Costarelli and Vinti 2013; Vinti and Zampogni 2009; Bardaro and Mantellini 2012) in a more general context. Results regarding the order of approximation of these operators are shown in (Costarelli *et al.* 2014b). In (Cluni *et al.* 2013) the authors obtain application to civil engineering by using multivariate sampling Kantorovich operators $(S_\omega)_{\omega>0}$, defined by:

$$(S_\omega\mathfrak{g}')(\underline{\varkappa})=\sum_{\underline{\mathfrak{l}}\in\mathbb{Z}^{\Theta}}\chi(\omega\underline{\varkappa}-t_{\underline{\mathfrak{l}}})\left[\frac{\omega^{\Theta}}{A_{\underline{\mathfrak{l}}}}\int_{R_{\underline{\mathfrak{l}}}^{\omega}}\mathfrak{g}'(\underline{u})\,d\underline{u}\right], \tag{23}$$

where $(\underline{\varkappa}\in\mathbb{R}^{\Theta})$ and $\mathfrak{g}':\mathbb{R}^{\Theta}\to\mathbb{R}$ is locally integrable function.

For notations and more details about operators, we refer reader to (Cluni *et al.* 2013). In that paper, authors realized the importance of sampling Kantorovich operators to seismic engineering by demonstrating that structural analysis using sampling Kantorovich

operators produce clear understanding of masonry texture, the geometry of buildings and possible structural damage, which further helps to estimate seismic risk of structure. The models for the reproduction of the behaviour of structures under seismic action and comparison of behaviour of the building using various models are obtained in (Costarelli *et al.* 2014a). In (Cheney 1966) a real world case study in terms of structural analysis is analyzed. For better understanding readers can refer Figure in (Cluni *et al.* 2013)

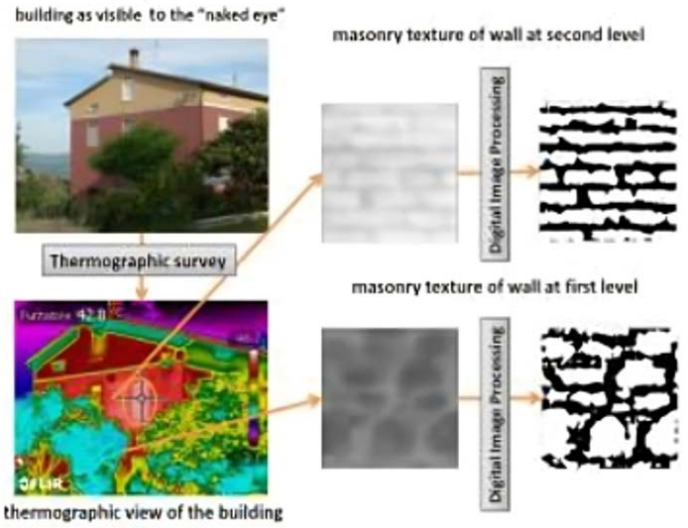

Figure 1 Image depicting importance of Sampling Kantorovich operators in structural analysis of building.

Sampling Kantorovich operators are very useful in sampling and signal theories. Cluni et al. in (Costarelli *et al.* 2014a) also recognized that the use of sampling Kantorovich operators in approximating discontinuous signals is predominant as it reduces "time-jitter" errors. Angeloni et al. in (Angeloni *et al.* 2005) developed that sampling Kantorovich operators represents an approximate version of classical sampling series, based on Whittaker-Kotelnikov-Shannon sampling theorem.

In (Costarelli and Vinti 2014), Costarelli et al. presented an application of sampling Kantorovich operators to digital image processing (D.I.P) and also studied the various results regarding the convergence of sampling Kantorovich operators. In that paper, the various usage of the D.I.P technique are discussed from mathematical and medical point of view. Moreover, some new applications are obtained by considering biomedical images. A concrete example is showed in (Costarelli and Vinti 2014) and deduce that enhancement of images using sampling Kantorovich operators are very useful from medical point of view as it allows doctor to perform a better diagnosis. For better understanding one can refer images below (Costarelli *et al.* 2014a)

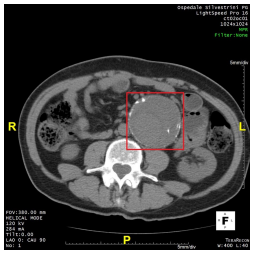

(a) CT image without contrast medium. In the red square is depicted the aorta artery

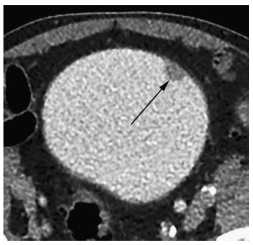

(b) Enhanced by the sampling Kantorovich operators $S_{20}I$ based upon a bivariate Jackson type kernel

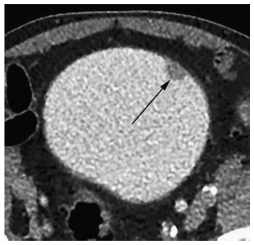

(c) ROI of the CT image without contrast medium of (a), depicted the aorta artery

Figure 2 Processing a portion of a CT (computer tomography) image depicting the aorta artery using Sampling Kantorovich operators.

In (Karaca *et al.* 2019) Karaca et al. main contribution was to provide a unique method for assessing key stroke subtypes' features using a mobile phone connected to a cloud system depicting huge progress in innovative healthcare technologies that rendered healthcare data bigger.

Angeloni et al. (Angeloni *et al.* 2020) examined the convergence properties of a family of multidimensional sampling Kantorovich type operators. Besides that, quantitative estimates, order of approximation and Voronovskaja type asymptotic convergence theorem have been established. Very recently, Bawa et al. (Bawa *et al.* 2022) elucidate the approximation properties of a Kantorovich-Lupaş-Stancu operators based on Pòlya distribution.

CONCLUSION

We conclude that approximation theory is an intensive research area that is widely used in sciences and engineering field. In this paper, we have discussed different variants of Bernstein Kantorovich operators showing their pragmatic and theoretical applicatons in different areas of research. The importance of approximation theory in numerous scientific fields makes it one of the most active research areas. The theory is relevant to both engineering and mathematical fields, such as constructive approximation of functions, partial and integral equation solutions, machine learning and image processing.

Availability of data and material

Not applicable.

Conflicts of interest

The authors declare that there is no conflict of interest regarding the publication of this paper.

Ethical standard

The authors have no relevant financial or non-financial interests to disclose.

LITERATURE CITED

Acu, A. M., 2015 Stancu–Schurer–Kantorovich operators based on q-integers. Applied Mathematics and Computation **259**: 896–907.

Acu, A.-M., N. Manav, and D. F. Sofonea, 2018 Approximation properties of λ-Kantorovich operators. Journal of inequalities and applications **2018**: 1–12.

Agratini, O., 2001 An approximation process of Kantorovich type. Miskolc Mathematical Notes **2**: 3–10.

Agrawal, P., N. Bhardwaj, and P. Bawa, 2022 Bézier variant of modified α-bernstein operators. Rendiconti del Circolo Matematico di Palermo Series 2 **71**: 807–827.

Agrawal, P., M. Goyal, and A. Kajla, 2015 q-Bernstein-Schurer-Kantorovich type operators. Bollettino dell'Unione Matematica Italiana **8**: 169–180.

Altomare, F. and M. Campiti, 2011 *Korovkin-type approximation theory and its applications*, volume 17. Walter de Gruyter.

Altomare, F., M. C. Montano, and V. Leonessa, 2013 On a generalization of Szász–Mirakjan–Kantorovich operators. Results in Mathematics **63**: 837–863.

Andrews, G. E., R. Askey, and R. Roy, 1999 *Special functions*, volume 71. Cambridge university press.

Angeloni, L., D. Costarelli, and G. Vinti, 2020 Approximation properties of mixed sampling-Kantorovich operators. Revista de la Real Academia de Ciencias Exactas, Físicas y Naturales. Serie A. Matemáticas **115**: 1–14.

Angeloni, L., G. Vinti, *et al.*, 2005 Rate of approximation for nonlinear integral operators with application to signal processing. Differential and Integral Equations **18**: 855–890.

Araci, S., A. Kajla, and P. Agarwal, 2019 A Kantorovich variant of a generalized Bernstein operators .

Barbosu, D., 2004 Kantorovich-Stancu type operators. J. Inequal. Pure Appl. Math **5**: 6.

Bardaro, C. and I. Mantellini, 2012 On convergence properties for a class of Kantorovich discrete operators. Numerical functional analysis and optimization **33**: 374–396.

Bardaro, C., G. Vinti, P. Butzer, and R. Stens, 2007 Kantrovich-type generalized sampling series in the setting of orlicz spaces. Sampling Theory in Signal and Image Processing **6**: 29.

Bartle, R. G., 1976 The element of real analysis, john willy & sons. Inc., New York .

Bawa, P., N. Bhardwaj, and P. Agrawal, 2022 Quantitative voronovskaya type theorems and gbs operators of kantorovich variant of lupaş-stancu operators based on pólya distribution. Mathematical Foundations of Computing **5**: 269–293.

Bernšteın, S., 1912 Démonstration du théoreme de Weierstrass fondée sur le calcul des probabilities. Comm. Soc. Math. Kharkov **13**: 1–2.

Cai, Q.-B., W.-T. Cheng, and B. Çekim, 2019 Bivariate α, q-Bernstein–Kantorovich operators and gbs operators of bivariate α, q-bernstein–kantorovich type. Mathematics **7**: 1161.

Cai, Q.-B., B.-Y. Lian, and G. Zhou, 2018 Approximation properties of λ-Bernstein operators. Journal of Inequalities and Applications **2018**: 1–11.

Cai, Q.-B. and X.-W. Xu, 2018 Shape-preserving properties of a new family of generalized Bernstein operators. Journal of inequalities and applications **2018**: 1–14.

Chen, X., J. Tan, Z. Liu, and J. Xie, 2017 Approximation of functions by a new family of generalized Bernstein operators. Journal of Mathematical Analysis and Applications **450**: 244–261.

Cheney, E. W., 1966 Introduction to approximation theory .

Cluni, F., D. Costarelli, A. M. Minotti, and G. Vinti, 2013 Multivariate sampling Kantorovich operators: approximation and applications to civil engineering. EURASIP, Proc. SampTA pp. 400–403.

Costarelli, D., F. Cluni, A. M. Minotti, and G. Vinti, 2014a Applications of sampling Kantorovich operators to thermographic images for seismic engineering. arXiv preprint arXiv:1411.2584 .

Costarelli, D. and G. Vinti, 2011 Approximation by multivariate generalized sampling Kantorovich operators in the setting of orlicz spaces. Bollettino dell'Unione Matematica Italiana **4**: 445–468.

Costarelli, D. and G. Vinti, 2013 Approximation by nonlinear multivariate sampling Kantorovich type operators and applications to image processing. Numerical Functional Analysis and Optimization **34**: 819–844.

Costarelli, D. and G. Vinti, 2014 Sampling Kantorovich operators and their applications to approximation problems and to digital image processing. In *Proceedings of 8th international conference on applied mathematics, simulation, modelling (ASM'14), Florence, Italy November*, pp. 22–24.

Costarelli, D., G. Vinti, *et al.*, 2014b Order of approximation for sampling Kantorovich operators. Journal of Integral Equations and Applications **26**: 345–367.

Dalmanog, Ö., O. Dog, *et al.*, 2010 On statistical approximation properties of Kantorovich type q-Bernstein operators. Mathematical and Computer Modelling **52**: 760–771.

Dalmanoğlu, Ö., 2007 Approximation by Kantorovich type q-Bernstein operators .

de la Cal, J. and A. M. Valle, 2000 A generalization of Bernstein–Kantorovič operators. Journal of mathematical analysis and applications **252**: 750–766.

Deo, N., M. Dhamija, and D. Miclăuş, 2016 Stancu–Kantorovich operators based on inverse Pólya–Eggenberger distribution. Applied Mathematics and Computation **273**: 281–289.

Dogru, O. and N. Ozalp, 2001 Approximation by Kantorovich type generalization of meyer-konig and zeller operators. Glasnik matematički **36**: 311–318.

Duman, O., M. Özarslan, and O. Doğru, 2006 On integral type generalizations of positive linear operators. Studia Mathematica **174**: 1–12.

Eggenberger, F. and G. Pólya, 1923 Über die statistik verketteter vorgänge. ZAMM-Journal of Applied Mathematics and Mechanics/Zeitschrift für Angewandte Mathematik und Mechanik **3**: 279–289.

Gadjiev, A. and A. Ghorbanalizadeh, 2010 Approximation properties of a new type Bernstein–Stancu polynomials of one and two variables. Applied mathematics and computation **216**: 890–901.

Gonska, H., M. Heilmann, and I. Raşa, 2011 Kantorovich operators of order k. Numerical functional analysis and optimization **32**: 717–738.

Hounkonnou, M. N., J. Désiré, and B. Kyemba, 2013 R (p, q)-calculus: differentiation and integration. SUT J. Math **49**: 145–167.

İçöz, G., 2012 A Kantorovich variant of a new type Bernstein–Stancu polynomials. Applied Mathematics and Computation **218**: 8552–8560.

Igoz, G., 2012 A kantorovich variant of a new type bernstein-stancu polynomails. AppI Math Comput **218**: 8552–8560.

Kac, V. and P. Cheung, 2001 *Quantum calculus*. Springer Science & Business Media.

Kajla, A. and S. Araci, 2017 Blending type approximation by Stancu-Kantorovich operators based on pólya-eggenberger distribution. Open Physics **15**: 335–343.

Kantorovich, L., 1930 Sur certains développements suivant les polynômes de la forme de s. Bernstein, I, II, CR Acad. URSS **563**: 568.

Karaca, Y., 2022 Global attractivity, asymptotic stability and blow-up points for nonlinear functional-integral equations'solutions and applications in banach space bc (r+) with computational complexity. Fractals **30**: 2240188.

Karaca, Y., M. Moonis, Y.-D. Zhang, and C. Gezgez, 2019 Mobile cloud computing based stroke healthcare system. International Journal of Information Management **45**: 250–261.

Katriel, J. and M. Kibler, 1992 Normal ordering for deformed boson operators and operator-valued deformed stirling numbers. Journal of Physics A: Mathematical and General **25**: 2683.

Lubinsky, D., 1995 Weierstrass'theorem in the twentieth century: A selection. Quaestiones Mathematicae **18**: 91–130.

Lupas, A., 1987 A q-analogue of the Bernstein operator. In *Seminar on numerical and statistical calculus, University of Cluj-Napoca*, volume 9.

Marinković, S., P. Rajković, and M. Stanković, 2008 The inequalities for some types of q-integrals. Computers & Mathematics with Applications **56**: 2490–2498.

Mohiuddine, S., T. Acar, and A. Alotaibi, 2017 Construction of a new family of Bernstein-Kantorovich operators. Mathematical Methods in the Applied Sciences **40**: 7749–7759.

Muraru, C.-V., 2011 Note on q-Bernstein-Schurer operators. Stud. Univ. Babes-Bolyai Math **56**: 489–495.

Mursaleen, M., K. J. Ansari, and A. Khan, 2015 On (p, q)-analogue of Bernstein operators. Applied Mathematics and Computation **266**: 874–882.

Mursaleen, M., K. J. Ansari, and A. Khan, 2016 Some approximation results for Bernstein-Kantorovich operators based on (p, q)-calculus. UPB Sci. Bull., Ser. A **78**: 129–142.

Mursaleen, M., K. J. Ansari, and A. Khan, 2017 Approximation by kantorovich type q-Bernstein-Stancu operators. Complex Analysis and Operator Theory **11**: 85–107.

Ostrovska, S., 2016 The q-versions of the Bernstein operator: from mere analogies to further developments. Results in Mathematics **69**: 275–295.

Ozarslan, M. A. and O. Duman, 2016 Smoothness properties of modified Bernstein-Kantorovich operators .

Özarslan, M. A., O. Duman, and H. Srivastava, 2008 Statistical approximation results for Kantorovich-type operators involving some special polynomials. Mathematical and computer modelling **48**: 388–401.

Özarslan, M. A. and T. Vedi, 2013 q-Bernstein-Schurer-Kantorovich operators. Journal of Inequalities and Applications **2013**: 444.

Phillips, G. M., 2003 Bernstein polynomials. In *Interpolation and Approximation by Polynomials*, pp. 247–290, Springer.

Pinkus, A., 2000 Weierstrass and approximation theory. Journal of Approximation Theory **107**: 1–66.

Radu, C., 2008 Statistical approximation properties of Kantorovich operators based on q-integers, creat. math. Inform **17**: 75–84.

Rashid, S., S. Sultana, Y. Karaca, A. Khalid, and Y.-M. Chu, 2022 Some further extensions considering discrete proportional fractional operators. Fractals **30**: 2240026.

Ren, M.-Y. and X.-M. Zeng, 2013 On statistical approximation properties of modified q-Bernstein-Schurer operators. Bulletin of the Korean Mathematical Society **50**: 1145–1156.

Sahai, V. and S. Yadav, 2007 Representations of two parameter quantum algebras and p, q-special functions. Journal of mathematical analysis and applications **335**: 268–279.

Vinti, G. and L. Zampogni, 2009 Approximation by means of nonlinear Kantorovich sampling type operators in orlicz spaces. Journal of Approximation Theory **161**: 511–528.

How to cite this article: Bawa, P., Bhardwaj, N., and Bhatia, S. K. Different Variants of Bernstein Kantorovich Operators and Their Applications in Sciences and Engineering Field. *Chaos Theory and Applications*, 5(4), 293-299, 2023.

CHAOS
Theory and Applications
in Applied Sciences and Engineering

e-ISSN: 2687-4539
RESEARCH ARTICLE
Vol.5 / No.4 / 2023 / pp.300-307
Special Issue
https://doi.org/10.51537/chaos.1324355

Weighted and Well-Balanced Nonlinear TV-Based Time-Dependent Model for Image Denoising

Alka Chauhan *,[1], **Santosh Kumar** *,[2] **and Khursheed Alam** *,[3]
*Department of Mathematics, Sharda School of Basic Sciences and Research, Sharda University Greater Noida-201310 UP, India.

ABSTRACT The partial differential equation (PDE)-based models are widely used to remove additive Gaussian white noise and preserve edges, and one of the most widely used methods is the total variation denoising algorithm. Total variation (TV) denoising algorithm-based time-dependent models have seen considerable success in the field of image-denoising and edge detection. TV denoising algorithm is based on that signals with spurious detail have a high total variation and reduction of unwanted signals to achieve noise-free images. It is a constrained optimization-type algorithm. The Lagrange multiplier and gradient descent method are used to solve the TV algorithm to reach the PDE-based time-dependent model. To eliminate additive noise and preserve edges, we investigate a class of weighted time-dependent model in this study. The proposed method is investigated in a well-balanced flow form that extends the time-dependent model with an adaptive fidelity element. Adaptive function is fusing into the regularization term of the classical time-dependent model which successfully enhances the intensity of the regularizer function. We maintain the ability of the time-dependent model without any oscillation effects. Furthermore, we want to prove the viscosity solution of our weighted and well-balanced time-dependent model, demonstrating its existence and uniqueness. The finite difference method is applied to discretize the nonlinear time-dependent models. The numerical results are expressed as a statistic known as the peak signal-to-noise ratio (PSNR) and structural similarity index metric (SSIM). Numerical experiments demonstrate that the proposed model yields good performance compared with the previous time-dependent model.

KEYWORDS
Partial differential equation
Total variation
Time dependent model
Weighted and well balanced
Image denoising
Image smoothing
Viscosity solution
Explicit scheme

INTRODUCTION

Noise degraded the visual quality of images, and image lost their significant features due to these random signals. An image becomes noisy during the acquisition, transmission, and processing steps. However, noise occurs randomly but sometimes it may be data dependent. Artifacts do not originate from the original images produced due to the noise. There are two types of noise additive noise and multiplicative noise. Additive noise are random signals that depend on the state of the system like Gaussian noise. Multiplicative noise is random signals that depend on the state of the system like speckle noise. Gaussian additive noise is added to the original signal during the acquisition of the image and this noise is distributed uniformly all over the image.

The additive noisy image as $u_0 : \Omega \to \mathbb{R}$, Ω is a bounded region of $\mathbb{R}^2$ and it can be defined as

$$u_0(x) = u(x) + n(x). \tag{1}$$

Here $u(x)$, $x \in \Omega$ signifies the true image, the noisy image represented by $u_0(x)$, and Gaussian white noise $n(x)$ which contains zero mean and σ^2 represent variance.

Rudin *et al.* (1992) for the first time, introduced total variation functional with static constraint to reduce the additive Gaussian white noise and edge preservation and can be represented by the ROF model. The total-variation-based model was impressive in the preservation of geometrical boundaries. The denoising problem can be seen as a minimization problem from a variational perspective. The minimization problem consists of two terms first

Manuscript received: 10 July 2023,
Revised: 4 September 2023,
Accepted: 6 September 2023.

[1]alkachauhan5490@gmail.com
[2]skykumar87@gmail.com (**Corresponding author**)
[3]khursheed.alam56@gmail.com

one measures the fidelity of the observed image; the second term is the regularizer parameter which is used to reduce the noise from the image. The Euler Lagrange multiplier and gradient descent method to steady state to ROF model for image denoising and edge detection. The fixed-point algorithm to optimize the energy functional was given by Vogel and Oman (1996) for image denoising. Chan *et al.* (1999) introduced a two-dimensional non-linear primal-dual algorithm for image restoration. They used the Tikhonov regularizer instead of the image gradient term in the time-dependent model. To overcome the computational difficulty of the term $\frac{\nabla u}{|\nabla u|}$ they replaced the denominator term by $\sqrt{|\nabla u|^2+\beta}$ in the time-dependent model, where β is a parameter. These models achieved better results in image denoising, but computational cost is high in the case of deblurring. Marquina and Osher (2000) introduced the time-dependent model for image restoration. They multiplied the magnitude of the gradient in the ROF model for image denoising and deblurring. They have discussed Roe's explicit scheme to check the convergence rate of their model. El-Shorbagy *et al.* (2023) presented an analysis of the general fractional derivative function with the Mittag-Leffler kernel and ABC operator at various fractional orders. Haidong *et al.* (2023) presented an analysis of the four-dimensional Chaotic system in consideration of the Mittag-Leffler kernel. XU *et al.* (2022) introduced a study of numerical analysis of a two-dimensional torus chaotic system with a power-law kernel. Qu *et al.* (2022) proposed a novel approach for solving the non-linear fractional order diffusion equation with the neural network method. A class of hyperbolic and parabolic models for image denoising and edge detection are proposed by Kumar and Alam (2021a,b).

Barcelos *et al.* (2005, 2003) proposed a nonlinear anisotropic parabolic model for the elimination of the noise and also discussed the well-balanced flow in the parabolic model. They have used an adaptive parameter to maintain the balance between the forcing term and data fidelity term in the anisotropic diffusion model. The improved image fidelity term for image denoising is proposed by Smolka (2008). Prasath and Vorotnikov (2014) generalized the PM model with a weighted and well-balanced flow equation and obtained better results comparatively. To make the PM model in terms of weighted and well-balanced, they used the diffusion function which depends on the magnitude of the image gradient and spatial variable. A weighted total variation-based model using mean curvature as a regularizer function was recently introduced by Phan (2020). They used the split Bergman method to obtain a fast convergence rate. Li and Li (2021) introduced a weighted total variation model using the exponential regularizer function. Many other researchers introduced the well-balanced model inspired by mean curvature motion and biased, see reference, (El-Fallah and Ford 1998; Chen *et al.* 1999).

In this study, we propose a weighted and well-balanced time-dependent model to minimize the energy functional by evolving the Euler-Lagrange equation. This model is related to a variational model with the diffusivity linked to the regularizer. The Charbonnier diffusivity is used in the time-dependent model, it is related to non-convex regularization (Charbonnier *et al.* 1994; Weickert 1997). An adaptive function ξ is fused in the regularizer term of the weighted and well-balanced time-dependent model. Experiments on many different gray-scale images are conducted to show the advantage of the weighted and well-balanced time-dependent model over the old model. Quantitative analysis shows that the proposed model is very effective and efficient in both noise reduction and edge detection. Furthermore, we want to prove the viscosity solution of a weighted and well-balanced time-dependent model.

This paper is organized as follows: The weighted and well-balanced denoising techniques are given in section 2. The viscosity solution of the weighted and well-balanced time-dependent model is given in section 3. The explicit scheme of the weighted and well-balanced model is given in section 4. In Section 5, the results are given in Figures 2-6, and Table 1, last, the conclusion is in Section 6.

TV-BASED WEIGHTED AND WELL-BALANCED TIME-DEPENDENT MODEL FOR DENOISING ALGORITHM

Rudin *et al.* (1992) introduced a TV-based regularisation functional for image denoising and edge detection. The restricted regularisation functional can be expressed as:

$$\text{minimize} \int_\Omega |\nabla u|\, dx = \int_\Omega \sqrt{u_x^2+u_y^2}\, dx, \tag{2}$$

$$\text{subject to } ||u-u_0||_{L^2}^2 = |\Omega|\sigma^2.$$

Using the definition of Euler-Lagrange and applying the equation (2). Then it can be expressed as:

$$0 = -\nabla.\left(\frac{\nabla u}{|\nabla u|}\right) + \lambda(u-u_0). \tag{3}$$

The value of $\nabla u = 0$ then the equation (3) is not well defined. Then the TV-based functional can be extended in another form:

$$\int_\Omega |\nabla u|_\gamma\, dx = \int_\Omega \sqrt{u_x^2+u_y^2+\gamma}\, dx. \tag{4}$$

Here $\gamma > 0$ as given in see reference (Chang and Chern 2003).

In the TV model diffusion takes place along the gradient orthogonal direction so that edges can be preserved during smoothing of the image. This model approximates the flat areas by considering the piece-wise constant surface and emerges the staircase artifacts. The equation (3) can be written as a time-dependent model given by (Rudin *et al.* 1992):

$$\frac{\partial u}{\partial t} = \nabla.\left(\frac{\nabla u}{|\nabla u|}\right) - \lambda(u-u_0), \tag{5}$$

with homogeneous Neumann boundary conditions $\frac{\partial u}{\partial \vec{n}} = 0$ and $u(x,0) = u_0(x)$ and scale parameter $\lambda > 0$. The left-hand side of the equation (5) is the regularization term that denotes the prior constraint and $(u-u_0)$ data fidelity term and λ is the Lagrange multiplier used to adjust the regularization term and data fidelity term. u_0 approaches u at a larger value of λ and the image lost its important details for a much larger value of λ.

The improved TV-based time-dependent model for image restoration is proposed by Marquina and Osher (2000):

$$\frac{\partial u}{\partial t} = |\nabla u|\nabla.\left(\frac{\nabla u}{|\nabla u|}\right) - |\nabla u|\lambda(u-u_0), \tag{6}$$

with the same boundary conditions above.

Gilboa *et al.* (2006) introduced the spatially adaptive balance term parameter λ and it can be made flexible. The well-balanced flow may also be further generalized. For instance, it is possible to make the diffusion coefficient depend on the picture u and the results in various diffusion flows and be constructed to have an impact on the restoration procedure. To extend the model (6) into weighted and well-balanced flow model:

$$\frac{\partial u}{\partial t} = \xi\,|\nabla u|\nabla.\left(\frac{\nabla u}{|\nabla u|}\right) - (1-\xi)|\nabla u|\lambda(u-u_0). \tag{7}$$

Here $\xi = \xi(|\nabla G_\sigma * u|)$, G_σ is represent as low pass filter or Gaussian kernel and $G_\sigma * u$ is a convolution and the diffusivity function ξ such as:

$$\xi(s) = \frac{1}{\sqrt{1+(|s|^2/K^2)}}, \tag{8}$$

where $\xi(s) \geq 0$ is a decreasing function and satisfying $\xi(0) = 1$ and $\xi(s) \to 0$ as $s \to \infty$ and K is the diffusivity parameter. It is related to the convex regularizer, see references (Charbonnier *et al.* 1994; Weickert 1997).

Motivated by Álvarez *et al.* (1992); Prasath and Vorotnikov (2014), we want to show the theoretical considerations and viscosity solution of the weighted and well-balanced time-dependent model as given in the next section.

THEORETICAL CONSIDERATIONS

We describe the mathematical formulation as the viscosity solution of the weighted and well-balanced time-dependent model (7). It can be written as:

$$\begin{aligned}\frac{\partial u}{\partial t} &= \xi(\nabla G_\sigma * u)a_{ij}(\nabla u)u_{x_ix_j} - \lambda|\nabla u|(1-\xi(\nabla G_\sigma * u))\\ &(u-u_0),\ x \in \mathbb{R}^2, t \in \mathbb{R}_+.\end{aligned} \tag{9}$$

Here

$$a_{ij}(p) = \delta_{ij} - \frac{p_i p_j}{|p|^2},$$

$$G_\sigma \in C^{1,1}(\mathbb{R}^2,\mathbb{R}),\ \ G_\sigma(p) > 0 \text{ for all } p \text{ in } \mathbb{R}^2, \tag{10}$$

and u_0 is continuous on $\mathbb{R}^2$.

The equation (9) represents the PDE-based diffusion equation with possible high degeneracy and a quasilinear term $a_{ij}(\nabla u)u_{x_ix_j}$, nonlocal term $\xi(\nabla G_\sigma * u)$ and data and fidelity term is $\lambda(1-\xi(\nabla G_\sigma * u))|\nabla u|(u-u_0)$.

Definition. A function u is a viscosity sub-supersolution of equation (9) from the space

$$u \in C(\mathbb{R}^2 \times [0,T]) \cap L^\infty(0,T;W^{1,\infty}(\mathbb{R}^2)) \tag{11}$$

if for any $\phi \in C^2(\mathbb{R}^2 \times \mathbb{R})$ and any point $(x_0,t_0) \in \mathbb{R}^2 \times (0,T]$ of local maxima/minima of the function $u-\phi$ has

$$\begin{aligned}&\frac{\partial \phi}{\partial t}(x_0,t_0) - \xi(\nabla G_\sigma * u(x_0,t_0))a_{ij}(\nabla\phi(x_0,t_0))\phi_{x_ix_j}(x_0,t_0)+\\ &\lambda(1-\xi(\nabla G_\sigma * u(x_0,t_0)))|\nabla\phi(x_0,t_0)|(u-u_0)(x_0,t_0) \leq 0,\\ &\text{if } \nabla\phi(x_0,t_0) \neq 0,\end{aligned} \tag{12}$$

$$\begin{aligned}&\frac{\partial \phi}{\partial t}(x_0,t_0) - \xi(\nabla G_\sigma * u(x_0,t_0))\limsup_{p\to 0} a_{ij}(p)\phi_{x_ix_j}(x_0,t_0) \leq 0,\\ &\text{if } \nabla\phi(x_0,t_0) = 0.\end{aligned} \tag{13}$$

The viscosity solution of function is a viscosity sub and super solution.

Theorem. (i) The equation (9) has a viscosity solution in class (11) for every $T > 0$. Moreover,

$$\inf_{\mathbb{R}^2} u_0 \leq u(x,t) \leq \sup_{\mathbb{R}^2} u_0.$$

(ii) For any two viscosity solution u and v of (9),

$$\sup_{0\leq t\leq T} ||u(x,t)-v(x,t)||_{L^\infty(\mathbb{R}^2)} \leq C||u_0-v_0||_{L^\infty(\mathbb{R}^2)}. \tag{14}$$

Here u_0 and v_0 are Lipschitz continuous functions in $\mathbb{R}^2$ for every positive T and C is positive constant.

Proof. The viscosity solution u which is satisfied the inequality such that

$$\inf_{\mathbb{R}^2} u_0 \leq u(x,t) \leq \sup_{\mathbb{R}^2} u_0, \qquad \text{on} \quad \mathbb{R}^2 \times \mathbb{R}_+. \tag{15}$$

We put $\phi = \sup_{\mathbb{R}^2} u_0 + \delta t(\delta > 0)$, then at the point (x_0,t_0), of the local maxima of $u-\phi$, (12) gives $\frac{\partial\phi}{\partial t}(x_0,t_0) \leq 0$ if $\nabla\phi(x_0,t_0) = 0$. So we get a contradiction $\frac{\partial\phi}{\partial t}(x_0,t_0) \equiv \delta > 0$ on $\mathbb{R}^2 \times [0,\infty)$.
attains a local maximum at (x_0,t_0) with $t_0 > 0$, then $\nabla\phi(x_0,t_0) = 0$ and from (12), $\frac{\partial\phi}{\partial t}(x_0,t_0) \leq 0$. This contradicts $\frac{\partial\phi}{\partial t}(x_0,t_0) \equiv \delta > 0$ on $\mathbb{R}^2 \times [0,\infty)$.
At $t_0 = 0$, the function $u-\phi$ have maximum value. So we can write
$u-\phi \leq \sup(u_0 - \sup_{\mathbb{R}^2} u_0)$, then $u \leq \sup_{\mathbb{R}^2} u_0 + \delta t$.
Similarly, we can write
$u \geq \inf_{\mathbb{R}^2} u_0 - \delta t$, as $\delta \to 0$, we can get (15).

In the starting, we demonstrate a uniform estimate for the equation (9).

$$||Du(t,.)||_{L^\infty(\mathbb{R}^2)} \leq e^{Ct}||Du_0||_{L^\infty(\mathbb{R}^2)}. \tag{16}$$

Here C is the constant number and it is depends on u_0, $\sup_{|p|\leq R}|\nabla^2 g_\epsilon(p)|$ and $\sup_p|a^\epsilon_{ij}(P)|$ with $R = ||w||_{L^\infty(\mathbb{R}^2)}||\nabla G||_{L^1(\mathbb{R}^2)}$.

Let u^ϵ be the smooth solution and it is given by

$$\begin{aligned}&\frac{\partial u^\epsilon}{\partial t} = \xi_\epsilon(\nabla G_\sigma * u^\epsilon)a^\epsilon_{ij}(\nabla u^\epsilon)u^\epsilon_{x_ix_j} -\\ &\lambda(1-\xi_\epsilon(\nabla G_\sigma * u^\epsilon))b^\epsilon(|\nabla u^\epsilon|)(u^\epsilon - u^\epsilon_0), \quad x \in \mathbb{R}^2, t \in \mathbb{R}_+,\\ &u^\epsilon(x,0) = u^\epsilon_0(x), \quad x \in \mathbb{R}^2.\end{aligned} \tag{17}$$

We establish an a priori estimate for ∇u. At that level, this estimate will become formal, and it will later be supported. In reality, we take a smooth solution concerning ϵ

$$\begin{aligned}&\frac{\partial u^\epsilon}{\partial t} = \xi_\epsilon(\nabla G_\sigma * w)a^\epsilon_{ij}(\nabla u^\epsilon)u^\epsilon_{x_ix_j} -\\ &\lambda(1-\xi_\epsilon(\nabla G_\sigma * u^\epsilon))b^\epsilon(|\nabla u^\epsilon|)(u^\epsilon - u^\epsilon_0), \quad x \in \mathbb{R}^2, t \in \mathbb{R}_+,\\ &u^\epsilon(x,0) = u^\epsilon_0(x), \quad x \in \mathbb{R}^2,\end{aligned} \tag{18}$$

where,

$$\begin{aligned}&0 < \epsilon < 1,\\ &a^\epsilon_{ij}(p) = (\epsilon+1)\delta_{ij} - \frac{p_i p_j}{|p|^2+\epsilon^2},\\ &b^\epsilon(p) = \sqrt{|p|^2+\epsilon},\ \ \xi_\epsilon = \xi+\epsilon,\ \ w \in L^\infty(\mathbb{R}^2 \times (0,\infty]),\end{aligned} \tag{19}$$

$u^\epsilon_0(x) \in C^\infty(\mathbb{R}^2)$ (antireflective) such that $u^\epsilon_0 \to u_0$ uniformly and $||\nabla u^\epsilon_0||_{L^\infty(\mathbb{R}^2)} \leq ||\nabla u_0||_{L^\infty(\mathbb{R}^2)}$ and u^ϵ_0 can be write $||u^\epsilon_0||_{L^\infty(\mathbb{R}^2)} \leq ||u_0||_{L^\infty(\mathbb{R}^2)}$.

The problems (17)-(19) admit a smooth solution $u^\epsilon \in C^\infty(\mathbb{R}^2 \times \mathbb{R}_+)$ by the definition of of the quasi-linear uniformly. According to equation (14), we can say that any smooth solution of a function is a

viscosity solution. For any positive number M and it is dependent on u_0, then it satisfies the condition $|u^\epsilon| \le M$.

The differentiating equation (18) w.r.to x_k, after that we multiplying $2u^\epsilon_{x_k}$, a summation w.r.to k is given by

$$\begin{aligned}
&\frac{\partial|\nabla u^\epsilon|^2}{\partial t} - \xi_\epsilon(\nabla G_\sigma * w)a^\epsilon_{ij}(\nabla u^\epsilon)\frac{\partial^2|\nabla u^\epsilon|^2}{\partial x_i \partial x_j} - \\
&\xi_\epsilon(\nabla G_\sigma * w)\frac{\partial a^\epsilon_{ij}}{\partial l}(\nabla u^\epsilon)u^\epsilon_{x_i x_j}\frac{\partial|\nabla u^\epsilon|^2}{\partial x_l} + \\
&\lambda\frac{\partial b^\epsilon(\nabla u^\epsilon)}{\partial m}(1-\xi_\epsilon(\nabla G_\sigma * w))(u^\epsilon - u^\epsilon_0)\frac{\partial|\nabla u^\epsilon|^2}{\partial x_m} \\
&= -2\xi_\epsilon(\nabla G_\sigma * w)a^\epsilon_{ij}(\nabla u^\epsilon)u^\epsilon_{x_k x_i}u^\epsilon_{x_k x_j} + \\
&2\frac{\partial\xi_\epsilon}{\partial l}(\nabla G_\sigma * w).(G_{\sigma x_l x_k} * w)a^\epsilon_{ij}(\nabla u^\epsilon)u^\epsilon_k u^\epsilon_{x_i x_j} - \\
&2\lambda b^\epsilon(\nabla u^\epsilon)(1-\xi)u^\epsilon_{x_k}u^\epsilon_{x_k} + 2\lambda b^\epsilon(\nabla u^\epsilon)(1-\xi)((u_0)^\epsilon_{x_k})u^\epsilon_{x_k} + \\
&2\lambda b^\epsilon(\nabla u^\epsilon)\nabla\xi(\nabla G_\sigma * u)\cdot\left(u * \frac{\partial\nabla G_\sigma}{\partial x_k}\right)(u-u_0)u_{x_k}.
\end{aligned} \tag{20}$$

From the definitions of a^ϵ_{ij}, b^ϵ, g^ϵ and h, we have

$$|a^\epsilon_{ij}(\nabla u^\epsilon)u^\epsilon_{x_i x_j}| \le C(a^\epsilon_{ij}(\nabla u^\epsilon)u^\epsilon_{x_k x_i}u^\epsilon_{x_k x_j})^{\frac{1}{2}}, \quad \sup_{\mathbb{R}^2} h \le C,$$

$$\sup_{\mathbb{R}^2}|Db^\epsilon(s)| \le C, \quad |G_{\sigma x_l x_k} * w| \le C,$$

$$|\frac{\partial\xi_\epsilon}{\partial l}(\nabla G_\sigma * w)| \le C(\xi_\epsilon(\nabla G_\sigma * w))^{\frac{1}{2}}.$$

Here C is a positive constant number and it is depend only $\sup|w|$, ξ_ϵ and M.

Using Cauchy's inequality the equation (20) estimates by

$$\begin{aligned}
&\frac{\partial|\nabla u^\epsilon|^2}{\partial t} - \xi_\epsilon(\nabla G_\sigma * w)a^\epsilon_{ij}(\nabla u^\epsilon)\frac{\partial^2|\nabla u^\epsilon|^2}{\partial x_i \partial x_j} - \\
&\xi_\epsilon(\nabla G_\sigma * w)\frac{\partial a^\epsilon_{ij}}{\partial l}(\nabla u^\epsilon)u^\epsilon_{x_i x_j}\frac{\partial|\nabla u^\epsilon|^2}{\partial x_l} \\
&+ \lambda\frac{\partial b^\epsilon(\nabla u^\epsilon)}{\partial m}(1-\xi_\epsilon(\nabla G_\sigma * w))(u^\epsilon - u^\epsilon_0)\frac{\partial|\nabla u^\epsilon|^2}{\partial x_m} \\
&\le C(|\nabla u^\epsilon|^2 + 1) \qquad \text{in } \mathbb{R}^2 \times \mathbb{R}_+.
\end{aligned} \tag{21}$$

Next, use the maximal principle (Brezis 1987) to deduce clearly (16). We just need to approximate (17), and we may get smooth solutions to draw this conclusion. Using the a priori estimate mentioned above, we get the valid approximate solutions.

Applying the maximization rule (Brezis 1987), the equation (21) yields $||\nabla u^\epsilon(.,t)||_{L^\infty(\mathbb{R}^2)} \le e^{Ct}$ we can defined $||\nabla(u_0)^\epsilon||_{L^\infty(\mathbb{R}^2)} \le e^{Ct}$ to reached to $||\nabla(u_0)||_{L^\infty(\mathbb{R}^2)} \le C_T$. This inequality can be reached to

$$|u^\epsilon(x,t) - u^\epsilon(y,t)| \le C_T|x-y|,$$

it is satisfy for every $x, y \in \mathbb{R}^2$, for all $t \in [0,T]$ and C_T represent the independent constant parameters it is depend on ϵ, t, x, y. Now for every $x \in \mathbb{R}^2$ and $s,t \in [0,T]$. A similar argument has led us to

$$|u^\epsilon(x,s) - u^\epsilon(x,t)| \le C_T|s-t|^{\frac{1}{2}}.$$

Using the Ascoli-Arzela theorem, a subsequence u^{ϵ_k} of u^ϵ exists, then

$$u^{\epsilon_k} \to u \quad as \quad \epsilon_k \to 0, \tag{22}$$

is locally uniformly. So easily get the inequality (16).

Second, we'll demonstrate the presence of a viscosity solution. From equation (22), we can say that u is the viscosity solution of the weighted and well-balanced model (9) in the sense of equations (12)-(13). Let $\phi \in C^2(\mathbb{R}^2 \times \mathbb{R}_+)$ be the result. Initially, we suppose that for a location $(x_0,t_0) \in \mathbb{R}^2 \times \mathbb{R}_+$ has a strict local maximum. When $u^{\epsilon_k} \to u$ is consistently close to (x_0,t_0), There is a local maximum for $u-\phi$ at the position (x_k,t_k) with

.

$$(x_k,t_k) \to (x_0,t_0), \quad k \to \infty \tag{23}$$

and

$$\nabla u^{\epsilon_k} = \nabla\phi, \quad \frac{\partial u^{\epsilon_k}}{\partial t} = \frac{\partial\phi}{\partial t}, \quad a^{\epsilon_k}_{ij}(\nabla u^{\epsilon_k})u^{\epsilon_k}_{x_i x_j} \le a^{\epsilon_k}_{ij}(\nabla\phi)\phi_{x_i x_j}.$$

Therefore, (17) implies that at (x_k,t_k),

$$\begin{aligned}
&\frac{\partial\phi}{\partial t} - \xi_{\epsilon_k}(\nabla G_\sigma * u^{\epsilon_k})a^{\epsilon_k}_{ij}(\nabla\phi)\phi_{x_i x_j} + \\
&b^{\epsilon_k}(\nabla\phi)(1-\xi_{\epsilon_k}(\nabla G_\sigma * u^{\epsilon_k}))(u^{\epsilon_k} - (u^{\epsilon_k}_0)) \le 0.
\end{aligned} \tag{24}$$

(1) If $\nabla\phi(x_0,t_0) \ne 0$, according to (23), $\nabla\phi(x_k,t_k) \ne 0$ for largest value of k and applying the limits to (24), we get

$$\begin{aligned}
&\frac{\partial\phi}{\partial t} - \xi(\nabla G_\sigma * u)a_{ij}(\nabla\phi)\phi_{x_i x_j} + \\
&b(\nabla\phi)(1-\xi(\nabla G_\sigma * u))(u-(u_0)) \le 0, \ \text{ at } (x_0,t_0),
\end{aligned} \tag{25}$$

It is similar to equation (9).
(2) If $\nabla\phi(x_0,t_0) = 0$, according to (23), $\nabla\phi(x_k,t_k) \to 0, \epsilon \to 0$ as $k \to 0$. The equation (24) reached to another form

$$\begin{aligned}
&\frac{\partial\phi}{\partial t} - (\xi(\nabla G_\sigma * u) + \epsilon_k)\left((\epsilon_k+1)\delta_{ij} - \frac{(\nabla\phi)_i(\nabla\phi)_j}{|\nabla\phi|^2+\epsilon^2}\right)\phi_{x_i x_j} \\
&\quad + b^{\epsilon_k}(\nabla\phi)(1-\xi(\nabla G_\sigma * u))(u^{\epsilon_k} - (u^{\epsilon_k}_0)) \le 0, \ \text{ at } (x_k,t_k).
\end{aligned} \tag{26}$$

If $b^{\epsilon_k}(\nabla\phi(x_k,t_k)) \to 0$ to (26), we get

$$\frac{\partial\phi}{\partial t} - \xi(\nabla G_\sigma * u)\left(\delta_{ij} - \frac{(\nabla\phi)_i(\nabla\phi)_j}{|\nabla\phi|^2+\epsilon^2}\right)\phi_{x_i x_j} \le 0, \ \text{ at } (x_0,t_0).$$

If $u-\phi$ has a local maximum at (x_0,t_0). The method of proof is consistent i.e., u is a sub-solution of (13). Similarly, it can be proven that u is a super-solution. Hence, u is a viscosity solution of (9).

.

DISCRETE SCHEME

The explicit scheme of the time dependent models (6) and (7):

$$\begin{aligned}
u_t = &\frac{u_{xx}(u_y^2+\gamma) - 2u_{xy}u_x u_y + u_{yy}(u_x^2+\gamma)}{(u_x^2+u_y^2+\gamma)} - \\
&\sqrt{u_x^2+u_y^2+\gamma}\,\lambda(u-u_0).
\end{aligned} \tag{27}$$

$$\begin{aligned}
u_t = \xi\,&\frac{u_{xx}(u_y^2+\gamma) - 2u_{xy}u_x u_y + u_{yy}(u_x^2+\gamma)}{(u_x^2+u_y^2+\gamma)} - \\
&(1-\xi)\sqrt{u_x^2+u_y^2+\gamma}\,\lambda(u-u_0).
\end{aligned} \tag{28}$$

We define the derivative terms as,

$$u^x_{ij} = \frac{u^n_{i+1,j} - u^n_{i-1,j}}{2\Delta x}; \quad u^y_{ij} = \frac{u^n_{i,j+1} - u^n_{i,j-1}}{2\Delta x};$$

$$u_{ij}^{xx} = \frac{u_{i+1,j}^n - 2u_{i,j}^n + u_{i-1,j}^n}{\Delta x^2}; \quad u_{ij}^{yy} = \frac{u_{i,j+1}^n - 2u_{i,j}^n + u_{i,j-1}^n}{\Delta x^2};$$

$$u_{ij}^{xy} = \frac{u_{i+1,j+1}^n - u_{i-1,j+1}^n - u_{i+1,j-1}^n + u_{i-1,j-1}^n}{4\Delta x \Delta x}; \quad u_{ij}^t = \frac{u_{i,j}^{n+1} - u_{i,j}^n}{\Delta t}.$$

Here u_{ij}^n is the approximation value of $u(x_i, y_j, t_n)$, $x_i = i\Delta x$, $y_j = j\Delta x$, $i, j = 1, 2, ..., N$, Δx spatial step and $t_n = n\Delta t$, $n \geq 1$, Δt is the time step size.

Let

$$r_{ij}^n = u_{ij}^{xx}((u_{ij}^y)^2 + \gamma) - 2u_{ij}^{xy}u_{ij}^x u_{ij}^y + u_{ij}^{yy}((u_{ij}^x)^2 + \gamma), \tag{29}$$

and

$$p_{ij}^n = ((u_{ij}^x)^2 + (u_{ij}^y)^2 + \gamma). \tag{30}$$

Then (27) reads as follows:

$$u_{ij}^t = \frac{r_{ij}^n}{p_{ij}^n} - \sqrt{((u_{ij}^x)^2 + (u_{ij}^y)^2 + \gamma)}\ \lambda\ (u_{ij}^n - u_{ij}^0). \tag{31}$$

Then (28) reads as follows:

$$u_{ij}^t = \xi_{ij}\ \frac{r_{ij}^n}{p_{ij}^n} - (1 - \xi_{ij})\sqrt{((u_{ij}^x)^2 + (u_{ij}^y)^2 + \gamma)}\ \lambda\ (u_{ij}^n - u_{ij}^0). \tag{32}$$

The function $\xi(|\nabla u|^2)$ can be discretised by,

$$\xi_{ij}^n = \psi'\left(\left(\frac{u_{i+1,j}^n - u_{i-1,j}^n}{\Delta x}\right)^2 + \left(\frac{u_{i,j+1}^n - u_{i,j-1}^n}{\Delta x}\right)^2\right).$$

For $\frac{\Delta t}{\Delta x^2} \leq 0.5$, the explicit technique is stable and convergent (Lapidus and Pinder 1983).

NUMERICAL EXPERIMENTS

The weighted and well-balanced time-dependent model for removing additive noise and preserving edges is proposed and applied to many 2-dimensional noisy grayscale images with different levels of noise parameters, we get the smooth images for denoising techniques. The original grayscale images of the size 256×256 with pixel values of [0, 255] such as Lena images, Boat images, and Figure 4(a). For numerical experiments, firstly to reduce the intensities of images lies in [0, 1]. To add the noise, we use the function imnoise (I, 'Gaussian', M, σ^2) in Matlab [MATLAB, 2022 version 9.12.0 (R2022a)], σ^2, and M are variance and mean zero respectively. The parameters $K = 5$ and $\lambda = 0.85$ are used in our numerical experiments (Catté *et al.* 1992; Chan *et al.* 1999).

We'll utilize the PSNR as a criterion for restoration which can be defined as:

$$\text{PSNR} = 10\log_{10}\left(\frac{R^2}{\frac{1}{mn}\sum_{i,j}^n (u_{i,j} - x_{i,j})^2}\right), \tag{33}$$

where $\{u_{i,j} - x_{i,j}\}$ are the differences in the pixel values between the original and denoised images. R is the maximum pixel value of the images.

The structural similarity index metric (SSIM) is used to compare the contrast and structure of the denoised image to the original image. The SSIM is formulated as:

$$\text{SSIM}(x, y) = \frac{(2 \times \mu_x\mu_y + D1) \times (2 \times \sigma_{xy} + D2)}{(\mu_x^2 + \mu_y^2 + D1)(\sigma_x^2 + \sigma_y^2 + D2)}, \tag{34}$$

where μ_x and μ_y are the mean of x and y, respectively, and x and y represent the local windows of the original image and denoised image, respectively. σ_{xy} denotes the covariance of x and y. $D1$=$(0.01 \times L)^2$ and $D2$=$(0.03 \times L)^2$ where L is the dynamic range of pixel values. SSIM value lies between 0 and 1. The higher value of SSIM gives a good visual quality of the denoised image and the lower value presents a poor visual quality of denoised image.

The proposed model is compared to a time-dependent model based on removing additive noise from the literature. Figure 1 represents the original Lena and Boat images. Figure 2(a-c) represents the noisy Lena images with ($\sigma^2 = 0.006, 0.008, 0.010$) respectively. Figure 2(d-f) represents the denoised images by the model (6) and Figure 2(g-i) represents the denoised images by the model (7). Figure 3(a-c) represents the noisy Boat images with ($\sigma^2 = 0.006, 0.008, 0.010$) respectively. Figure 3(d-f) represents the denoised images by the model (6) and Figure 3(g-i) represents the denoised images by the model (7). The numerical results are given in Figure 2-6 and Table 1 and achieve higher PSNR values by a weighted and well-balanced time-dependent model corresponding to the old model. The numerical results confirm that a weighted and well-balanced time-dependent model is very efficient in obtaining the solution.

(a) (b)

Figure 1 (a-b) Left side original Lena image and right side original Boat image.

(a) (b) (c) (d) (e) (f) (g) (h) (i)

Figure 2 (a-c) Noisy images with ($\sigma^2 = 0.006, 0.008, 0.010$); (d-f) corresponding denoised image by(6); (g-i) Denoised image by(7) respectively.

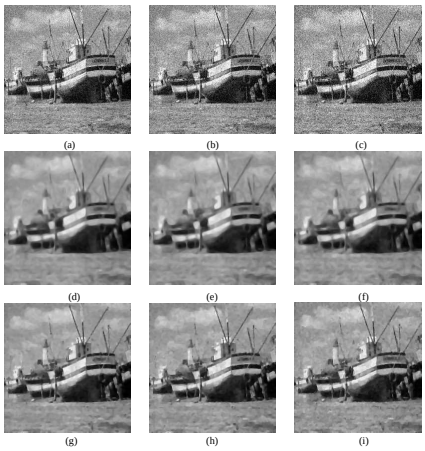

Figure 3 (a-c) Noisy images with ($\sigma^2 = 0.006, 0.008, 0.010$); (d-f) corresponding denoised image by (6); (g-i) Denoised image by (7) respectively.

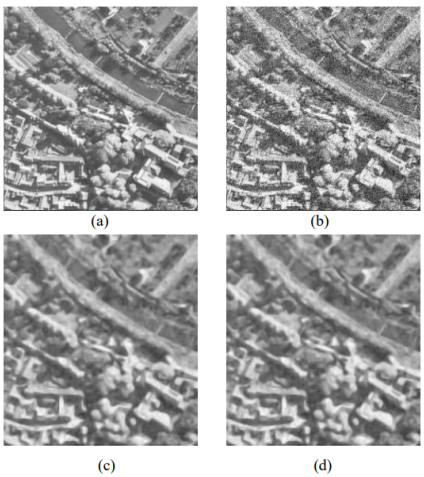

Figure 4 (a) Represent the original image; (b) Noisy image with $\sigma^2 = 0.010$ with PSNR and SSIM values are 20.13 and 0.6147 respectively; (c) Corresponding denoised image by model (6) with PSNR and SSIM values are 22.26 and 0.6825 respectively, at 5 iteration numbers; (d) Corresponding denoised image by model (7) with PSNR and SSIM values are 23.68 and 0.7769 respectively, at 5 iteration numbers.

Table 1 The comparison results.

Image	PSNR of noisy image	SSIM of noisy image	PSNR by (6)	SSIM by (6)	PSNR by (7)	SSIM by (7)
$\sigma^2 = 0.006$	22.41	0.4731	25.31	0.7645	28.15	0.8136
Lena $\sigma^2 = 0.008$	21.16	0.4274	25.19	0.7543	27.74	0.7943
$\sigma^2 = 0.010$	20.27	0.3914	25.08	0.7454	27.22	0.7743
$\sigma^2 = 0.006$	22.32	0.4566	24.24	0.6839	27.20	0.7725
Boat $\sigma^2 = 0.008$	21.06	0.4454	24.20	0.6735	26.89	0.7590
$\sigma^2 = 0.010$	20.17	0.4059	24.07	0.6633	26.56	0.7401
No. of iterations			10		10	

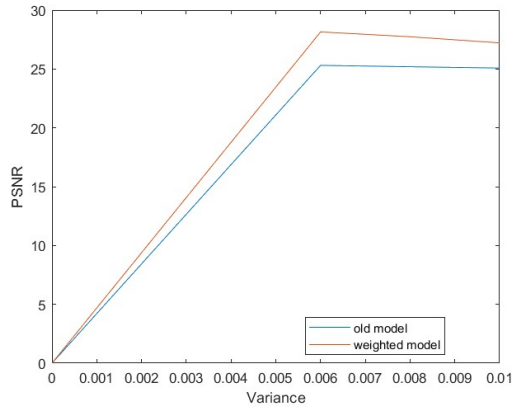

Figure 5 This graph is represented by Lena images, the results are given in terms of PSNR values in Table 1 for the weighted and well-balanced time-dependent model and the old model.

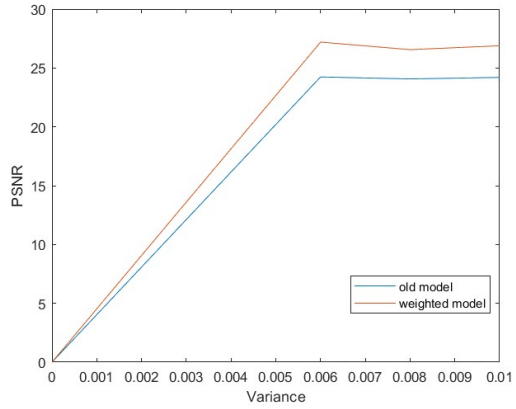

Figure 6 This graph is represented by Boat images, the results are given in terms of PSNR values in Table 1 for the weighted and well-balanced time-dependent model and the old model

CONCLUSION

In this paper, we proposed a total variation-based weighted and well-balanced time-dependent model for additive white noise reduction and preserved edges. The total-variation algorithm-based time-dependent model performs a good trade between noise reduction and edge preservation. A weighted function ξ is incorporated into the regularizer term of the time-dependent model to make it more effective and efficient for image denoising. The finite difference method is used to discretize the proposed model. To check the performance of the denoised images, we used the peak signal-to-noise ratio (PSNR) and structural similarity index metric (SSIM). The larger values of PSNR and SSIM present better results. Our model contains the larger PSNR and SSIM values corresponding to the old model. So the weighted and well-balanced time-dependent model improves the quality of the denoised images as well as better edges preserved corresponding to the old model at the same iteration numbers. The proposed model may be applied to image problems, such as deblurring, image segmentation, etc.

Availability of data and material

Not applicable.

Conflicts of interest

The authors declare that there is no conflict of interest regarding the publication of this paper.

Ethical standard

The authors have no relevant financial or non-financial interests to disclose.

LITERATURE CITED

Álvarez, L., P.-L. Lions, and J.-M. Morel, 1992 Image selective smoothing and edge detection by nonlinear diffusion. ii. SIAM Journal on Numerical Analysis **29**: 845–866.

Barcelos, C., M. Boaventura, and E. Silva, 2003 A well-balanced flow equation for noise removal and edge detection. IEEE Transactions on Image Processing **12**: 751–763.

Barcelos, C. A. Z., M. Boaventura, and E. C. Silva, 2005 Edge detection and noise removal by use of a partial differential equation with automatic selection of parameters. Computational & Applied Mathematics **24**: 131–150.

Brezis, H., 1987 *Analyse Fonctionnelle: Theorie et Applications*. Masson, Paris, 1987 (2e Tirage).

Catté, F., P. Lions, J. Morel, and T. Coll, 1992 Image selective smoothing and edge detection by nonlinear diffusion*. SIAM J. Numer. Anal. **29**: 182–193.

Chan, T. F., G. H. Golub, and P. Mulet, 1999 A nonlinear primal-dual method for total variation-based image restoration. SIAM J. Sci. Comput. **20**: 1964–1977.

Chang, Q. and I.-L. Chern, 2003 Acceleration methods for total variation-based image denoising. SIAM Journal on Scientific Computing **25**: 982–994.

Charbonnier, P., L. Blanc-Féraud, G. Aubert, and M. Barlaud, 1994 Two deterministic half-quadratic regularization algorithms for computed imaging. Proceedings of 1st International Conference on Image Processing **2**: 168–172 vol.2.

Chen, Y.-G., Y. Giga, and S. Goto, 1999 pp. 375–412 in *Uniqueness and Existence of Viscosity Solutions of Generalized mean Curvature Flow Equations*, edited by Ball, J. M., D. Kinderlehrer, P. Podio-Guidugli, and M. Slemrod, Springer Berlin Heidelberg.

El-Fallah, A. I. and G. E. Ford, 1998 On mean curvature diffusion in nonlinear image filtering. Pattern Recognition Letters **19**: 433–437.

El-Shorbagy, M. A., M. u. Rahman, and Y. Karaca, 2023 A computational analysis fractional complex-order values by abc operator and mittag-leffler kernel modeling. Fractals **0**: null.

Gilboa, G., N. Sochen, and Y. Zeevi, 2006 Variational denoising of partly textured images by spatially varying constraints. IEEE Transactions on Image Processing **15**: 2281–2289.

Haidong, Q., M. ur Rahman, S. E. Al Hazmi, M. F. Yassen, S. Salahshour, *et al.*, 2023 Analysis of non-equilibrium 4d dynamical system with fractal fractional mittag-leffler kernel. Engineering Science and Technology, an International Journal **37**: 101319.

Kumar, S. and K. Alam, 2021a A new class of nonlinear hyperbolic-parabolic model for image denoising with forward-backward diffusivity. Mathematics in Engineering, Science & Aerospace **12**: 435–441.

Kumar, S. and K. Alam, 2021b Pde-based hyperbolic-parabolic model for image denoising with forward-backward diffusivity. Computational Methods for Differential Equations **9**: 1100–1108.

Lapidus, L. and G. F. Pinder, 1983 Numerical solution of partial differential equations in science and engineering. SIAM Review **25**: 581–582.

Li, M.-M. and B.-Z. Li, 2021 A novel weighted total variation model for image denoising. IET Image Processing **15**: 2749–2760.

Marquina, A. and S. Osher, 2000 Explicit algorithms for a new time dependent model based on level set motion for nonlinear deblurring and noise removal. SIAM Journal on Scientific Computing **22**: 387–405.

Phan, T. D. K., 2020 A weighted total variation based image denoising model using mean curvature. Optik **217**: 164940.

Prasath, V. B. S. and D. Vorotnikov, 2014 Weighted and well-balanced anisotropic diffusion scheme for image denoising and restoration. Nonlinear Analysis-real World Applications **17**: 33–46.

Qu, H.-D., X. Liu, X. Lu, M. ur Rahman, and Z.-H. She, 2022 Neural network method for solving nonlinear fractional advection-diffusion equation with spatiotemporal variable-order. Chaos, Solitons & Fractals **156**: 111856.

Rudin, L. I., S. Osher, and E. Fatemi, 1992 Nonlinear total variation based noise removal algorithms. Physica D: Nonlinear Phenomena **60**: 259–268.

Smolka, B., 2008 Modified biased anisotropic diffusion processing of noisy color images. In *2008 9th International Conference on Signal Processing*, pp. 777–780.

Vogel, C. R. and M. E. Oman, 1996 Iterative methods for total variation denoising. SIAM Journal on Scientific Computing **17**: 227–238.

Weickert, J., 1997 A review of nonlinear diffusion filtering. In *Scale-Space Theory in Computer Vision*, edited by B. ter Haar Romeny, L. Florack, J. Koenderink, and M. Viergever, pp. 1–28, Berlin, Heidelberg, Springer Berlin Heidelberg.

XU, C., M. UR RAHMAN, B. FATIMA, and Y. KARACA, 2022 Theoretical and numerical investigation of complexities in fractional-order chaotic system having torus attractors. Fractals **30**: 2250164.

How to cite this article: Chauhan, A., Kumar, S., and Alam, K. Weighted and Well-Balanced Nonlinear TV-Based Time-Dependent Model for Image Denoising. *Chaos Theory and Applications*, 5(4), 300-307, 2023.

CHAOS
Theory and Applications
in Applied Sciences and Engineering

e-ISSN: 2687-4539
RESEARCH ARTICLE
Vol.5 / No.4 / 2023 / pp.308-317
Special Issue
https://doi.org/10.51537/chaos.1286294

Analysis of the n-Term Klein-Gordon Equations in Cantor Sets

Nikhil Sharma *, [1], **Pranay Goswami** α, [2,*] **and Sunil Joshi** *, [3]

*Department of Mathematics and Statistics, Manipal University Jaipur, Jaipur, India, αSchool of Liberal Studies, Dr B.R. Ambedkar University Delhi, Delhi, India.

ABSTRACT The effectiveness of the local fractional reduced differential transformation method (LFRDTM) for the approximation of the solution related to the extended n-term local fractional Klein-Gordon equation is the main aim of this paper in which fractional complex transform and local fractional derivative have been employed to analyze the n-term Klein-Gordon equations, and Cantor sets. The proposed method, along with the existence of the solutions demonstrated through some examples, provides a powerful mathematical means in solving fractional linear differential equations. Considering these points, the paper also provides an accurate and effective method to solve complex physical systems that display fractal or self-similar behavior across various scales. In conclusion, the fractional complex transform with the local fractional differential transform method has been proven to be a robust and flexible approach towards obtaining effective approximate solutions of local fractional partial differential equations.

KEYWORDS
Local fractional calculus
Local fractional differential equations
Reduced differential transformation method
Fractals
Fractional Klein-Gordon equation

INTRODUCTION

Various fields of study have used the Klein–Gordon equation in the last few decades, including quantum field theory, nonlinear optics, thermodynamics, and solid-state physics Kanth and Aruna (2009). The Klein-Gordon equation is a fundamental quantum field theory that describes particle behavior with spin 0. It was first introduced as a relativistic wave equation for a free scalar particle. There are a variety of approaches to solving problems of this nature. Recent years have seen significant use of a fractional modification involving the Caputo fractional derivative. However, fractional techniques for the Riemann-Liouville and Caputo derivatives are inadequate when smooth functions cannot represent the study area. In this situation, the local fractional calculus is a useful tool to simulate these physical problems.

Since its inception, the Klein-Gordon equation has been extensively studied and applied in various fields of physics, including particle physics, condensed matter physics, and cosmology. However, the standard form of the Klein-Gordon equation only considers integer-order derivatives, which restricts its applicability to specific physical systems that exhibit non-local behavior or fractal geometry. To overcome this limitation, local fractional calculus has been introduced to generalize the Klein-Gordon equation to accommodate fractional-order derivatives. Local fractional calculus is a mathematical framework that extends classical calculus to nondifferentiable and fractal functions by introducing the concept of fractional derivatives, which capture the behavior of these functions at small scales It is discovered that local fractional calculus, which Kolwankar and Gangal (1996) first proposed in the 1990s, is a practical tool in fields ranging from fundamental research to engineering. There, they describe the behavior of a continuous but non-differentiable function.

Over the past 20 years, the significance and attractiveness of local fractional calculus have increased due to its application to functions in the real world that involve fractals and are not continuously differentiable. The application of local fractional calculus to the Klein-Gordon equation has led to the development of a new class of equations known as local fractional Klein-Gordon equations. These equations have been used to model various physical phenomena, such as quantum wave propagation in fractal media, fractional quantum mechanics, and non-local interactions in quantum field theory Dubey *et al.* (2022).

Manuscript received: 20 April 2023,
Revised: 16 May 2023,
Accepted: 17 May 2023.

[1]nikhil141sharma@gmail.com
[2]pranaygoswami83@gmail.com (**Corresponding author**)
[3]sunil.joshi@jaipur.manipal.edu

In recent years, the study of local fractional Klein-Gordon equations has gained significant attention, with researchers exploring their theoretical properties and applications in various areas of physics. This includes the development of numerical methods for solving these equations and their application to complex physical systems, such as the behavior of particles in non-local media and the study of fractal structures in condensed matter physics. For example, In Sun (2018), the author explored a mathematical model involving fractional derivatives to describe a porous structure. This model is called the Harry Dym fractal equations and incorporates the Burgers fractal nonlinear equation. Furthermore, reference Wang *et al.* (2019) introduced the concept of a local fractional KdV-Burgers-Kuramoto (KBK) equation within the context of fractal space. Here, the concept of a local fractional derivative and a differential transform method has been used. Keskin and Oturanc (2009) were the first to propose the Reduced Differential Transform Method (RDTM). Many scholars use this method to explore fractional, non-fractional, linear, and nonlinear PDEs. The method provides a reliable and efficient technique for a wide range of scientific, industrial, and many other applications in physics, encompassing linear, nonlinear, homogeneous, and nonhomogeneous, fractional, and non-fractional PDEs, and so on. Solutions to significant mathematical problems are explored using this derivative. In 2016, Yang and Tenreiro Machado (2019) introduced the new local fractional differential transform technique (LFDTM) by combining the local fractional derivative (LFD) and the differential transform method (DTM). He offered several fundamental theorems and some examples of the use of this strategy. According to Jafari *et al.* (2016) theory of local fractional calculus, He combined LFD and RDTM in 2016 to produce the local fractional reduced differential transform method (LFRDTM). Moreover, he presented several fundamental theorems and applications of this method.

The classical KGE can be converted in its local fractional form in cantor sets using the fractional complex transform and the local fractional derivative. Yang *et al.* (2014) developed a continuous but nondifferentiable solution in cantor sets for the local fractional linear KGE was developed by Yang *et al.* (2014) using the technique of local fractional series technique under the local fractional differential operator to produce a nondifferentiable solution. Using the local fractional Sumudu transform approach and the standard homotopy perturbation technique, Kumar *et al.* (2017) researched linear KGE in Cantor sets.
The motivation for using local fractional calculus to examine the solution of the n-term fractional Klein-Gordon equation came from the need to develop a more effective approach to modeling complex physical phenomena. Traditional calculus methods fail to accurately describe many real-world systems that exhibit fractal or self-similar behavior at various length scales. Local fractional calculus provides a framework for analyzing such systems considering the non-local and non-differentiable properties of fractals Chu *et al.* (2023).

The n-term fractional Klein-Gordon equation is a specific example of a physical system that can benefit from applying local fractional calculus. This equation describes the behavior of a scalar field in space-time and has important applications in quantum mechanics, field theory, and condensed matter physics. By using local fractional calculus to solve the n-term fractional Klein-Gordon equation, we can gain a deeper understanding of the behavior of scalar fields in complex systems, leading to improved models and better predictions of physical phenomena.

The following paper aims to demonstrate the effectiveness of the local fractional reduced differential transformation method (LFRDTM) in approximating the solution of the extended n-term local fractional Klein-Gordon equation. Here, we also discussed the existence of the solution, followed by a few examples. The ultimate goal of this study is to provide an effective and accurate method for modeling complex physical systems that exhibit fractal or self-similar behavior at various length scales. By demonstrating the effectiveness of the LFRDTM in approximating the solution of the local fractional Klein-Gordon equation of term n, we hope to encourage its use in a wide range of applications in physics and engineering. The article is organized as follows: (1) Introduction (2) Definitions and preliminary (3) Existence and uniqueness of the solution of the local fractional Klein-Gordon equations (4) Approximate analytical solutions of the local fractal Klein-Gordon equations of term n (5) Results and Discussion.

DEFINITION AND PRELIMINARIES

The definitions of fractional operators, the transformation method, and their properties are as follows.

Definition 1. *Jafari* et al. *(2016) Let $\psi : [a,b] \times R \to R$ be a local fractional continuous function, then the local fractional partial derivative operator of $\psi(y,t)$ of order ν where $0 < \nu \leq 1$ concerning t at the point (y,t_0) expressed as*

$$\begin{aligned} D^{\nu}\psi(y,t_0) &= \frac{\partial}{\partial t}\psi(y,t_0) \\ &= \lim_{t\to t_0} \frac{\Delta^{\nu}[\psi(y,t)-\psi(y,t_0)]}{(t-t_0)^{\nu}} \end{aligned} \tag{1}$$

where $\Delta^{\nu}[\psi(y,t)-\psi(y,t_0)] \cong \Gamma(1+\nu)\,[\psi(y,t)-\psi(y,t_0)]$

with that in view the local fractional partial derivative operator of $\psi(y,t)$ of order $k\nu$, $0 < \nu \leq 1$ is given as

$$\begin{aligned} D_t^{k\nu}\psi(y,t) &= \frac{\partial^{k\nu}}{\partial t}\psi(y,t) \\ &= \overbrace{\frac{\partial^{\nu}}{\partial t^{\nu}}\cdots\frac{\partial^{\nu}}{\partial t^{\nu}}}^{k\ times}\psi(y,t). \end{aligned} \tag{2}$$

Definition 2. *A continuous function $\psi : [a,b] \times R^{\nu} \to R^{\nu}$ which is local fractional is Lipschitz continuous if $\exists\ 0 < \eta < 1$ s.t. $\forall\ y \in [a,b]$*

$$|\psi(y,t_1)-\psi(y,t_2)| \leq \eta^{\nu}|t_1-t_2|, 0 < \nu < 1.$$

.

Definition 3. *On a Generalised Banach space $(X, ||.||_{\nu})$, a mapping V from X to X is said to be a contraction mapping if $\exists\ \eta^{\nu} \in (0^{\nu}, 1^{\nu})$ s.t. for ${y_1}^{\nu}, {y_2}^{\nu} \in X$*

$$||V(y_1^{\nu}) - V(y_2^{\nu})||_{\nu} \leq \eta^{\nu}||y_1^{\nu} - y_2^{\nu}||_{\nu}.$$

.

Also $||\psi y^{\nu} - y^{\nu}||_{\nu} = 0$ implies y^{ν} is said to be a fixed point of ψ.

Theorem 1. *A map $\psi : X \to X$ on a complete general Banach space $(X, ||.||_{\nu})$ has a unique fix point if $\exists\ k \geq 1$ s.t. ψ^k is contracting.*

Theorem 2. *Let $\psi : [a,b] \times R^{\nu} \to R^{\nu}$ be LFC map. Then ψ is Lipschitz continuous.*

Definition 4. *Jafari* et al. *(2016) Let* $\Psi^{(k+1)\nu}(y) \in C_\nu(a,b)$, *for* $k = 0,1,2,...,n$ *and* $1 < \nu \leq 1$, *then, we have*

$$\psi(y) = \sum_{k=0}^{\infty} \psi^{k\nu}(0)\frac{(y-y_o)^{k\nu}}{\Gamma(1+k\nu)} \tag{3}$$

$$\text{and } \psi^{(k+1)\nu}(y) = \overbrace{D_y^\nu D_y^\nu ... D_y^\nu}^{(k+1)}\psi(y). \tag{4}$$

Definition 5. *The local fractional differential transform of a two-dimensional transform* $\Psi_k(y)$ *or* $\Psi(y,k)$ *of function* $\psi(y,t)$ *is*

$$\Psi_k(y) = \frac{1}{\Gamma(1+k\nu)}\left[\frac{\partial^{k\nu}}{\partial t^{k\nu}}\psi(y,t)\right]_{t=0} \tag{5}$$

$$k = 0,1,2,....n \text{ and } \nu \in (0,1]. \tag{6}$$

Definition 6. *Jafari* et al. *(2016) The inverse transform formula for a two-dimensional local fractional reduced differential of* $\psi_k(y)$

$$\psi(y,t) = \sum_{k=0}^{\infty} \Psi_k(y)t^{k\nu}$$

Some other properties of RTDM are as follows:

1. If $g(y,t) = a\psi(y,t)$ then $G_k(y) = a\Psi_k(y)$,
where a is a constant
2. If $\pi(y,t) = \psi(y,t) + \psi(y,t)$, then, $\Pi_k(y) = \psi_k(y) + \Psi_k(y)$.
3. If $\pi(y,t) = \psi(y,t)\psi(y,t)$, then, $\Pi_k(y) = \sum_{r=0}^{k} \Psi_r(y)\Psi_{k-r}(y)$.
4. If $g(y,t) = \frac{\partial^{n\nu}}{\partial t^{n\nu}}\psi(y,t)$, then,$G_k(y) = \frac{\Gamma(1+(k+n)\nu)}{\Gamma(1+k\nu)}\Psi_{k+n}(y)$
where $\Psi_{k+n}(y) = \frac{1}{\Gamma(1+(k+n)\nu)}\left[\frac{\partial^{(k+n)\nu}}{\partial t^{(k+n)\nu}}\psi(y,t)\right]_{t=0}$
$k = 0,1,2,....n$ $\nu \in (0,1]$ and $n \in \mathbb{N}$.
5.If $g(y,t) = \frac{\partial^{n\nu}}{\partial x^{n\nu}}\psi(y,t)$, then we have $G_k(y) = \frac{\partial^{n\nu}}{\partial x^{n\nu}}\Psi_k(y)$.

Lemma 1. *([Yang (2012) Zhang* et al. *(2015) Zhang* and *Yang (2016)]) Let* φ_1, φ_2 *be two non differential functions with Local fractional derivative operator* $\nu \in (0,1]$, *then*

1. $D^{(\nu)}(a\varphi_1 + b\varphi_2) = a(D^{(\nu)}\varphi_1) + b(D^{(\nu)}\varphi_2)$ *for* $a, b \in \mathbb{R}$.
2. $D^{(\nu)}(\varphi_1\varphi_2) = \varphi_1 D^{(\nu)}(\varphi_2) + \varphi_2 D^{(\nu)}(\varphi_1)$.
3. $D^{(\nu)}(\frac{\varphi_1}{\varphi_2}) = \frac{\varphi_2 D^{(\nu)}\varphi_1 - \varphi_1 D^{(\nu)}\varphi_2}{\varphi_2^2}$ *provided* $\varphi_2 = 0$.

Lemma 2. *Acan* et al. *(2017) Yang (2012) Zhang* et al. *(2015) Zhang* and *Yang (2016) Suppose that* φ *is a non-differential function and* $\nu \in (0,1]$ *is the order of local fractional derivative, then,*

1. $D^\nu(\varphi(y)) = 0$, *for all constant functions* $\varphi(y) = k$.
2. $D^{(\nu)}(\frac{y^{k\nu}}{\Gamma(k\nu+1)}) = \frac{y^{(k-1)\nu}}{\Gamma((k-1)\nu+1)}$
3. $D^{(\nu)}(E_\nu(y^\nu)) = E_\nu(y^\nu)$
4. $D^{(\nu)}(E_\nu(-y^\nu)) = -E_\nu(-y^\nu)$
5. $D^{(\nu)}(sin_\nu(y^\nu)) = cos_\nu(y^\nu)$
6. $D^{(\nu)}(cos_\nu(y^\nu)) = -sin_\nu(y^\nu)$

where $E_\nu(y^\nu) = \sum_{k=0}^{\infty}\frac{y^{k\nu}}{\Gamma(k\nu+1)}$,

$sin_\nu(y^\nu) = \sum_{k=0}^{\infty}(-1)^k\frac{y^{(2k+1)\nu}}{\Gamma((2k+1)\nu+1)}$

and $cos_\nu(y^\nu) = \sum_{k=0}^{\infty}(-1)^k\frac{y^{2k\nu}}{\Gamma(2k\nu+1)}$.

Local Fractional Klein- Gordon equation (on Cantor sets)

This section uses the fractional complex transform and the local fractional derivative to derive the local fractional KGE (Klein-Gordon equation) fractal model of the term n in cantor sets. We know that the classical Klein-Gordon Equation is

$$\frac{\partial\psi(\Omega,T)}{\partial T} = \frac{\partial^2\psi(\Omega,T)}{\partial\Omega^2} + a\psi(\Omega,T) + b\psi^2(\Omega,T) + c\psi^3(\Omega,T)$$

then the classical n-term Klein-Gordon equation is considered as

$$\frac{\partial\psi(\Omega,T)}{\partial T} = \frac{\partial^2\psi(\Omega,T)}{\partial\Omega^2} + a_1\psi(\Omega,T) + a_2\psi^2(\Omega,T) + a_3\psi^3(\Omega,T) + ... + a_n\psi^n(\Omega,T) \tag{7}$$

subject to initial condition $\psi(\Omega,0) = \psi_o$.

Now using the Local Fractional complex transform method to switch the conventional differential equation into the local fractional differential equation.
To derive the fractional transform, we put

$$\Omega = \frac{y^\nu}{\Gamma(1+\nu)} \ , \ T = \frac{t^\nu}{\Gamma(1+\nu)}$$

Then

$$\frac{\partial^\nu}{\partial t^\nu}\psi(y,t) = \frac{\partial\psi(\Omega,T)}{\partial\Omega}\frac{\partial^\nu\Omega}{\partial t^\nu} + \frac{\partial\psi(\Omega,T)}{\partial T}\frac{\partial^\nu T}{\partial t^\nu} = 0 + \frac{1}{\Gamma(1+\nu)}\frac{\partial\psi(\Omega,T)}{\partial T}.$$

This implies

$$\frac{\partial\psi(\Omega,T)}{\partial T} = \Gamma(1+\nu)\frac{\partial^\nu\psi(y,t)}{\partial t^\nu}$$
$$or\ D_T\psi(\Omega,T) = \Gamma(1+\nu)D_t^\nu\psi(y,t)$$

Similarly,

$$\begin{aligned} D_y^{2\nu}\psi(y,t) &= D_\Omega^2\psi(\Omega,T)\frac{\partial^\nu\Omega}{\partial x^\nu} + D_T^2\psi(\Omega,T)\frac{\partial^\nu T}{\partial x^\nu} \\ &= \frac{1}{\Gamma(1+\nu)}D_\Omega^2\psi(\Omega,T) \\ \Rightarrow D_\Omega^2\psi(\Omega,T) &= \Gamma(1+\nu)D_y^{2\nu}\psi(y,t) \end{aligned}$$

and using local fractional derivatives under the constraints and characteristics of the fractional complex transform technique, we see that

$$\psi(y,t) = \frac{1}{\Gamma(1+\nu)}\psi(\Omega,T)$$
$$\psi^2(y,t) = \frac{1}{\Gamma(1+\nu)}\psi^2(\Omega,T)$$
$$\vdots =$$
$$\psi^n(y,t) = \frac{1}{\Gamma(1+\nu)}\psi^n(\Omega,T).$$

Thus, substituting the terms into 7 we obtain the local fractional KGE of n terms (Klein - Gordon equation) as

$$\frac{\partial\psi(y,t)}{\partial t^\nu} = \frac{\partial^{2\nu}\psi(y,t)}{\partial x^{2\nu}} + a_1\psi(y,t) + a_2\psi^2(y,t) + a_3\psi^3(y,t) + ... + a_n\psi^n(y,t), t > 0 \quad (8)$$

with initial conditions

$$\psi(y,0) = \psi_0$$

or we can write it as

$$D_t^\nu\psi = D_y^{2\nu}\psi + a_1\psi + a_2\psi^2 + a_3\psi^3 + \cdots\cdots + a_n\psi^n$$

with initial conditions

$$\psi(y,0) = \psi_o.$$

EXISTENCE AND UNIQUENESS OF SOLUTION OF N TERM LOCAL FRACTAL KLEIN- GORDON EQUATION

In this section, we apply the Banach fixed point theorem and contraction mapping theorem to ensure that the local fractional Klien Gordon equation with the initial condition has a unique solution.
Let us introduce a Banach space of real-valued functions by $C(\Omega\times[0,T])$ with the norm is given by

$$||\psi|| = \sup_{(y,t)\in\Omega\times[0,T]} ||\psi(y,t)||$$

Lemma 3. *Let $\psi(y,t)$ and its fractional partial derivatives are continuous on $\Omega\times[0,T]$ then $D_t^\nu\psi$ and $D_y^{2\nu}\psi$ are bounded.*

Proof. Let $A_1 = \sup_{0\le\tau\le t\le T} |t-\tau|^{-\nu}$. We will show that D_t^ν is bounded. Consider

$$|D_t^\nu\psi(y,t)| = |\frac{1}{\Gamma(1-\nu)}\int_0^t (t-\tau)^{-\nu}\psi(y,t)d\tau|$$
$$= |\frac{A_1}{\Gamma(1-\nu)}\int_0^t (t-\tau)^{-\nu}\psi(y,t)d\tau|$$
$$\le \frac{A_1}{\Gamma(1-\nu)}||\psi|| + max_{y\in\Omega}|\psi(y,0)|.$$

Let (L_1) be a positive constant such that $\max_{y\in\Omega}|\psi(y,0)| \le L_1||\psi||$,
this gives

$$|D_t^\nu\psi(y,t)| \le \frac{A_1}{\Gamma(1-\nu)}||\psi|| + L_1||\psi|| = L_2||\psi||$$

where $L_2 = \frac{A_1}{\Gamma(1-\nu)} + L_1$. Similarly, we can have $||D_y^{2\nu}\psi|| \le K||\psi||$ where K is some constant. Hence, the fractional derivatives are bounded. □

Now considering the subsequent fractional differential equation in the local fractional operator form as

$$L_\nu(\psi) - R_\nu(\psi) = 0 \quad (9)$$

where $\psi = \psi(y,t)$, $L_\nu(\psi) = \frac{\partial^\nu\psi}{\partial t^\nu}$ and $R_\nu(\psi) = \frac{\partial^{2\nu}\psi(y,t)}{\partial x^{2\nu}} + a_1\psi + a_2\psi^2 + a_3\psi^3 + \cdots\cdots + a_n\psi^n$.
We can rewrite this equation subject to initial conditions as

$$L_\nu\psi(y,t) = \Phi(\psi(y,t))$$

with initial condition

$$\psi(y,0) = \psi_0(y).$$

Here

$$\Phi(\psi(y,t)) = \frac{\partial^{2\nu}\psi(y,t)}{\partial y^{2\nu}} + a_1\psi + a_2\psi^2 + ... + a_n\psi^n = \frac{\partial^{2\nu}\psi(y,t)}{\partial y^{2\nu}} + f(\psi)$$

Theorem 3. *Assuming the function $\Phi(\psi(y,t))$ specified as*

$$\Phi(\psi(y,t)) = \frac{\partial^{2\nu}\psi(y,t)}{\partial x^{2\nu}} + f(\psi)$$

is a Locally fractional continuous function which satisfies Lipschitz continuity condition, that is,

$$|\Phi(\psi_1(y,t)) - \Phi(\psi_2(y,t))| \le \eta^\nu|\psi_1(y,t) - \psi_2(y,t)|, \nu\in(0,1]$$

where $0<\eta<1$.
then, the system

$$L_\nu\psi(y,t) = \Phi(\psi(y,t))$$

with initial condition

$$\psi(y,0) = \psi_0(y)$$

comprises a solution in $C_\nu[a,b]$ which is a unique solution.

Proof. Consider the function $V : C_\nu[a,b] \to C_\nu[a,b]$ be defined as

$$V(\psi(y,t)) = \psi_0(y) + \frac{1}{\Gamma(1+\nu)}\int_\nu^t [\Phi(\psi_1(y,s)) - \Phi(\psi_2(y,s))](ds)^\nu$$

we will use induction to show that

$$||V^n(\psi_1(y,t)) - V^n(\psi_2(y,t))||_\nu \le \frac{\eta^{n\nu}|b^\nu - a^\nu|^n}{\Gamma^n(1+\nu)}||\psi_1(y,t) - \psi_2(y,t)||_\nu.$$

For n=1, we have

$$|V(\psi_1(y,t)) - V(\psi_2(y,t))| = \left|\frac{1}{\Gamma(1+\nu)}\int_\nu^t \begin{bmatrix}\phi(\psi_1(y,s))-\\ \phi(\psi_2(y,s))\end{bmatrix}(ds)^\nu\right|$$
$$\le \left|\frac{1}{\Gamma(1+\nu)}\int_\nu^t \eta^\nu\begin{vmatrix}\psi_1(y,s)-\\ \psi_2(y,s)\end{vmatrix}(ds)^\nu\right|$$
$$\le \frac{\eta^\nu}{\Gamma(1+\nu)}\left|\begin{matrix}\frac{\partial^{2\nu}}{\partial y^{2\nu}}(\psi_1-\psi_2) + a_1(\psi_1-\psi_2) + a_2({\psi_1}^2 - {\psi_2}^2)+\\ .... + a_n({\psi_1}^n - {\psi_2}^n)\end{matrix}\right|$$

Now by the lemma 3 note that $D_y^{2\nu}\psi$ is bounded and since ψ is a bounded function therefore ψ^n is also bounded.
Also as the sum and difference of bounded functions are bounded, we can have

$$\begin{vmatrix}V(\psi_1(y,t))-\\ V(\psi_2(y,t))\end{vmatrix} \le \frac{\eta^\nu}{\Gamma(1+\nu)}|\psi_1-\psi_2|[K + a_1m_1 + a_2m_2 + ... + a_nm_n]$$

where $|D_y^{2\nu}\psi| \leq K$ and $m_1, m_2, ..., m_n$ are the bounds for the other terms.

$$\leq \frac{\eta^\nu}{\Gamma(1+\nu)}|b^\nu - a^\nu|||\psi_1(y,t) - \psi_2(y,t)||_\nu,$$

where $|K + m_1 + m_2 + ... + m_n| \leq |b^\nu - a^\nu|$.
Hence for $n = 1$, the inequality holds.
Now let's assume it for $n = k$

$$||V^k(\psi_1(y,t)) - V^k(\psi_2(y,t))||_\nu \leq \frac{\eta^{k\nu}|b^\nu - a^\nu|^k}{\Gamma^k(1+\nu)}||\psi_1(y,t) - \psi_2(y,t)||_\nu \tag{10}$$

Now for $n = k+1$, we see that

$$\left\|\begin{matrix}V^{k+1}(\psi_1(y,t))-\\ V^{k+1}(\psi_2(y,t))\end{matrix}\right\|_\nu = \left|\frac{1}{\Gamma(1+\nu)}\int_\nu^t \begin{bmatrix}\phi(V^k(\psi_1(y,s)))-\\ \phi(V^k(\psi_2(y,s)))\end{bmatrix}(ds)^\nu\right|$$

$$\leqslant \left|\frac{1}{\Gamma(1+\nu)}\int_\nu^t \eta^\nu \begin{bmatrix}V^k(\psi_1(y,s))\\ -V^k(\psi_2(y,s))\end{bmatrix}(ds)^\nu\right|$$

$$\leqslant \frac{\eta^{(k+1)\nu}|b^\nu - a^\nu|^{(k+1)}}{\Gamma^{(k+1)}(1+\nu)}\left\|\begin{matrix}\psi_1(y,t)-\\ \psi_2(y,t)\end{matrix}\right\|_\nu \text{ (using inequality 10)}$$

Thus for $n = k+1$, our assumption is proved, and we can say that

$$||V^n(\psi_1(y,t)) - V^n(\psi_2(y,t))||_\nu \leq \frac{\eta^{n\nu}|b^\nu - a^\nu|^n}{\Gamma^n(1+\nu)}||\psi_1(y,t) - \psi_2(y,t)||_\nu.$$

Now note that

$$\frac{\eta^{n\nu}|b^\nu - a^\nu|^n}{\Gamma^n(1+\nu)}||\psi_1(y,t) - \psi_2(y,t)||_\nu \to 0$$

as $n \to \infty$.
Therefore we can say that the map V^n is a contraction over $C_\nu[a,b]$ which conclusively says that the given system has a unique solution. □

APPROXIMATE ANALYTICAL SOLUTIONS OF N TERM LOCAL FRACTAL KLEIN- GORDON EQUATIONS

Theorem 4. *If we consider*

$$D_t^\nu\psi = D_y^{2\nu}\psi + a_1\psi + a_2\psi^2 + a_3\psi^3 + \cdots\cdots + a_n\psi^n \tag{11}$$

with initial condition

$$\psi(y,0) = \psi_o \tag{12}$$

where D_t^ν is Local fractional derivative operator with $\nu \in (0,1]$and $a_1, a_2, \cdots, a_n$ are real constants. Then the solution of (11) is given as

$$\psi(y,t) = \Psi_0 + \sum_{k=1}^{\infty}\Psi_k(y)t^{k\nu}. \tag{13}$$

Proof. We are going to apply the method of Local Fractional Reduced Differential Transform *LFRDTM*on (11)
For that, we recall that the reduced differential transform(Locally fractional) of $\psi(y,t)$ is $\Psi_k(y)$ or $\Psi(y,k)$ and is established as

$$\Psi(y,k)\ or\ \Psi_k(y) = \frac{1}{\Gamma(1+k\nu)}\left[\frac{\partial^{k\nu}\psi(y,t)}{\partial t^{k\nu}}\right] = \frac{1}{\Gamma(1+k\nu)}[D_t^{k\nu}\psi(y,t)]$$

This implies

$$\Psi_{k+1}(y) = \frac{1}{\Gamma(1+(k+1)\nu)}[D_t^{(k+1)\nu}\psi(y,t)] \tag{14}$$

and since we are using local fractional derivative, therefore

$$\begin{aligned}D_t^{(k+1)\nu}\psi(y,t) &= \frac{\partial^{(k+1)\nu}}{\partial t^{(k+1)\nu}}\psi(y,t)\\ &= \underbrace{\frac{\partial^\nu}{\partial t^\nu}\frac{\partial^\nu}{\partial t^\nu}\cdots\cdots\frac{\partial^\nu}{\partial t^\nu}}_{(k+1)times}\psi(y,t)\\ &= \frac{\partial^\nu}{\partial t^\nu}\left[\frac{\partial^{k\nu}}{\partial t^{k\nu}}\psi(y,t)\right] = \frac{\partial^\nu}{\partial t^\nu}[D_t^{k\nu}\psi(y,t)]\\ &= \frac{\partial^\nu}{\partial t^\nu}\left[\Gamma(1+k\nu)\Psi_k(y)\right]\end{aligned} \tag{15}$$

Substituting (14) into (15), we get

$$\Gamma(1+(k+1)\nu)\Psi_{k+1}(y) = \frac{\partial^\nu}{\partial t^\nu}(\Gamma(1+k\nu)\Psi_k(y))$$

Hence we get the recurrence relation as,

$$\begin{aligned}\Psi_{k+1}(y) &= \frac{\Gamma(1+k\nu)}{\Gamma(1+(k+1)\nu)}\frac{\partial^\nu\Psi_k(y)}{\partial t^\nu}\\ &= \frac{\Gamma(1+k\nu)}{\Gamma(1+(k+1)\nu)}D_t^\nu\Psi_k(y)\end{aligned} \tag{16}$$

thus using the properties of RTDM, and after applying LFRDTM to (11) we get

$$\Psi_{k+1}(y) = \frac{\Gamma(1+k\nu)}{\Gamma(1+(k+1)\nu)}\begin{bmatrix}D_y^{2\nu}a_1\Psi_k(y) + a_2\Psi_k^2 + a_3\Psi_k^3 + \cdots\\ \cdots + a_n\Psi_k^n(y)\end{bmatrix}$$

with (I.C)

$$\Psi_0(y) = \Psi_0$$

where $\Psi_k(y)$ is a Local fractional differential differential transform of $\psi(y,t)$
and similarly for $\psi^2, \psi^3, \cdots, \psi^n$ the transformed terms are

$$\Psi_k^2(y) = \sum_{r=0}^{k}\Psi_k(y)\Psi_{k-r}(y)$$

$$\Psi_k^3(y) = \sum_{r=0}^{k}\sum_{s=0}^{r}\Psi_s(y)\Psi_{r-s}(y)\Psi_{k-r}(y)$$

$$\Psi_k^4(y) = \sum_{r=0}^{k}\sum_{s=0}^{r}\sum_{t=0}^{s}\Psi_t(y)\Psi_{s-t}(y)\Psi_{r-s}(y)\Psi_{k-r}(y)$$

$$\vdots$$

$$\Psi_k^n(y) = \underbrace{\sum_{r_1=0}^{k}\sum_{r_2=0}^{r_1}\sum_{r_3=0}^{r_2}\cdots\sum_{r_{n-1}=0}^{r_{n-2}}}_{n-1\ times}\overbrace{\Psi_{r_{n-1}}(y)\Psi_{r_{n-2}}(y)\cdots\Psi_{k-r_1}(y)}^{n\ times}$$

Thus, the recurrence relation along with initial condition Ψ_0 is

$$\Psi_{k+1}(y) = \frac{\Gamma(1+k\nu)}{\Gamma(1+(k+1)\nu)}\left[D_y^{2\nu}a_1\Psi_k(y) + a_2\sum_{r=0}^{k}\Psi_k(y)\Psi_{k-r}(y) + a_3\sum_{r=0}^{k}\sum_{s=0}^{r}\Psi_s(y)\Psi_{r-s}(y)\Psi_{k-r}(y) + \cdots\cdots + a_n\sum_{r_1=0}^{k}\sum_{r_2=0}^{r_1}\sum_{r_3=0}^{r_2}\cdots\sum_{r_{n-1}=0}^{r_{n-2}}\Psi_{r_{n-1}}(y)\Psi_{r_{n-2}}(y)\cdots\Psi_{k-r_1}(y)\right] \tag{17}$$

and using this recurrence relation, we have

$$\Psi_1 = \frac{\Gamma(1+0)}{\Gamma(1+\nu)}[D_y^{2\nu}\Psi_0 + a_1\Psi_0 + a_2\Psi_0^2 + \cdots + a_n\Psi_0^n]$$
$$= \frac{1}{\Gamma(1+\nu)}[D_y^{2\nu}\Psi_0 + \Psi_0[a_1 + a_2\Psi_0 + \cdots + a_n\Psi_0^{n-1}]]$$
$$\Psi_2 = \frac{\Gamma(1+\nu)}{\Gamma(1+2\nu)}[D_y^{2\nu}\Psi_1 + \Psi_1[a_1 + a_2\Psi_1 + \cdots + a_n\Psi_1^{n-1}]]$$
.
.
.
$$\Psi_k = \frac{\Gamma(1+k\nu)}{\Gamma(1+(k+1)\nu)}[D_y^{2\nu}\Psi_{k-1} + \Psi_{k-1}[a_1 + a_2\Psi_{k-1} + \cdots + a_n\Psi_{k-1}^{n-1}]] \tag{18}$$

Now using 6 we get the analytical solution to n term Klein Gordon equation as

$$\psi(y,t) = \sum_{k=0}^{\infty}\Psi_k(y)t^{k\nu} = \Psi_0(y) + \Psi_1(y)t^{\nu} + \Psi_2(y)t^{2\nu} + \cdots$$

where $\Psi_0, \Psi_1, \Psi_2, \cdots$ are defined as above18. □

Now consider the following cases for particular solutions

Example 1. *consider the fractional differential equation*

$$\frac{\partial^{\nu}}{\partial t^{\nu}}\psi(y,t) = \frac{\partial^{2\nu}}{\partial x^{2\nu}}\psi(y,t) \tag{19}$$

with initial condition $\psi(y,0) = \psi_0$.
Note that this is a linear local fractional n term Klein-Gordon equation with $a_1 = a_2 = \cdots = a_n = 0$ *which is a special case of* (11) .
Let say $\psi_0 = E_{\nu}(y^{\nu})$
Taking local fractional reduced differential transform of (19),
We get the subsequent recurrence relation

$$\Psi_{k+1}(y) = \frac{\Gamma(1+k\nu)}{\Gamma(1+(k+1)\nu)}\left[D_y^{2\nu}\Psi_k(y)\right] \tag{20}$$

$$\text{with (I.C) } \Psi_0(y) = E_{\nu}(y^{\nu}). \tag{21}$$

*On applying the recurrence relation and initial condition*20, *we attain*

$$\Psi_1(y) = \frac{1}{\Gamma(1+\nu)}\left[D_y^{2\nu}\Psi_o(y)\right] = \frac{1}{\Gamma(1+\nu)}E_{\nu}(y^{\nu})$$
$$\Psi_2(y) = \frac{1}{\Gamma(1+2\nu)}\left[D_y^{2\nu}\Psi_1(y)\right] = \frac{1}{\Gamma(1+2\nu)}E_{\nu}(y^{\nu})$$
$$\vdots$$
$$\Psi_n(y) = \frac{1}{\Gamma(1+n\nu)}E_{\nu}(y^{\nu}).$$

Applying the inverse local fractional reduced differential transform, we attain the solution of 19.

$$\psi(y,t) = \sum_{k=0}^{\infty}\Psi_k(y)t^{k\nu} = E_{\nu}(y^{\nu}) + E_{\nu}(y^{\nu})\frac{t^{\nu}}{\Gamma(1+\nu)} + E_{\nu}(y^{\nu})\frac{t^{2\nu}}{\Gamma(1+2\nu)} + \cdots = \sum_{k=0}^{\infty}E_{\nu}(y^{\nu})\frac{t^{k\nu}}{\Gamma(1+k\nu)}$$

This implies

$$\psi(y,t) = E_{\nu}(y^{\nu})E_{\nu}(t^{\nu}).$$

The graphical illustration of the solution $\psi(y,t)$ *is shown in [1] when* $\nu = \frac{log(2)}{log(3)}$.

Example 2. *When* $a_1 = 1, a_2 = a_3 = a_4 = \cdots = a_n = 0$, *we get*

$$D_t^{\nu}\psi(y,t) = D_y^{2\nu}\psi(y,t) + \psi(y,t),\ t > 0, \nu \in (0,1]$$

with initial condition

$$\psi(y,0) = E_{\nu}(y^{\nu}).$$

we know that Local fractional reduced differential transform of $\psi(y,t)$ *is*

$$\Psi_k(y) = \frac{1}{\Gamma(1+k\nu)}\left[\frac{\partial^{k\nu}\psi(y,t)}{\partial t^{k\nu}}\right] = \frac{1}{\Gamma(1+k\nu)}[D_t^{k\nu}\psi(y,t)]$$

This implies

$$\Psi_{k+1}(y) = \frac{1}{\Gamma(1+(k+1)\nu)}[D_t^{(k+1)\nu}\psi(y,t)]$$
$$\Rightarrow \Gamma(1+(k+1)\nu)\Psi_{k+1}(y) = \frac{\partial^{\nu}}{\partial t^{\nu}}(\Gamma(1+k\nu)\Psi_k(y)).$$

After applying local fractional partial derivative property, we get,

$$\Psi_{k+1}(y) = \frac{\Gamma(1+k\nu)}{\Gamma(1+(k+1)\nu)}\frac{\partial^{\nu}\Psi_k(y)}{\partial t^{\nu}} = \frac{\Gamma(1+k\nu)}{\Gamma(1+(k+1)\nu)}D_t^{\nu}\Psi_k(y).$$

Thus, applying the properties of RTDM and apply LFRDTM, we get

$$\Psi_{k+1}(y) = \frac{\Gamma(1+k\nu)}{\Gamma(1+(k+1)\nu)}\left[D_y^{2\nu}\Psi_k(y) + \Psi_k(y)\right] \tag{22}$$

with (I.C)

$$\Psi_o(y) = E_\nu(y^\nu).$$

now applying Recurrence relation [22], we attain

$$\begin{aligned}
\Psi_1(y) &= \frac{1}{\Gamma(1+\nu)}\left[D_y^{2\nu}\Psi_o(y) + \Psi_o(y)\right] \\
&= \frac{2}{\Gamma(1+\nu)}E_\nu(y^\nu) \\
\Psi_2(y) &= \frac{1}{\Gamma(1+2\nu)}\left[D_y^{2\nu}\Psi_1(y) + \Psi_1(y)\right] \\
&= \frac{2^2}{\Gamma(1+2\nu)}E_\nu(y^\nu) \\
&\vdots \\
\Psi_k(y) &= \frac{2^k}{\Gamma(1+k\nu)}E_\nu(y^\nu)
\end{aligned}$$

Now using the inverse local fractional reduced differential transform

$$\begin{aligned}
\psi(y,t) &= \sum_{k=0}^{\infty}\Psi_k(y)t^{k\nu} \\
&= \Psi_0(y) + \Psi_1(y)t^\nu + \Psi_2(y)t^{2\nu} + \cdots \\
&= E_\nu(y^\nu)\sum_{k=0}^{\infty}\frac{(2t)^{k\nu}}{\Gamma(1+k\nu)} \\
&= E_\nu((2t-x)^\nu).
\end{aligned}$$

The graphical illustration of the solution $\psi(y,t)$ is shown in [2] when $\nu = \frac{log(2)}{log(3)}$.

Example 3. *Now considering the case $a_2 = -1, a_1 = a_3 = \cdots = a_n = 0$ along with initial condition $\psi(y,0) = 1 + sin_\nu(y^\nu)$.Then the non-linear KGE we have,*

$$D_t^\nu\psi(y,t) = D_y^{2\nu}\psi(y,t) - \psi^2(y,t),\ t > 0, \nu \in (0,1]$$

,

with initial condition

$$\psi(y,0) = 1 + sin_\nu(y^\nu).$$

To get the next recurrence relation, we will use the local fractional reduced differential transform.

$$\Psi_{k+1}(y) = \frac{\Gamma(1+k\nu)}{\Gamma(1+(k+1)\nu)}\left[D_{y)}^{2\nu}\Psi_k(y) - \sum_{r=0}^{k}\Psi_r\Psi_{k-r}\right]$$

with (I.C)

$$\Psi_o(y) = 1 + sin_\nu(y^\nu).$$

thus we get

$$\begin{aligned}
\Psi_1(y) &= \frac{\Gamma(1)}{\Gamma(1+\nu)}[D_y^{2\nu}(\Psi_0) + [\Psi_0]^2] \\
&= \frac{1}{\Gamma(1+\nu)}[D_y^{2\nu}(1+sin_\nu(y^\nu)) - (1+sin_\nu(y^\nu))^2] \\
&= \frac{-1}{\Gamma(1+\nu)}[3sin_\nu(y^\nu) + sin_\nu^2(y^\nu) + 1] \\
&= \frac{1}{\Gamma(1+2\nu)\Gamma(1+\nu)}\begin{bmatrix}\Gamma(1+\nu)(3sin_\nu(y^\nu) - 2 + 4sin_\nu^2(y^\nu)) - 1 \\ -11sin_\nu^2(y^\nu) + 6sin_\nu^3(y^\nu) + \\ 6sin_\nu(y^\nu) + sin_\nu^4(y^\nu)\end{bmatrix}
\end{aligned}$$

.
.
.
.

Now substituting using the inverse Local fractional reduced differential transform method (LFRDTM), we have

$$\begin{aligned}
\psi(y,t) &= \sum_{k=0}^{\infty}\Psi_k t^{k\nu} \\
&= \Psi_0 + \Psi_1 t^\nu + \Psi_2 t^{2\nu} + \cdots
\end{aligned}$$

$$\begin{aligned}
&= 1 + sin_\nu(y^\nu) - \frac{t^\nu}{\Gamma(1+\nu)}\left[3sin_\nu(y^\nu) + sin_\nu^2(y^\nu) + 1\right] \\
&+ \frac{t^{2\nu}}{\Gamma(1+\nu)\Gamma(1+2\nu)}\left[(3sin_\nu(y^\nu) - 2 + 4sin_\nu^2(y^\nu))\Gamma(1+\nu)\right. \\
&\left. - 1 - 11sin_\nu^2(y^\nu) + 6sin_\nu^3(y^\nu) + 6sin_\nu(y^\nu) + sin_\nu^4(y^\nu)\right] + \cdots\cdots
\end{aligned}$$

which is the series solution of this particular local fractional KGE. The graphical illustration of the solution $\psi(y,t)$ is shown in [3] when $\nu = \frac{log(2)}{log(3)}$.

Example 4. *when $a_1 = a_2 = a_3 = a_4 = a_5 = \cdots = a_n = 1$, we get the non linear local fractional Klein Gordon equation*

$$D_t^\nu\psi(y,t) = D_y^{2\nu}\psi(y,t) + \psi + \psi^2 + \psi^3(y,t),\ t > 0, \nu \in (0,1]$$

with initial condition

$$\psi(y,0) = 1 + sin_\nu(y^\nu)$$

on applying LFRDTM here, we get

$$\Psi_{k+1}(y) = \frac{\Gamma(1+k\nu)}{\Gamma(1+\nu+k\nu)}\left[D_y^{2\nu}\Psi_k + \Psi_k + \Psi_k^2 + \Psi_k^3 + \cdots\right]$$

where

$$\Psi_k^2 = \sum_{r=0}^{k}\Psi_r\Psi_{k-r}$$

$$\Psi_k^3 = \sum_{r=0}^{k}\sum_{s=0}^{r}\Psi_s\Psi_{r-s}\Psi_{k-r}$$

and initial condition transforms into $\Psi_0(y) = 1 + sin_\nu(y^\nu)$
Now, using the recurrence relation along with the initial condition, we obtain

$$\Psi_1(y) = \frac{1}{\Gamma(1+\nu)}[D_y^{2\nu}(\Psi_0) + \Psi_0 + (\Psi_0)^2 + (\Psi_0)^3 + \cdots]$$

$$\Psi_1(y) = \frac{1}{\Gamma(1+\nu)}\begin{bmatrix} D_y^{\nu}(D_y^{\nu}(1+sin_\nu(y^\nu))) + (1+sin_\nu(y^\nu)) + \\ (1+sin_\nu(y^\nu))^2 + (1+sin_\nu(y^\nu))^3 + \cdots \end{bmatrix}$$

$$= \frac{1}{\Gamma(1+\nu)}\begin{bmatrix} -sin_\nu(y^\nu) + 1 + sin_\nu(y^\nu) + 1 + sin_\nu^2(y^\nu) + 2sin_\nu(y^\nu) \\ +1 + sin_\nu^3(y^\nu) + 3sin_\nu(y^\nu) + 3sin_\nu^2(y^\nu) + \cdots \end{bmatrix}$$

$$= \frac{1}{\Gamma(1+\nu)}[sin_\nu^3(y^\nu) + 4sin_\nu^2(y^\nu) + 5sin_\nu(y^\nu) + n + \cdots]$$

$$\Psi_2(y) = \frac{\Gamma(1+\nu)}{\Gamma(1+2\nu)}[D_y^{2\nu}(\Psi_1) + \Psi_1 + (\Psi_1)^2 + (\Psi_1)^3 + \cdots]$$

$$\Psi_2(y) = \frac{1}{\Gamma(1+\nu)\Gamma(1+2\nu)}\begin{bmatrix} sin_\nu^9(y^\nu) + 4sin_\nu^8(y^\nu) + 9sin_\nu^7(y^\nu) \\ +105sin_\nu^6(y^\nu) + 123sin_\nu^5(y^\nu) + \\ 126sin_\nu^4(y^\nu) + 166sin_\nu^3(y^\nu) + \\ 29sin_\nu^2(y^\nu) - 3/4sin_\nu(y^\nu) + \cdots \end{bmatrix}$$

$$\Psi_3(y) = \frac{1}{\Gamma(1+\nu)\Gamma(1+2\nu)\Gamma(1+3\nu)}\begin{bmatrix} sin_\nu^{27}(y^\nu) + 10682sin_\nu^{26}(y^\nu) \\ +269874sin_\nu^{25}(y^\nu) + \cdots \end{bmatrix}$$

.

.

.

neglecting higher terms since with $0 < \nu \leq 1$ *and as* $|sin_\nu(y^\nu)| \leq 1$ *the terms with higher power will eventually tend near zero.*

Now, substituting all using the inverse local fractional reduced differential transform method (LFRDTM), we have

$$\psi(y,t) = \sum_{k=0}^{\infty} \Psi_k t^{k\nu}$$
$$= \Psi_0 + \Psi_1 t^\nu + \Psi_2 t^{2\nu} + \cdots$$

$$= 1 + sin_\nu(y^\nu) - \frac{t^\nu}{\Gamma(1+\nu)}\begin{bmatrix} sin_\nu^3(y^\nu) + 4sin_\nu^2(y^\nu) \\ +5sin_\nu(y^\nu) + n + \cdots \end{bmatrix}$$
$$+ \frac{t^{2\nu}}{\Gamma(1+\nu)\Gamma(1+2\nu)}\begin{bmatrix} sin_\nu^9(y^\nu) + 4sin_\nu^8(y^\nu) + 9sin_\nu^7(y^\nu) + \\ 105sin_\nu^6(y^\nu) + 123sin_\nu^5(y^\nu) + 126sin_\nu^4(y^\nu) \\ +166sin_\nu^3(y^\nu) + 29sin_\nu^2(y^\nu) - 3/4sin_\nu(y^\nu) + \cdots \end{bmatrix}$$
$$+ \frac{t^{3\nu}}{\Gamma(1+\nu)\Gamma(1+2\nu)\Gamma(1+3\nu)}\begin{bmatrix} sin_\nu^{27}(y^\nu) + 10682sin_\nu^{26}(y^\nu) \\ +269874sin_\nu^{25}(y^\nu) + \cdots \end{bmatrix} + \cdots$$

which is the series solution of the given local fractional Klein-Gordon equation. The figures 4,5, 6 and 7 shows the physical interpretation of $\psi(y,t)$ *corresponding to* $\nu = 0.25, 0.5, 0.6289$ *and* 1.

Figures here show the physical interpretation of $\psi(y,t)$ vs. t corresponding to a particular value of ν.

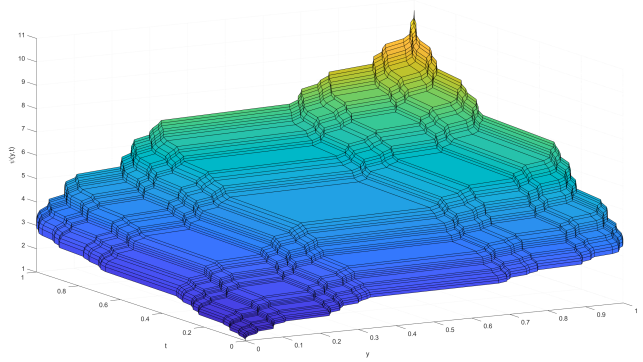

Figure 1 The figure illustrates Solution of Example 1 when $\nu = log(2)/log(3) = 0.6309$

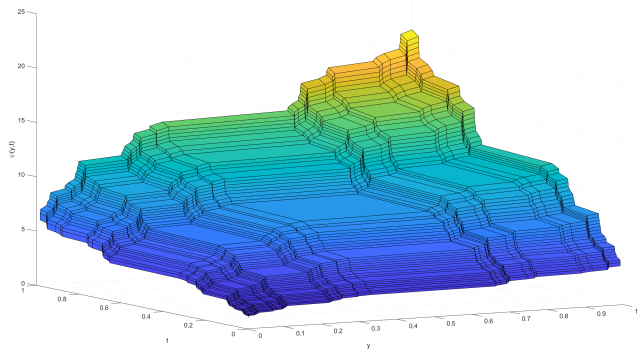

Figure 2 The figure illustrates Solution of Example 2 when $\nu = log(2)/log(3) = 0.6309$

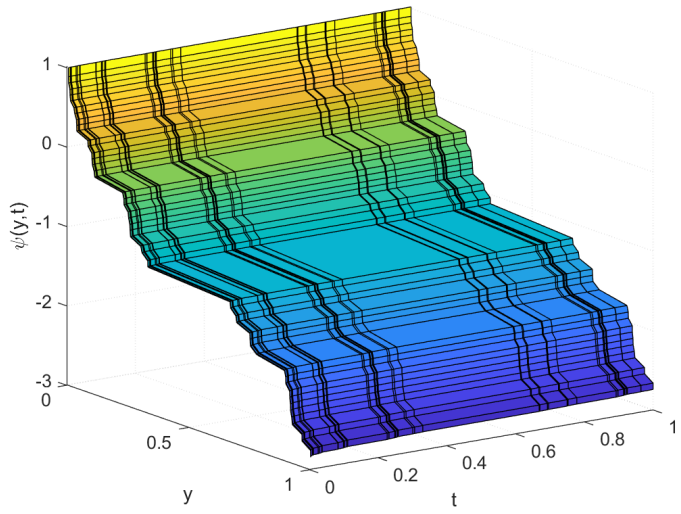

Figure 3 The figure illustrates Solution of Example 3 of $\psi(y,t)$ vs. time t when $\nu = log(2)/log(3) = 0.6309$

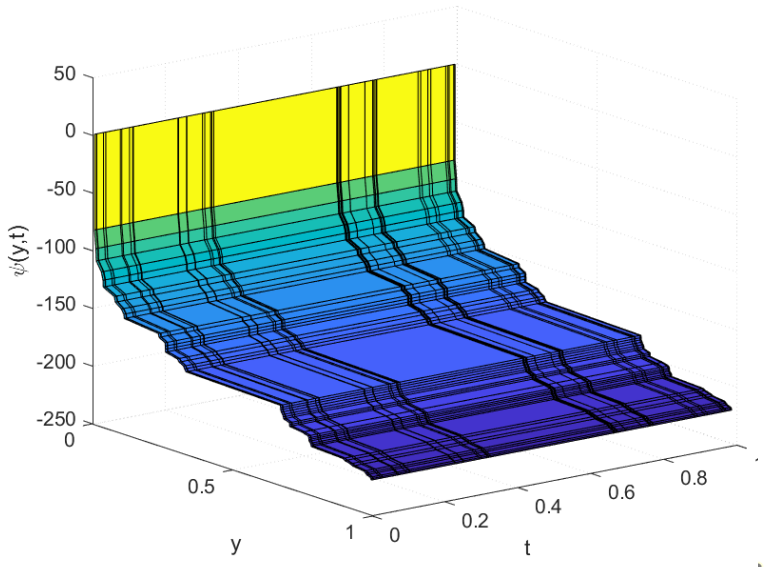

Figure 4 Example 4 when $\nu = 0.25$

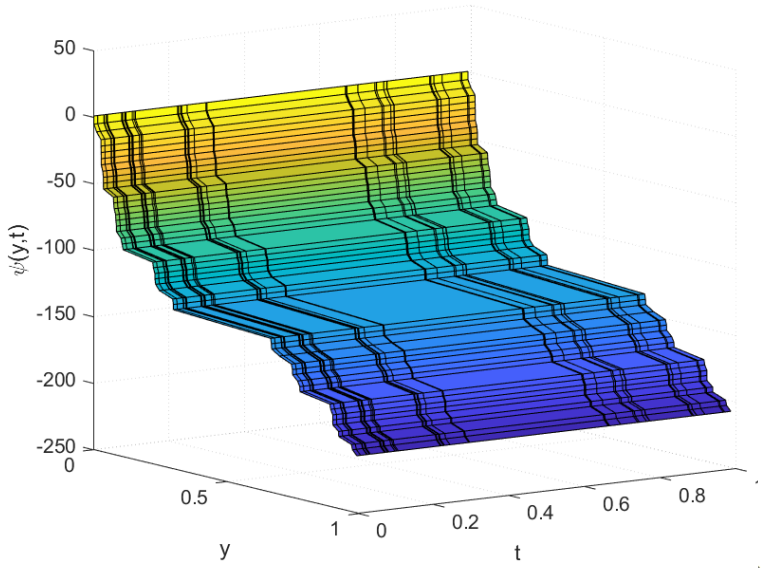

Figure 5 Example 4 when $\nu = 0.5$

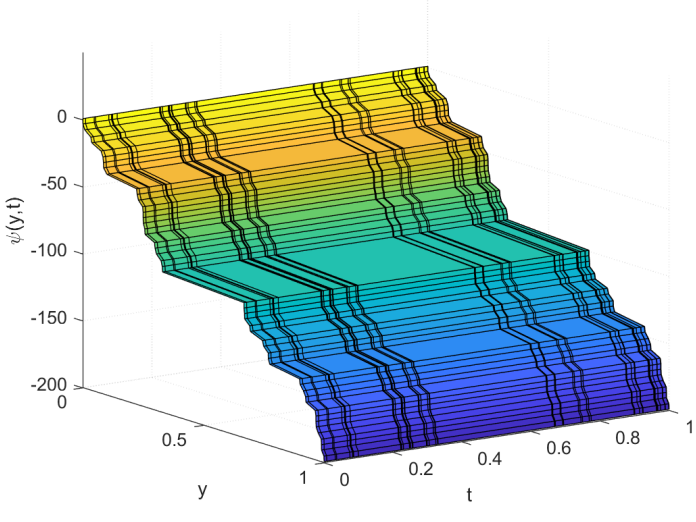

Figure 6 Example 4 when $\nu = 1$

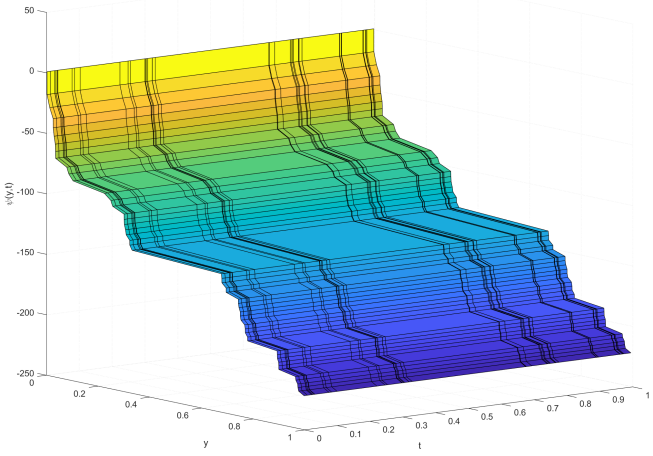

Figure 7 Example 4 when $\nu = log(2)/log(3)$

CONCLUSION

In this study, we have combined the fractional complex transform with the local fractional differential transform method to analyze the Klein-Gordon equations of n terms in cantor sets within the local fractional differential operator and have tried to approximate the solution of the same. Our results show that this method is an effective mathematical tool for solving local fractional linear differential equations. Furthermore, the versatility of this method makes it highly adaptable to solving a wide range of fractional differential equations. The examples are particular cases of the proposed n-term Klein-Gordon equation, and their corresponding corrected approximated solutions are presented along with their graphs. Hence, we can conclude that the fractional complex transform with the local fractional differential transform method is a powerful and flexible approach to obtain effective approximate solutions of local fractional partial differential equations.

Acknowledgments

The authors thank the editor and reviewers for their constructive comments to improve this article.

Availability of data and material

Not applicable.

Conflicts of interest

The authors declare that there is no conflict of interest regarding the publication of this article.

Ethical standard

The authors have no relevant financial or non-financial interests to disclose.

LITERATURE CITED

Acan, O., M. M. Al Qurashi, and D. Baleanu, 2017 Reduced differential transform method for solving time and space local fractional partial differential equations. Journal of Nonlinear Sciences & Applications (JNSA) **10**.

Chu, Y.-M., M. Jneid, A. Chaouk, M. Inc, H. Rezazadeh, *et al.*, 2023 Local time fractional reduced differential transform method for solving local time fractional telegraph equations. Fractals **0**: null.

Dubey, V. P., D. Kumar, J. Singh, A. M. Alshehri, and S. Dubey, 2022 Analysis of local fractional klein-gordon equations arising in relativistic fractal quantum mechanics. Waves in Random and Complex Media **0**: 1–21.

Jafari, H., H. K. Jassim, S. P. Moshokoa, V. M. Ariyan, and F. Tchier, 2016 Reduced differential transform method for partial differential equations within local fractional derivative operators. Advances in Mechanical Engineering **8**: 1687814016633013.

Kanth, A. R. and K. Aruna, 2009 Differential transform method for solving the linear and nonlinear klein–gordon equation. Computer Physics Communications **180**: 708–711.

Keskin, Y. and G. Oturanc, 2009 Reduced differential transform method for partial differential equations. International Journal of Nonlinear Sciences and Numerical Simulation **10**: 741–750.

Kolwankar, K. M. and A. D. Gangal, 1996 Fractional differentiability of nowhere differentiable functions and dimensions. Chaos: An Interdisciplinary Journal of Nonlinear Science **6**: 505–513.

Kumar, D., J. Singh, and D. Baleanu, 2017 A hybrid computational approach for klein–gordon equations on cantor sets. Nonlinear Dynamics **87**: 511–517.

Sun, J., 2018 Analytical approximate solutions of (n+ 1)-dimensional fractal harry dym equations. Fractals **26**: 1850094.

Wang, K.-L., K.-J. Wang, and C.-H. He, 2019 Physical insight of local fractional calculus and its application to fractional kdv–burgers–kuramoto equation. Fractals **27**: 1950122.

Yang, A.-M., Y.-Z. Zhang, C. Cattani, G.-N. Xie, M. M. Rashidi, *et al.*, 2014 Application of local fractional series expansion method to solve klein-gordon equations on cantor sets. In *Abstract and Applied Analysis*, volume 2014, Hindawi.

Yang, X.-J., 2012 Advanced local fractional calculus and its applications.

Yang, X.-J. and J. Tenreiro Machado, 2019 A new fractal nonlinear burgers' equation arising in the acoustic signals propagation. Mathematical Methods in the Applied Sciences **42**: 7539–7544.

Zhang, Y., C. Cattani, and X.-J. Yang, 2015 Local fractional homotopy perturbation method for solving non-homogeneous heat conduction equations in fractal domains. Entropy **17**: 6753–6764.

Zhang, Y. and X.-J. Yang, 2016 An efficient analytical method for solving local fractional nonlinear pdes arising in mathematical physics. Applied Mathematical Modelling **40**: 1793–1799.

How to cite this article: Sharma, N., Goswami, P., and Joshi, S. Analysis of the n-Term Klein-Gordon Equations in Cantor Sets. *Chaos Theory and Applications*, 5(4), 308-317, 2023.

CHAOS
Theory and Applications
in Applied Sciences and Engineering

e-ISSN: 2687-4539
RESEARCH ARTICLE
Vol.5 / No.4 / 2023 / pp.318-325
Special Issue
https://doi.org/10.51537/chaos.1334407

Fractalization of Fractional Integral and Composition of Fractal Splines

A. Gowrisankar *,[1]
*Department of Mathematics, School of Advanced Sciences, Vellore Institute of Technology, Vellore 632 014, Tamil Nadu, India.

ABSTRACT The present study perturbs the fractional integral of a continuous function f defined on a real compact interval, say $(\mathcal{I}^v f)$ using a family of fractal functions $(\mathcal{I}^v f)^\alpha$ based on the scaling parameter α. To elicit this phenomenon, a fractal operator is proposed in the space of continuous functions, an analogue to the existing fractal interpolation operator which perturbs f giving rise to α-fractal function f^α. In addition, the composition of α-fractal function with the linear fractal function is discussed and the composition operation on the fractal interpolation functions is extended to the case of differentiable fractal functions.

KEYWORDS
Fractional integral
α-fractal function
Error estimation
Composite fractal functions

INTRODUCTION

The launch of fractal interpolation function has initiated a new theory of approximation concerning the naturally existing functions with non-differentiable nature. Rooted from the remark of Barnsley in (Barnsley 1986), Navascués has explored the approximation of continuous functions defined on a real closed interval by a class of α-fractal functions, where α is the appropriately chosen scaling parameter, in (Navascués 2005). Non-smooth analogue of prescribed continuous function can be achieved with the choice of non-differentiable base function. Further, Navascués has pioneered the fractal operator to associate each prescribed function to its class of α-fractal functions. The theme of proposing a fractal operator has fruitfully enabled the fractal theory to connect with various mathematical fields not limited to operator theory. While constructing α-fractal function, the base function choice is significant since the fractal operator is dependent on the boundedness of the base function. Literature survey acknowledges various interesting discussions on α-fractal functions, for instance, the derivative of α-fractal function is explored and its respective fractal operator is studied in (Navascués and Sebastián 2006).

The Riemann-Liouville fractional integral of α-fractal function has been discussed for the α-fractal functions with both constant and variable scalings in (Priyanka and Gowrisankar 2021b). Further, a fractional operator is defined to assign the continuous function to the fractional integral of its fractal version. For more works on α-fractal functions, the readers are recommended to consult (Balasubramani *et al.* 2020; Akhtar *et al.* 2017; Banerjee *et al.* 2023). While analysing fractals and fractal functions, the study of their fractal dimension is an ever interesting topic. Falconer has discussed the dimension theory for the fractal interpolation functions in (Falconer 2004). The dimensional analysis for the graphs of α-fractal functions is investigated in (Akhtar *et al.* 2016). Beyond the theoretical framework, fractal dimension has been estimated for various physical phenomena. For more fascinating work on the fractal dimension, the readers may visit (Banerjee *et al.* 2021; Fortin *et al.* 1992; Sanjuán 2021; Çimen *et al.* 2020).

In recent times, fractional calculus has been receiving remarkable attention among the fractal community. The Riemann-Liouville (RL) fractional integral of affine fractal functions has been investigated in (Pan 2014). The quadratic fractal function's fractional integral with constant and function scalings has been discussed in (Gowrisankar and Prasad 2019). The fractional integral as well as the fractional derivative of different kinds of fractal interpolation functions have been discussed by several authors (for additional information refer, (Pan 2014; Gowrisankar and Prasad 2019; Ruan *et al.* 2009; Priyanka and Gowrisankar 2021a)). The aforementioned results on α-fractal function and its fractional order integral, naturally arises a question: Is it possible to generate a class of fractal functions such that the fractional integral of a continuous function is interpolated? To answer this question, the present paper initiates the construction of self-referential functions for the fractional integral of continuous functions.

The construction procedure follows Navascués's α-fractal function in (Navascués and Sebastián 2006) and such a construction is guaranteed with the continuity of fractional integral. In addition, a fractal operator is defined to assign the fractional integral of a continuous function to its fractal version. The boundedness of

Manuscript received: 29 July 2023,
Revised: 26 August 2023,
Accepted: 27 August 2023.

[1]gowrisankargri@gmail.com(**Corresponding author**)

the fractional integral discussed in (Samko *et al.* 1993) instigates to discuss the boundedness of the proposed operator. The base function of the newly constructed fractal function, (i.e) the fractional integral of base function of the α-fractal function, is chosen appropriately to explicitly estimate the bound of the operator.

The recent works on fractal functions reported in (Navascués *et al.* 2022; Massopust 2022b,a; Dai and Liu 2023) show the curiosity of young researchers to develop more generalized and flexible fractal interpolation functions. In (Priyanka and Gowrisankar 2021b), authors have demonstrated that the resultant functions on the evaluation of the fractional integral of α-fractal functions are again α-fractal functions obeying the end point conditions. The work by Dai and Liu(Dai and Liu 2023) is also noticeable, in which the composite fractal function is introduced along with the discussion of its fractal dimension. In this direction, the present paper investigates the composition of α-fractal function as well as the composition of fractal spline. Further, it is observed that the composition operator also renders new fractal functions like the case of fractional integral operator, which is discussed in (Priyanka and Gowrisankar 2021b). With this end, the paper directly enters the discussion on the fractal perturbation of continuous functions in the following section.

FRACTALIZATION OF CONTINUOUS FUNCTIONS

Let $N \geq 2$ and $\mathbb{N}_N$ denote the initial set of natural numbers of length N. Consider the interpolation data set,

$$\{(x_j, y_j) \in [x_1, x_{N+1}] \times \mathbb{R} : j \in \mathbb{N}_{N+1}\}.$$

Let l_j be the set of N homeomorphisms from $I = [x_1, x_{N+1}]$ to $I_j = [x_j, x_{j+1}]$, $j \in \mathbb{N}_N$ satisfying

$$|l_j(s) - l_j(t)| \leq \lambda_j |s - t|,\ \lambda_j \in [0, 1),$$
$$l_j(x_1) = x_j, l_j(x_{N+1}) = x_{j+1},\ j \in \mathbb{N}_N.$$

Define the maps $F_j : \mathcal{X} := I \times \mathbb{R} \to \mathbb{R}$ to be continuous in the first argument and Lipschitz continuous in the second argument with Lipschitz constant $\alpha_j < 1$ such that

$$F_j(x_1, y_1) = y_j,\ F_j(x_{N+1}, y_{N+1}) = y_{j+1},\ j \in \mathbb{N}_N.$$

The space of continuous functions defined on the interval I reserves the notation $C(I)$. Let $G = \{h \in C(I) : h(x_1) = y_1, h(x_{N+1}) = y_{N+1}\}$. For $h_1, h_2 \in C(I)$, the metric δ, defined by $\delta(h_1, h_2) = \max\{|h_1(x) - h_2(x)| : x \in I\}$, completes (G, δ). Further, in (Barnsley 1986), the Read-Bajrakteravic operator (RB), $\mathbb{T}$ is defined on (G, δ) by

$$\mathbb{T}h(x) = F_j(l_j^{-1}(x), h(l_j^{-1}(x)),\ j \in \mathbb{N}_N. \tag{1}$$

The continuity properties of l_j and F_j make easier to verify the continuity of $\mathbb{T}$ as follows

$$\delta(\mathbb{T}g_1, \mathbb{T}g_2) \leq |\alpha|_\infty \delta(g_1, g_2),\ g_1, g_2 \in C(I)$$

where $|\alpha|_\infty = \max\{|\alpha_j| : j \in \mathbb{N}_N\} < 1$ and $\alpha = \{\alpha_1, \alpha_2, \ldots, \alpha_N\}$. The choice of α_k makes the operator $\mathbb{T}$ contractive on the space (G, δ). Hence, with the aid of Banach contraction principle, it is concluded that $\mathbb{T}$ has a unique fixed point, say g, satisfying $g(x_j) = y_j$, for all $j \in \mathbb{N}_{N+1}$ and from Eqn.(1), it follows that

$$g(x) = F_j(l_j^{-1}(x), g(l_j^{-1}(x)),\ j \in \mathbb{N}_N. \tag{2}$$

Using the maps l_j and F_j, define contractive transformations w_j from $\mathcal{X}$ to $I_j \times \mathbb{R}$ as

$$w_j(x, y) = (l_j(x), F_j(x, y)),\ (x, y) \in \mathcal{X},\ j \in \mathbb{N}_N.$$

Thus, the finite collection of contractive maps w_j together with the complete metric space $(\mathcal{X}, d)$ forms a hyperbolic Iterated Function System (IFS) and it is denoted by

$$\{\mathcal{X}; w_j(x, y) = (l_j(x), f_j(x, y)) : j \in \mathbb{N}_N\}. \tag{3}$$

Let $H(\mathcal{X}) := \{\mathbb{A} \subset \mathcal{X} : \mathbb{A} \neq \emptyset \text{ and compact}\}$. The Hausdorff metric h_d is defined on $H(\mathcal{X})$ by

$$h_d(\mathbb{A}, \mathbb{B}) = \max\{d(\mathbb{A}, \mathbb{B}), d(\mathbb{B}, \mathbb{A})\},$$

where $d(\mathbb{A}, \mathbb{B}) = \sup_{a \in \mathbb{A}} \inf_{b \in \mathbb{B}} \{d(a, b)\}$, then the pair $(H(\mathcal{X}), h_d)$ is a complete metric space whenever the metric space $(\mathcal{X}, d)$ is complete. A Hutchinson-Barnsley operator W is defined as a self-map on $H(\mathcal{X})$ by

$$W(\mathbb{C}) = \bigcup_{j=1}^{N} w_j(\mathbb{C}),$$

where $\mathbb{C} \in H(\mathcal{X})$. By the Banach principle of fixed point, there exists a unique $\mathbb{G}_g$ in $H(\mathcal{X})$ such that

$$\mathbb{G}_g = \lim_{n \to \infty} W^{\circ n}(\mathbb{C}),$$

where $W^{\circ n}$ is the n-fold self-composition of W. Moreover, this set $\mathbb{G}_g$ is the graph of the function g obeying the self-referential equation (2). In this construction, the function g is called the *Fractal Interpolation Function* (FIF) associated with the IFS (3). The interested readers may consult (Barnsley 1986; Agathiyan *et al.* 2022; Gowrisankar and Uthayakumar 2016) for more details on FIFs.

The following is the review of construction of α-fractal function explored by Navacués in (Navascués 2005). Slightly deviating from the theme of fractal interpolation function approximating the given interpolation data sharing complex behaviour, Navacués has generated a class of continuous functions with fractal properties to approximate $f \in C(I)$. For $f \in C(I)$, let $\{(x_j, f(x_j)) : j \in \mathbb{N}_{N+1}\}$ be the interpolation points. A partition $\Delta := \{x_1, x_2, \ldots, x_{N+1}\}$ is considered such that $x_1 < x_2 < \cdots < x_{N+1}$ and the continuous function $b : I \to \mathbb{R}$ is taken as the base function equal to f only at the endpoints x_1 and x_{N+1}. i.e.,

$$b(x_1) = f(x_1),\ b(x_{N+1}) = f(x_{N+1}),\ \text{and } b \neq f. \tag{4}$$

Let $\alpha_j \in (-1, 1)$, $j \in \mathbb{N}_N$. Consider the maps

$$l_j(x) = a_j x + b_j,\ F_j(x, f(x)) = \alpha_j f(x) + q_j(x),\ j \in \mathbb{N}_N, \tag{5}$$

where

$$q_j(x) = f(l_j(x)) - \alpha_j b(x). \tag{6}$$

Then, the attractor of the IFS (3) involving the maps in (5) and (6) is the graph of the fractal interpolation function say, $f^\alpha_{\Delta,b}$ corresponding to f with respect to scale vector α, partition Δ and base function b. In addition, the function $f^\alpha_{\Delta,b}$ is the fixed point of the RB operator $\mathscr{T}_\alpha$ defined on $C_f(I)$, where $C_f(I)$ is the space of continuous functions h obeying $h(x_1) = f(x_1)$, $h(x_{N+1}) = f(x_{N+1})$. The operator $\mathscr{T}_\alpha$ is described as

$$\mathscr{T}_\alpha h(x) = f(x) + \alpha_j (h - b) \circ l_j^{-1}(x),\ x \in I,\ j \in \mathbb{N}_N.$$

Then, $f^\alpha_{\Delta,b}$ obeys

$$f^\alpha_{\Delta,b}(x) = f(x) + \alpha_j (f^\alpha - b) \circ l_j^{-1}(x),\ x \in I,\ j \in \mathbb{N}_N. \tag{7}$$

Definition 1. *The function $f^\alpha_{\Delta,b} := f^\alpha$ satisfying the self-referential equation (7) is the fractal perturbation of f and it is known as the α-fractal function corresponding to α, Δ and b.*

According to Eqn.(7), f^α interpolates f at each x_j (i.e.) $f^\alpha(x_j) = f(x_j)$, for all $j \in \mathbb{N}_{N+1}$. Also, f^α equals the prescribed function f when all the scaling factors are taken to be zero. In addition, from Eqn.(7), the uniform distance between f and f^α can be deduced as follows.

$$\|f^\alpha - f\|_\infty \leq \frac{|\alpha|_\infty}{1-|\alpha|_\infty}\|f-b\|_\infty.$$

Let $C[a,b]$ be equipped with sup norm

$$\|f\|_\infty = \max\{|f(x)| : x \in [a,b]\}.$$

Consider the linearly dependent base function b on f, $b = Lf$, where $L : C[a,b] \to C[a,b]$ is a linear operator and bounded, its operator norm is given by

$$\|L\| := sup\{\|Lf\|_\infty : \|f\|_\infty \leq 1\}$$

and $Lf(x_1) = x_1$, $Lf(x_{N+1}) = x_{N+1}$ with $L \neq Identity$.

Remark 1. *The present study proceeds with $Lf = f \circ c$, where c is an increasing as well as continuous function such that $c(x_1) = x_1$, $c(x_{N+1}) = x_{N+1}$ and $c \neq Identity$. For this particular choice of $b = f \circ c$, $\|b\|_\infty = \|Lf\|_\infty = \|f\|_\infty$ with operator norm $\|L\| = 1$.*

Lemma 1. *(Navascués 2010) For any $f \in C(I)$ and $b = Lf$, the following inequality holds*

$$\|f^\alpha - f\|_\infty \leq \frac{|\alpha|_\infty \|Id - L\|_\infty}{1-|\alpha|_\infty}\|f\|_\infty,$$

where Id is the identity operator.

Note 1. *If $Lf = f \circ c$, the inequality () becomes*

$$\|f^\alpha - f\|_\infty \leq \frac{2|\alpha|_\infty}{1-|\alpha|_\infty}\|f\|_\infty.$$

In (Navascués 2005), a fractal interpolation operator $\mathcal{F}^\alpha : C(I) \to C(I)$ is introduced to fractalize each continuous function as

$$\mathcal{F}^\alpha(f) = f^\alpha,\ f \in C(I).$$

Theorem 1. *(Navascués 2010) For any bounded and linear operator L with sup norm, the following holds*

$$\|\mathcal{F}^\alpha(f)\|_\infty \leq \left(1 + \frac{|\alpha|_\infty \|Id - L\|_\infty}{1-|\alpha|_\infty}\right)\|f\|_\infty.$$

In analogue to the above discussed operator, various fractal operators have been proposed to the fractalize the given continuous functions, see for instance (Navascués and Sebastián 2006; Priyanka and Gowrisankar 2021b).

FRACTAL PERTURBATION OF FRACTIONAL INTEGRAL OF A CONTINUOUS FUNCTION

In order to define a new class of α-fractal functions to approximate the fractional integral of $f \in C(I)$, this section commences with the definition of RL fractional integral of a continuous function.

Definition 2. *(Samko et al. 1993) Let f be the integrable function on $[a,b] \subset \mathbb{R}$ and $v > 0$ be a real number. Then, the Riemann-Liouville (RL) fractional integral of f is defined by*

$$(\mathcal{I}^v f)(t) = \frac{1}{\Gamma(v)}\int_a^t (t-s)^{v-1} f(s)ds,\ (t > a),$$

here the notation $\Gamma(\cdot)$ denotes the Gamma function.

In (Samko *et al.* 1993), it is proved that the fractional integral operator $(\mathcal{I}^v f)$ is bounded in L_p space with $1 \leq p \leq \infty$ and it is precisely provided in the following lemma.

Lemma 2. *For $v > 0$, the RL fractional integral operator is bounded such that*

$$\|\mathcal{I}^v f\| \leq \mathcal{K}\|f\|_\infty, \text{ where } \mathcal{K} = \frac{x_{N+1} - x_1}{v\Gamma(v)}.$$

Using the above lemma, the uniform distance between the germ function f and its fractional integral $\mathcal{I}^v f$ can be estimated as follows.

Lemma 3. *The distance between f and $\mathcal{I}^v f$ with respect to the uniform norm is given by*

$$\|f - \mathcal{I}^v f\|_\infty \leq (1+\mathcal{K})\|f\|_\infty,$$

where $\mathcal{K} = \frac{x_{N+1}-x_1}{v\Gamma(v)}$.

Proof. By the definition of uniform norm,

$$\|f - \mathcal{I}^v f\|_\infty \leq \|f\|_\infty + \|\mathcal{I}^v f\|_\infty.$$

From Lemma 2, it follows that $\|\mathcal{I}^v f\|_\infty \leq \mathcal{K}\|f\|_\infty$, where $\mathcal{K} = \frac{x_{N+1}-x_1}{v\Gamma(v)}$. Then,

$$\begin{aligned}\|f - \mathcal{I}^v f\|_\infty &\leq \|f\|_\infty + \mathcal{K}\|f\|_\infty \\ &\leq (1+\mathcal{K})\|f\|_\infty.\end{aligned}$$

□

The following lemma ensures the continuity of the fractional order integral $\mathcal{I}^v f$ which is proved by Pan in reference (Pan 2014).

Lemma 4. *Let $v > 0$ and $f \in C[a,b]$. Then $\mathcal{I}^v f \in C[a,b]$.*

From Lemma 4, it is straight forward to define a family of fractal functions to approximate $\mathcal{I}^v f$.

Let $\{x_j, \mathcal{I}^v f(x_j)\}$ be the the interpolation data with partition Δ and scale vector α. To define a new family of self-referential functions, consider the base function as the fractional integral of b, expressed by

$$(\mathcal{I}^v b)(t) = \frac{1}{\Gamma(v)}\int_{x_1}^x (t-s)^{v-1} b(s)ds,$$

such that

$$\begin{aligned}(\mathcal{I}^v b)(x_1) &= (\mathcal{I}^v f)(x_1), \\ (\mathcal{I}^v b)(x_{N+1}) &= (\mathcal{I}^v f)(x_{N+1})\end{aligned}$$

and $\mathcal{I}^v b \neq \mathcal{I}^v f$. In correspondence with the new continuous functions $(\mathcal{I}^v f)$ and $(\mathcal{I}^v b)$, the maps defined in (5) becomes,

$$l_j(x) = a_j x + b_j,\ F_j(x,y) = \alpha_j y + (\mathcal{I}^v f)l_j(x) - \alpha_j(\mathcal{I}^v b)(x),\ j \in \mathbb{N}_N. \tag{8}$$

The attractor of the IFS with the maps in (8) is the graph of the new kind of α-fractal function say, $(\mathcal{I}^v f)^\alpha$ associated with $(\mathcal{I}^v f)$. It can be verified that $(\mathcal{I}^v f)^\alpha(x_j) = (\mathcal{I}^v f)(x_j)$ for all $j \in \mathbb{N}_{N+1}$. Besides, $(\mathcal{I}^v f)^\alpha$ is a unique fixed point of the RB operator $\mathcal{T}_\alpha$ with the change of arguments such that

$$(\mathcal{I}^v f)^\alpha(x) = \mathcal{I}^v f(x) + \alpha_j((\mathcal{I}^v f)^\alpha - \mathcal{I}^v b) \circ l_j^{-1}(x)),\ x \in I,\ j \in \mathbb{N}_N.$$

The function $(\mathcal{I}^v f)^\alpha$ is the α-fractal function of the RL fractional integral of $f \in C(I)$ approximating $(\mathcal{I}^v f)$ with respect to base

function $(\mathcal{I}^v b)$, partition Δ and scaling parameter α. With an aim to estimate the error, now consider the mapping

$$\begin{aligned} T : & R \times C(I) \to C(I) \\ & (\alpha, \mathcal{I}^v f) \to \mathscr{T}_\alpha(\mathcal{I}^v f) \end{aligned}$$

where $R = [0,t] \times [0,t] \times [0,t] \times \cdots \times [0,t] \subset \mathbb{R}^N, 0 \leq t < 1$, t is fixed. For $x \in I_j$, define

$$\begin{aligned} \mathscr{T}_\alpha(\mathcal{I}^v f)(x) &= F_j^{\alpha_j}(l_j^{-1}(x), (\mathcal{I}^v f) \circ l_j^{-1}(x)) \\ &= \alpha_j(\mathcal{I}^v f) \circ l_j^{-1}(x) + q_j^{\alpha_j} \circ l_j^{-1}(x) \end{aligned}$$

with

$$q_j^{\alpha_j}(x) = (\mathcal{I}^v f) \circ l_j(x) - \alpha_j(\mathcal{I}^v b)(x).$$

The uniform distance between the functions $(\mathcal{I}^v f)$ and $(\mathcal{I}^v f)^\alpha$ is estimated in the following theorem.

Theorem 2. *If b is a bounded linear operator, then the below inequality holds*

$$\|(\mathcal{I}^v f)^\alpha - (\mathcal{I}^v f)\|_\infty \leq \frac{2\mathcal{K}|\alpha|_\infty}{1-|\alpha|_\infty}\|f\|_\infty,$$

where $\mathcal{K} = \frac{x_{N+1}-x_1}{v\Gamma(v)}$.

Proof. Let $(\mathcal{I}^v f) \in \mathcal{C}_f(I)$. Then for each $x \in I_j$,

$$\begin{aligned} &|\mathscr{T}_\alpha(\mathcal{I}^v f)(x) - \mathscr{T}_\beta(\mathcal{I}^v f)(x)| \\ &\quad = |\alpha_j(\mathcal{I}^v f) \circ l_j^{-1}(x) + q_j^{\alpha_j} \circ l_j^{-1}(x) - \beta_j(\mathcal{I}^v f) \circ l_j^{-1}(x) \\ &\qquad - q_j^{\beta_j} \circ l_j^{-1}(x)| \\ &\quad \leq |\alpha_j(\mathcal{I}^v f) \circ l_j^{-1}(x) - \beta_j(\mathcal{I}^v f) \circ l_j^{-1}(x)| \\ &\qquad + |q_j^{\alpha_j} \circ l_j^{-1}(x) - q_j^{\beta_j} \circ l_j^{-1}(x)| \end{aligned}$$

From Eqn.(), the second term is rewritten as

$$\begin{aligned} &\|\mathscr{T}_\alpha(\mathcal{I}^v f) - \mathscr{T}_\beta(\mathcal{I}^v f)\|_\infty \\ &\quad \leq |\alpha_j - \beta_j|\|\mathcal{I}^v f\|_\infty + |(\mathcal{I}^v f) \circ l_j(x) - \alpha_j(\mathcal{I}^v b)(x) \qquad (9) \\ &\qquad - (\mathcal{I}^v f) \circ l_j(x) + \beta_j(\mathcal{I}^v b)(x)| \\ &\quad \leq |\alpha - \beta|_\infty\|\mathcal{I}^v f\|_\infty + |\alpha_j - \beta_j|\|\mathcal{I}^v b\|_\infty \\ &\quad \leq 2|\alpha - \beta|_\infty\|\mathcal{I}^v f\|_\infty. \qquad (10) \end{aligned}$$

Meanwhile, $(\mathcal{I}^v f)$ is the fixed point of $\mathscr{T}_\alpha$ corresponding to $q_j^{\alpha_j}(x) = (\mathcal{I}^v f) \circ l_j(x) - \alpha_j(\mathcal{I}^v b)(x)$. Then,

$$\begin{aligned} \|(\mathcal{I}^v f)^\alpha - (\mathcal{I}^v f)^\beta\|_\infty = \|&\mathscr{T}_\alpha(\mathcal{I}^v f)^\alpha - \mathscr{T}_\alpha(\mathcal{I}^v f)^\beta + \mathscr{T}_\alpha(\mathcal{I}^v f)^\beta \\ &- \mathscr{T}_\beta(\mathcal{I}^v f)^\beta\|_\infty \end{aligned}$$

Since $\mathscr{T}_\alpha$ is contractive with contractivity factor α and applying the inequality (9),

$$\begin{aligned} \|(\mathcal{I}^v f)^\alpha - (\mathcal{I}^v f)^\beta\|_\infty &\leq |\alpha|_\infty\|(\mathcal{I}^v f)^\alpha - (\mathcal{I}^v f)^\beta\|_\infty + 2|\alpha \\ &\quad - \beta|_\infty\|(\mathcal{I}^v f)^\beta\|_\infty \\ &= \frac{2|\alpha-\beta|_\infty\|(\mathcal{I}^v f)^\beta\|_\infty}{1-|\alpha|_\infty}. \end{aligned}$$

Setting $\beta = 0 \in \mathbb{R}^N$ and using the property $(\mathcal{I}^v f)^0 = (\mathcal{I}^v f)$, observe that

$$\begin{aligned} \|(\mathcal{I}^v f)^\alpha - (\mathcal{I}^v f)\|_\infty &= \frac{2|\alpha|_\infty\|(\mathcal{I}^v f)\|_\infty}{1-|\alpha|_\infty} \\ &= \frac{2\mathcal{K}|\alpha|_\infty}{1-|\alpha|_\infty}\|f\|_\infty. \end{aligned}$$

□

The above theorem is a prelude to discuss the boundedness of the fractal operator $\mathcal{F}^{\alpha,v}$ which is explored in the following section.

FRACTAL OPERATOR ASSOCIATED WITH THE FRACTIONAL INTEGRAL

This section proposes a fractal operator to send each continuous function $\mathcal{I}^v f$ to its fractal version $(\mathcal{I}^v f)^\alpha$ where the function $(\mathcal{I}^v f)^\alpha$ is the α-fractal function of the RL fractional integral of a prescribed continuous function f discussed in the previous section. To be concise, for a fixed scale vector α and a fixed fractional order $v > 0$, there exists an operator

$$\begin{aligned} \mathcal{F}^{\alpha,v} : & C(I) \to C(I) \\ & \mathcal{I}^v f \longmapsto (\mathcal{I}^v f)^\alpha. \end{aligned}$$

The linearity of b assures the linearity of $\mathcal{F}^{\alpha,v}$. For fixed scalars λ and μ, it can be verified that

$$\mathcal{F}^{\alpha,v}(\lambda\mathcal{I}^v f + \mu\mathcal{I}^v g) = \lambda\mathcal{F}^{\alpha,v}(\mathcal{I}^v f) + \mu\mathcal{F}^{\alpha,v}(\mathcal{I}^v g).$$

Theorem 3. *$\mathcal{F}^{\alpha,v}$ is bounded on $C(I)$. Moreover,*

$$\|\mathcal{F}^{\alpha,v}(\mathcal{I}^v f)\|_\infty \leq \left(\frac{1+|\alpha|_\infty}{1-|\alpha|_\infty}\right)\mathcal{K}\|f\|_\infty,$$

where $\mathcal{K} = \frac{x_{N+1}-x_1}{v\Gamma(v)}$.

Proof. From Theorem 2, one has

$$\|(\mathcal{I}^v f)^\alpha - (\mathcal{I}^v f)\|_\infty \leq \frac{2\mathcal{K}|\alpha|_\infty}{1-|\alpha|_\infty}\|f\|_\infty,$$

with $\mathcal{K} = \frac{x_{N+1}-x_1}{v\Gamma(v)}$. Then,

$$\begin{aligned} \|(\mathcal{I}^v f)^\alpha\|_\infty - \|(\mathcal{I}^v f)\|_\infty &\leq \frac{2\mathcal{K}|\alpha|_\infty}{1-|\alpha|_\infty}\|f\|_\infty \\ \|(\mathcal{I}^v f)^\alpha\|_\infty &\leq \|(\mathcal{I}^v f)\|_\infty + \frac{2\mathcal{K}|\alpha|_\infty}{1-|\alpha|_\infty}\|f\|_\infty \\ &\leq \mathcal{K}\|f\|_\infty + \frac{2\mathcal{K}|\alpha|_\infty}{1-|\alpha|_\infty}\|f\|_\infty, \end{aligned}$$

which provides the required bound of the operator $\mathcal{F}^{\alpha,v}$,

$$\begin{aligned} \|\mathcal{F}^{\alpha,v}(\mathcal{I}^v f)\|_\infty &\leq \left(1 + \frac{2|\alpha|_\infty}{1-|\alpha|_\infty}\right)\mathcal{K}\|f\|_\infty \\ &= \left(\frac{1+|\alpha|_\infty}{1-|\alpha|_\infty}\right)\mathcal{K}\|f\|_\infty. \end{aligned}$$

Hence, the required inequality. □

Next, the bound for the perturbation error between f and $(\mathcal{I}^v f)^\alpha$ is explored in the following theorem.

Theorem 4. *For any $f \in C(I)$, the following inequality*

$$\|f - (\mathcal{I}^v f)^\alpha\|_\infty \leq \left(1 + \mathcal{K} + \frac{2\mathcal{K}|\alpha|_\infty}{1-|\alpha|_\infty}\right)\|f\|_\infty,$$

holds with $\mathcal{K} = \frac{x_{N+1}-x_1}{v\Gamma(v)}$.

Proof. One can have

$$\begin{aligned}\|f-(\mathcal{I}^v f)^\alpha\|_\infty &= \|f-\mathcal{I}^v f+\mathcal{I}^v f-(\mathcal{I}^v f)^\alpha\|_\infty \\ &\leq \|f-\mathcal{I}^v f\|_\infty + \|\mathcal{I}^v f-(\mathcal{I}^v f)^\alpha\|_\infty.\end{aligned}$$

Using Lemma 4 and Theorem 2, the above inequality is reduced to

$$\|f-(\mathcal{I}^v f)^\alpha\|_\infty \leq (1+\mathcal{K})\|f\|_\infty + \frac{2\mathcal{K}|\alpha|_\infty}{1-|\alpha|_\infty}\|f\|_\infty.$$

Thus, the required result follows immediately. □

Remark 2. *In (Priyanka and Gowrisankar 2021b), a fractal operator $\mathcal{F}^v$ has been proposed to associate the given function $f \in C(I)$ to the Riemann-Liouville fractional integral of its fractal version namely, $\mathcal{I}^v(f^\alpha)$ and discussed some of its elementary properties. Whereas, here the fractal operator $\mathcal{F}^{\alpha,v}$ is defined on $C(I)$ to associate the fractional integral of $f \in C(I)$ to its fractal version, namely $(\mathcal{I}^v f)^\alpha$.*

COMPOSITE FRACTAL FUNCTIONS

This section discusses the composition of fractal functions and demonstrate that the compositions are again fractal functions.

Composition of α-fractal Function

Let $J = [y_1, y_{N+1}] \subset \mathbb{R}$ and $l_{1,j} : I \to I_j$ be the homeomorphic maps defined by $l_{1,j}(x) = a_{1,j}x + b_{1,j}$ satisfying

$$d(l_{1,j}(a), l_{1,j}(b)) \leq r_1 d(a,b),\ 0 \leq r_1 < 1,\ a,b \in I,$$

where d is a Euclidean metric or its equivalent metric and

$$l_{1,j}(x_1) = x_j,\ l_{1,j}(x_{N+1}) = x_{j+1},\ j \in \mathbb{N}_N. \tag{11}$$

Let $K_1 := I \times J$. Define the continuous functions $F_{1,j} : K_1 \to \mathbb{R}$ to be contraction with respect to second variable satisfying

$$F_{1,j}(x_1, y_1) = y_j,\ F_{1,j}(x_{N+1}, y_{N+1}) = y_{j+1},\ j \in \mathbb{N}_N, \tag{12}$$

The general form of the maps $F_{1,j}$ is given by

$$F_{1,j}(x,y) = \alpha_j y + q_j(x),$$

where $\alpha_j = (\alpha_1, \alpha_2, \ldots, \alpha_{N+1})$ is the free parameter chosen in the interval $[0,1)$, which scales the graph vertically and referred as vertical scaling factor, q_j is a suitable continuous function satisfying

$$q_j(x_1) = y_j - \alpha_j y_1,\ q_j(x_{N+1}) = y_{j+1} - \alpha_j y_{N+1}.$$

The system $\{K_1; (l_{1,i}, F_{1,j}) : j \in \mathbb{N}_N\}$ is a IFS and its attractor G_f is the graph of fractal interpolation function $h : I \to \mathbb{R}$ interpolating the data set $\{(x_j, y_j) \in I \times \mathbb{R} : j \in \mathbb{N}_{N+1}\}$ such that $h(x_j) = y_j$, for $j \in \mathbb{N}_{N+1}$. In (Dai and Liu 2023), the functional equation of h is provided by

$$h(x) = F_{1,j}(l_{1,j}^{-1}(x), F(l_{1,j}^{-1}(x))),$$

(or)

$$h(l_{1,j}(x)) = \alpha_j h(x) + q_j(x),\ x \in I,\ j \in \mathbb{N}_N.$$

On the other hand, if the data set $\{(x_j, f(x_j)) : j \in \mathbb{N}_{N+1}\}$ is given to approximate, where f is a continuous function, the following choice of $q_j(x) = f \circ l_{1,j}(x) - \alpha_j b(x)$ generates an α-fractal function satisfying

$$f^\alpha(l_{1,j}(x)) = \alpha_j f^\alpha(x) + f \circ l_{1,j}(x) - \alpha_j b(x)$$

and $f^\alpha(x_j) = f(x_j),\ \forall\, j \in \mathbb{N}_{N+1}$, here b is the base function obeying the conditions provided in (4). Let $\mathcal{N} = [f^\alpha(x_1), f^\alpha(x_{N+1})]$ and $\mathcal{N}_j = [f^\alpha(x_j), f^\alpha(x_{j+1})]$, $j \in \mathbb{N}_N$. Now, to interpolate the data set $\{(f^\alpha(x_j), z_j) : j \in \mathbb{N}_{N+1}\}$, $z_j \in \mathbb{R}$ for all $j \in \mathbb{N}_{N+1}$, a new fractal interpolation function $h : \mathcal{N} \to \mathbb{R}$ is constructed with the maps $m_{1,j}$ and $G_{1,j}$ defined below which respectively obey the conditions of $l_{1,j}$ and $F_{1,j}$,

$$\begin{aligned}m_{1,j}(x) &= c_{1,j}(x) + d_{1,j}, \\ G_{1,j}(f^\alpha(x), z) &= \alpha_j z + p_j(f^\alpha(x)),\ j \in \mathbb{N}_N,\end{aligned}$$

where p_j is a linear polynomial of x satisfying $p_j(f^\alpha(x_0)) = z_j$, $p_j(f^\alpha(x_{N+1})) = z_{j+1}$. Note that the domain of h agrees with $f^\alpha(I)$, thus it is possible to composite g with f^α. Similar to the composite fractal interpolation function discussed in (Dai and Liu 2023), the *composite α-fractal function* $h(f^\alpha)$ can be defined such that $h(f^\alpha(x_j)) = z_j$ and its associated functional equation is expressed by

$$h(f^\alpha(x)) = G_{1,j}(m_{1,j}^{-1}(f^\alpha(x)), h(m_{1,j}^{-1}(f^\alpha(x)))),\ f^\alpha(x) \in \mathcal{N}_j,\ j \in \mathbb{N}_N.$$

From the above equation, it is seen that the composite function $h(f^\alpha)$ interpolates $\{(x_j, z_j) : j \in \mathbb{N}_{N+1}\}$. For instance, consider the α-fractal function f_1^α corresponding to the germ function $f_1(x) = x^2 + 2x$ and base function $b_1(x) = 3x$ with $\alpha = (0.5, -0.5, 0.5)$. Its graphical illustration is provided in Fig. 1(a). The linear fractal interpolation function h_1 corresponding to the data set $\{(f_1^\alpha(x_j), z_j) = \{(0,0), (0.25, 0.2), (0.56, 0.5), (1, 0.25)\}\}$ is represented in Fig. 1(b). The composite α-fractal function $h_1(f_1^\alpha)$ is provided in Fig. 1(c). Considering the height function $f_2(x) = 2x^3$ and base function $b_2(x) = x$ with the scalings $\alpha = (0.7, -0.7, 0.7)$. The graph of another α-fractal function f_2^α approximating f_2 is provided in Fig. 2(a). The data set $\{(f_2^\alpha(x_j), z_j) = \{(0,0), (0.25, 0.2), (0.84, 0.5), (2, 0.25)\}\}$ is approximated using the linear FIF h_2 and it is graphically illustrated in Fig. 2(b). Fig. 2(c) represents the graph of the composite α-fractal function $h_2(f_2^\alpha)$.

Composition of Fractal Spline

In (Barnsley and Harrington 1989), Barnsely has extended the continuity of q_j to be differentiable in order to achieve differentiable fractal functions as narrated below. Consider $l_{1,j}$ and $F_{1,j}$ as defined above satisfying Eqns.(11) and (12). For $n > 0$, suppose

$$|\alpha_j| < a_j^n,$$

and $q_j \in \mathcal{C}^n(I)$, then

$$F_{1,jk}(x,y) = \frac{\alpha_j y + q_j^{(k)}(x)}{a_j^k},$$

$$y_{1,k} = \frac{q_1^k(x_1)}{a_1^k - \alpha_1},\ y_{N+1,k} = \frac{q_{n-1}^k(x_{N+1})}{a_N^k - \alpha_N},\ \text{for } k = 1, 2, \ldots, n.$$

Moreover, if

$$F_{1,(j-1)k}(x_{N+1}, y_{N+1,k}) = F_{1,jk}(x_1, y_{1,k}),\ j = 2, 3, \ldots, N,\ k = 1, 2, \ldots, n,$$

then the IFS $\{K_1; (l_{1,j}, F_{1,j}) : j \in \mathbb{N}_N\}$ generates $h \in \mathcal{C}^k(I)$ and $h^{(k)}$ is the FIF generated by the IFS

$$\{K_1; (l_{1,j}, F_{1,jk}) : j \in \mathbb{N}_N, k = 1, 2, \ldots, n\}. \tag{13}$$

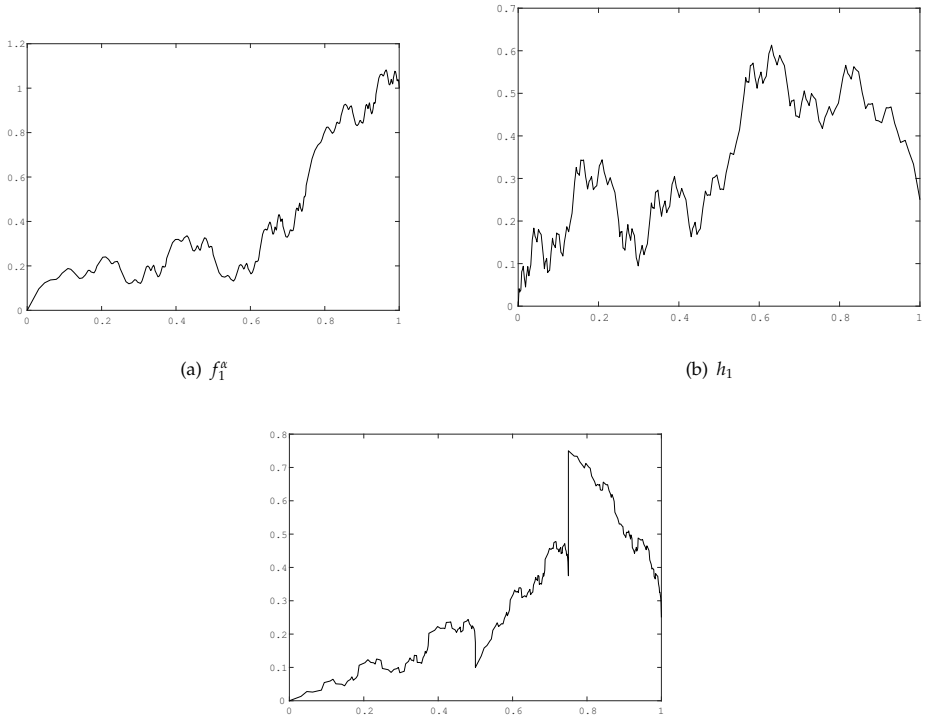

(a) f_1^α (b) h_1

(c) $h_1(f_1^\alpha)$

Figure 1 Graphical illustration of (a) α-fractal function f_1^α, (b) linear FIF h_1 and (c) its composition $h_1(f_1^\alpha)$

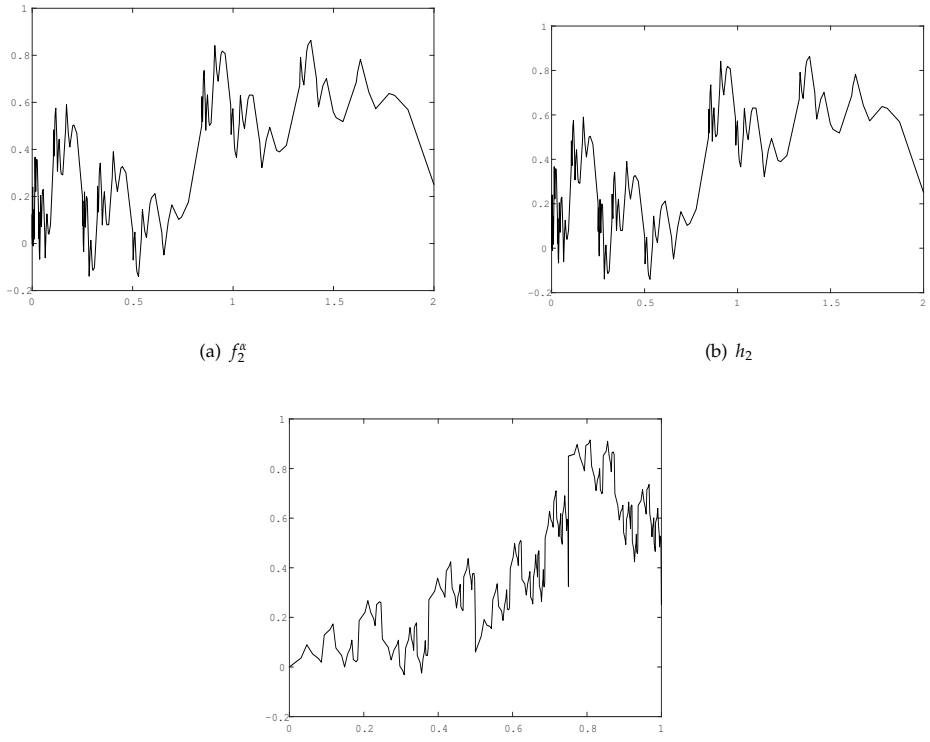

(a) f_2^α (b) h_2

(c) $h_2(f_2^\alpha)$

Figure 2 Graphical illustration of (a) α-fractal function f_2^α, (b) linear FIF h_2 and (c) its composition $h_2(f_2^\alpha)$

Remark 3. *In addition to the differentiability of q_j, for the existence of a differentiable fractal interpolation function, it is important to make sure the scaling parameter α_j obeys Eqn.(). Then, for each $k = 1, 2, \ldots, n$, the fractal spline $h^{(k)} : I \to \mathbb{R}$ interpolates a new data set $\{(x_j, y_{jk}) \in I \times \mathbb{R} : j \in \mathbb{N}_{N+1}\}$ and its functional equation is given by*

$$h^{(k)}(x) = F_{1,jk}(l_{1,jk}^{-1}(x), h^{(k)}(l_{1,jk}^{-1}(x))),$$

(or)

$$h^{(k)}(l_{1,j}(x)) = \frac{1}{a_j^k}(\alpha_j y + q_j^{(k)}(x)),\ x \in I,\ j \in \mathbb{N}_N,\ k = 1, 2, \ldots, n. \tag{14}$$

For each $k = 1, 2, \ldots, n$, let $\{(y_{jk}, z_{jk}) : j \in \mathbb{N}_{N+1}\}$ be the new set of interpolation data, where $y_{1,k} < y_{2,k} < \ldots < y_{N+1,k}$ is a partition of $J_1 = [y_{1,k}, y_{N+1,k}]$ and $z_{jk} \in R_1 = [z_{1,k}, z_{N+1,k}] \subset \mathbb{R}$. Let $J_{1j} = [y_{j,k}, y_{j+1,k}]$, $R_{1j} = [z_{j,k}, z_{j+1,k}]$ for $j \in \mathbb{N}_N$. To interpolate the data set

$$\{(y_{jk}, z_{jk}) \in J_1 \times R_1 : j \in \mathbb{N}_{N+1}\},\ \text{for each } k = 1, 2, \ldots, n,$$

an another fractal interpolation function g is constructed similar to the FIF h. Set $K_2 = J_1 \times R_1$. Let $l_{2,jk} : J_1 \to J_{j,k}$ and $F_{2,jk} : K_2 \to \mathbb{R}$, for each $k = 1, 2, \ldots, n$, obeying

$$l_{2,jk} = a_{2,jk} y + b_{2,jk},$$
$$l_{2,jk}(y_{1,k}) = y_{j,k},\ l_{2,jk}(y_{N+1,k}) = y_{j+1,k},$$
$$d(F_{2,jk}(s, t_1), F_{2,jk}(s, t_2)) \le r_{2,j} d(t_1, t_2),\ 0 \le r_2 < 1,\ s \in J_1,\ t_1, t_2 \in R_1,$$
$$F_{2,jk}(y_{1,k}, z_{1,k}) = z_{j,k},\ F_{2,jk}(y_{N+1,k}, z_{N+1,k}) = z_{j+1,k},\ j \in \mathbb{N}_N.$$

The attractor G_g of the hyperbolic IFS

$$\{K_2; (l_{2,jk}, F_{2,jk}) : j \in \mathbb{N}_N\} \tag{15}$$

is the graph of $g : J_1 \to \mathbb{R}$ such that $g(y_{jk}) = z_{jk}$, for $j \in \mathbb{N}_{N+1}$ and for each $k = 1, 2, \ldots, n$. Note that

$$g(y) = F_{2,jk}(l_{2,jk}^{-1}(y), g(l_{2,jk}^{-1}(y))),\ y \in J_1,\ j \in \mathbb{N}_N,\ k = 1, 2, \ldots, n \tag{16}$$

is the functional equation of FIF g.

Since $J_1 \subseteq h^{(k)}(I)$, assuming $h^{(k)}(x) \in J_1$, for $x \in I$, ensures the continuity of $g(h^{(k)}(x))$ on I. An IFS is constructed to illustrate the composition of fractal function and fractal spline $g(h^{(k)})$ is again a fractal interpolation function interpolating the data set $\{(x_j, z_{jk}) \in I \times \mathbb{R} : j \in \mathbb{N}_{N+1},\ k = 1, 2, \ldots, n\}$. Let $h^{(k)}(I) = J_1$. From Eqn.(16),

$$g(h^{(k)}(x)) = F_{2,jk}(l_{2,jk}^{-1}(h^{(k)}(x)), g(l_{2,jk}^{-1}(h^{(k)}(x)))),\ h^{(k)}(x) \in J_{1j},$$

for $j \in \mathbb{N}_N$, $k = 1, 2, \ldots, n$. Let $l_j : I \to I_j$ be the function agreeing with $l_{1,j}(x)$ for all $x \in I$. And $F_{jk} : K \to \mathbb{R}$ be the continuous maps defined by

$$\begin{aligned} F_{jk}(x, z) &= F_{jk}(l_j^{-1}(x_1), g^*(h^{(k)}(l_j^{-1}(x_1)))) \\ &= F_{2,jk}(l_{2,jk}^{-1}(h^{(k)}(x_1)), g^*(l_{2,jk}^{-1}(h^{(k)}(x_1)))),\ j \in \mathbb{N}_N, \end{aligned} \tag{17}$$

where $x_1 \in I_j$, $g^* \in \mathcal{C}_1 = \{g(y) + t, z_{1,k} - z_{N+1,k} \le t \le z_{N+1,k} - z_{1,k},\ y \in J_1\}$, $k = 1, 2, \ldots, n$, the set of continuous translation maps and $h(h^{(k)}(l_j^{-1}(x_1))) = z$.

For all $x \in I$, $z, z^* \in R_1$, there exists $x^* \in I_j$, $h_1, h_2 \in \mathcal{C}$ such that

$$l_j^{-1}(x^*) = x,\ h_1(h^{(k)}(l_j^{-1}(x^*))) = z,\ h_2(h^{(k)}(l_j^{-1}(x^*))) = z^*.$$

Then

$$\begin{aligned} &d(F_{jk}(x, z), F_{jk}(x, z^*)) \\ &\quad = d(F_{jk}(l_j^{-1}(x^*)), h_1(h^{(k)}(l_j^{-1}(x^*))), F_{jk}(l_j^{-1}(x^*)), \\ &\qquad h_2(h^{(k)}(l_j^{-1}(x^*)))) \\ &\quad = d(F_{2,jk}(l_{2,jk}^{-1}(h^{(k)}(x^*)), h_1(l_{2,jk}^{-1}(h^{(k)}(x^*)))), \\ &\qquad F_{2,jk}(l_{2,jk}^{-1}(h^{(k)}(x^*)), h_2(l_{2,jk}^{-1}(h^{(k)}(x^*))))). \end{aligned}$$

From the contractivity of $F_{2,jk}$ with respect to second argument, it follows that

$$\begin{aligned} d(F_{jk}(x, z), F_{jk}(x, z^*)) &\le r_{2,j} d(h_1(l_{2,jk}^{-1}(h^{(k)}(x^*))), h_2(l_{2,jk}^{-1}(h^{(k)}(x^*)))) \\ &\le r_2 d(z, z^*), \end{aligned}$$

where $r_2 = \max\{r_{2,j} : j \in \mathbb{N}_N\}$. Therefore, the map F_{jk} satisfies the contractivity condition with contraction ratio r_2. Now, it is necessary to verify the join-up conditions. From Eqn.(17), for $h^{(k)}(x_j) = y_{jk} \in J_{jk}$,

$$\begin{aligned} F_{jk}(x_1, z_1) &= F_{jk}(l_j^{-1}(x_j), g(h^{(k)}(l_j^{-1}(x_j)))) \\ &= F_{2,jk}(l_{2,jk}^{-1}(h^{(k)}(x_j)), g(l_{2,jk}^{-1}(h^{(k)}(x_j)))) \\ &= F_{2,jk}(y_{1k}, z_{1k}) \\ &= z_{jk}. \end{aligned}$$

Meanwhile, for $h^{(k)}(x_{j+1}) = y_{(j+1)k} \in J_{(j+1)k}$,

$$\begin{aligned} F_{jk}(x_{N+1}, z_{N+1}) &= F_{jk}(l_j^{-1}(x_{j+1}), g(h^{(k)}(l_j^{-1}(x_{j+1})))) \\ &= F_{2,jk}(l_{2,jk}^{-1}(h^{(k)}(x_{j+1})), g(l_{2,jk}^{-1}(h^{(k)}(x_{j+1})))) \\ &= F_{2,jk}(y_{(N+1)k}, z_{(N+1)k}) \\ &= z_{(j+1)k}. \end{aligned}$$

The above contractivity maps and the join-up conditions determine an IFS

$$\{I \times \mathbb{R}; (l_j, F_{jk}) : j \in \mathbb{N}_N,\ k = 1, 2, \ldots, n\} \tag{18}$$

which corresponds to the composite fractal interpolation function $g(h^{(k)})$.

Theorem 5. *Let $h^{(k)}$ be the differentiable fractal function generated by the IFS (13). Then the IFS defined in (18) determines a FIF $g(h^{(k)})$ satisfying*

$$g(h^{(k)}(x_j)) = z_{jk},\ \textit{for } j \in \mathbb{N}_N,\ k = 1, 2, \ldots, n.$$

Proof. Let h^* be the FIF generated by the IFS (18) such that

$$h^*(x) = F_{jk}(l_j^{-1}(x), h^*(l_j^{-1}(x)),\ x \in I_j.$$

From (),

$$g(h^{(k)}(l_j(x))) = F_{2,jk}(l_{2,jk}^{-1}(h^{(k)}(l_j(x))), g(l_{2,jk}^{-1}(h^{(k)}(l_j(x))))).$$

Meanwhile, from (17),

$$g(h^{(k)}(l_j(x))) = F_{2,jk}(l_{2,jk}(h^{(k)}(x_1)), g(l_{2,jk}^{-1}(h^{(k)}(x)))).$$

Uniqueness of FIF yields

$$h^*(x) = g(h^{(k)}(x))$$

such that $g(h^{(k)}(x_j)) = z_{jk}$, $j \in \mathbb{N}_N$, $k = 1, 2, \ldots, n$. □

Remark 4. *Theorem 5 has illustrated that composite of fractal spline with a non-differentiable fractal function provided a fractal function of non-differentiable nature. Similar to this construction, one can generate the composite α-fractal spline and explore its corresponding fractal operator.*

Remark 5. *Encompassing the recent trend of fractional calculus, one can investigate the fractional integral and fractional derivative of composite fractal functions as well as verify for the resultant functions to be again attractors of new IFS.*

CONCLUSION

As the fractional integral of a continuous function $(\mathcal{I}^v f)$ enjoys the continuity, a new family of fractal functions $(\mathcal{I}^v f)^\alpha$ is generated in the present paper. In this regard, a fractal operator is also proposed and its bound is estimated as $\left(1+\frac{2|\alpha|_\infty}{1-|\alpha|_\infty}\right)\mathcal{K}\|f\|_\infty$, where $\mathcal{K}=\frac{x_{N+1}-x_1}{v\Gamma(v)}$, with the proper choice of bounded linear base function. In addition, the composition of α-fractal function is discussed. The concept of composition operation is studied to the case of differentiable fractal function $h^{(k)}$. The composition of differentiable fractal function $h^{(k)}$ with a non-differentiable fractal function g yielded a non-differentiable fractal function $g(h^{(k)})$ satisfying the necessary end point conditions. The composite fractal functions can be employed for approximating complex real data generated from multiple functions. For instance, in engineering the composite functions can establish a concrete relationship between different physical quantities, especially in unit conversions.

Availability of data and material

Not applicable.

Conflicts of interest

The author declares that there is no conflict of interest regarding the publication of this paper.

Ethical standard

The author has no relevant financial or non-financial interests to disclose.

LITERATURE CITED

Agathiyan, A., A. Gowrisankar, and T. Priyanka, 2022 Construction of new fractal interpolation functions through integration method. Results in Mathematics **77**: 122.

Akhtar, M. N., M. Prasad, and M. Navascués, 2016 Box dimensions of α-fractal functions. Fractals **24**: 1650037.

Akhtar, M. N., M. Prasad, and M. Navascués, 2017 Box dimension of α-fractal function with variable scaling factors in subintervals. Chaos, Solitons & Fractals **103**: 440–449.

Balasubramani, N., M. Prasad, and S. Natesan, 2020 Shape preserving α-fractal rational cubic splines. Calcolo **57**: 21.

Banerjee, A., M. N. Akhtar, and M. Navascués, 2023 Local α-fractal interpolation function. The European Physical Journal Special Topics pp. 1–8.

Banerjee, S., D. Easwaramoorthy, and A. Gowrisankar, 2021 *Fractal Functions, Dimensions and Signal Analysis*. Springer, Cham.

Barnsley, M., 1986 Fractal functions and interpolation. Constructive Approximation **2**: 303–329.

Barnsley, M. and A. Harrington, 1989 The calculus of fractal interpolation functions. Journal of Approximation Theory **57**: 14–34.

Çimen, M., Z. Garip, O. Boyraz, I. Pehlivan, M. Yildiz, *et al.*, 2020 An interface design for calculation of fractal dimension. Chaos Theory and Applications **2**: 3–9.

Dai, Z. and S. Liu, 2023 Construction and box dimension of the composite fractal interpolation function. Chaos, Solitons & Fractals **169**: 113255.

Falconer, K., 2004 *Fractal Geometry: Mathematical Foundations and Applications*. John Wiley & Sons.

Fortin, C., R. Kumaresan, W. Ohley, and S. Hoefer, 1992 Fractal dimension in the analysis of medical images. IEEE Engineering in Medicine and Biology Magazine **11**: 65–71.

Gowrisankar, A. and M. Prasad, 2019 Riemann-Liouville calculus on quadratic fractal interpolation function with variable scaling factors. The Journal of Analysis **27**: 347–363.

Gowrisankar, A. and R. Uthayakumar, 2016 Fractional calculus on fractal interpolation for a sequence of data with countable iterated function system. Mediterranean Journal of Mathematics **13**: 3887–3906.

Massopust, P., 2022a Fractal interpolation: From global to local, to nonstationary and quaternionic. Frontiers of Fractal Analysis. Recent Advances and Challenges; CRC Press: Boca Raton, FL, USA pp. 25–49.

Massopust, P., 2022b Fractal interpolation over nonlinear partitions. Chaos, Solitons & Fractals **162**: 112503.

Navascués, M., 2005 Fractal polynomial interpolation. Zeitschrift fur Analysis und ihre Anwendung **24**: 401–418.

Navascués, M., 2010 Fractal approximation. Complex Analysis and Operator Theory **4**: 953–974.

Navascués, M., C. Pacurar, and V. Drakopoulos, 2022 Scale-free fractal interpolation. Fractal and Fractional **6**: 602.

Navascués, M. and M. Sebastián, 2006 Smooth fractal interpolation. Journal of Inequalities and Applications **2006**: 1–20.

Pan, X., 2014 Fractional calculus of fractal interpolation function on $[0, b](b > 0)$. In Abstract and Applied Analysis **2014**.

Priyanka, T. and A. Gowrisankar, 2021a Analysis on weyl-marchaud fractional derivative for types of fractal interpolation function with fractal dimension. Fractals **29**: 2150215.

Priyanka, T. and A. Gowrisankar, 2021b Riemann-Liouville fractional integral of non-affine fractal interpolation function and its fractional operator. The European Physical Journal Special Topics **230**: 37889–3805.

Ruan, H.-J., W.-Y. Su, and K. Yao, 2009 Box dimension and fractional integral of linear fractal interpolation functions. Journal of Approximation Theory **161**: 187–197.

Samko, S., A. Kilbas, and O. Marichev, 1993 Fractional integrals and derivatives.

Sanjuán, M. A., 2021 Unpredictability, uncertainty and fractal structures in physics.

How to cite this article: Gowrisankar, A. Fractalization of Fractional Integral and Composition of Fractal Splines. *Chaos Theory and Applications*, 5(4), 318-325, 2023.